UNIVERSITAT POLITÈCNICA DE CATALUNYA

Doctoral Programme:

AUTOMATITZACIÓ AVANÇADA I ROBÒTICA

Doctoral Thesis

INSTRUMENTATION, MODEL IDENTIFICATION AND CONTROL OF AN EXPERIMENTAL IRRIGATION CANAL

Carlos Alberto Sepúlveda Toepfer

Supervisors: PhD Manuel Gómez V. and PhD José Rodellar B.

Institut d'Organització i Control de Sistemes Industrials

October 2007

To my two Silvias

Abstract

This thesis aims to develop control algorithms for irrigation canals in an experimental framework.

These water transport systems are difficult to manage and present low efficiencies in practice. As a result, an important percentage of water is lost, maintenance costs increase and water users follow a rigid irrigation schedule. All these problems can be reduced by automating the operation of irrigation canals.

In order to fulfil the objectives, a laboratory canal, called Canal PAC-UPC, was equipped and instrumented in parallel with the development of this thesis. In general, the methods and solutions proposed herein were extensively tested in this canal.

In a broader context, three main contributions in different irrigation canal control areas are presented.

Focusing on gate-discharge measurements, many submerged-discharge calculation methods are tested and compared using Canal PAC-UPC measurement data. It has been found that most of them present errors around $10\,\%$, but that there are notable exceptions. Specifically, using classical formulas with a constant 0.611 contraction value give very good results (MAPE<$6\,\%$), but when data is available, a very simple calibration formula recently proposed in Ferro (2001) significantly outperform the rest (MAPE<$3\,\%$). As a consequence, the latter is encouragingly proposed as the basis of any gate discharge controller.

With respect to irrigation canal modeling, a detailed procedure to obtain data-driven linear irrigation canal models is successfully developed. These models do not use physical parameters of the system, but are constructed from measurement data. In this case, these models are thought to be used in irrigation canal control issues like controller tuning, internal controller model in predictive controllers, or simply as fast and simple simulation platforms. Much effort is employed in obtaining an adequate model structure from the linearized Saint-Venant equations, yielding to a mathematical procedure that verifies the existence of an integrator pole in any type of canal working under any hydraulic condition. Time-domain and frequency-domain results demonstrate the accuracy of the resulting models approximating a canal working around a particular operation condition, in either simulation or experimentation.

Regarding to irrigation canal control, two research lines are exploited. First, a new water level control scheme is proposed as an alternative between decentralized and centralized control. It is called Semi-decentralized scheme and aims to resemble the centralized control performance while maintaining an almost decentralized structure. Second, different water level

control schemes based on Proportional Integral (PI) control and Predictive Control (PC) are studied and compared. The simulation and laboratory results show that the response and performance of this new strategy against offtake discharge changes, are almost identical to the ones of the centralized control, outperforming the other tested PI-based and PC-based schemes. In addition, it is verified that PC-based schemes with good controller models can counteract offtake discharge variations with less level deviations and in almost half the time than PI-based schemes.

In addition to these three main contributions, many other smaller developments, minor results and practical recommendations for irrigation canal automation are presented throughout this thesis.

Acknowledgments

There are lots of people that I have to thank after four years of research, study, hard work and unforgettable experiences.

First, I would like to express my enormous gratitude to my two thesis supervisors, Professor Manuel Gómez and Professor José Rodellar, for offering me the great opportunity to study at UPC, a prestigious university located in a beautiful city, doing something that I really enjoy. Their wisdom and expert guidance have been indispensable in the elaboration of this thesis and without their efforts, I would not have had the support to finish this work. It was a pleasure to work under the supervision of these two true gentlemen.

I would like to thank my mentor at UdeC, Professor Daniel Sbarbaro, for his help and guidance in the embryonic stage of the research.

Thanks to the laboratory personnel of the Hydraulic and Hydrological Engineering Section, Juan Pomares, Jaime Ambrós, Robert McAllon and others for their help and meticulous work in the construction of the laboratory canal.

Appreciation is also extended to my "occasional" laboratory assistants and friends: Silvia Arriagada, Joaquim Blesa, Rodrigo Concha, Claudiu Iurian, Gustavo Mazza and Francisco Núñez. Their help was invaluable in particular periods of this work and I think I will never be able to reward the patience they had with a so perfectionist and demanding boss.

I would need more than a lifetime to thank all what my beloved wife, Silvia Arriagada, has made for me. She has worked a lot to make this possible. Without her, I would not have been capable to bring this to an end. This thesis is also hers.

Additionally, I wish to thank for the generous support provided by the Spanish Ministry of Science and Education through BES-2003-2042 grant.

Finally, special thanks go to my parents, Silvia Toepfer and Luis Sepúlveda; brothers, Lucho, Jorge and Rodrigo; friends and colleagues, Anaïs, Belén, Cesca, Kat, Raquel, Úrsula, Andrés, Alejandro, Antonio, Beniamino, Carles, David, Germán, Hans, Jordi, José Luis, Quim and Vicente for their continuous encouragement and support.

People like this is essential to make research possible.

<div align="right">

Carlos Sepúlveda Toepfer

Barcelona

October 26, 2007

</div>

Contents

List of Figures

List of Tables

Nomenclature

$\mathbf{\Phi}_k$ Vector of past input and output measures at instant k

$\mathbf{\Theta}$ Vector of model parameters

$\mathbf{I}$ Identity matrix

ν Kinematic viscosity

$\overline{Q}_i$ Reach's i, transport area, water discharge downstream boundary condition

$\overline{X}$ x position of the end of the transport area (the start of the storage area)

$\overline{Z}_i$ Reach's i, transport area, water level downstream boundary condition

A Wetted cross-sectional area

B Water width

b Gate or weir width

C Water wave celerity

C_c Contraction coefficient

C_d Discharge coefficient

C_{rw} Rectangular weir discharge coefficient

C_{vw} V-notch weir discharge coefficient

d Delay in amount of instants

e_k Model error at instant k

F Froude number

$F1$ Upstream gate discharge transfer function

$F2$ Downstream gate discharge transfer function

$F3$ Offtake discharge transfer function

g Gravity acceleration

h Head above the weir

h_1 Gate upstream water level

h_2 Water depth at vena contracta generated by the gate

h_3 Gate downstream water depth

k Discrete time instant variable

l Gate opening

l_i Reach's i upstream gate opening

O Weir height or gate position

P Wetted perimeter

Q Volumetric water discharge

q Forward shift time operator

q Water discharge around a working point

q^{-1} Backward shift time operator

Q_0 Initial time water discharge condition

Q_i Reach's i, transport area, water discharge upstream boundary condition

Q_{i+1} Water discharge delivered to reach $i+1$

Q_{Li} Reach's i offtake discharge

s Laplace variable

S_0 Bottom slope

S_f Friction slope

T Sampling period

t Time

u System input

V Water velocity

V_{si} Water volume stored behind gate $i+1$

x Longitudinal coordinate in the flow direction

y System output

Z Water level

z Water level around a working point

z Z-transform complex variable

Z_0 Initial time water level condition

Z_i Reach's i, transport area, water level upstream boundary condition

z_k Output measure at instant k

Z_{si} Reach's i downstream water level

List of abbreviations

ARIMAX   Auto-Regressive Integrated Moving Average with eXogenous Input

ARIX   Auto-Regressive Integrated with eXogenous input

ARX   Auto-Regressive with eXogenous Input

ASCE   American Society of Civil Engineers

ASTM   American Society for Testing and Materials

BIBO   Bounded-Input Bounded-Output

Canal PAC-UPC Canal de Prueba de Algoritmos de Control - Universitat Politècnica de Catalunya

CARDD   Canal Automation for Rapid Demand Deliveries

DAQ   Data AcQuisition

HEC-RAS   Hydrologic Engineering Center - River Analysis System

ID   Integrator Delay

IDZ   Integrator Delay Zero

ISO   International Organization for Standardization

LAD   Least Absolute Deviations

LQ   Linear Quadratic

LQG   Linear Quadratic Gaussian

LQR   Linear Quadratic Regulator

MAE   Mean Absolute Error

MAPE   Mean Absolute Percentage Error

ME   Mean Error

MIMO   Multiple-Input Multiple-Output

MPE   Mean Percentage Error

ODE   Ordinary Differential Equation

P	Proportional
PC	Predictive Control
PDE	Partial Differential Equation
PI	Proportional Integral
PID	Proportional Integral Derivative
PRBS	Pseudo Random Binary Sequence
PV	Process Variable
QP	Quadratic Programming
RMSE	Root Mean Square Error
SCADA	Supervisory Control And Data Acquisition
SIC	Simulation of Irrigation Canals
SISO	Single-Input Single-Output
SP	Set Point
TITO	Two-Input Two-Output
USBR	U.S. Department of the Interior, Bureau of Reclamation
WLS	Weighted Least Squares

Glossary

B

Black-box model   No physical insight is available or used, but the chosen model structure belongs to families that are known to have good flexibility and have been "successful in the past", p. 10.

bode diagram   Logarithmic magnitude and phase plot of a transfer function, that gives information of this function evaluated in the s-plane imaginary axis. In a more practical view, it shows what happens with the amplitude and the phase of the response of a system, when it is excited with a sinusoidal input at a given frequency.

C

Control theory   Branch of Mathematics and Engineering which deals with the design, identification and analysis of systems with a view towards controlling them, i.e., to make them perform specific tasks or make them behave in a desired way.

G

Grey-box model   This is the case when some physical insight is available, but several parameters remain to be determined from observed data. It is useful to consider two sub-cases: - Physical Modeling: A model structure can be built on physical grounds, which has a certain number of parameters to be estimated from data. This could, e.g., be a state space model of given order and structure. - Semi-physical modeling: Physical insight is used to suggest certain nonlinear combinations of measured data signal. These new signals are then subjected to model structures of black box character, p. 10.

H

hydraulic jump   The sudden and usually turbulent passage of water in an open channel from low stage, below critical depth, to high stage, above critical depth. During this passage, the velocity changes from supercritical to subcritical. There is considerable loss of energy during the jump, p. 46.

I

irrigation canal   Permanent irrigation conduit constructed to convey water from the source of supply to one or more farms, p. 8.

P

Parameter Estimation   Estimating the values of parameters based on measured/empirical data.

R

radial gate   Gate with a curved upstream plate and radial arms hinged to piers or other supporting structures on which the gate pivots.

S

sluice gate   Gate that can be opened or closed by sliding it in supporting guides.

state-space model   Mathematical model of a physical system as a set of input, output and state variables related by first-order differential equations. To abstract from the number of inputs, outputs and states, the variables are expressed as vectors and the differential and algebraic equations are written in matrix form, p. 8.

System Identification   General term to describe mathematical tools and algorithms that build dynamical models from measured data, p. 86.

T

transfer function   Mathematical representation of the relation between the input and output of a linear time-invariant system, p. 9.

W

weir   1. Low dam or wall built across a stream to raise the upstream water level, termed fixed-crest weir when uncontrolled. 2. Structure built across a stream or channel for the purpose of measuring flow, sometimes called a measuring weir or gauging weir. Types of weirs include broad-crested, sharp-crested, drowned, and submerged.

White-box model   This is the case when a model is perfectly known; it has been possible to construct it entirely from prior knowledge and physical insight.

Chapter 1

Introduction

1.1 Background

Irrigation is the artificial application of water to the soil usually for assisting in growing crops. In crop production, irrigation is mainly used to replace missing rainfall in periods of drought, but also to protect plants against frost.

At the global scale, approximately $2\,788\,000\,\mathrm{km^2}$ of agricultural land is equipped for irrigation in the world. $68\,\%$ of this area is located in Asia, $17\,\%$ in America, $9\,\%$ in Europe, $5\,\%$ in Africa and $1\,\%$ in Oceania. Most of this vast area is gridded by irrigation canals.

Irrigation canals are artificial systems developed to transport water from main water reservoirs to several water-demanding agricultural farms during irrigational seasons (see figure 1.1). Generally, they cover very long distances: their length can range from hundreds of meters to hundred of kilometers. Along these canals, farms are located close to them and distributed all over the way.

A typical configuration, considered as a prototype case study in this thesis, is the one depicted in figure 1.1b. A main canal transports water from a big reservoir to the farms and controls the water flow by modifying the openings of several gates. These hydraulic structures are situated in the waterway in order to regulate discharge in relation to ongoing irrigation demands. Water is supplied only in fixed locations of the canal; generally, a few meters upstream of each gate. In real situations, these water offtakes are usually performed by pumps or weirs.

It is not trivial to manage this type of systems. Water must be transported, minimizing the losses and assuring that every farm receives the stipulated amount of water at its corresponding frequency. Besides, the inherent characteristics of these systems increase the complexity of the problem. These systems present very long delays in the water transport (from minutes to hours), delay that even varies depending on the provided discharge. Moreover, there are important dynamical effects produced generally by changes in the amount of supplied water, that produce

(a) Aerial Photo
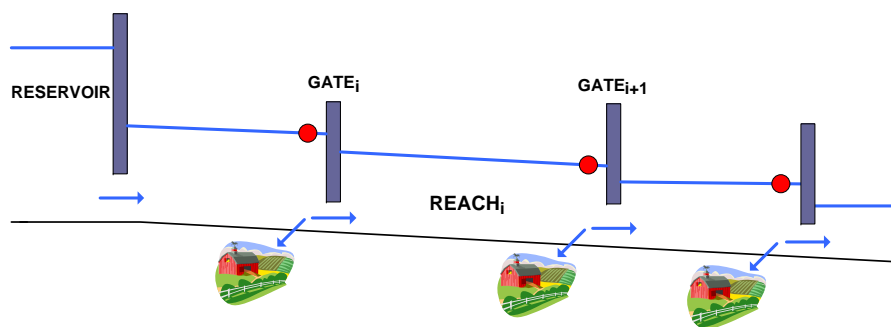
(b) Idealized scheme

Figure 1.1: Irrigation canal

in different degrees depending on the case, interferences in the delivers of the whole system (coupling). Historically, these problems and the availability of water have motivated the creation in many countries of irrigation associations with their own irrigation statutes and rules.

Despite these measures, it is estimated that between $15\,\%$ and $21\,\%$ of water set aside for irrigation is lost, because of unappropriate transport management policies.

Regulation of an irrigation water delivery system generally relies on manual or open-loop techniques. The use of this type of managing strategies has the following drawbacks according to researchers around the world:

- Routing known flow changes and accounting for unknown flow disturbances and flow measurement errors using manual control is a difficult and time-consuming process (Wahlin and Clemmens, 2006).

- Low efficiency in terms of delivered water versus water taken from the resource (Litrico and Georges, 1999b).

- Large water losses (Rivas Pérez et al., 2007).

- The performance is limited and the costs of operation are relatively high (Litrico and Georges, 1999b).

- Poor timing of irrigation, a consequence of manual water scheduling on the supply canals and tendency to oversupply water, as a lack of water has obviously averse effects on the yield (Mareels et al., 2005).

For these reasons, the research community have paid attention in improving the operational management of these systems by applying control engineering tools.

Generally speaking, the goal of any irrigation canal automation is to maintain water levels as constant as possible at the offtakes by moving intermediate check gates in an automatic operation. This type of objective is requested for the following reason: either if irrigation water is taken out of the system by pumps or weirs, a constant level ensures water availability neither wasting water nor interfering other irrigations. Furthermore, there are several other benefits that can be gained. For instance, the erosion of the canal covering is reduced leading to lower maintenance costs, canal overflows are eliminated thereby saving water, etc..

There are only a few practical implementations to date. Most of them are based on automatic gates using local control, but there are also cases of supervisory control of a complete canal like in the Canal de Provence system (France) and in the Central Arizona Project canal system (USA) (Rogers and Goussard, 1998). However, there is a growing interest around the world in automating irrigation canal systems. For example, a large irrigation system in Victoria

(Australia) is being fully automated, which is reported as the largest Supervisory Control And Data Acquisition (SCADA) system of its kind in the world (Mareels et al., 2005).

In general, the following elements are required to design and implement an irrigation canal control system:

- Instrumentation to measure relevant variables and to operate gates.

- A good dynamical model of the canal to design, analyze and simulate control solutions.

- A control strategy that can cope with irrigation canal managing problems and fulfil water level regulation requirements.

The mix of these basic requirements with the particular interest to develop more practical implementations of fully automated irrigation canals to be able to transfer this knowledge to real canals, lays the foundations of these thesis. This idea is presented in terms of specific objectives in the following section.

1.2   Objective of the thesis

The overall objective of this work is **to develop linear control algorithms for multiple-pool irrigation canals and test them in a newly installed experimental facility.**

This objective intrinsically comprises several tasks that should be done to attain the final goal:

- To instrument a new laboratory canal and create a canal management system capable of implementing control algorithms.

- To improve the accuracy of actuators and water measurements as far as possible.

- To develop a methodology capable of producing good linear models to design and tune controllers and test control solutions.

- To develop and implement different control schemes and test them experimentally.

1.3   Methodology used

In brief, the methodology employed goes along as follows: first, the literature reporting the research on canal control methods is reviewed and studied in order to lay the theoretical foundations of the thesis; second, the laboratory canal is equipped with the sensors, control gates and data acquisition systems to serve as an adequate experimental platform; third, several water-measurements calibration-methods are tested with experimental data to find the most appropriate ones; fourth, simulation and experimentation is used to obtain linear models; and fifth,

control algorithms are designed, tested and compared through numerical simulation and experimental work.

Literature review It was decided to base this work mainly on journal papers and books. Most of the reviewed irrigation canal control papers were published in the last ten years.

Canal PAC-UPC instrumentation Most of the instrumentation comes from suppliers specialized in water. The methods used to connect, shield and route measurement signals follows general wiring recommendations and a large number of trial and error attempts. The motorization of the gates was implemented with typical gate servomotors and optimized as far as possible in situ.

Calibration of measurements Water level measurements were properly conditioned, filtered and periodically calibrated with manual limnimeters to increase as far as possible the measurement accuracy. Discharge was always calculated using hydraulic discharge formulas from journal papers or water measurement manuals. Many methods were tested experimentally and the ones with the higher performance results were selected to be implemented and used in laboratory.

Canal modeling The model analysis starts from the Saint-Venant equations to have an insight into the linearized phenomenons. From there on, only discharge-based models and linear structures are considered for irrigation canal control algorithms. In order to obtain data-driven models, methods and techniques common in the system identification area were used. Both, simulation and experimental data were employed.

Canal automation Only PI-based and Predictive Control (PC)-based techniques were used. All methods where designed with the aid of identified canal models. The schemes were tested in computational simulation and in laboratory. The laboratory implementation was performed on a real-time software platform with direct communication with canal gates and water level sensors.

1.4   Thesis layout

The present thesis is organized in six chapters and a few appendices. Some of these chapters are based on developments from former chapters, but in general, all of them can be read independently as self-contained entities.

Chapter 2 presents a deep revision of the irrigation canal control research during the last ten years.

Chapter 3 shows and describes the laboratory canal specially constructed to test irrigation canal control developments in practice.

Chapter 4 presents several of the most common discharge calculation and calibration methods for weirs and gates and collects the results of their implementation in the Canal PAC-UPC.

Chapter 5 looks deeply into the linear properties of a Saint-Venant pool model and develops a particular methodology to obtain data-driven pool models from real canal measurements.

Chapter 6 describes how to design and implement an irrigation canal automation. It is centered primarily on the water level control, testing PI-based and PC-based control schemes for the Canal PAC-UPC and presenting a new strategy called Semi-decentralized control. All of them are tested under different conditions and the results are analyzed in terms of regulation performance.

With respect to the conclusions of the thesis, they are presented in detail at the end of each chapter and the most important concepts are summarized in Chapter 7.

Chapter 2

Literature Review

As has been previously remarked in Chapter 1, the control of irrigation canals is not an easy task to carry out without a solid background knowledge on the theme. Fortunately, this subject has attracted the attention of many researchers around the world in the last decades. This chapter summarizes the most important developments and results found in the specialized research literature on Control of Irrigation Canals in the last ten years.

2.1 System characteristics and the control problem

In Malaterre et al. (1998) and in Ruiz et al. (1998) there is a survey about the different types of controllable variables in canal systems, in order to assure the availability of water for the final users. These are:

- Supplied water discharges

- Water depth levels where water is diverted for irrigation

- Stored water volumes

The truth is that what is really supplied to the farmers are always discharges, but the difficulties that has the measurement of this variable, make it less attractive. In contrast, the fact of controlling the water levels in the extraction zones, produce the same effect of water availability for the farmers, contributing additional advantages like, for example, preventing canal overflows and increasing the stability of the system. Choosing to control the storaged water volumes has the advantage that this variable is less sensitive to the disturbances (unexpected water extractions), but at the cost of incrementing the response times of the system. Therefore the most used policy is considering the water levels in the extraction zones as control objective.

On the other hand, the final control action is always limited to control the gates or valves position or pumping actions. However, according to the same works and Malaterre and Baume

(1999), it is also usual to solve the control problem using only discharges, and afterwards use local controllers or discharge formulas inversion, in order to obtain the necessary actions over the actuators.

In the operational point of view, generally, it is more often required a regulation effect, in front of previous known demands, than a change in the operational working point (Clemmens et al., 1998). However, the system has also unknown disturbances due to: inaccuracies in the measurement of the supplied discharge, filtration of the canals, non-authorized water extractions and changes in the demand.

A frequency analysis around a given working point, as the one made in Litrico and Fromion (2004c), gives valuable information about the different types of behaviors that can appear. According to the geometrical characteristics of the canal and the hydraulic conditions of the flow that circulates through it, the system can exhibit (small slope canals) or not (high slope canals) resonant modes, can have long delays (whose values depend mainly on the canal's length) that vary according to the circulating water discharge and can also have pure integrating dynamics (single pole in the origin).

2.2 Irrigation canal models for automatic control purposes

The modeling of an irrigation canal is carried out dividing the canal into pools (section of a canal between two gates or any similar device), characterizing then the water dynamics at each reach separately and, finally, including the water regulation devices equations as boundary conditions between reaches.

As detailed in Henderson (1966), the water flow through a reach can be well characterized by the Saint-Venant equations, a nonlinear hyperbolic Partial Differential Equation (PDE) system. On the other hand, the governing equations of the devices that are usually found in an irrigation canal (gates, weirs, etc.) are of nonlinear nature. In this manner, the solution of a complete irrigation canal model does not exist analitically and can only be done by means of advanced numerical methods (finite volume, finite differences, method of characteristics, etc.).

Clearly these models are not adequate for their use in automatic control design and implementation. For this reason, a series of authors have proposed different and diverse simplified types of models for control.

In Malaterre and Baume (1998) there is a survey about all types of models that had been used, until that date, in the canal control literature. They cover a large spectrum that includes: Saint-Venant model linearizations, infinite order linear transfer functions, finite order nonlinear models, finite order linear models (state-space models), finite order linear models (transfer functions), neural networks based models, fuzzy logic based models and petri nets based models.

In all these alternatives, Single-Input Single-Output (SISO) approaches that model each

reach separately and Multiple-Input Multiple-Output (MIMO) approaches that model a whole canal, have been used. In both cases, some models include the actuators dynamics and models that do not.

In the last years, the literature shows the inclusion of new models and improvements to the already existing ones. First of all, we will refer to models that use some physical knowledge about the canal for its formulation. Second, we will review some black-box models along with identification techniques.

In Schuurmans et al. (1999b,a) a model, proposed by the same authors in 1995, is evaluated. This one approximates each canal's reach as a pure integrator plus a delay, the reason why it is called Integrator Delay (ID) Model. The input variables of the model are the reach's inflow and outflow discharges and what is obtained is the water level at the end of it. In this model, the delay is obtained in an algebraic manner as a function of the physical parameters of each reach, and the storage area (integrative part) is obtained by means of the canal's backwater curve. In order to include the actuators, linearized models of them were used. The model's validation in the time domain, with experimental data, showed an acceptable performance when the system was operated with small movements around a working point. In the frequency domain, the model showed a good fit in the low frequencies, but a bad fit in the high frequencies. In other words, there exist some evidence that the model does not perform well in the short-term period. For this reason, the model manifested an incapability to approximate resonant modes when they exist. They put emphasis on remarking, however, that the modeling of these modes is not so important, because they are generally filtered in control applications. This model has been also used to generate state-space MIMO models and in Clemmens and Schuurmans (2004a,b); Wahlin (2004); Montazar et al. (2005) and van Overloop et al. (2005).

Few years ago, improvements to the ID model have been also proposed in Litrico and Fromion (2004a,b). There, the inclusion of a transfer function to approximate better the high frequency range was proposed. The model was called Integrator Delay Zero (IDZ) Model and this additional transfer function was considered for the influences of the inflow and outflow discharges. In that work, the algebraic expressions that describe the model parameters were also modified.

Another model in the same line as the preceding ones was the one presented in Rodellar et al. (1993) and in Gómez et al. (2002), where the Muskingum model was used to model the water transport and, also, an integrator was used to characterize the water level variations upstream a gate (extraction zone).

Another approach was the one used in Litrico and Georges (1999a,b), where a simplification of the Saint-Venant equations was used to model a reach by means of the Hayami model. Due to the similarities that the authors observed between this model and a standard second-order plus delay one, they used the Method of Moments to obtain the parameters of this last one as a

function of the Hayami parameters.

For the particular modeling case where rivers are used for irrigation purposes, in Litrico (2001a,b) system identification techniques were used to obtain the parameters of a Diffusive Wave model (another simplification of the Saint-Venant model) with the aid of experimental data.

For canals, in Litrico and Fromion (2004c) and in Litrico et al. (2005) they developed and used a methodology for obtaining numerically the frequency response of a reach, including the gates, by means of the linearization of the Saint-Venant equations around an operation point and the knowledge of the hydraulic and geometric parameters of the canal.

A different approach was used, for example, in Malaterre and Rodellar (1997) and in Malaterre (1998). In that paper, a state-space MIMO model was generated, using the linearized Preissmann method in order to solve the Saint-Venant equations directly and construct, in that manner, a state observer. A linearized version of all gates equations were also included in order to generate a model that, by knowing the gate's openings, can calculate all water levels in the irrigation water extraction zones. This approach includes all system coupling effects and in general generates very large matrices.

In the same line of thought, Reddy and Jacquot (1999) used a linearization of the Saint-Venant equations using the Taylor series and a finite difference approximation to develop state-space MIMO model. A Kalman filter was also designed to estimate values for the state variables that were not measured.

In Durdu (2005), they developed a state-space MIMO model using another finite difference method. The difference was that in that work they developed a state estimator based on fuzzy logic rules.

Another state-space MIMO model was used in Seatzu (1999, 2000) and in Seatzu and Usai (2002). In that case the modeling was performed around a particular hydraulic regime, called uniform regime, that is the only one that has an algebraic solution by linearizing the Saint-Venant equations. Additionally, the model used as inputs, gate openings, and as outputs, not the water depth levels, but rather, the storaged water volumes in each reach.

Nonlinear irrigation canal models for control has also been developed. In Dulhoste et al. (2004), a model was developed by means of a nonlinear approximation with Lagrange polynomials of the Saint-Venant equations. In de Halleux et al. (2003), they went one step ahead and used the Saint-Venant model, but only for a zero-slope rectangular canal without friction. In Sanders and Katopodes (1999) the canal was modeled solving numerically the original Saint-Venant equations as an adjoint problem discretized with the Leap-Frog scheme. In Soler et al. (2004) a numerical scheme solving the Saint Venant equations using the method of the characteristics has been developed to calculate desired trajectories for control gates.

The modeling problem has also been faced from the Black-box model and Grey-box model

identification point of view.

In Akouz et al. (1998); Ruiz and Ramírez (1998); Sawadogo et al. (1998, 2000); Rivas et al. (2002) and in Rodellar et al. (2003) Auto-Regressive Integrated with eXogenous input (ARIX) and Auto-Regressive Integrated Moving Average with eXogenous Input (ARIMAX) Black-box models were used without getting too deep into the analysis or validation issues. The majority of these models used or the discharge or the gate opening at the beginning of the reach as model input and, the water level at its end, as output. In some cases the reach's outflow discharge and the water delivered for irrigation (when it was initially known) were used as known disturbances. All of them used data obtained by computational simulation of the Saint-Venant equations.

In Weyer (2001) a more deeper work was performed for model identification of the Haughton Main Channel reaches in Australia. Three gray-box models were used, based on elementary mass balances and gate equations. Because, in this case, the canal has overflow gates, the inputs to the model were water levels over the gates and its outputs, water levels in the extraction zones. Linear and nonlinear first order, second order and second order plus integrator (third order) models were proven. All of them included explicitly the delay. The obtained results, by means of model validation against real data, showed that the only model that could reproduce the effect of the waves was the nonlinear third order model. However, the first and second order ones could follow the tendencies in most of the cases. In the final conclusions they emphasized the need to study more the cases with gates in submerged regime and the use of closed loop identification, in order to estimate models using smaller variations and shorter experimentation times. The results of this work were extended in Eurén and Weyer (2007) in several aspects:

- The irrigation channel was equipped with both overshot and undershot gates.

- The overshot gates operated in both submerged and free flow.

- There were several gates at each regulator structure and they had different positions.

- The flows and pools were larger.

The results presented in this paper are very encouraging, since the system identification models were able to accurately simulate the water levels more than $12\,\mathrm{h}$ ahead of time.

System identification applied on irrigation canals was also studied in Ooi et al. (2005). The results showed that the St. Venant equations can adequately capture the dynamics of real channels, but that to estimate their parameters from real data is more accurate than using only physical knowledge. On the other hand, system identification models were as accurate as the St. Venant equations with estimated parameters and, consequently, they should be preferred over the St. Venant equations for control and prediction purposes since they are much easier to use.

2.3 Types of control algorithms developed for irrigation canals

Malaterre et al. (1998); Malaterre and Baume (1998) and Ruiz et al. (1998) gave a survey of the control algorithms that had been developed until 1998 for canal irrigation control. They cover a large spectrum of approaches and techniques, among which can be mentioned: monovariable heuristical methods, Proportional Integral Derivative (PID) Control, Smith Predictor scheme, Pole Placement Control, Predictive Control, Fuzzy Logic Control, Model Inversion methods, Optimization methods, Robust Control, Adaptive Control and Nonlinear Control.

Due to the diversity of proposed methods and distinct performance criteria used, the American Society of Civil Engineers (ASCE) Task Committee on Canal Automation Algorithms developed in Clemmens et al. (1998) two standard cases (Test Canal 1 and Test Canal 2) to test and evaluate automatic control algorithms. These cases are based on real canals and normal operation conditions as, for example, scheduled and unscheduled water discharge offtakes and correct and incorrect knowledge of the canal physical parameters. In that work, a series of evaluation criteria are likewise given in order to standardize the evaluation of control algorithm performance.

In spite of the important amount of studies that have been done about the subject (the majority of them in computational simulation), as denoted by Rogers and Goussard (1998) and by Burt and Piao (2004), until now the few real canals that are managed in an automatic form use, in their majority, at the most PID control based techniques. It has been used, aside from several heuristic techniques, in the form of Proportional Integral (PI) control in many cases, PI plus filter (PIF) in cases with resonance problems, and occasionally PID. These developments can be found in North America, Asia and Europe, but mostly in the USA.

Going back to the academical knowledge developed, it is also important to mention that some of the cited methods have used only feedback strategies and others only feedforward strategies, while others have made use of combinations of both (Malaterre et al., 1998). Feedback produces a corrective control action in order to return the controlled variable to its nominal value, inclusively in presence of unknown disturbances, whereas feedforward can compensate the inherent delays of the system by anticipating the needs of the canal users.

In Bautista and Clemmens (1999) they tested a classical open-loop method, called Gate Stroking. The conclusion was that an adequate irrigation canal controller should be implemented, when possible, with feedback and feedforward capabilities. That is especially true for canals that need large water volume variations, to arrive to another steady state condition, and for those characterized by a low Froude number.

2.3.1 PID control

From 1998 on, the works based on PID control have focused in improving the tuning of this types of controllers. To achieve this goal, two common practices have been identified from the literature: the use of simplified mathematical models and the employment of strategies that lead to decoupling the influences, produced by the control action of a reach over all the adjacent ones.

Schuurmans et al. (1999b) proposed a control where every reach was controlled by its upstream gate. In order to achieve this, a supervisory control was used. It calculated which should be the input discharge, and then a local controller moved the gate so as to obtain the required discharge. The reach's outflow discharge and the water demands were also included as known disturbances, so as to decouple, in a better way, the interaction between reaches. The philosophy was, thus, to include the local controller in order to minimize the nonlinear effects that a gate induces on the canal operation. The tuning of these controllers was based on the ID Model and a filter was also used, so as to filter the canal inherent resonance.

In Malaterre and Baume (1999) optimum PI controller tunings were calculated in conjunction with their corresponding performances for different cases. In that work, different manipulated variable choices and decoupling strategies were tested. They arrived at the conclusion that the best results are obtained with a supervisory control that calculates for each reach their optimum inflow discharge, and a series of local slave controllers that calculate the gate openings taking into account the water level variations induced by the gate movements. Better result were also obtained when the local controllers ran at a sampling time 5 times faster than the supervisory controller, but with a considerable increase in the control effort.

Other work that treated the decentralized Proportional (P) and PI controller tuning was Seatzu (1999). They proposed the use of a state feedback diagonal matrix and a H_2 norm minimization, so as to obtain an optimal tuning. Seatzu (2000) proposed the same scheme, now seeking to place the eigenvalues and eigenvectors of the controlled MIMO system to some optimal values, obtained previously with the Linear Quadratic Regulator (LQR) method. Besides, in a later work (Seatzu and Usai, 2002), a research was made in order to know when this controller plus an observer was robust against modeling errors.

In Wahlin and Clemmens (2002) three classical controllers were tested on the ASCE Test Canal 1: PI Control, PI Control with upstream and downstream decouplers as proposed by Schuurmans in 1992 (they were tested separatelly and together) and a heuristic control called Canal Automation for Rapid Demand Deliveries (CARDD). In all cases the control variables were the gate openings and feedforward control was implemented by means of a volume compensation method. The results showed that the best option was the control with both decouplers and that feedforward strategy was indispensable for all the cases. A control deterioration was also ob-

served when the canal parameters were not accurate and when the gate movement restrictions were included.

Afterwards, in Clemmens and Schuurmans (2004a) and in Clemmens and Schuurmans (2004b), a methodology was developed and tested in which, using a modified PI structure in order to compensate the delay of each reach, they structured a state feedback matrix with some non-zero elements. Then, formulating a LQR objective function and solving the Ricatti equation, they found the parameters of this feedback. They identified that using the trick of making zero some elements of the feedback matrix, was equivalent to use different decoupling logics and that the use of the whole matrix was equal to implement a completely centralized controller. They also made a performance study for all possible controllers, going from the complete centralization to the total decentralization. The conclusion was that, the centralized controller and the PI that sends information to all upstream reaches and to the closest downstream one, were the best options in the performance point of view. Another thing worth to mention is that they observed a possible control system destabilization when there exist a minimum gate movement restriction.

Other similar PI scheme working together with a centralized controller was used in Montazar et al. (2005). van Overloop et al. (2005) also performed a decentralized PI tuning solving an optimization problem, but using, instead of one model for each flow condition, a set of models. The idea behind was the obtention of a more stable controller.

Litrico et al. (2005) used each reach's frequency response to tune PI controllers. Making use of the gain margin obtained for different discharge conditions, a series of robust controllers were calculated. In this manner, they achieved robustness against operation condition changes. The test performed in a laboratory canal showed also a great correspondence between the observed and the expected performances.

A more detailed robustness analysis was performed in Litrico and Fromion (2006) and in Litrico et al. (2006). They proposed a new method to tune robust distant downstream proportional integral (PI) controllers for an irrigation canal pool. This tuning rules are appropriate to obtain specific robust margins and error characteristics. Implementation issues are also addressed.

Finally, in Litrico et al. (2007) a classical closed loop PI tuning method, called ATV method, was adapted for irrigation canal decentralized level controllers. The method needs to induce sustained level oscillations to characterize the stability margins of the controlled system. In this paper, these parameters were linked with many tunings rules in order to obtain a good water level regulation performance in irrigation canals.

2.3.2 Robust control

In addition to the robust PI controllers previously mentioned, other robust control techniques have also been employed.

Litrico and Georges (1999b) suggested two irrigation canal controllers design methodologies: the a priori computation of a robust Smith Predictor and the trial and error tuning of a robust Pole Placement controller. Both of them used a nominal linear model and multiplicative uncertainty. These schemes were compared with the performance given by a PID tuned with the Haalman method, suitable for time delay dominant systems. The research concluded that a PID without a filter was faster, but also oscillating. In this context, the robust controllers fulfilled the established performance and robust requirements without major problems.

Litrico (2001b) developed another methodology for robust controllers based on internal models, in this case, for the Gimone river in France. This river, in particular, has two water irrigation offtakes. They used the Hayami model and a multiplicative model uncertainty representation. The formulation was the following: they parameterized the filter value in order to obtain it, subsequently, assuring the closed loop robust stability.

2.3.3 Optimal control

In spite of the use of this technique for tuning another types of controllers, there are few recent studies about it.

In Malaterre (1998) they used a MIMO Linear Quadratic (LQ)-optimal control for irrigation canals. This control was developed together with a previously mentioned state observer. It could handle unexpected and beforehand scheduled demands. Additionally, the MIMO structure of the controller exhibited big advantages to counteract canal coupling and transport delay effects. Among the disadvantages of the method, they mentioned the large dimension of vectors and matrices, that the model validity is assured only for subcritical flows and the difficulty of LQ-optimal control to include gates restrictions.

In Reddy and Jacquot (1999) a proportional-plus-integral controller was developed for an irrigation canal with five pools using the linear optimal control theory. Different strategies were tested and it was found that the performance of regional constant-volume control algorithms was as good as the performance of a global control algorithm, whereas the performance of regional constant-level control algorithms was marginally acceptable.

More recently Durdu (2005) used a Linear Quadratic Gaussian (LQG) control strategy for irrigation canals in order to test different state observers.

2.3.4   Predictive control

Similarly as occurs with Optimal control, there are few recent works that address the canal control with Predictive control techniques, and the ones that do, use in general classical techniques in this area.

Malaterre and Rodellar (1997) performed a multivariable predictive control of a two reaches canal using a state space model. They observed that the increase of the prediction horizon produced a change in the controller behavior, varying the control perspective from a local to a global problem.

Following the research line of Rodellar et al. (1989) and Rodellar et al. (1993), Gómez et al. (2002) presented a decentralized predictive irrigation canal control. They used the Muskingum model plus a storage model in order to perform the water dynamic predictions in each reach. In order to decouple the system, the controller used an estimation of the future discharges and the hypothesis of being linearly approaching the reference, to finally reach it, at the end of the prediction horizon. Because the control law solution was given in terms of reach's inflow discharge, they used a local controller to adjust the gate opening to the required discharge.

Akouz et al. (1998) used decentralized predictive controllers to manage three reaches of the ASCE Test Canal 2, acting on each reach's inflow discharge. They didn't include in the control, feedforward compensation for known scheduled demands or reach's outflow discharges. The same technique was used in Ruiz and Ramírez (1998), including the reach's outflow discharge as a known disturbance. In Sawadogo et al. (1998), and later in Sawadogo et al. (2000), they presented a similar decentralized adaptive predictive control, but that used the reach's head gate opening as controllable variable and the reach's tail gate opening and the irrigation offtake discharge as known disturbances.

A decentralized adaptive predictive controller was also presented in Rivas et al. (2002). Here the manipulated variable was the inflow discharge and they did not include the known disturbances. In order to achieve some kind of robustness they used dead bands and normalization in the adaptation of the model.

Sometimes it is convenient to take into account actuator and process constraints when controlling a particular system. In this respect, a constrained predictive control scheme was developed in Rodellar et al. (2003) to manage irrigation canals. It was based on a linear model that used gate openings and water levels as input and output variables respectively, and one of the novelties of the method was that it takes into account explicitly in the control problem that gates should not come out of water. Constraints on the movement velocity of the gates were also considered and the results exhibited an improvement in the control performance in comparison with the predictive unconstrained case.

More recently, Wahlin (2004) tested a MIMO Constrained Predictive controller using a state

space model based on Schuurmans ID model. They performed tests where the controller either knew or did not know the canal parameters and with and without the minimum gate movement restriction. While many gate operation restrictions could be included in the control law, the minimum gate movement restriction could only be applied as a dead band in the control action once calculated. The reason for this is that this type of constrains are very difficult to implement in a controller. The results showed that it was possible to control the canal in question, but with a performance not superior than a centralized PI. Nevertheless, they conjectured that the problem was attributable to the modeling errors of the ID Model. In that case, a better model would be required in order to implement the predictive control. Additionally, they observed that the minimum gate movement restriction worsened, in a high degree, the control performance.

There are also some real implementations of predictive control in laboratory canals. In Begovich et al. (2004), a multivariable predictive controller with constraints was implemented in real-time to regulate the downstream levels of a four-pool irrigation canal prototype. In Silva et al. (2007), a predictive controller, based on a linearization of the Saint Venant equations, has been also implemented on an experimental water canal.

2.3.5   Nonlinear Control

Because of the complexity of the original nonlinear model, there are not many research works that had faced the nonlinear control for these types of systems.

In Sanders and Katopodes (1999), they used a nonlinear optimization method for controlling one canal reach adjusting its gate openings. The computation times were near the three minutes with Pentium processors.

Dulhoste et al. (2004) made a controller based on the dynamic state feedback linearization. The control was tested for set-point changes, infiltration and water extraction cases. There were good results on computational simulation for different length rectangular canals.

In de Halleux et al. (2003), they described and analyzed a general stability condition for water velocities and levels in open channels. With the aid of it, they proposed and applied a controller to a two-reaches no-friction horizontal computer-simulated canal.

In Soler et al. (2004), the nonlinear numerical scheme has been combined with a typical predictive control performance criterion to compute gate trajectories in an open-loop operation.

2.4   Conclusion

In brief, this chapter reviews the conceptual/theoretical dimension and the methodological dimension of the literature in irrigation canal control and discovers research questions or hypotheses that are worth researching in later chapters.

Chapter 3

The Canal PAC-UPC

This chapter describes some technical aspects of a laboratory canal that has been specially designed to test irrigation canal control algorithms. This canal has been built and instrumented in parallel with the development of this PhD thesis and is going to be used as an experimental platform in all subsequent chapters.

3.1 History

The construction of this canal was mainly possible thanks to the financing granted by the Spanish Ministry of Science and Education (MEC) through research project REN2002-00032.

The canal itself was designed and constructed by the laboratory personnel of the Hydraulic and Hydrological Engineering Section of the Department of Hydraulic, Maritime and Environmental Engineering of the UPC. The construction started in 2003. Part of the evolution of the canal can be seen in figure 3.1.

Most of the design, acquisition and final implementation of the instrumentation and of the motorization of the canal felt under the responsibility of this thesis work.

After several years of hard work, the Canal PAC-UPC is nowadays completely operative (see figure 3.2) in order to study control issues in irrigation canals.

3.2 General description

Canal PAC-UPC is the acronym of "Canal de Prueba de Algoritmos de Control - Universitat Politècnica de Catalunya". The english translation of this name would be: "Technical University of Catalonia - Control Algorithms Test Canal".

As the name already suggests, it is a laboratory canal specially designed to develop basic and applied research in the irrigation canals control area and in all subjacent areas like irrigation canal instrumentation, irrigation canal modeling, water measurements, etc..

(a) January 8th, 2004

(b) February 25th, 2005

Figure 3.1: Construction of the Canal PAC-UPC

Figure 3.2: Lateral view of the Canal PAC-UPC in operation

It is located in the Laboratory of Physical Models inside the North Campus of the UPC. This laboratory occupies a $2000\,\mathrm{m}^2$ surface area and has an underground water reservoir of approximately $250\,\mathrm{m}^3$.

The original idea was to make a rectangular canal that could exhibit notorious transport delays in order to resemble real irrigation canal control problems. For this reason, it was decided to construct a sufficiently-long zero-slope rectangular canal. Because of the lack of space inside the laboratory, the canal was designed with a serpentine shape so as to attain the maximum canal length in the most condensed space. With this particular design, the result was a $220\,\mathrm{m}$ long, $44\,\mathrm{cm}$ width and $1\,\mathrm{m}$ depth canal on a $22.5\,\mathrm{m} \times 5.4\,\mathrm{m}$ surface area. A detailed scheme of this laboratory canal is presented in figure 3.3.
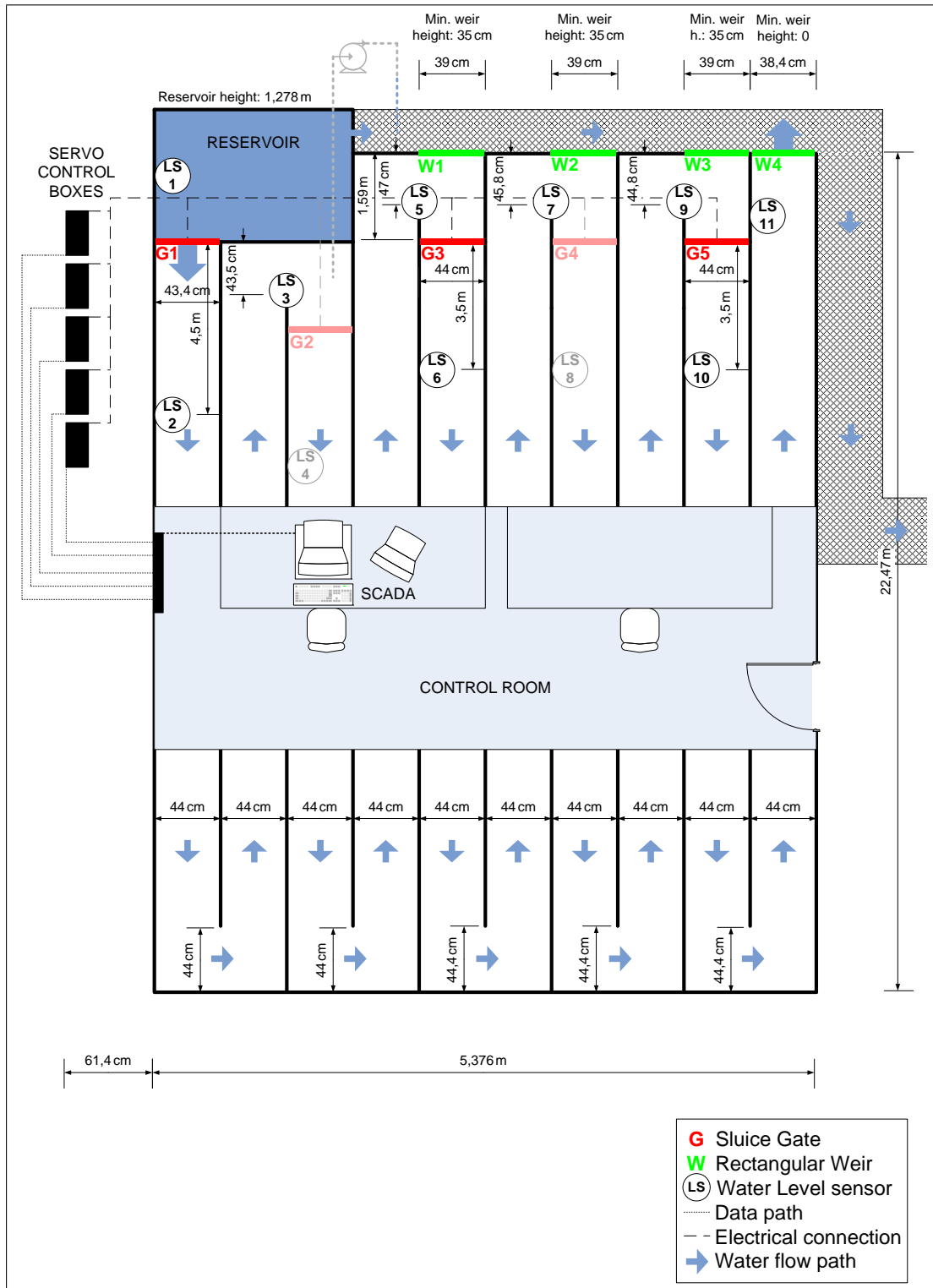
Figure 3.3: Schematic diagram of the top view of the Canal PAC-UPC

As illustrated by figure 3.3, the canal has currently:

- 1 head reservoir

- 3 vertical sluice gates

- 4 rectangular weirs

- 9 water level sensors

- 1 control room

Some items stand transparent in figure 3.3, because the canal has the capacity to include 2 additional gates and 2 more level sensors, which are planned to be placed in the future.

In the present condition, it is possible to arrange the canal with several pool configurations, i.e. a canal with only one very long pool, a canal with one long pool and one short pool, etc.. In this thesis work, the canal is going to be configured in order to obtain a 3-pool canal with 2 intermediate offtakes and a weir end as schematized in figure 3.4
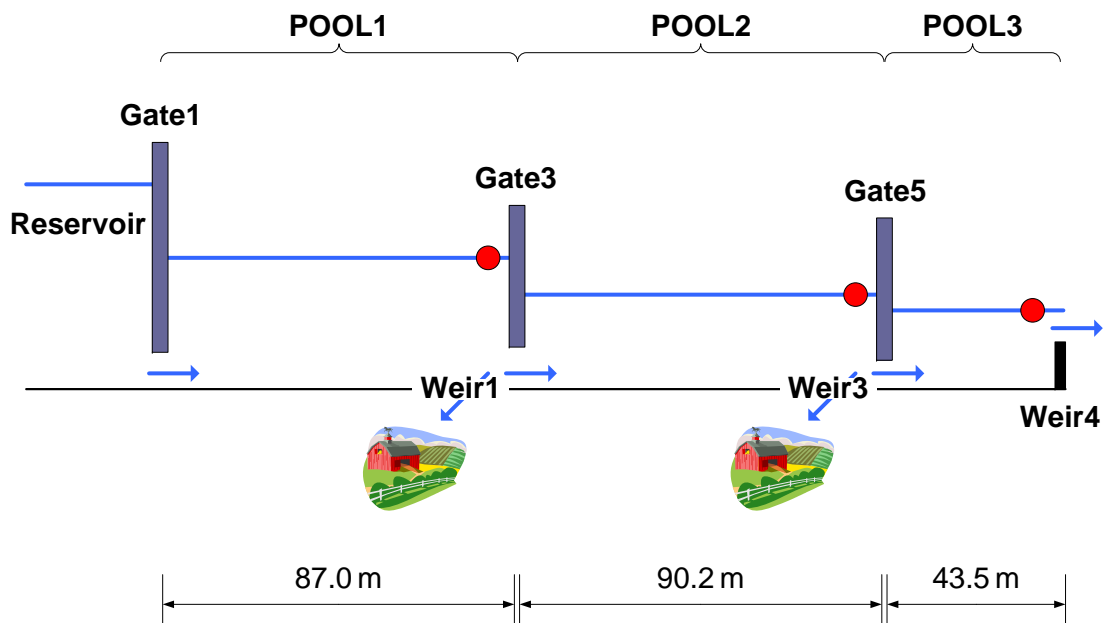
Figure 3.4: Canal PAC-UPC pool configuration in this thesis

With a canal configuration like this, it is possible to obtain delays of tens of seconds (approx. $30\,\mathrm{s}$, $35\,\mathrm{s}$ and $20\,\mathrm{s}$ for pools 1, 2 and 3 respectively), to have couplings effects among pools and to produce offtake discharge changes. All these characteristics provide a good platform to emulate irrigation canal control problems.

3.3 Water supply

The $250\,\mathrm{m}^3$ underground laboratory reservoir supplies the water to the canal. The water follows a path that is depicted in the aerial photo of figure 3.5.

Figure 3.5: Water path from the pumps to the canal head

The water can be delivered to the canal using any of the three available pumps (P). These pumps have pumping capacities of $100\,\mathrm{L/s}$, $200\,\mathrm{L/s}$ and $300\,\mathrm{L/s}$ respectively.

The water is raised to a constant level reservoir (CLR) that is connected to two parallel canals with triangular weirs (TW) at the downstream ends through two electric valves. With these valves, it is possible to regulate the discharge that is delivered, whose value can be known very accurately by measuring the head water. Two manual limnimeters are located over the weirs to perform these level measurements.

At this point, the water not entering the canals is returned to the underground reservoir and the measured discharge is conveyed through two pipes up to the canal head (shown in figure 3.6).

The canal has also a small constant level reservoir at its head. The objective of this element is twofold: to dissipate the flow energy and to provide the canal with enough and virtually unlimited water.

The canal takes water from this reservoir through Gate1, which is normally under submerged conditions. This gate can regulate the canal inflow by adjusting the gate opening. The water that is not used is also returned to the underground reservoir.

Under normal operation conditions, the discharge delivered to the canal reservoir should be between $100\,\mathrm{L/s}$ and $150\,\mathrm{L/s}$. Naturally, this value determines the maximum discharge that can be supplied to the canal, while the minimum discharge is a value close to zero given by the

(a) Head reservoir

(b) Gate1

Figure 3.6: Canal head

minimum available gate opening.

3.4 Gates

(a) Gates

(b) Control boxes

Figure 3.7: Sluice gates in the Canal PAC-UPC

The gates of the canal are vertical sluice gates (see figure 3.7) and were designed and con-
structed by the laboratory personnel. They are made of methacrylate reinforced with a metal
skeleton in order to provide enough rigidity and a low weight. The vertical movement of the
gates is guided by metal frameworks embedded in the canal and is executed by three-phase ser-
vomotors. These servomotors are located on top of the gates and are commanded by control
boxes situated next to the canal. This particular gate motorization enables only constant speed
movements of about $1 \, \text{cm/s}$.

The control boxes allow either the local or the distant operation of the gates. In local operation mode, it is possible to open, close or stop a gate, while in the distant operation mode it is possible to give an external reference signal in order to approximately position the gate at a desired opening. From these control boxes, it is also possible to have a real-time measurement of all the current gate openings.

3.5   Weirs

The rectangular weirs of the canal are used to extract a water discharge and to measure its value in different sections of the canal, so as to emulate the effect of offtake discharges in real irrigation canals. Figure 3.8 shows some of the canal weirs in photos.

(a) Opened weir   (b) Closed weir

Figure 3.8: Rectangular weirs in the Canal PAC-UPC

These weirs have a width of approximately $39\,\mathrm{cm}$ and were constructed starting from a $35\,\mathrm{cm}$ canal height, except for the canal end weir (Weir4) that starts from the canal base. From this minimum height, it is possible to raise the height of any weir by placing measured-height PVC pieces in specially designed metal rails. Each weir has its own set of pieces. There are pieces of $5\,\mathrm{cm}$, $10\,\mathrm{cm}$, $20\,\mathrm{cm}$ and $35\,\mathrm{cm}$. With different combinations of these pieces, it is possible to cover a broad range of weir heights.

Weir 4 plays also an important role in the overall canal operation. By raising and lowering this weir height, it is possible to change the minimum water level value throughout the whole

canal. Here, the head value acts as a reference value for the other pools, a phenomena that allows to work with different combinations of discharges and water level values, leading to different hydraulic conditions.

3.6   Sensors

3.6.1   Water level sensors

The canal has currently nine level sensors located in strategic places. Specifically, these sensors are situated upstream and downstream of each gate and at every rectangular weir (see figure 3.3 for details). Their mission is twofold: to take level measurements where water is taken from the canal and to enable the calculation of gate and weir discharges by means of appropriate hydraulic relationships.

These sensors are submergible pressure sensors and were acquired from the specialized manufacturer SOFREL. Their specific model is CNPI and they can measure water depths up to $2\,\mathrm{m}$. One of these sensors is shown in figure 3.9.

Figure 3.9: Type of water level sensor used in the Canal PAC-UPC

These sensors are mainly oriented for level measurements in real canals. Consequently, this work had to deal with practical problems similar to the ones encountered in the field.

The installation of the sensors inside the canal was carried out in a the following way: the bodies of the sensors were firmly attached to the internal side of the lateral walls at $3\,\mathrm{cm}$ from the floor and their cables were routed to the control room separately from any power cable to avoid electrical noise.

Following appropriate wiring and signal filtering procedures, they are able to provide precise level measurements. The way they are connected is sketched in figure 3.10.
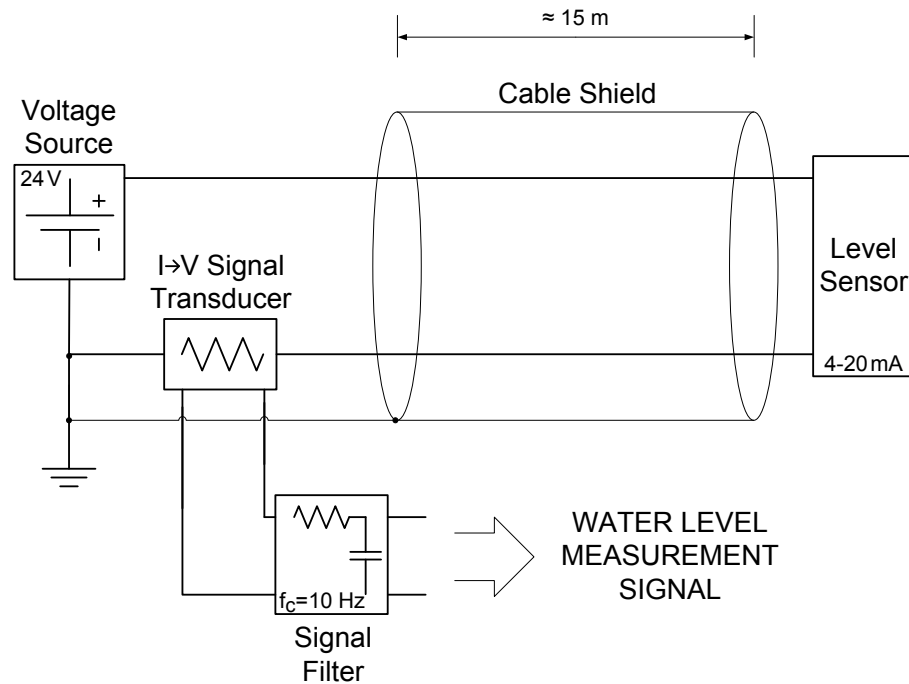
Figure 3.10: Connection diagram of a level sensor

Once installed in the canal, these sensors where calibrated against manual limnimeter measurements. The calibration procedure was as follows: the weirs were closed and the canal was filled with a certain amount of water; one hour after, level measurements were carried out in calm water and the process was repeated. As a result, several data points were collected and an experimental calibration curve was computed for each sensor using linear regression analysis. The calibration curve of one of the level sensors is presented in figure 3.11 as an example.
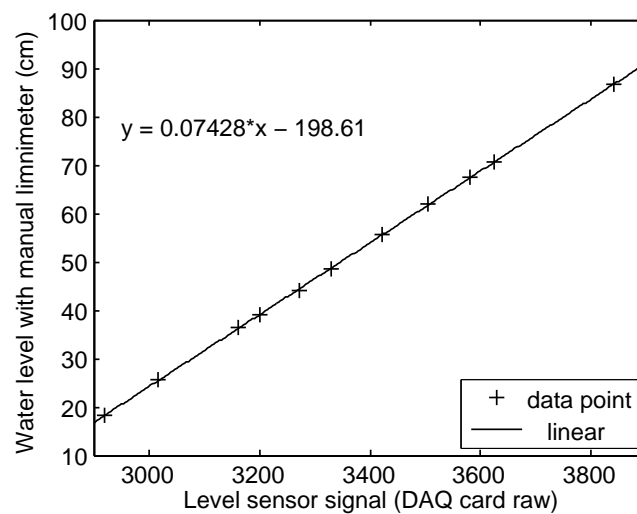
Figure 3.11: Calibration curve of level sensor 11

These level sensors are based on pressure measurements. These type of measurements are

robust against turbulent water, but can be biased by effects related to the water temperature. Hence, it is recommendable to perform periodic sensor recalibrations, specially between the seasons of the year.

3.6.2   Gate position sensors

Each servomotor has a position measuring gear embedded in the motor chassis. This gear rotates when the gate is opened or closed and by means of this event the gate opening is sent to the control box. What actually happens is that the gear is mechanically connected to a potentiometer, thereby giving different resistance values for different gate openings. This signal is successively transformed up to the control room computer. The flow path of this gate position measurement signal is summarized in figure 3.12.
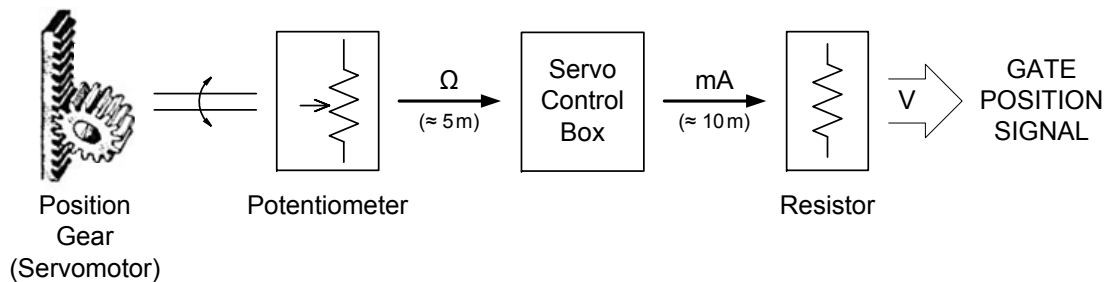
Figure 3.12: Flow path of the gate position signal

If the calibration step is performed with data arising from opening and closing a gate, it is possible to see that the data points group along two different calibration curves. This peculiarity is highlighted in figure 3.13 for the calibration data of Gate 1.
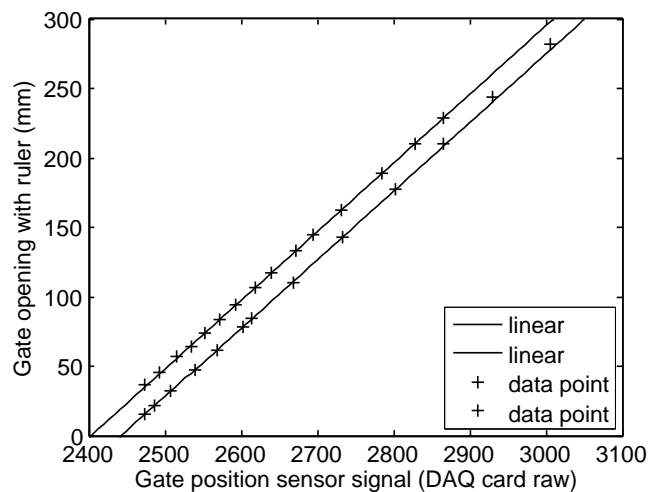
Figure 3.13: Gate 1 position calibration data

One of these data subsets correspond to move the gate upwards and the other to move it

downwards. This is due to the inaccuracy of the position measurement method: any mechanical system based on gears present gaps between the teeth. As a result, when the rotation direction is inverted in this case, there is an interval of time during which the potentiometer do not move, generating two different electrical readings for the same position depending on the gate moving direction.

This is a problem for calibration. One possible solution is to pass through a unique calibration line equidistantly from both data subsets. This would produce a permanent measurement error. In this case, this error would be approximately $\pm 1\,\mathrm{cm}$. In order to improve the measurement accuracy another option was taken: a correction algorithm was implemented in the SCADA software by using two calibration curves and a gate moving direction detection method. This approach does not entirely solve the problem, but most of the time works fine for the required precision. Nevertheless, gate opening measurements were performed always manually when calibrating gate discharge equations.

3.6.3 Flowmeter

For comparison and calibration purposes, the canal is equipped with a movable flow velocity sensor. This flowmeter has been manufactured by NIVUS and consist of an OCM EM control box and a doppler-based wedge-mouse one-dimensional flow velocity sensor.

This device can measure velocities up to $6\,\mathrm{m/s}$ and working in combination with a level sensor is able to measure discharge. This device needs a strictly parallel flow in order to give good measurement. Consequently, it should be placed at a considerable distance from any hydraulic structure.

In the Canal PAC-UPC, this device has been placed downstream of Gate 1 in order to have an independent measurement of the canal inflow. The preferred way to measure gate discharges throughout this thesis will be to calibrate and use gate discharge hydraulic equations, a method that has been proven to be highly accurate and robust in our laboratory tests. Essentially, the flowmeter measurement provides a way to continuously validate these discharge calculations, but it is not used in the control system of the canal.

3.7 Control room

The Canal PAC-UPC has a control room over the canal. All sensors are wired to it and from there it is also possible to operate the servomotor control boxes.

The brain of the control room is a $3.06\,\mathrm{GHz}$ Pentium®4 processor, $1\,\mathrm{GiB}$ memory desktop computer equipped with three Advantech® Data AcQuisition (DAQ) cards. Illustrative photos are presented in figure 3.14.

(a) Control room

(b) Control computer

Figure 3.14: Canal PAC-UPC control installations

3.7.1 Advantech DAQ cards

The models of the data acquisition cards inside the computer are PCI-1711, PCI-1720 and PCI-1750. All three cards are situated in PCI-slots and perform different tasks in the canal operation.

The PCI-1711 is a multifunction DAQ card that has 16 analog inputs and 2 analog outputs. In this case, these inputs are used to receive the 9 level sensor measurements, the 3 gate position signals and 1 flow velocity signal. On the other hand, the analog outputs are used to give position reference values to Gate1 and Gate3.

The PCI-1720 completes the set of required analog outputs. This card dispose of 4 analog outputs, but connection incompatibilities between the control boxes and this card allow the use of only one of these outputs. Thus, this card takes over the operation of Gate5.

The PCI-1750 has not been used in this work, but can manage external alarm signals and receive orders from independent control button panels.

All these cards can achieve very fast sampling rates, but water measurements in irrigation canals do not need a so continuous update. Hence, they are operated at a much slower rate. In particular, level measurements and gate openings are acquired at $10\,\mathrm{Hz}$ and gate opening set-points are delivered every $10\,\mathrm{s}$.

The resolution of the measurements deserve special attention. This resolution depends on the sensor resolution and on the DAQ card resolution. The PCI-1711 has a $12\,\mathrm{bit}$ resolution. That means that the card is able to distinguish 4096 different values when using the complete input range. However, this is seldom the case. In this case, the sensor signal ranges are considerably smaller, yielding water level measurements and gate openings with a resolution slightly smaller than $1\,\mathrm{mm}$.

3.8 Software

The data acquisition cards provide the hardware to receive and send electrical signals from the computer. However, a specialized computer program is completely indispensable to manage this huge amount of information and to provide a basis where to perform discharge computations and to implement control algorithms.

3.8.1 Base software

In this case, it was decided to use the software package MATLAB$^{\circledR}$. In particular, real-time programs can be easily implemented by using three of its components: Simulink$^{\circledR}$, Real-Time Workshop$^{\circledR}$ and Real-Time Windows Target. Each one of them plays a particular role.

Simulink is a platform for multidomain simulation and model-based design for dynamic systems. It provides an interactive graphical environment and a customizable set of block libraries.

For instance, using its block library or user-written blocks, it is possible to develop a complete Supervisory Control And Data Acquisition (SCADA) program for the Canal PAC-UPC.

On the other hand, Real-Time Workshop generates C code from Simulink programs in order to be used by real-time and non-real-time applications.

Finally, Real-Time Windows Target enables to run Simulink in real-time on a personal computer. With this Simulink add-on product, it is possible to create and control a real-time execution entirely through Simulink.

The procedure to deploy a program is the following. First, the program is opened in Simulink. Then, using Real-Time Workshop, a C code version of this program is generated and compiled. Finally, the program is started in a real-time execution on Microsoft Windows.

3.8.2   Canal PAC-UPC SCADA program

A SCADA software is a type of application to perform data collection and control at the supervisory level. In a program like this, it is possible to perform many tasks online such as: to read and plot sensor measurements, to use this information to calculate related variables, to run and tune control algorithms, to store results, etc.. These tasks and many others were implemented in a Simulink program specifically designed in this thesis for the Canal PAC-UPC.

As illustrated by the main window of this program shown in figure 3.15, it is essentially a large block diagram, made up of logic blocks, routing blocks, equation blocks, visualization blocks, etc., which is fed with real measurements and user-specified values.
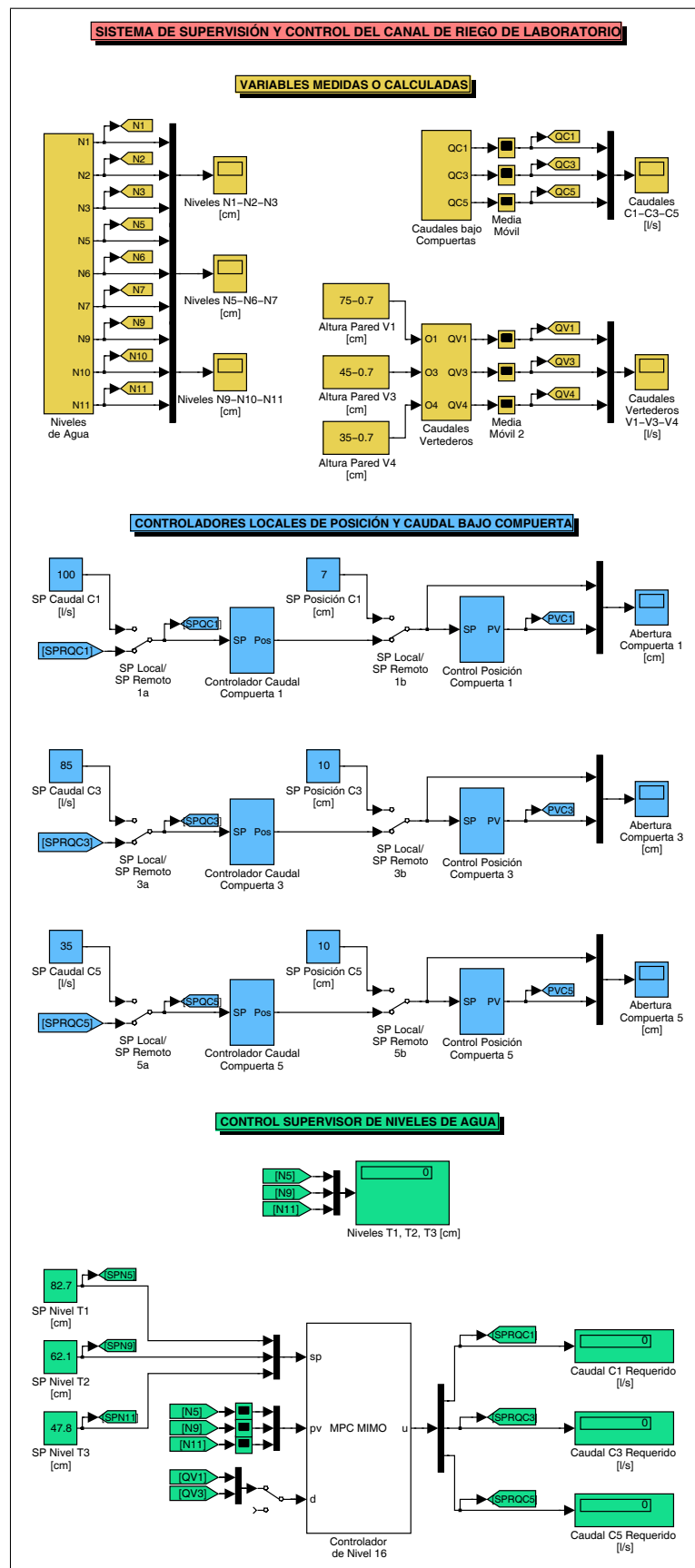
Figure 3.15: Main window of the Canal PAC-UPC SCADA program
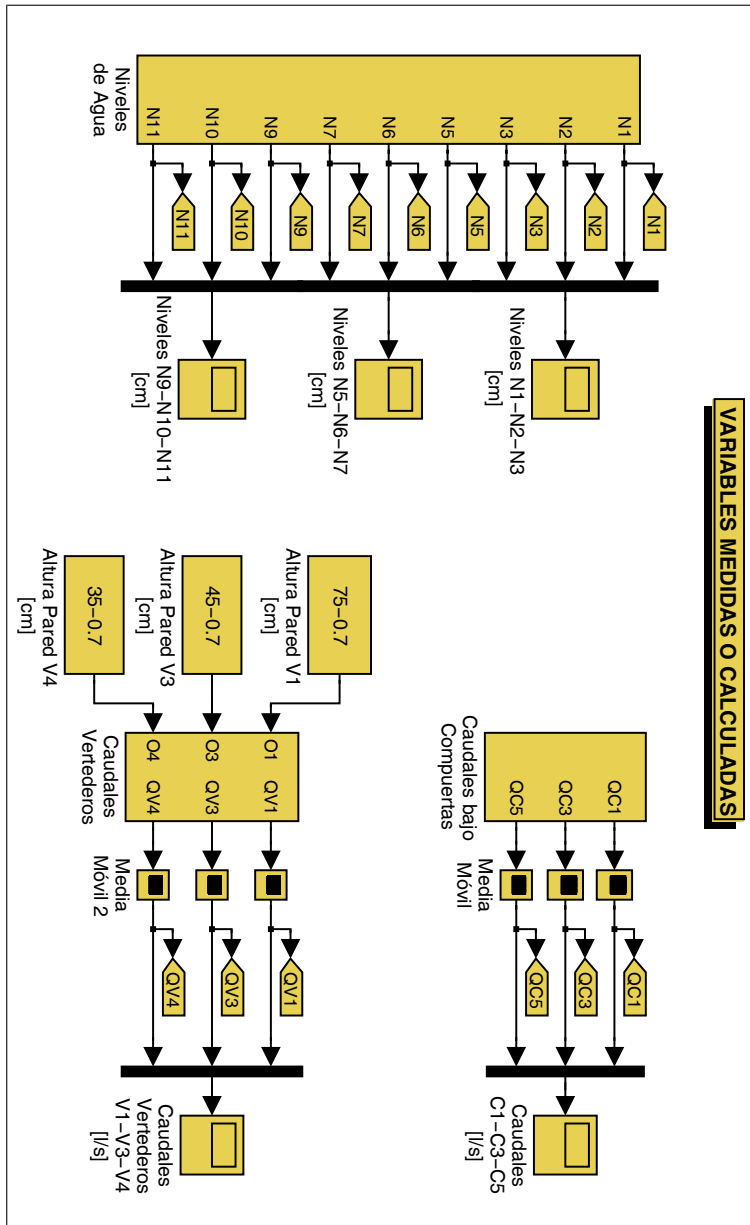
Figure 3.16: Canal PAC-UPC SCADA program: Data acquisition and signal processing module
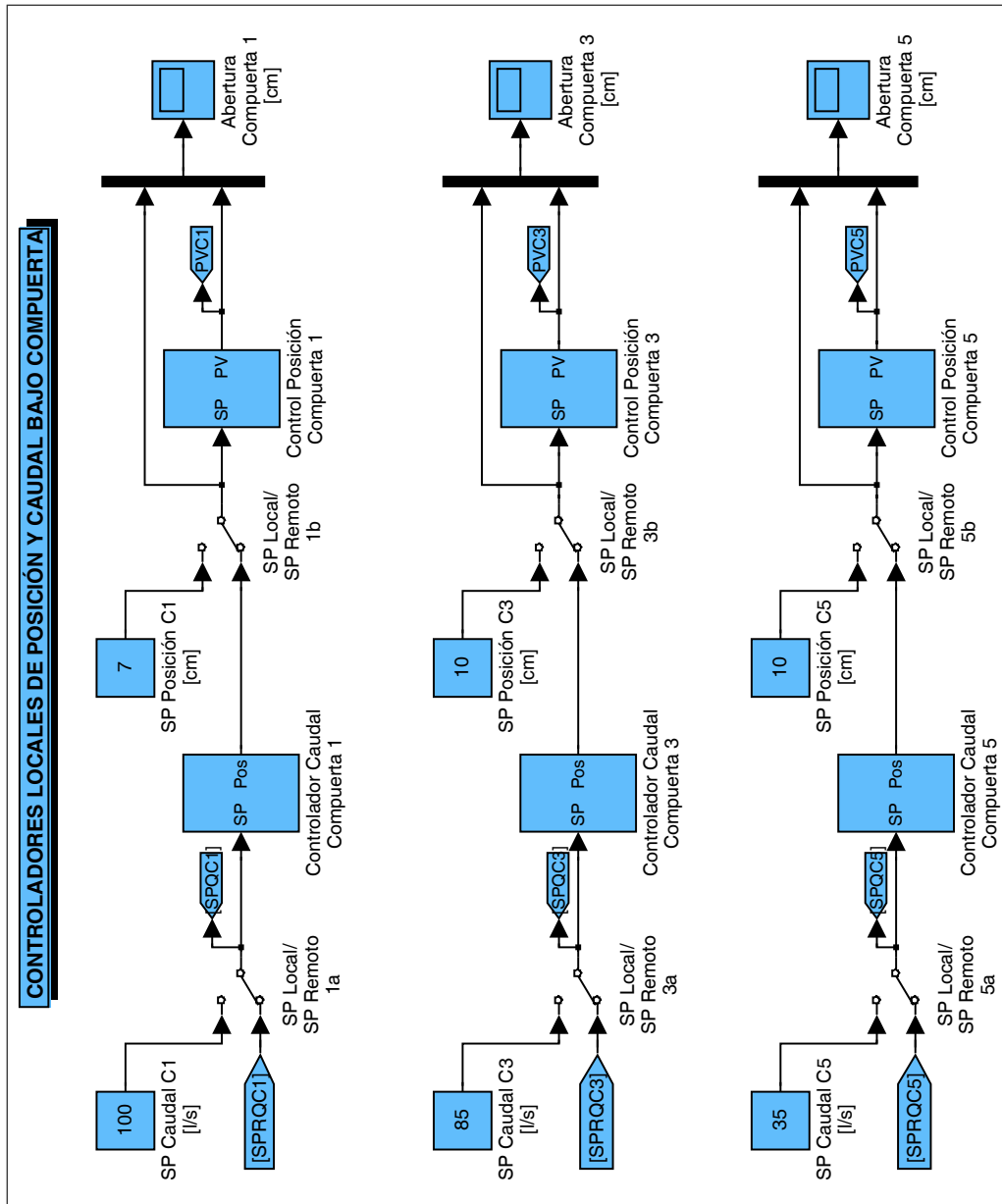
Figure 3.17: Canal PAC-UPC SCADA program: Gate position and gate discharge control module
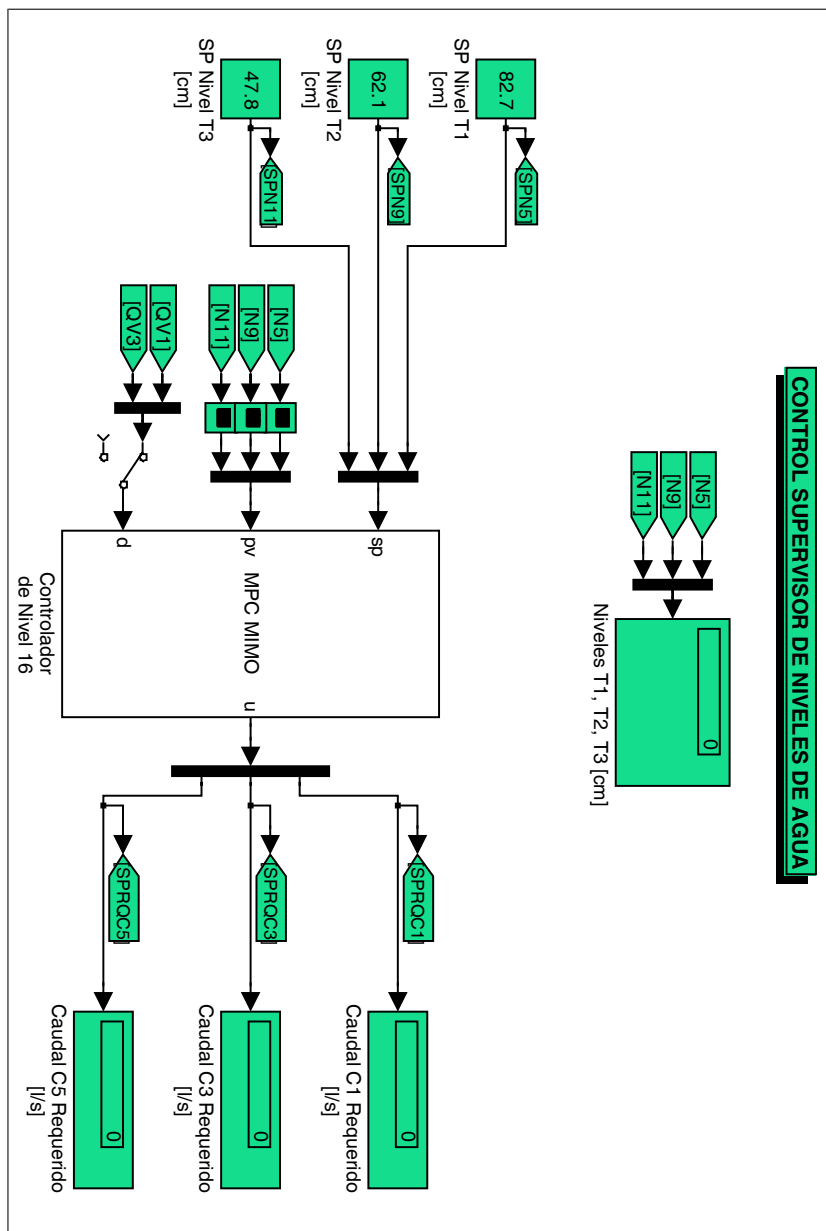
Figure 3.18: Canal PAC-UPC SCADA program: Supervisory water level control module

Specifically, the SCADA program performs the following tasks:

- Measurements

    - Filters water level signals.

    - Stores and reads calibration curves in order to transform sensor signals into real measurements.

    - Calculates gate discharges and weir discharges.

    - Calculates moving averages of some signals when required.

    - Diminishes gate position sensor errors due to precision gear rotation changes.

    - Stores all measurements in data files.

    - Displays the evolution of system variables during a given time-window in different zoomable graphs.

- Gate position control

    - Enables the introduction of user-defined gate opening set-points or to receive external reference values from gate discharge controllers.

    - Fools the control boxes in order to allow manual operation of gates from the control room.

    - Overrides the original position control devices and takes over this task, in order to reduce the gate positioning error.

    - Enables gate repositioning with larger trajectories to diminish positioning errors due to mechanical minimum gate movement restrictions.

- Gate discharge control

    - Enables the introduction of user-defined gate discharge set-points or to receive external reference values from water level controllers.

    - Calculates gate openings necessary to reach gate discharge references by inverting gate discharge formulas with predictions of level changes.

    - Calculates the maximum discharge that a gate can deliver at a present time instant.

- Water level control

    - Accepts water level set-points online.

    - Enables the implementation of many types of water level control schemes to calculate adequate gate discharges.

    - Provides a library of level control implementations to test different irrigation canal control solutions.

3.9   Conclusion

This chapter has described in detail the Canal PAC-UPC. Its purpose, operation and several of their elements has been presented along with technical details and operational constrains.

An important practical knowledge related to the instrumentation of canals has been acquired, touching on topics like treatment of measurement errors, signal processing techniques, calibration of sensors, etc.. All this know-how is indispensable when working with real canals.

This chapter has also presented one of the product of this thesis: an own, non-commercial, SCADA software for the Canal PAC-UPC. Many of the elements, solutions and procedures used in its development are applicable to similar systems in real canals.

Based on the overall chapter content, it is possible to confirm that this laboratory canal provides a good platform where to test irrigation canal automation issues.

Chapter 4

Calibration of Weirs and Sluice Gates

This chapter deals with some issues related to discharge measurements in canals; particulary in our laboratory canal: the Canal PAC-UPC. It describes mathematical and empirical formulations to calculate discharge, the calibration of our weirs and sluice gates, and some results obtained from our observations.

4.1 Introduction

Open channel flow is defined as the flow in any channel where the water flows with a free surface. Open channel flow is not under pressure; gravity is the main force that can produce flow in open channels, and a progressive declive in water surface elevation always occurs as the flow moves downstream. Examples of open channel flow include: rivers, streams, creeks, discharges from tailings ponds, and other uncovered conduits. Closed channels, such as adits, tunnels, sewers, and ventilation shafts, can be treated as open channels when flowing partially full and not under pressure.

Measuring discharge in open channels can be a difficult task. There are two types of approaches:

1. Measure directly all the involved variables (flow area and mean velocity).

2. Define a so called control section, where there is a single relationship between Q/h, so by measuring water depths we can derive the Q value. Example of control sections are weirs, parshall flumes, flumes and gates.

This chapter focus on discharge characteristics of two types of hydraulic structures that belong to the second group: weirs and gates.

4.2 Weirs

Weirs are typically installed in open channels to determine discharge (flow rate). Since the geometry of the weir is known and all water flows through it, the depth of water flowing over the weir (head) is an indication of the discharge value. Two different geometries are considered below.

4.2.1 Sharp-edged v-notch (triangular) weirs

The discharge is directly related to the water depth above the crotch (bottom) of the V; this distance is called head (h). The V-notch design assumes that small changes in discharge to have a large change in depth allowing more accurate head measurement than with a rectangular weir.
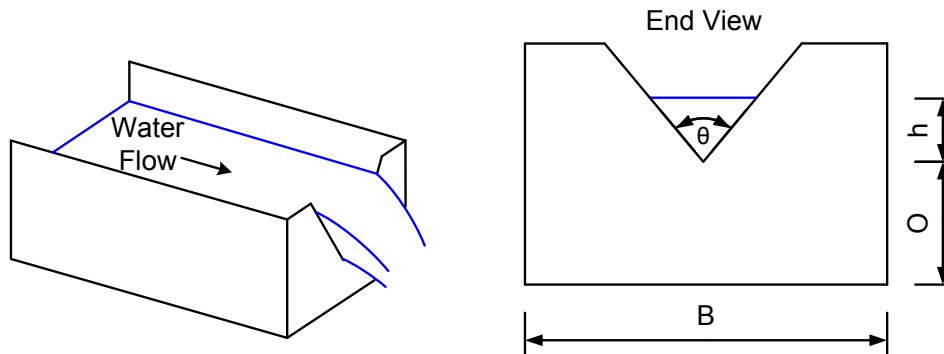
Figure 4.1: V-notch weir scheme

The 90° V-notch weir is most accurate when measuring discharges of less than $0.03 \, \mathrm{m^3/s}$. The maximum discharge that can be accurately measured is approximately $0.3 \, \mathrm{m^3/s}$. The sides of the notch are inclined outwardly at $45°$ from the vertical.

The V-notch weir equations have become somewhat standardized. The water measurement manuals of the International Organization for Standardization (ISO), the American Society for Testing and Materials (ASTM) and the U.S. Department of the Interior, Bureau of Reclamation (USBR) all suggest using the Kindsvater-Shen equation, which is presented below:

$$Q = \frac{8}{15}\sqrt{2g}\, C_{vw} \tan\left(\frac{\theta}{2}\right)(h + corr_h)^{5/2} \tag{4.1}$$

where C_{vw} is the v-notch weir discharge coefficient, h is the head (m) and $corr_h$ is the head correction factor (m). Particulary for the 90° V-notch:

$$C_{vw} = 0.578$$

$$corr_h = 8.847 \times 10^{-4} \, \mathrm{m}$$

In this way, we used only (4.1) to calculate the discharges given by our two v-notch weirs.

4.2.2 Sharp-edged rectangular weirs

The rectangular weir is the most commonly used thin plate weir. As its name suggests, it has a rectangular opening of a certain width (b). It is more suitable for larger flows, because the width can be chosen so that it can pass the expected flow at a suitable depth.
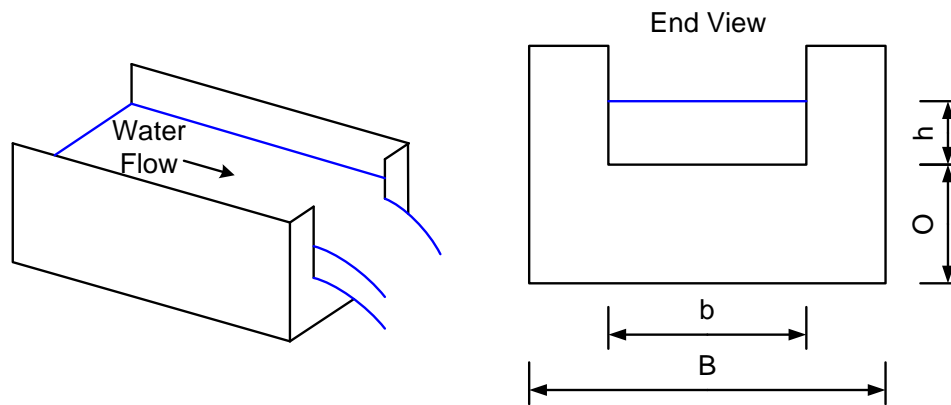
Figure 4.2: Rectangular weir scheme

Depending on its width the weir can be "suppressed", "partially contracted" or "fully contracted". Suppressed means there are no contractions. A suppressed weir's notch width (b) is equal to the channel width (B); thus, there really is not a notch; the weir is flat all the way along the top. For a weir to be fully contracted, ($B - b$) must be greater than $4h_{max}$, where h_{max} is the maximum expected head on the weir. A partially contracted weir has $B - b$ between 0 and $4h_{max}$. Weir contractions produce the water flow lines to converge through the notch.

To provide a single reliable, accurate method to model all rectangular weirs (suppressed, partially contracted, and fully contracted), the ISO, the ASTM and the USBR, all recommend using the Kindsvater-Carter method for all rectangular weirs. The equation is the following:

$$Q = \frac{2}{3}\sqrt{2g}\,C_{rw}(b + corr_b)(h + corr_h)^{3/2} \tag{4.2}$$

where C_{rw} is the rectangular weir discharge coefficient, h is the head (m), the sum $b + corr_b$ is called "effective width" (m) and the sum $h + corr_h$ is called "effective head" (m).

The value of $corr_h$ is normally taken as 0.001 m. The discharge coefficient C_{rw} is a function of b/B and h/O, and $corr_b$ is a function of b/B. In general these relationships are of linear nature and are given, in technical manuals, by graphs and equations. Particulary for our canal, we obtained these relationships empirically. We measured head values, using a limnimeter, and discharges with our v-notch weirs.

Putting all constant values together, and taking into account the fact that b/B is fixed for a particular weir, (4.2) yields:

$$Q = C_{gen}\left(\frac{h}{O}\right)(h + 0.001)^{3/2} \tag{4.3}$$

From (4.3) one can see that the discharge can be calculated by measuring h. However, the mathematical expression of function $C_{gen}\left(\frac{h}{O}\right)$ is not exactly known and has to be determined for each particular weir. This task can be performed by taking head-discharge data pairs using other measuring devices and reordering (4.3) as $\frac{Q}{(h+0.001)^{3/2}} = C_{gen}\left(\frac{h}{O}\right)$. Using this approach, $C_{gen}\left(\frac{h}{O}\right)$ can be obtained solving a linear regression problem. It should be noted that with this approach, the weir width b is included in the general coefficient C_{gen} and does not need to be measured.

We have three rectangular weirs in operation: Weir 1, Weir 3 and Weir 4. Although not needed in this case, their widths are $0.434\,\text{m}$, $0.44\,\text{m}$ and $0.44\,\text{m}$ respectively. All measurements were performed after waiting a two-hours stabilization period. The calibration data and the obtained relationships are detailed in table B.1, table B.2 and table B.3, and in figure 4.3, figure 4.4 and figure 4.5.
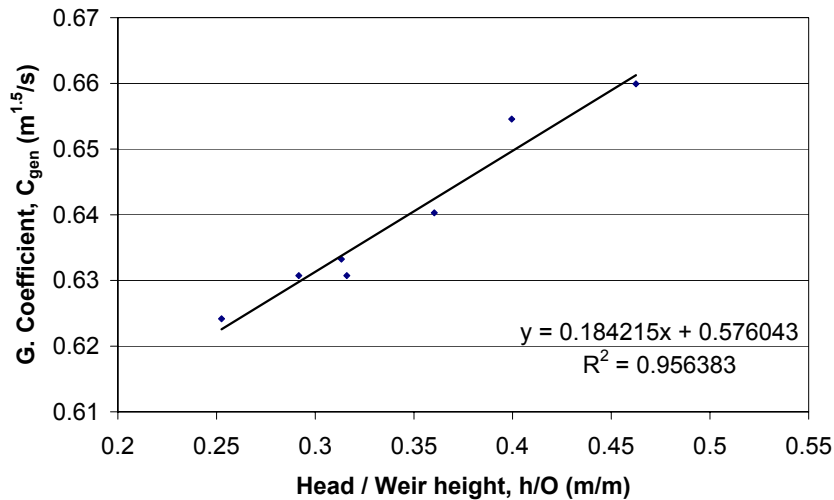
Figure 4.3: Weir 1 Calibration curve
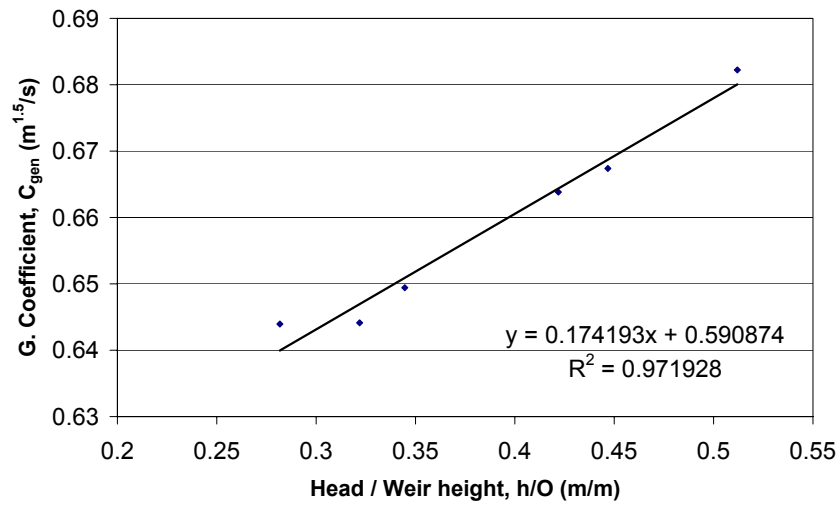
Figure 4.4: Weir 3 Calibration curve
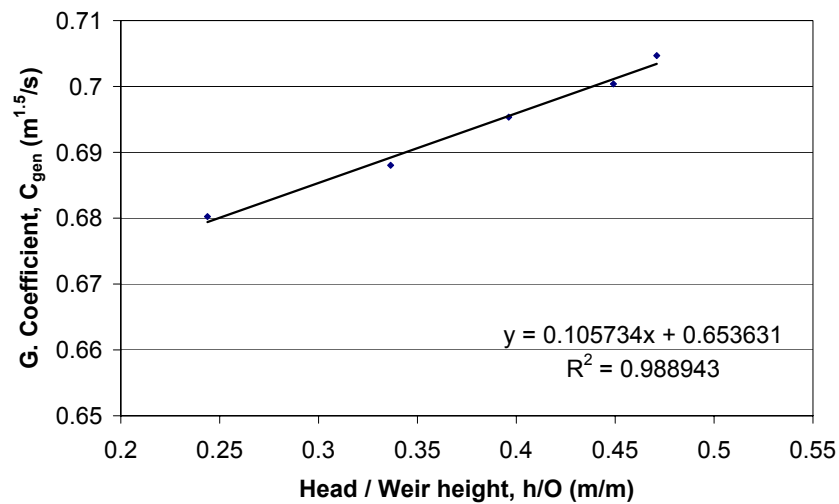
Figure 4.5: Weir 4 Calibration curve

Now, with the information given by these graphs and (4.3), the weir discharges Q can be accurately calculated measuring the head h.

As it can be observed in figures 4.3, 4.4 and 4.5, all linear relationships have a high correlation number. That means that the relationships suggested by technical manuals are valid for our rectangular weirs too. A more detailed comparison between the curves and equations given in manuals and our empirical equations, reveals that they differ slightly. However, it is worth to remember that the curves and equations given in technical manuals must follow some strict installation guidelines to ensure their applicability. In this case, it was not always possible to follow exactly these guidelines: the main reason for the discrepancies in our opinion.

4.3   Sluice gates

A gate is a hydraulic structure widely used for controlling discharge and water depth in irrigation and drainage canals. However, it can also be used as a convenient discharge measuring device.

Depending on the intended purpose and the particular mechanical design, there are different types of gates, many of them widely used in irrigation canal applications: vertical lift gates, radial (tainter) gates, roller gates, flap gates, overshoot gates and so forth.

A sluice gate is traditionally a wooden or metal plate, vertical (vertical lift gates) or curve (radial (tainter) gates), which slides in grooves in the sides of the channel. Sluice gates are commonly used to control water levels and flow rates in rivers and canals.

Raising a sluice gate allows water to flow under it. The term sluice gate refers to any gate that operates by allowing water to flow under it. When a sluice gate is fully lowered, water sometimes spills over the top, in which case the gate operates as a weir.

Usually a mechanism drives the sluice gate up and down. This may be a simple, hand-operated, worm drive or rack and pinion drive, or it may be electrically or hydraulically powered.

This section is focused on vertical lift gates mainly because the laboratory canal has only this type of gates. However, the majority of the following developments can also be applied to other types of sluice gates.

4.3.1   Flow conditions

It is very important to remark the existence of two particular working flow conditions when dealing with sluice gates:

1. The free flow condition

2. The submerged flow condition.

Both conditions are sketched in figure 4.6 and figure 4.7 respectively.

Under a free flow condition (see figure 4.6), a hydraulic jump occurs downstream from the sluice gate in a channel. The downstream conjugate depth of the jump h_3 may be calculated by taking the water depth at vena contracta h_2 as the upstream conjugate depth.

A submerged flow occurs when the tailwater depth is greater than the downstream conjugate depth of h_2. As illustrated in figure 4.7, instead of being in presence of a normal hydraulic jump, this particular condition develops a submerged hydraulic jump. The contact of this hydraulic jump with the volume of water above it induces a turbulent water recirculation. This phenomena produces typically a backwater flow in the surface layer.
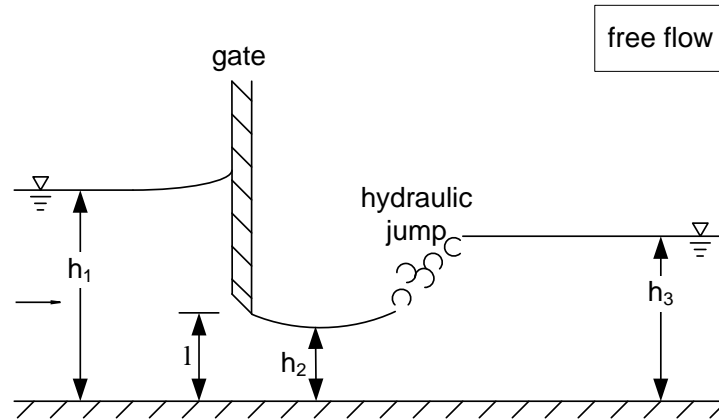
Figure 4.6: Sketch of free flow
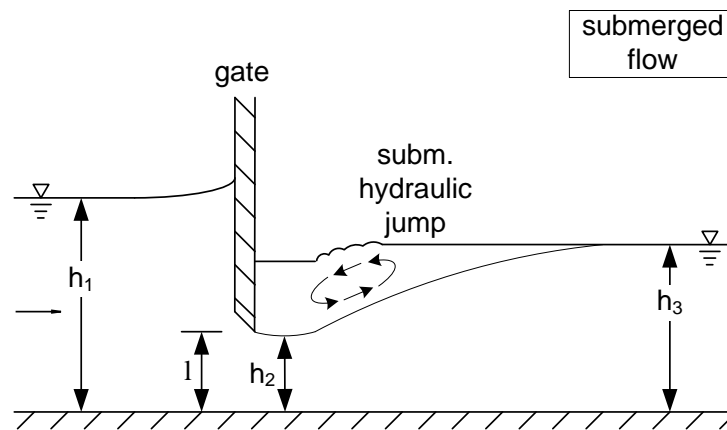
Figure 4.7: Sketch of submerged flow

To determine whether the jump will be free or submerged is another problem. In this respect, there are several formulas that have been obtained theoretically or empirically by many researchers. Moreover, there are some formulas that do not consider an absolute frontier, but a gradually changing transition. Because this topic is out of the scope of this work, the following simple condition presented in Swamee (1992) was used when needed to distinguish both working flow conditions:

$$\text{Free flow:} \qquad h_1 \geq 0.81 h_3 \left(\frac{h_3}{l} \right)^{0.72} \qquad (4.4)$$

$$\text{Submerged flow:} \qquad h_3 < h_1 < 0.81 h_3 \left(\frac{h_3}{l} \right)^{0.72} \qquad (4.5)$$

4.3.2 Flow rate formulas

4.3.2.1 Classical theoretical formulation

Calculating the discharge under a sluice gate is not a trivial matter. In theory, the sluice flow rate formula can be accurately obtained if the contraction coefficient is known (Henderson, 1966). The most common flow rate expression makes use of the conservation of energy, mass and momentum in the sluice gate - hydraulic jump flow. This procedure yields the following equation:

$$Q = C_d \, l \, b \, \sqrt{2g \, h_1} \tag{4.6}$$

In (4.6), l is the gate opening, b is the gate width and h_1 is the upstream water level. In this context, the discharge coefficient C_d is given by two equations (one for each flow condition), functions of the contraction coefficient C_c, b, h_1 and, for the submerged condition, the downstream water level h_3:

$$\text{Free flow:} \qquad C_d = \frac{C_c}{\sqrt{1 + \eta}} \tag{4.7}$$

$$\text{Submerged flow:} \qquad C_d = C_c \frac{\left[\xi - \sqrt{\xi^2 - \left(\frac{1}{\eta^2} - 1 \right)^2 \left(1 - \frac{1}{\lambda^2} \right)} \right]^{1/2}}{\frac{1}{\eta} - \eta} \tag{4.8}$$

where $\eta = C_c b / h_1$, $\xi = (1/\eta - 1)^2 + 2(\lambda - 1)$ and $\lambda = h_1 / h_3$.

Unfortunately, the contraction coefficient varies with: the amount of gate opening, shape of the gate lip, upstream water depth, gate type and so forth (Lin et al., 2002). Thus, it is very difficult to know its true value for all operating conditions in practice. That is why there are other approaches that combine some theoretical and some practical knowledge in order to simplify the task. Some of them are presented in the next sections.

4.3.2.2 Classical empirical formulations

Free Flow A good survey that includes many of these approaches for the free flow condition can be found in Montes (1997, 1999); Webby (1999) and in Speerli and Hager (1999). One common approach is to use (4.6) and determine an empirical constant value or, moreover, a relationship for C_d or C_c. Writing this in a mathematical form leads:

$$Q = C_d \, l \, b \, \sqrt{2g \, h_1}$$

with $C_d = f(h_1, l)$ or $C_d = k_0$.

Submerged Flow As mentioned in Clemmens et al. (2003), few studies are available in the literature. There are two common approaches: use (4.6) as well, including the effect of the downstream water level h_3 in the discharge coefficient C_d or modify (4.6) in order to incorporate h_3 explicitly (Malaterre and Baume, 1998). That is:

$$Q = C_d\, l\, b\, \sqrt{2g\, h_1}$$

with $C_d = f(h_1, h_3, l)$ or $C_d = k_0$, or

$$Q = C_d\, l\, b\, \sqrt{2g\, (h_1 - h_3)} \tag{4.9}$$

with $C_d = f(h_1, l)$ or $C_d = k_0$.

It is worth to note that a particular sluice gate in a normal irrigation canal operates, the most of the time, either in the free flow condition or in the submerged flow condition. Moreover, they are usually operated in a very narrow range, which explains, in some cases, the use of fixed discharge coefficient values. However this is not always advisable, because the discharge coefficient can suffer abrupt changes around a particular working point. In this context, it is very clarifying the experimental research performed by Henry (1950). Figure 4.8 shows the variation of C_d (using (4.6)) under free and submerged flow as obtained by him.
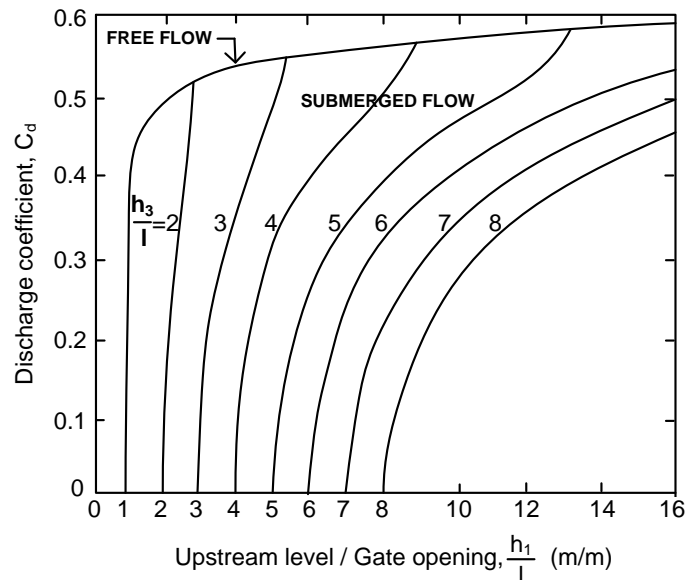
Figure 4.8: Variation of Discharge coefficient

From figure 4.8 one can observe that C_d can be very sensitive to small changes in any of the involved variables. For free flow, C_d progressively increases to a constant value of 0.611. Under submerged flow conditions, C_d is zero when $h_1 = h_3$. Any increase in h_1 above h_3 results in

rapid increase in C_d until h_1 attains a maximum value at which the flow is free.

4.3.2.3 Some empirical discharge calculation methods

- Rajaratnam and Subramanya (1967) performed the first modern study about sluice gate discharge calculation. They expressed the discharge through a vertical lift gate as:

$$\text{Free Flow:} \qquad Q = C_d \, l \, b \, \sqrt{2g \left(h_1 - C_c \, l\right)} \qquad (4.10)$$

$$\text{Submerged Flow:} \qquad Q = C_d \, l \, b \, \sqrt{2g \left(h_1 - h_2\right)} \qquad (4.11)$$

A value of 0.61 was used for C_c and the analysis of experimental data indicated that C_d was uniquely related to l/h_1 for both conditions. For $l/h_1 < 0.3$ this relationship was almost linear with $C_d = 0.0297 \, l/h_1 + 0.589$. As can be noted, (4.11) makes use of h_2, the water level at the vena contracta. Because its value is very difficult to be measured accurately (this zone has standing recirculation flows), it must be predicted. After certain simplifications they obtained:

$$h_2 = lC_d \left(2 \left(1 - \frac{lC_d}{h_3} \right) + \sqrt{4 \left(1 - \frac{lC_d}{h_3} \right)^2 + \left(\frac{h_3}{lC_d} \right)^2 - 4 \left(\frac{h_1}{lC_d} - \frac{h_1}{h_3} \right)} \right) \qquad (4.12)$$

- In Swamee (1992), they obtained discharge coefficient equations for (4.6), performing nonlinear regression on Henry's nomogram (figure 4.8). For both hydraulic conditions they obtained:

$$\text{FF:} \quad C_d = 0.611 \left(\frac{h_1 - l}{h_1 + k_0 l} \right)^{k_1} \qquad (4.13)$$

$$\text{SF:} \quad C_d = 0.611 \left(\frac{h_1 - l}{h_1 + k_0 l} \right)^{k_1} \left(k_2 \left(\frac{k_3 h_3 \left(\frac{h_3}{l} \right)^{k_4} - h_1}{h_1 - h_3} \right)^{k_5} + 1 \right)^{-k_6} \qquad (4.14)$$

where $k_0, k_1, \ldots, k_6$ are constants with the following values: $k_0 = 15$, $k_1 = 0.072$, $k_2 = 0.32$, $k_3 = 0.81$, $k_4 = 0.72$, $k_5 = 0.7$ and $k_6 = 1$. Later on, the same approach was used in Swamee et al. (1993, 2000) and Ghodsian (2003) for side sluice gates and other sluice gates configurations, by finding other equation constants for each particular case.

- In Ferro (2000), the stage-discharge relationship was deduced by a theoretical analysis, based on the application of the Π-theorem of the dimensional analysis and the incomplete self-similarity theory, coupled with an experimental investigation carried out by using a laboratory flume. This study was completed in Ansar (2001) and Ferro (2001) to enhance

the applicability of the method and cover the submerged flow condition case. The strength of this formulation resides on the use of correctly chosen adimensional variables, which can describe accurately the physical phenomena. In this case, the resolution of the problem lead to two adimensional variables, H/l and K/l, which are related by the following equation:

$$\frac{K}{l} = k_0 \left(\frac{H}{l}\right)^{k_1} \tag{4.15}$$

with

$$K = \sqrt[3]{\frac{\left(\frac{Q}{b}\right)^2}{g}} \tag{4.16}$$

$$H = \begin{cases} h_1 & \text{in Free Flow} \\ h_1 - h_3 & \text{in Submerged Flow} \end{cases} \tag{4.17}$$

The constants k_0 and k_1 should be easily obtained by fitting (in Excel, SPSS, or any other statistical software) the available field data to a power model. Consequently, the overall result for the gate discharge is:

$$\text{Free Flow:} \qquad Q = b \sqrt{g \left(l \, k_0 \left(\frac{h_1}{l}\right)^{k_1}\right)^3} \tag{4.18}$$

$$\text{Submerged Flow:} \qquad Q = b \sqrt{g \left(l \, k_0' \left(\frac{h_1 - h_3}{l}\right)^{k_1'}\right)^3} \tag{4.19}$$

where k_0, k_1, k_0' and k_1' are constants to be obtained from experimental data. The method is recommended with 15 or more data points and was proven with mixtures of data sets in order to obtain mean design values. Special care should be taken when working with Reynolds numbers $Re = Q/(b\,\nu)$ below $10\,000$. In such cases, real fluid effects (viscous effects) are highly noticeable and the Reynolds number should be included as another variable in (4.18) and (4.19) (Montes, 1997; Ansar, 2001). However, the later work of Shahrokhnia and Javan (2006) observed that this influence has less effects on the average estimation error of discharge, at least in their particular case (radial gates).

- Simulation of Irrigation Canals (SIC) is a commercial software, developed by the "Modeling and Regulation of Water Transfers" research team of the Irrigation Research Unit of Cemagref Montpellier (France), that includes their own empirical gate discharge equations. All of them can be found in the SIC software manual (see CEMAGREF, 2004, vol. II). For undershot gates these are:

$(h_3/h_1 \leq \alpha) \Rightarrow$ Free Flow

$$Q = b\sqrt{2g}\left(\mu\, h_1^{3/2} - \mu_1(h_1 - l)^{3/2}\right) \tag{4.20}$$

$(h_3/h_1 > \alpha) \wedge (h_3 \leq \alpha_1 h_1 + (1 - \alpha_1)l) \Rightarrow$ Partially Submerged Flow

$$Q = b\sqrt{2g}\left(k_F\,\mu\, h_1^{3/2} - \mu_1(h_1 - l)^{3/2}\right) \tag{4.21}$$

$(h_3/h_1 > \alpha) \wedge (h_3 > \alpha_1 h_1 + (1 - \alpha_1)l) \Rightarrow$ Totally Submerged Flow

$$Q = b\sqrt{2g}\left(k_F\,\mu\, h_1^{3/2} - k_{F1}\,\mu_1(h_1 - l)^{3/2}\right) \tag{4.22}$$

where

$$\alpha = 1 - 0.14\frac{h_3}{l}; \quad \alpha_1 = 1 - 0.14\frac{h_3 - l}{l}$$
$$\mu = \mu_0 - \frac{0.08}{\frac{h_1}{l}}; \quad \mu_1 = \mu_0 - \frac{0.08}{\frac{h_1}{l} - 1}$$

$$k_F = \begin{cases} 1 - (1 - \frac{x}{\sqrt{1-\alpha}})^{-2\alpha+2.6} & \text{if } x = \sqrt{1 - \frac{h_3}{h_1}} > 0.2 \\ 5x(1 - (1 - \frac{0.2}{\sqrt{1-\alpha}})^{-2\alpha+2.6}) & \text{if } x = \sqrt{1 - \frac{h_3}{h_1}} \leq 0.2 \end{cases}$$

$$k_{F1} = \begin{cases} 1 - (1 - \frac{x_1}{\sqrt{1-\alpha_1}})^{-2\alpha_1+2.6} & \text{if } x_1 = \sqrt{1 - \frac{h_3-l}{h_1-l}} > 0.2 \\ 5x_1(1 - (1 - \frac{0.2}{\sqrt{1-\alpha_1}})^{-2\alpha_1+2.6}) & \text{if } x_1 = \sqrt{1 - \frac{h_3-l}{h_1-l}} \leq 0.2 \end{cases}$$

Additionally, when α or α_1 go out of the range [0.4 0.75], their values are fixed to the closest boundary.

As can be observed, this formulation considers two subdivisions for the submerged case: the partially submerged condition (4.21) and the totally submerged condition (4.22). Additionally, it uses their own distinguish condition and two variables, k_F and k_{F1}, in order to "weight" the terms of the free flow equation for different degrees of submergence. The only user defined parameter is μ_0, which is function of the classical discharge coefficient C_d, from the free flow equation (4.6), and defined by $\mu_0 = 2/3\,C_d$. Thus, C_d should be calculated from measurement data or selected among the values recommended in technical handbooks ($C_d \approx 0.6$).

- Hydrologic Engineering Center - River Analysis System (HEC-RAS) is a very popular

(freeware) software developed at the HEC, which is a division of the Institute for Water Resources - U.S. Army Corps of Engineers, that allows to perform one dimensional steady and unsteady flow river hydraulics calculations. This software models vertical lift gates in the following manner (HEC, 2002):

$(h_3/h_1 \leq 0.67) \Rightarrow$ Free Flow

$$Q = C_d \, l \, b \, \sqrt{2g \, h_1} \tag{4.23}$$

$(0.67 < h_3/h_1 < 0.8) \Rightarrow$ Partially Submerged Flow

$$Q = C_d \, l \, b \, \sqrt{2g \, 3(h_1 - h_3)} \tag{4.24}$$

$(h_3/h_1 \geq 0.8) \Rightarrow$ Totally Submerged Flow

$$Q = C_d' \, l \, b \, \sqrt{2g \, (h_1 - h_3)} \tag{4.25}$$

where C_d and C_d' are fixed user defined values.

This approach is conceptually similar to the one used in SIC (three different working conditions), but with less effort in the calculation of the discharge coefficients.

4.3.3 Submerged sluice gate calibration study

4.3.3.1 Introduction

In Clemmens et al. (2003), it is remarked that discharge measurement errors for gates working in the free flow condition are normally $\pm 5 \, \%$. On the opposite, there are reported discharge errors of up to $50 \, \%$ in the submerged flow condition.

The problem lies clearly in the submerged flow modeling structures. This explains, in some sense, the proliferation of several variations of the free flow or the orifice flow model structures with their empirical discharge coefficient expressions or curves.

This modeling problem affects mainly three aspects:

1. Gate discharge field calculations

2. Gate discharge software modeling

3. Gate discharge control

Discharge calculation accuracy is very important from an environmental and an economical point of view. On the other hand, open channel flow software modeling is nowadays a very useful design tool. There is a great effort to model the water behavior accurately. However, a bad modeling of the boundary conditions (in this case, for example, a sluice gate) could lead to wrong results, no matter the sophistication of the hydraulic modeling method. Furthermore, if one has a good gate discharge model, it is also possible to accurately predict the required gate opening in order to obtain a desired discharge. This is particularly important in the case of using gates as actuators for automatic control purposes.

The objective of this study is to find the best models in terms of accuracy and reliability for our laboratory requirements, focusing mainly in the analysis and comparison of several submerged discharge modeling methods.

In order to achieve the objective of this study the following steps will be developed in the next sections:

1. To take relevant measurement data from our laboratory canal.

2. To perform the calibration step for those methods that require it.

3. To evaluate and compare all methods.

4.3.3.2 Methodology

Hydraulic data was taken from our laboratory canal. Because this is a zero-slope canal, the gates work, most of the time, in submerged flow condition. There are three gates: Gate 1, Gate 3 and Gate 5. Gate 1 works usually with an upstream water level (h_1) much higher than the downstream water level (h_3) (i.e. high hydraulic head) and small gate openings ($2\,\text{cm} \leq l \leq 9\,\text{cm}$). On the contrary, Gate 3 and Gate 5 work with small water level differences ($h_1 - h_3 \leq 15\,\text{cm}$) and higher gate openings ($4\,\text{cm} \leq l \leq 20\,\text{cm}$).

A collection of steady state points ($1\,\text{h}$ stabilization time) was taken for Gate 1, Gate 3 and Gate 5. The task was performed using a triangular weir as discharge measurement instrument, a $0.1\,\text{mm}$ precision limnimeter as water depth measuring device and a $0.5\,\text{mm}$ precision ruler to measure the openings of the gates.

The data sets for Gate 1, Gate 3 and Gate 5 are given in Table C.1, Table C.2 and Table C.3 respectively.

Using all the collected information, the majority of the submerged discharge formulations presented in this chapter were implemented and used. These are:

- The C_c=0.611 method

- The Henry method

- The Rajaratnam method

- The Swamee method

- The Ferro method

- The SIC method

- The HEC-RAS method

The $C_c=0.611$ method consists in using a constant contraction coefficient value of 0.611 in the theoretical formula given by (4.8). This value is recommended in many research works and in technical manuals references. The other methods were already explained previously.

The SIC method, the Ferro method and the HEC-RAS method needed a previous calibration stage.

The SIC method was formulated in a linear regression form in order to estimate μ_0 using the least squares approach. A similar approach was used to estimate the parameters of the HEC-RAS method. The difference was that in this case the data collection was separated in two groups: one for the totally submerged condition and other for the remaining conditions.

The calibration of the Ferro method (4.19) can be formulated in a linear manner, if the natural logarithm is applied in both equation sides. Then, the problem can also be solved in a linear regression form using the least squares approach. However, this procedure, although most of the time gives good results, is not advisable in all cases. One of the least squares assumptions is that the error variance remains constant for all points (homoscedastic errors). This assumption is violated in this case because the involved adimensional variables, H/l and K/l, propagate constant measurement errors in a strictly growing form. As a consequence, there are different error variances for different points (heteroscedastic errors). For example, an "errorless" head measurement, $H = 1$, and a gate opening measurement with an average error, $l = 1 \pm 0.1$, would produce an average error of:

$$e_{H/l} = \frac{H}{l}\left(\frac{e_H}{H} + \frac{e_l}{l}\right) = \pm 0.1$$

With $H = 2$, this error increase to $e_{H/l} = \pm 0.2$. Summing up that then these variables are log-transformed in their linear regression form, there is a high probability of heteroscedasticity. When there exists strong evidence that this problem is clearly affecting the least squares fit, a more robust curve fitting method should be employed. In this particular case, the Least Absolute Deviations (LAD) method with the original nonlinear equation form, gave very good results (the fit is less influenced by greater errors). In that case the optimization problem has the following form:

$$\min_{k_0,\,k_1} \frac{1}{N} \sum_i^N \left| Y_i - k_0\, X_i^{k_1} \right| \tag{4.26}$$

Other alternatives are Weighted Least Squares (WLS), MM-estimators, and so forth.

The calibration results are summarized in table 4.1.

Table 4.1: Calibration results for Gate 1, Gate 3 and Gate 5

	SIC	HEC-RAS		Ferro	
Gate Id.	μ_0	C_d	C_d'	k_0'	k_1'
Gate 1	0.3356	0.438	0.609	0.9176	0.3489
Gate 3	0.3347	0.388	0.678	0.9482	0.3202
Gate 5	0.3790	0.405	0.768	1.0097	0.3154

At this point, all methods were evaluated in terms of predicted discharge errors, using the same data sets, in order to analyze and compare the model-fitting properties of each approach.

4.3.3.3   Results

These results are presented in two forms. First of all, discharge predictions and their residuals are shown graphically, in order to observe tendencies and assess performance in a more qualitative way. Next, different mean error indices are calculated and contrasted, in order to obtain numerical values that permit a quantitative evaluation of each discharge calculation method.

The predicted discharges, calculated from the application of each method to the experimental data from Table C.1, Table C.2 and Table C.3, are shown for Gate 1, Gate 3 and Gate 5 in figure 4.9, figure 4.10 and figure 4.11 respectively. The discharge errors of these predictions are shown, separately, in figure 4.12, figure 4.13 and figure 4.14.
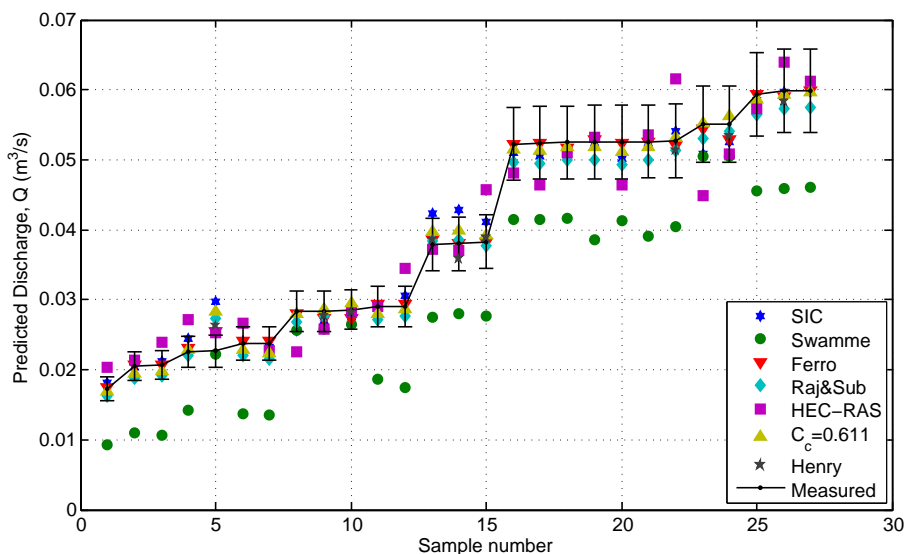
Figure 4.9: Gate 1 predicted discharges with $\pm 10\%$ error bars
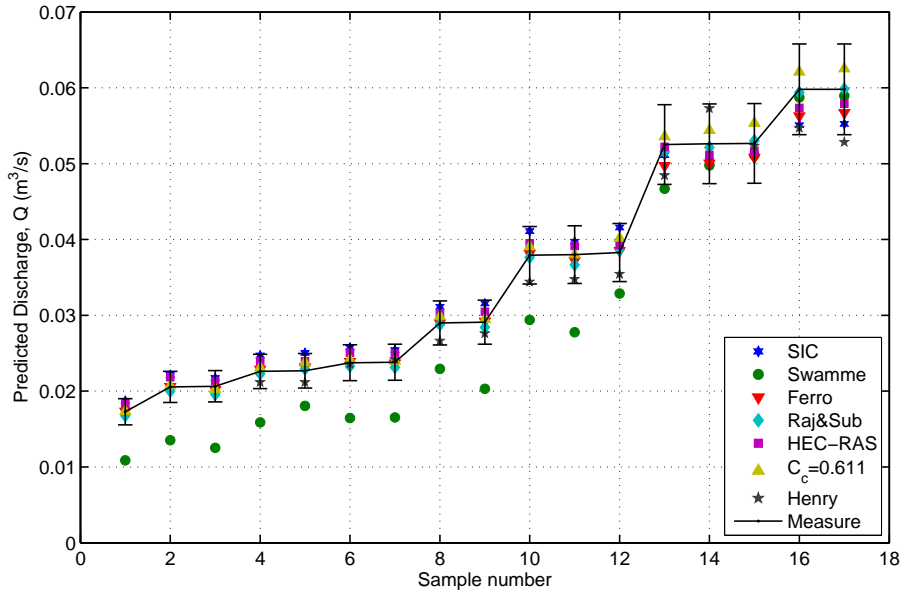
Figure 4.10: Gate 3 predicted discharges with $\pm 10\,\%$ error bars
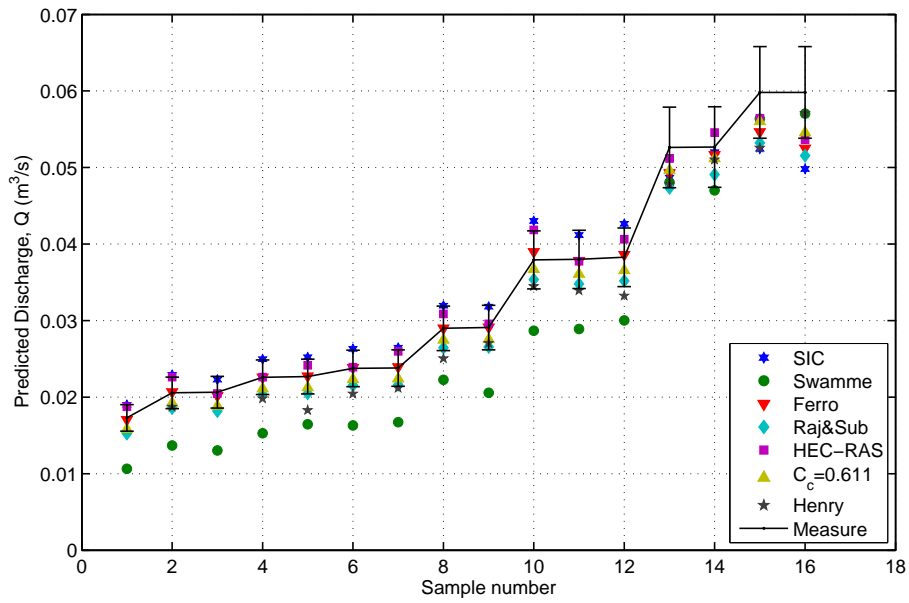
Figure 4.11: Gate 5 predicted discharges with $\pm 10\,\%$ error bars
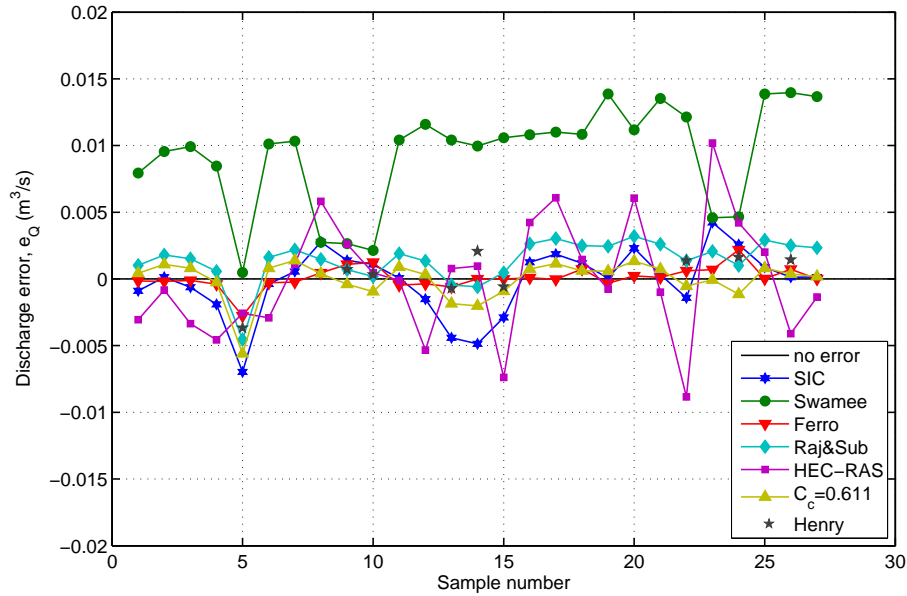
Figure 4.12: Gate 1 discharge errors
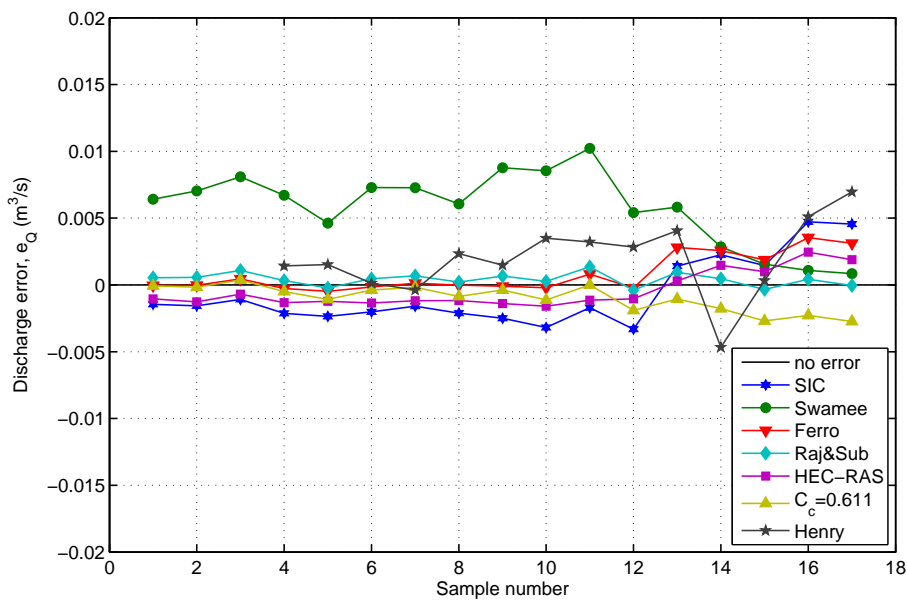
Figure 4.13: Gate 3 discharge errors
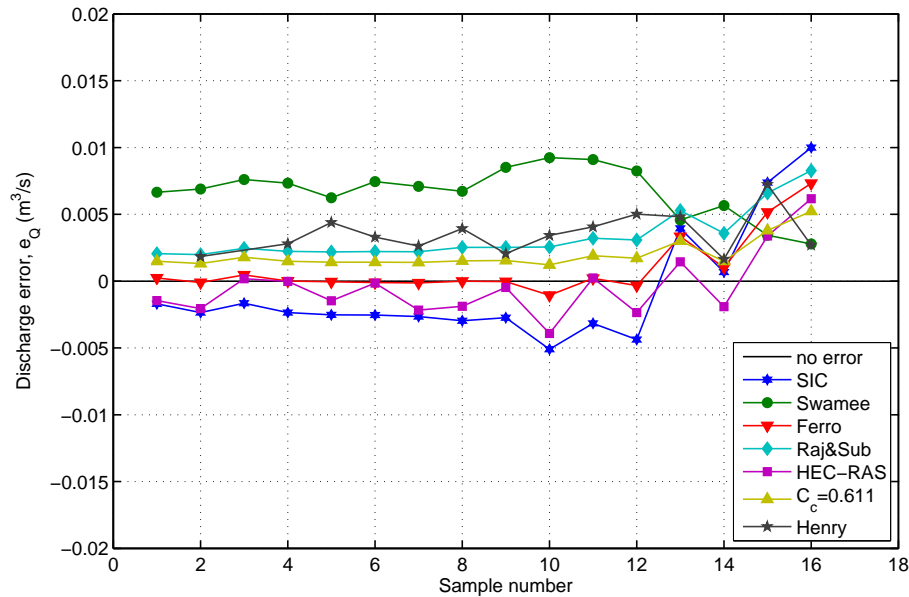
Figure 4.14: Gate 5 discharge errors

The first feature that shows up from observing the figures, is that, in the operational range of this study, the Swamee method gave a very poor performance, exhibiting high discharge errors in all the studied gates. In fact, the direct inspection of Henry's nomogram (the Swamee method only gives equations for Henry's curves) gave more accurate results in the majority of the cases, when it was possible its application (there were several points that went out of the range of the nomogram ($1 < h_1/l \leq 16$)).

Without taking into account the Swamee method, the rest of the methods fell, in general, within the $\pm 10\,\%$ error margin.

The Ferro method performed very well in all three gates, displaying a very good fit (this method, the SIC and the HEC-RAS method were calibrated using the same data as in this evaluation) with very small errors in most of the cases. The HEC-RAS fit, although oscillating around zero, seems to be more erratic. The SIC method has a similar behaviour.

Surprisingly, the use of a constant contraction coefficient value of 0.611 in the theoretical formulas gave very good results. The discharge predictions were very accurate with low dispersion.

The results given by the Rajaratnam method and the Henry method look also good. In most of the cases, they predicted discharges with small error in a reliable manner.

In order to evaluate quantitatively these results, the error based performance indices of table 4.2 were used.

The Mean Error (ME), the Mean Absolute Error (MAE) and the Root Mean Square Error (RMSE) are indices measured in the same units as the error. They can be influenced in some way, if the errors depend on the magnitude of the measurements. Conversely, the Mean Percentage

Table 4.2: Performance indices

Index	Formula
MAPE	$\dfrac{100}{N} \sum\limits_{i=1}^{N} \left| \dfrac{Y_i - \hat{Y}_i}{Y_i} \right|$
MPE	$\dfrac{100}{N} \sum\limits_{i=1}^{N} \dfrac{Y_i - \hat{Y}_i}{Y_i}$
ME	$\dfrac{1}{N} \sum\limits_{i=1}^{N} \left(Y_i - \hat{Y}_i \right)$
MAE	$\dfrac{1}{N} \sum\limits_{i=1}^{N} \left| Y_i - \hat{Y}_i \right|$
RMSE	$\sqrt{\dfrac{1}{N} \sum\limits_{i=1}^{N} \left(Y_i - \hat{Y}_i \right)^2}$

Error (MPE) and the Mean Absolute Percentage Error (MAPE) are relative indices given in percentage.

The ME and the MPE are signed measures of error which indicate whether the predictions are biased, i.e. whether they tend to be disproportionately positive or negative. Bias is normally considered a bad thing, but it is not the bottom line. On the other hand, the MAE, the MAPE and the RMSE are indices that incorporate the bias as well as the variance of the errors. The RMSE takes normally precedence over the others because has a close relationship with the standard deviation, but it is more sensitive than the other measures to the occasional large error.

The results for each gate are summarized in table 4.3, table 4.4 and table 4.5. In order to simplify comparison purposes, these results are also given in bar charts. They are shown in figures 4.15 - 4.20.

Table 4.3: Performance of each method for Gate 1 data

Method	MAPE (%)	MPE (%)	ME (m^3/s)	MAE (m^3/s)	RMSE (m^3/s)
SIC	5.11	-1.47	-0.0002	0.0017	0.0024
Swamee	25.73	25.73	0.0093	0.0093	0.0101
Ferro	1.61	-0.15	0.0001	0.0005	0.0008
Raj & Sub	5.05	3.36	0.0014	0.0018	0.0021
HEC-RAS	9.38	-1.67	0.0000	0.0034	0.0043
Cc=0.611	3.14	-0.29	0.0000	0.0010	0.0014
Henry	4.08	-0.27	0.0003	0.0014	0.0017

Table 4.4: Performance of each method for Gate 3 data

Method	MAPE (%)	MPE (%)	ME (m³/s)	MAE (m³/s)	RMSE (m³/s)
SIC	7.00	-4.03	-0.0006	0.0023	0.0025
Swamee	21.13	21.13	0.0058	0.0058	0.0064
Ferro	2.09	1.41	0.0008	0.0010	0.0016
Raj & Sub	1.80	1.49	0.0004	0.0005	0.0006
HEC-RAS	4.04	-2.57	-0.0004	0.0013	0.0013
Cc=0.611	2.56	-2.35	-0.0010	0.0010	0.0014
Henry	6.48	4.98	0.0020	0.0027	0.0033

Table 4.5: Performance of each method for Gate 5 data

Method	MAPE (%)	MPE (%)	ME (m³/s)	MAE (m³/s)	RMSE (m³/s)
SIC	10.21	-5.48	-0.0008	0.0035	0.0042
Swamee	23.88	23.88	0.0067	0.0067	0.0070
Ferro	2.42	1.73	0.0010	0.0012	0.0024
Raj & Sub	9.61	9.61	0.0033	0.0033	0.0038
HEC-RAS	5.21	-2.68	-0.0004	0.0018	0.0024
Cc=0.611	5.95	5.95	0.0020	0.0020	0.0023
Henry	10.57	10.57	0.0036	0.0036	0.0038
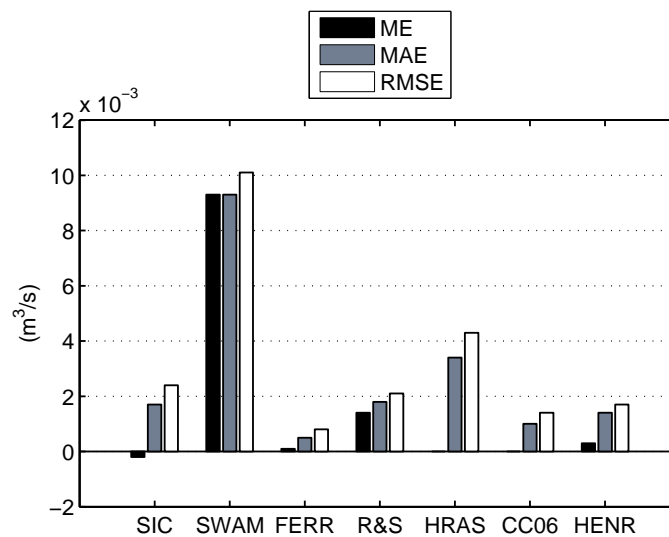
Figure 4.15: ME, MAE and RMSE for Gate 1
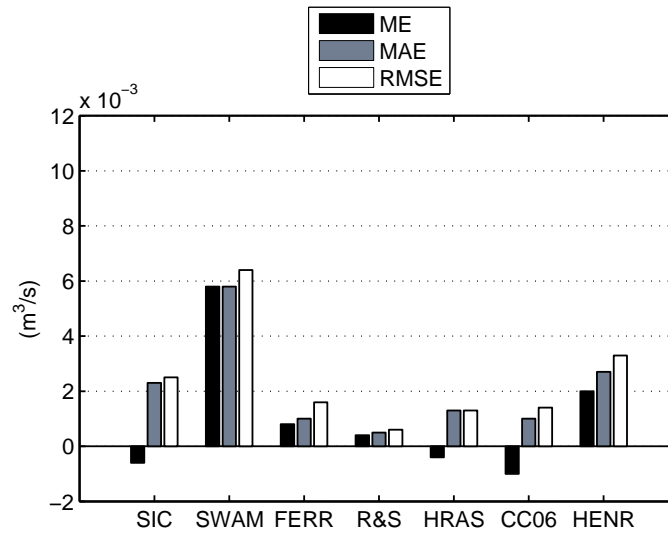
Figure 4.16: ME, MAE and RMSE for Gate 3
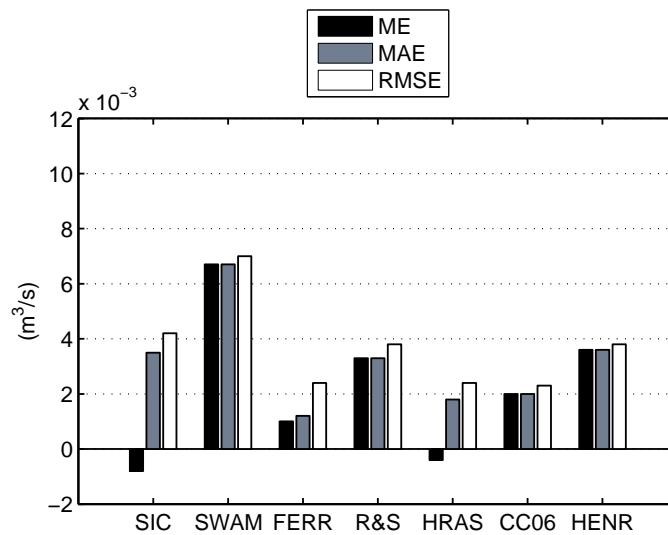
Figure 4.17: ME, MAE and RMSE for Gate 5
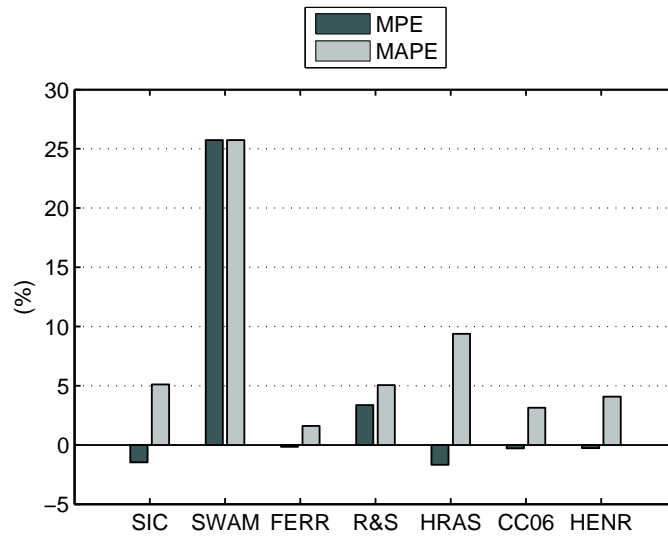
Figure 4.18: MPE and MAPE for Gate 1
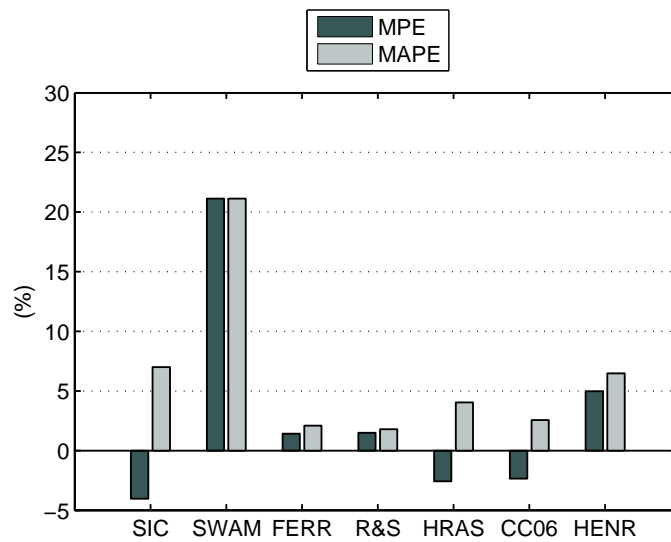
Figure 4.19: MPE and MAPE for Gate 3
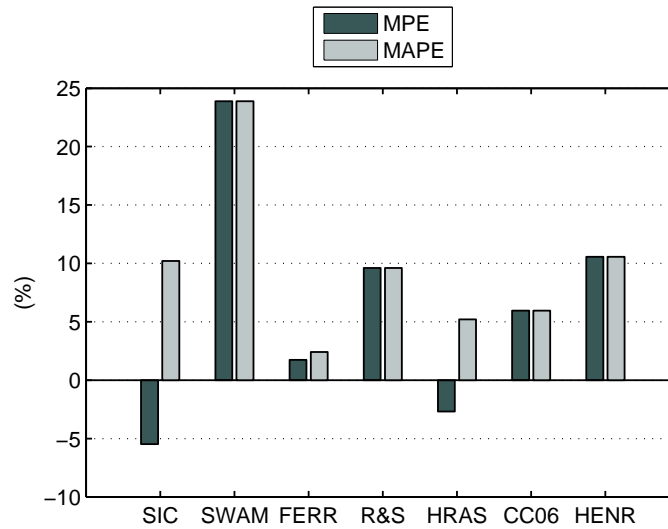
Figure 4.20: MPE and MAPE for Gate 5

The performance results are in good agreement with the qualitative results. The Swamee method presented a very high bias error for all three gates. In all the tests, it underestimated the gate discharges in more than $20\,\%$.

The rest of the methods can be joined into two groups under a performance point of view.

The first group is integrated with methods whose results oscillate in the $2\,\%$-$10\,\%$ MAPE range, depending on the particular studied gate. This group is integrated with the SIC method, the HEC-RAS method, the Rajaratnam method and the Henry method.

The second group showed a high performance consistency through gates. For example, the C_c=0.611 method had the following MAPE values: $3.14\,\%$, $2.56\,\%$ and $5.95\,\%$. The other method in this group had the best overall performance results: the Ferro method. This fact is exemplified by its low MAPE values: $1.61\,\%$, $2.09\,\%$ and $2.42\,\%$.

The last performance test involves the evaluation of the SIC method, the HEC-RAS method and the Ferro method using *typical* calibration values. This values were obtained from manuals and research works, and are summarized in table 4.6.

Table 4.6: Typical calibration values

Method	Calibration values	
SIC	$\mu_0 = 0.4$	
Ferro	$k_0' = 1.0559$	$k_1' = 0.3344$
HEC-RAS	$C_d = 0.6$	$C_d' = 0.8$

Because there was a clear pattern among all gates, these results are only presented for Gate 3 using the MPE and the MAPE for simplicity reasons. These results are shown in figure 4.21.
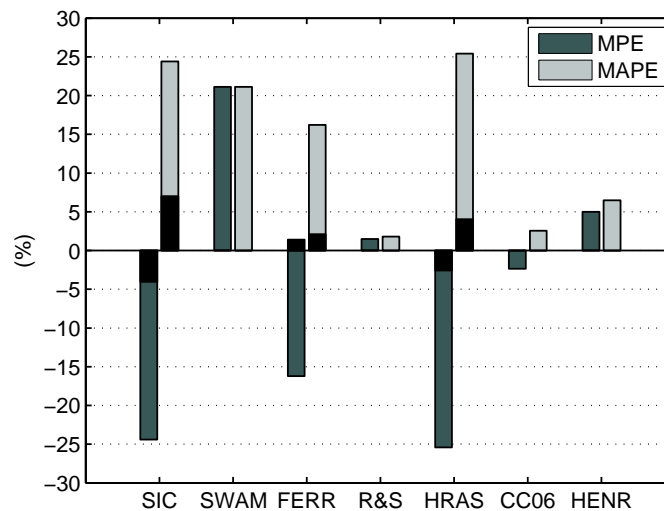
Figure 4.21: Performance degradation without calibration - Gate 3

This test showed a high increment of the errors (essentially bias errors) when using typical calibration values (prior errors were colored in black). As a matter of fact, the performance degradation was so pronounced (MAPEs $\approx 20\,\%$) that, in general, the rest of methods performed far better than them. Additionally, the performance results from the untuned Ferro method were always better than the ones obtained using the untuned, HEC-RAS and SIC, methods.

4.3.3.4 Discussion

One of the most impressing issues from the results section was the poor performance exhibited in these tests by the Swamee method. However, this point can be made clear after comparing Henry's original nomogram with Swamee's approximation. This comparison is sketched in figure 4.22.

As it can be seen in figure 4.22, Swamee's discharge equations produce only a good fit for $h_3/l < 5$. For $h_3/l \geq 5$, there are clear differences between both diagrams. Besides, these differences tend to increase with the quotient h_3/l. Therefore, the poor results obtained in this case were only an example of these fitting errors: most of the data lied in that range.

All the rest of the methods achieve a more than acceptable performance. However, there are some differences that are worth to remark.

A difference should be made when comparing the results of methods that were calibrated using field information with the ones that were not. It is clear that these methods should perform much better than the others, because, in this case, they were calibrated using the same data that were, subsequently, used for model validation. However, with the particular exception of the Ferro method, the SIC method and the HEC-RAS method performed, in general, equally than
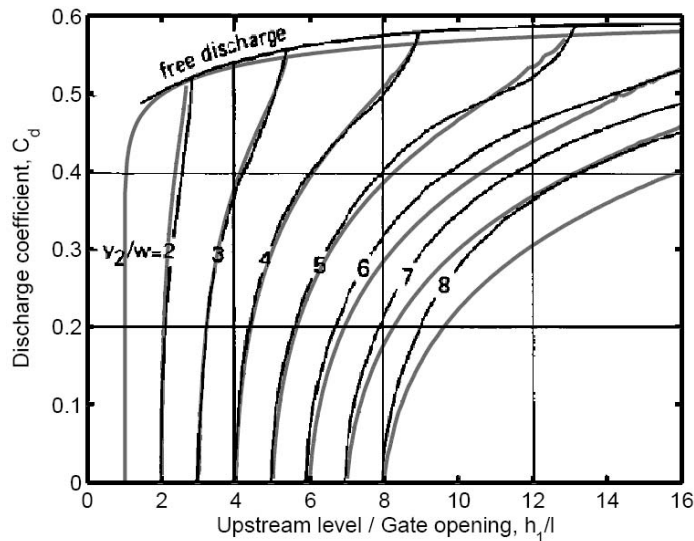
Figure 4.22: Comparison between Henry's nomogram (black) and Swamee's approx. (gray)

the other methods. This result was not previously expected, taking into account the fact that both were the only ones, that make use of a subdivision of the submerged flow to cover the flow transition behavior. On the other hand, the Ferro method has a very simple equation structure (very suitable for model inversion gate discharge control) and obtained the best performance results, facts that encourage its use when calibration data is available. However, care should be taken when using these three methods without data to perform calibration: there is a high probability of uncertain discharge values and high errors when using default calibrations. When previous data is not available, this experiment showed that is more safe to use one of the other methods.

Among the methods that do not use a calibration stage, it was a real surprise the high performance exhibited by the method that used a constant contraction coefficient value. This approach made use of a totally theoretical formulation with the, 0.611, empirically obtained average contraction coefficient value. The real contraction coefficient was never measured, so there is no evidence of its variation in this case. However, there are several research works (Rajaratnam and Subramanya, 1967; Montes, 1997; Yen et al., 2001; Lin et al., 2002) that suggest that, at least for vertical lift gates working in free flow, this parameter does not suffer great variations. Perhaps, the main drawbacks of this method are that its equation structure is rather troublesome to perform model inversion and that it will always exhibit a tendency to bias errors, for gates with slightly different average contraction values.

With respect to the other two classical methods, the Rajaratnam method and the Henry method, both of them gave good results, but there is a big difference between them: it is far easier to use Rajaratnam's discharge coefficient curve than Henry's nomogram. As a matter of fact, there is a high probability that an important part of its errors arise from interpolation of

curves and visual inspection problems. Furthermore, there are not equations, nowadays, that can describe accurately the whole range of the nomogram (demonstrated by Swamee's method results). In contrast, the Rajaratnam's curve was easily approximated by a line, in the range of interest, and gave similar performance results. Automatized calculations for the Rajaratnam method can also be done in this manner. However, this model inversion is also difficult to accomplish.

4.4   Conclusions

This chapter has tackled different aspects related to discharge measurements in our laboratory canal that are also applicable to other similar installations and bigger canals. The main conclusions of this chapter are the following:

- Hydraulic structures, like weirs and gates, have demonstrated a great skill in measuring water discharges, as a cheaper option than flow gages.

- Rectangular weirs should be carefully calibrated when default installation guidelines are not strictly followed and/or when equation applicability is not always assured. After that, they can be used as good measurement devices.

- Apart form the Swamee method, all the other tested gate discharge methods had small discharge prediction errors under submerged conditions (MAPE $\leq 10\,\%$).

- When calibration data was available, the best performance was obtained by the Ferro method (MAPE $\leq 3\,\%$). When no a priori data were available, using a fixed contraction value of 0.611 in the classical theoretical formula, was found to be a very good option (MAPE $\leq 6\,\%$).

- The Ferro method is also found to be a very good candidate to perform model inversion based - gate discharge control.

- The good success in calibrating the hydraulic structures of our laboratory canal using methods from other researchers, validate their design to use them as commonly encountered irrigation canal devices.

In a broader context, this chapter has achieved two goals:

1. The empirical validation of the use of several discharge calculation methods.

2. The complete calibration of our hydraulic structures, a task that now permits the accurate measurement of water discharges through the canal.

Both goals give now enough support to continue with:

- Open channel flow modeling approaches that use discharges as known variables.

- Automatic control of discharges through hydraulic structures.

- Automatic control of water levels in canals.

Chapter 5

Canal Identification for Control Purposes

This chapter gives some guidance on how to obtain linear black-box models of irrigation canal pools using system identification techniques.

First of all, some general properties of the irrigation canal pools are deducted, based on the use of the linearized Saint-Venant equations to model the water behavior.

Then, different aspects of the system identification procedure like the sampling time, the model structure, the experiment design, etc., are studied, in order to avoid possible modeling problems and, in that manner, obtain a good linear model capable to be used in control systems designs.

The results obtained in the time domain and in the frequency domain show that one can achieve very accurate models, provided the system identification procedure is designed with care having in mind the intrinsic properties of the system.

The research reveals that it is not convenient to perform a black-box irrigation canal system identification without having a certain knowledge of the system.

5.1   Introduction

5.1.1   About the importance of models in automatic control

The use of a good model of a process to be controlled is essential for almost all the currently existent control techniques (Shook et al., 1992). In addition to the possibility to test the control strategy to be implemented by means of computational simulation of the model, many control techniques use the model explicitly in the design stage of the controller or/and in the calculation of the control action (in this case check gates movements).

In the situation where the model is used in the design stage or in the computation of the

control action, unfortunately, the complexity of the characteristics of the model (nonlinearities, delays, instability, etc), is usually directly proportional to the complexity of the control techniques and their implementation. For example, a linear and rational model opens the possibility to apply numerous and well-known linear control theories and standard techniques, which are relatively easy to implement. A nonlinear model, in contrast, requires much more effort and time to solve the control problem. Therefore, it is always desirable to have the simplest model that can reproduce the behavior of the system. However, the "closest to exact" behavior of a system is always obtained, when it can be obtained, by very complex models. For example, all the existing processes are actually nonlinear. Linearity is only a simplification of the problem. So, models for control purposes should be made as a trade-off between simplicity and accuracy of the model in concordance with the automation goal.

5.1.2 About irrigation canal models

Models that involve water are generally obtained making use of simplifications of the Navier-Stokes Equations, because of the complexity in dealing directly with them. For irrigation canals, one of the most accepted and used model in simulations is the system given by the Saint-Venant Equations (Henderson, 1966), because of its capacity to represent the characteristics of real interest. However, this system is a nonlinear partial differential equation system, which has analytical solution only in very special cases, forcing the employment of numerical methods to solve it properly. As a model for computational simulation it is very accurate, but as model for control, it is clearly not appropriate for the reasons exposed before. This is why, usually, linearizations or simplifications of the Saint-Venant equations are recurrently studied by the irrigation control research community (Schuurmans et al., 1995, 1999a; Litrico and Fromion, 2004c; Weyer, 2001). These models are based on physical parameters of the real system. This approach has advantages and drawbacks. The advantages are that a physical model is reliable and has a very strong connection with the theoretical concepts. The main drawback is that it is necessary to feed the model with many parameters that have to be determined (from theoretical and/or experimental results) and an error in this determination can lead to a bad model performance. For example, a bad determination or small variation of the Manning number (a coefficient related to the friction of canals) can produce quite different results.

The scope of this chapter is to study the application of black box models to the problem of modeling irrigation canals for control purposes. These models do not necessarily have a physical meaning; they only focus on reproducing the behavior of a system, and are obtained from input-output experimental collected data, in a process that is called System Identification.

5.2 Model of a pool

5.2.1 Mathematical model
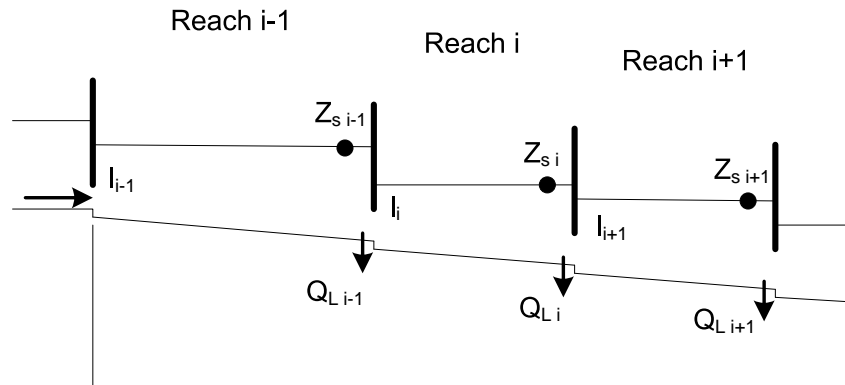
Figure 5.1: Irrigation canal schematic

A simplified view of a typical irrigation canal can be observed in figure 5.1. As mentioned before, it receives water from a source and lets the water flow with a small slope. The intermediate check gates, represented by vertical lines, regulate with their openings (l_i) the desired discharge, so as to maintain the water depth level ($Z_{s\,i}$) in the zones, where water is diverted for irrigational purposes ($Q_{L\,i}$).

For modeling intentions, a natural way of partitioning a canal is dividing it into reaches (also called pools). A reach is a portion of a canal between two check gates. So, a normal canal can have several reaches with different characteristics (length, slope, width, etc.). However, all the reaches share a common structure, focusing the problem of modeling an irrigation canal to find a suitable model for reaches. In that manner, the problem can be solved by an addition of the same model structure with only different parameter values.

In the specialized literature there are several approaches to obtain this model. In this work, two facts will be taken into account: the location of water extractions (offtakes), generally near the end of a reach, and the gradual change of the water behavior when approaching to an obstacle like a cross-gate, resembling the characteristics of a water reservoir. To put this practical knowledge in a mathematical model, an imaginary bound can be created, which separates the reach, in an absolute manner, in a water transport area and in a water storage area (see figure 5.2). It should be noted that the location of this imaginary bound is not so crucial; as it defines a particular size of the storage area, it will be correctly chosen whenever that area remains small enough in relation to the reach's total size.

Making use of the Saint-Venant equations (Henderson, 1966) to model the transport zone and of the mass conservation principle to model the storage, that leads to the following mathematical model:
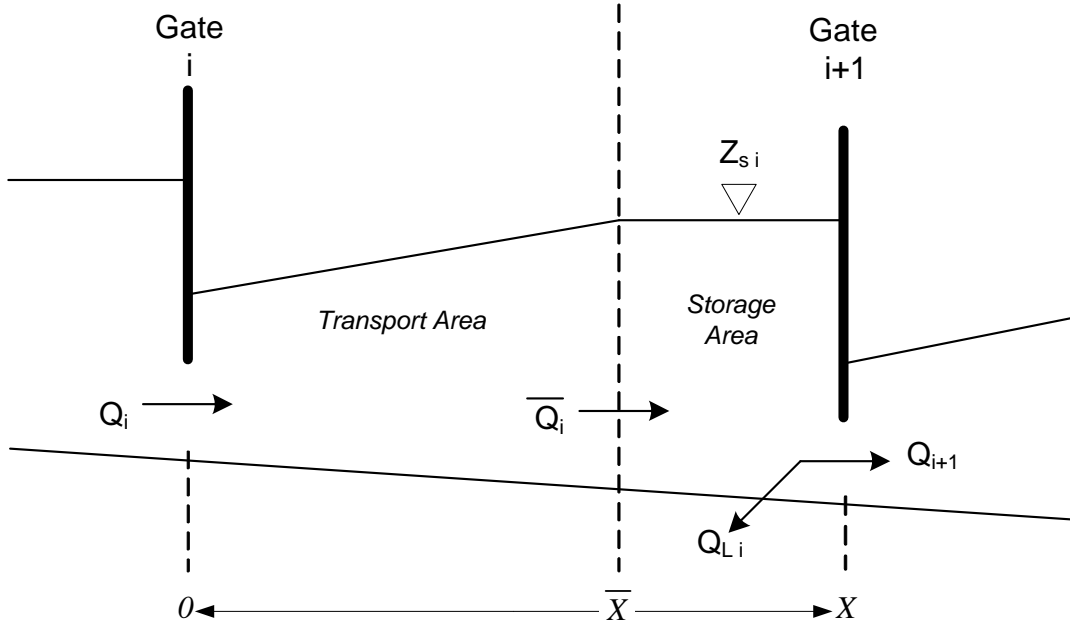
Figure 5.2: Simplified representation of a reach

- Transport

$$\frac{\partial A}{\partial t} + \frac{\partial Q}{\partial x} = 0 \tag{5.1}$$

$$\frac{\partial Q}{\partial t} + \frac{\partial}{\partial x}\left(\frac{Q^2}{A}\right) + gA\frac{\partial Z}{\partial x} = gA(S_0 - S_f) \tag{5.2}$$

with initial conditions: $Z(x,0) = Z_0(x)$, $Q(x,0) = Q_0(x)$ and boundary conditions: $Z(0,t) = Z_i(t)$, $Q(0,t) = Q_i(t)$, $Z(\overline{X},t) = \overline{Z}_i(t)$, $Q(\overline{X},t) = \overline{Q}_i(t)$.

- Storage

$$\overline{Q}_i(t) - Q_{i+1}(t) - Q_{Li}(t) = \frac{dV_{si}(t)}{dt} \tag{5.3}$$

In the transport equations (5.1)-(5.2), x is the longitudinal coordinate in the flow direction, t is the time, $A = A(x,t)$ is the wetted cross-sectional area of the pool, $Q = Q(x,t)$ is the water discharge, $Z = Z(x,t)$ is the water depth, S_0 is the bottom slope, S_f is the friction slope of the canal and g is the gravity acceleration. Besides, it should be noted that the wetted cross-sectional area (A) depends explicitly on the water depth (Z) and on the shape of the cross-section of the canal.

In the storage equation (5.3), $\overline{Q}_i(t)$ is the water discharge that enters the zone, $Q_{i+1}(t)$ is the water discharge delivered to the next reach, $Q_{Li}(t)$ is the water discharge extracted for irrigation purposes and $V_{si}(t)$ is the water volume (that is a function of the water depth $Z_{si}(t)$ and the geometry of that zone) stored behind gate $i+1$.

As can be seen from figure 5.2 and equations (5.1), (5.2) and (5.3), the values of the variables in the interface, denoted by an upper line $\left(\overline{Z}_i(t), \overline{Q}_i(t)\right)$, provide the link between both areas. Normally, they are not known a priori, but making use of extra mass and energy conservation relationships among that particular point and the described zones, the problem can be solved.

In summary, the model consists in a system of two nonlinear Partial Differential Equations (PDEs) and one nonlinear (sometimes linear) Ordinary Differential Equation (ODE). Because of the reasons given before, the model is little advantageous for control purposes. In the search for a more convenient model, a linearization around an operational condition will be performed.

5.2.2 Linearization of the model

Linearization is carried out replacing in the model described by (5.1), (5.2) and (5.3), the expressions of the variables around a working point, namely, $Z(x,t) = Z_0(x) + z(x,t)$ and $Q(x,t) = Q_0 + q(x,t)$, and neglecting all the second-order terms (Litrico and Fromion, 2004c). For the Saint-Venant equations (5.1) and (5.2), this yields:

$$B_0 \frac{\partial z}{\partial t} + \frac{\partial q}{\partial x} = 0 \tag{5.4}$$

$$\frac{\partial q}{\partial t} + 2V_0 \frac{\partial q}{\partial x} - \beta_0\, q + \left(C_0{}^2 - V_0{}^2\right) B_0 \frac{\partial z}{\partial x} - \gamma_0\, z = 0 \tag{5.5}$$

with $\gamma_0 = V_0{}^2 \frac{dB_0}{dx} + gB_0 \left[(1+\kappa) S_0 - \left(1 + \kappa - F_0{}^2 (\kappa-2)\right) \frac{\partial Z_0}{\partial x}\right]$, $\beta_0 = -\frac{2g}{V_0}\left(S_0 - \frac{\partial Z_0}{\partial x}\right)$ and $\kappa = \frac{7}{3} - \frac{4S_0}{3B_0 P_0} \frac{\partial P_0}{\partial Z}$, in case Manning equation is used to represent the friction slope S_f.

In (5.4) and (5.5), $F_0 = \frac{V_0}{C_0}$ is the Froude number, P_0 is the wetted perimeter, $C_0 = \sqrt{\frac{gA_0}{B_0}}$ is the water wave celerity and $V_0 = \frac{Q_0}{A_0}$ is the water velocity; all of them evaluated at the operational condition. Using the linearized form, the boundary conditions of the model are now: $q(0,t) = q_i(t)$, $q(\overline{X},t) = \overline{q}_i(t)$, and $z(0,t) = z_i(t)$, $z(\overline{X},t) = \overline{z}_i(t)$.

One way to obtain a solution for this system is applying the Laplace transform and then reordering. This produces the following system of ordinary differential equations in the variable x, with a complex parameter s (the Laplace variable):

$$\frac{\partial}{\partial x} \begin{bmatrix} q(x,s) \\ z(x,s) \end{bmatrix} = A(x,s) \begin{bmatrix} q(x,s) \\ z(x,s) \end{bmatrix} {}^{1} \tag{5.6}$$

with $A(x,s) = \begin{bmatrix} 0 & -B_0(x)s \\ \dfrac{-s + \beta_0(x)}{B_0(x)\left(C_0(x)^2 - V_0(x)^2\right)} & \dfrac{2V_0(x)B_0(x)s + \gamma_0(x)}{B_0(x)\left(C_0(x)^2 - V_0(x)^2\right)} \end{bmatrix}$.

---

[1]In the following any $f(s)$ will correspond to $\mathcal{L}\{f(t)\}$, the laplace transform of $f(t)$, which is a complex-valued function.

Because matrix A depends on the variable x, there is not a closed solution to the differential equation, and therefore, it is necessary to use a numerical integration method to obtain the solution. Only the case where A is not dependent on x has an analytical solution. This special case is called uniform regime and is characterized by having the same water depth and the same water flow throughout a canal.

It has been proven in Litrico and Fromion (2004c) that the problem can be solved numerically very efficiently, if it can be discretized by several "mini uniform regimes problems" in a way as illustrated in figure 5.3.
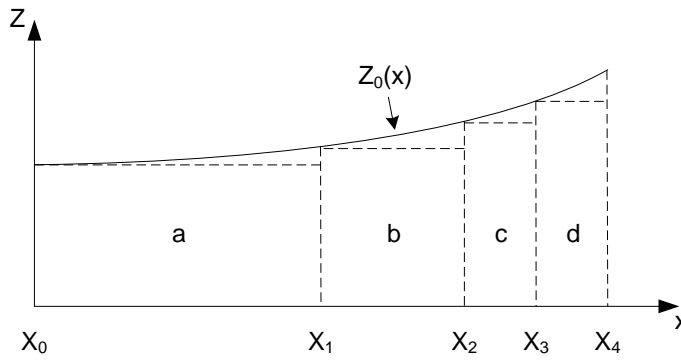
Figure 5.3: Schematic representation of a backwater curve approximated by uniform regimes

Using this approach, the solution of (5.6) is given in the following manner:

$$\begin{bmatrix} q(\overline{X},s) \\ z(\overline{X},s) \end{bmatrix} = \Gamma\left(\overline{X},0\right) \begin{bmatrix} q(0,s) \\ z(0,s) \end{bmatrix} = \begin{bmatrix} \gamma_{11}(s) & \gamma_{12}(s) \\ \gamma_{21}(s) & \gamma_{22}(s) \end{bmatrix} \begin{bmatrix} q(0,s) \\ z(0,s) \end{bmatrix} \tag{5.7}$$

where the transfer function matrix Γ should be calculated using:

$$\Gamma\left(x_n = \overline{X}, x_0 = 0\right) = \prod_{k=n-1}^{0} e^{A\left(x_k,s\right)h_k} \tag{5.8}$$

with $h_k = (x_{k+1} - x_k)$.

It should be noted that the term $e^{A(x_k,s)h_k}$ correspond to the exponential of a matrix (evaluated at x_k), which yields in this case:

$$e^{A\left(x_k,s\right)h_k} = \begin{bmatrix} \dfrac{\lambda_2(s)\,e^{\lambda_1(s)h_k} - \lambda_1(s)\,e^{\lambda_2(s)h_k}}{\lambda_2(s) - \lambda_1(s)} & \dfrac{c\left(e^{\lambda_1(s)h_k} - e^{\lambda_2(s)h_k}\right)s}{\lambda_2(s) - \lambda_1(s)} \\ \dfrac{\lambda_1(s)\,\lambda_2(s)\left(e^{\lambda_2(s)h_k} - e^{\lambda_1(s)h_k}\right)}{c\left(\lambda_2(s) - \lambda_1(s)\right)s} & \dfrac{\lambda_2(s)\,e^{\lambda_2(s)h_k} - \lambda_1(s)\,e^{\lambda_1(s)h_k}}{\lambda_2(s) - \lambda_1(s)} \end{bmatrix} \tag{5.9}$$

where

$$\lambda_{1,2}(s) = \frac{1}{f}\left(as + b \pm \sqrt{cs^2 + ds + e}\right)$$

with

$$a = 2B_0(x_k)V_0(x_k)$$

$$b = \gamma_0(x_k)$$

$$c = 4C_0{}^2(x_k)B_0{}^2(x_k)$$

$$d = 4B_0(x_k)\left(V_0(x_k)\gamma_0(x_k) - \left(C_0{}^2(x_k) - V_0{}^2(x_k)\right)B_0(x_k)\beta_0(x_k)\right)$$

$$e = \gamma_0{}^2(x_k)$$

$$f = 2B_0(x_k)\left(C_0{}^2(x_k) - V_0{}^2(x_k)\right)$$

In the solution expressed by (5.7) using (5.8) and (5.9), s is the laplace variable, $\overline{X}$ is the x position of the end of the transport area (the start of the storage area) and Γ is the transfer function matrix that describes exactly all the input-output relationships of the linearized Saint-Venant equations in the laplace domain. In fact, it is possible with this formula to determine the value of the water flow and of the water depth at $\overline{X}$, by knowing their values at the start of the canal and by knowing the transfer function matrix.

Now, since usually the water depths are the outputs and the water flows the inputs of a hydraulic model, it is convenient to express this matrix relationship in the same manner. This is performed with basic algebraic matrix manipulations to (5.7), which in this particular case yields:

$$\begin{bmatrix} z(0,s) \\ z(\overline{X},s) \end{bmatrix} = \begin{bmatrix} -\dfrac{\gamma_{11}(s)}{\gamma_{12}(s)} & \dfrac{1}{\gamma_{12}(s)} \\ \gamma_{21}(s) - \dfrac{\gamma_{22}(s)\,\gamma_{11}(s)}{\gamma_{12}(s)} & \dfrac{\gamma_{22}(s)}{\gamma_{12}(s)} \end{bmatrix} \begin{bmatrix} q(0,s) \\ q(\overline{X},s) \end{bmatrix} \tag{5.10}$$

With (5.10), the water depth at the beginning and at the end of the transport area depend, in a deterministic manner, on the water flow that enters and that leaves that area. This is the end of the derivation presented in Litrico and Fromion (2004c) to solve the linearized Saint-Venant equations. However, this work aims to extend this linear model to include the influence of the storage at the end of the pool and to consider explicitly the offtake discharge as an independent variable. It is thought that this addition can be carried out in the following way.

To complete the model, it is necessary to linearize the storage equation given by (5.3). Following the same procedure as with the Saint-Venant equations, we obtain:

$$\overline{q}_i(t) - q_{i+1}(t) - q_{L\,i}(t) = \frac{dz_{s\,i}(t)}{dt}A_{s\,i} \tag{5.11}$$

Applying the Laplace transform to (5.11) and replacing it in the expression for $z(\overline{X},s)$ from

(5.10) assuming that $z_{s\,i}(s) \approx z(\overline{X}, s)$, the following equation is obtained after reordering:

$$z_{s\,i}(s) = \frac{\gamma_{21}(s)\,\gamma_{12}(s) - \gamma_{22}(s)\,\gamma_{11}(s)}{\gamma_{12}(s) - s\,\gamma_{22}(s)\,A_{s\,i}}\,q_i(s) + \frac{\gamma_{22}(s)}{\gamma_{12}(s) - s\,\gamma_{22}(s)\,A_{s\,i}}\,(q_{i+1}(s) + q_{L\,i}(s)) \tag{5.12}$$

(5.12) represents a linearized model (directly derived from the Saint-Venant equations) for a reach working around an operational point. It can be seen that the water level of interest $z_{s\,i}$ (the one where water is diverted for irrigation) can be obtained, if the water discharges that enter (q_i) and that exit the reach (q_{i+1} and $q_{L\,i}$) are known. However, in order to obtain the transfer functions that relate those variables, it is necessary to know a considerable amount of information, including the design parameters and the water depths of the reach, all of them at small enough longitudinal discrete positions of the reach (in order to reproduce accurately the characteristics of interest of the reach).

Since the goal of this work is to design an appropriate and simple black-box (without information about physical parameters) modeling procedure for a canal reach, that can fulfill the control automation requirements, this model is not going to be used explicitly. However, it will be used to study the main properties that a simpler model should have and to decide which model structure is more adequate for the purposes established.

5.2.3 Properties of the linearized model

It is extremely important to know the transfer function characteristics of a system (e.g poles, zeros, etc.) for identification and control purposes. However only the uniform regime case has a clear analytical expression that can be analyzed. This is absolutely true, but an analytical expression can always be derived, using the fact that any shape of backwater curve of any type of reach can be well approximated using different number of terms in (5.8).

Using this approach and after some manipulations, it can be conjectured by empirical induction (see Appendix A) that the structure of (5.12) will always be (no matter the reach or the operational condition) of the form:

$$z_{s\,i}(s) = \frac{1}{s}\left(\frac{n_1(s)}{d_1(s)\,d_2(s)}\,q_i(s) - \frac{n_2(s)}{d_2(s)}\,q_{i+1}(s) - \frac{n_2(s)}{d_2(s)}\,q_{L\,i}(s)\right) \tag{5.13}$$

Expression (5.13) has been developed considering that the offtake is located at the end of the reach. However, if the offtake is located in between the pool, a similar structure can be obtained (see also Appendix A):

$$z_{s\,i}(s) = \frac{1}{s}\left(\frac{n_1(s)}{d_1(s)\,d_2(s)\,d_3(s)}\,q_i(s) - \frac{n_3(s)}{d_3(s)}\,q_{i+1}(s) - \frac{n_2(s)}{d_2(s)\,d_3(s)}\,q_{L\,i}(s)\right) \tag{5.14}$$

In (5.13) and (5.14), $n_1(s)$, $n_2(s)$ and $n_3(s)$ are irrational numerator expressions, $d_1(s)$,

$d_2(s)$ and $d_3(s)$ are irrational denominator expressions (all of them include exponentiation and roots of s polynomials) and $\frac{1}{s}$ correspond to an integration in the time-domain (integrator pole).

From model structures (5.13) and (5.14) several conclusions can be drawn. Some of them are the following:

- The existence of an integrator pole (real pole in the origin) denotes that the system is marginally stable. If any of the inputs of the system is excited with a finite impulse input, the output magnitude will be bounded. However, if the system is given a step as an input, the system's output could increase indefinitely. So, this system is not a Bounded-Input Bounded-Output (BIBO) system. For system identification and control designs, this type of systems should be treated with special care; otherwise very bad performance behaviors could appear.

- When the offtake is located at the end of the reach, its transfer function and the one of the discharge that enters the next reach, i.e. the transfer functions of $q_{L\,i}$ and q_{i+1} are identical. That means that for model system identification, it is enough to identify the transfer function of one of them to know the other. However, when the offtake is somewhere else, their transfer functions are different because of their numerators.

- The irrational terms of all the transfer functions imply that an approximation by rational transfer functions (with a Padé approximations for example) would be more or less accurate, depending on the number of terms used to approximate the irrationality. Hence, it is expected that the rational transfer function approximation would have more terms than the irrational original one.

- The denominators of all the transfer functions share common terms. That means that the dynamical responses obtained by the inputs of the models are similar. Technically speaking, the transfer functions of the model have some poles in common.

The appearance of the integrator pole, or in other words, that a reach have similarities with a swimming pool or tank is not a real surprise and is, in some sense, expected. As mentioned before, this pole appears clearly in the uniform case regime and has been successfully included in several simplified models proposed by other researchers (Integrator Delay (ID) model (Schuurmans et al., 1999b), Integrator Delay Zero (IDZ) model (Litrico and Fromion, 2004a), etc.). However, there are some research works that did not include this characteristic in their models. That is why it was found important to go a step forward in the generalization of this feature for any type of reach (slope, cross section, width, length, etc.) working around any flow condition (discharge, backwater curve, etc.).

5.2.4　Characteristics of some type of pools

In addition to the general properties presented above, there are also some particular characteristics that are worth to review. These characteristics are going to be studied, analyzing the Bode diagram (or frequency response) of the downstream water level z_{si} using different discharges for the water inflow q_i as in Litrico and Fromion (2004c).

The Bode diagram is a logarithmic magnitude and phase plot of a transfer function, that gives information of this function evaluated in the s-plane imaginary axis. In a more practical view, it shows what happens with the amplitude and the phase of the response of a system, when it is excited with a sinusoidal input at a given frequency. In this case, the Bode diagram is obtained numerically around a given operational backwater curve (by means of the linearized Saint-Venant equations), calculating the whole matrix product series (5.8) for each frequency point $s = j\omega$ and replacing the results in (5.12).

There is a natural question that arise at this point: why to study the Bode diagram of a pool that is going to be identified?

The answer to this question is the following: there are some pool characteristics that have a direct relationship with some modeling issues. Thus, the Bode diagram can be useful to get an insight into: the required number of parameters when using a linear model structure (model order), the validity range of a particular linear model, the number of models required to cover a given operating range, etc.. For example, a pool exhibiting high resonant peaks in the Bode diagram due to the effect of water waves traveling back and forth through it, requires a model structure with more parameters (higher order) than a pool that does not exhibit this behavior.

Moreover, it is known that operating points of the same pool could exhibit considerable differences in the steady state gain, amount of delay, etc.. All this information can be obtained analyzing the Bode diagram of a pool.

To illustrate these points, two pool configuration are going to be studied: one short flat pool and one long slopping pool.

5.2.4.1　Short flat pools

The Bode diagram of such a pool is presented in figure 5.4 for three different operational discharges, namely $14\,\mathrm{m}^3/\mathrm{s}$, $7\,\mathrm{m}^3/\mathrm{s}$ and $1.75\,\mathrm{m}^3/\mathrm{s}$.

In order to carry out a detailed analysis of the diagram, several areas have been marked (dotted ellipses):

(1) This area shows that in the very long-term, a pool like this acts as a pure integrator (swimming-pool or tank). However, the gain of this integrator varies for different working conditions (in this case the discharge value).
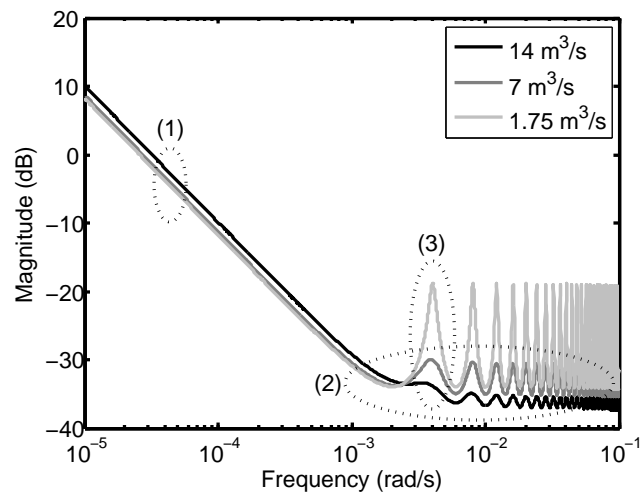
(a) Bode Magnitude
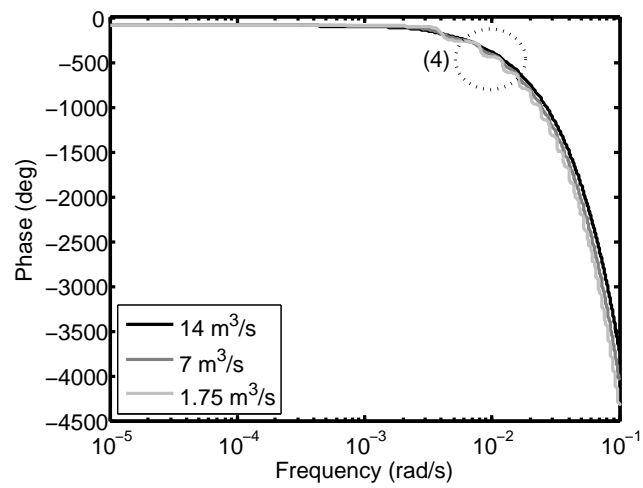
(b) Bode Phase

Figure 5.4: Bode diagram between q_i and $z_{s\,i}$ for short flat pool

(2) The change in the slope of the diagram in this area reveals the appearance of a zero in the transfer function. In this case, this zero is related to the propagation of a shock wave through the pool when there is a change in the water inflow or in the water outflow.

(3) Each oscillation in this diagram denotes the existence of a resonant mode. That means that the water depth of this type of pools have a natural tendency to oscillation. However, the magnitude and frequency of this oscillations vary depending on the discharge and on the water level. These resonant modes have a close relationship with the shock-waves traveling back and forth through the pool. As a matter of fact, they occur approximately at a frequency equal to the time that takes the shock wave to go and return from one extreme of the pool to the other.

(4) A decreasing curve in the phase margin reveals the existence of a delay between the input and the output of a system. In this case, the time that takes a discharge change at the beginning of the pool to modify the downstream water level. The amount of delay also changes for different discharge values and water level conditions.

5.2.4.2 Long slopping pools

A typical Bode diagram of this type of pools is presented in figure 5.5 for three different operational discharges, namely $80\,\mathrm{m^3/s}$, $40\,\mathrm{m^3/s}$ and $10\,\mathrm{m^3/s}$.

The result of the analysis of the dotted areas of this Bode diagram is given below:

(1) This zone shows the integral part of the behavior. Hence, this system also resembles a water tank under certain conditions. As expected, this behavior appears in the long-term response, but the integral gain changes with the discharge or the water level.

(2) This area shows some changes in the slope of the diagram. First, there is an increment in the slope attributable to the presence of another pole. Finally, the curve rises because of the presence of some zeros in the system. The whole set models the presence of a shock-wave when changing the water inflow. This shock-wave travels through the whole pool until arriving to the end of the pool. The distortion of this shock-wave through the way is also determined by this zone of the diagram.

(3) This type of pools does not develop resonant modes in the frequency response. That means that the shock waves that arrive to the end of the pool are not reflected back.

(4) The decreasing curve in the phase margin is an evidence of the existence of delay in the system. As a matter of fact, the frequency were the phase is $360°$ is the inverse of the delay in seconds. Thus, the deviation of these curves for different discharges show variations of the delay for different discharge conditions.
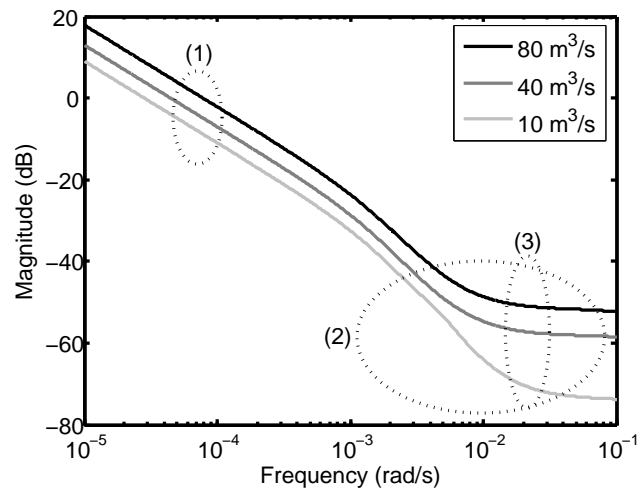
(a) Bode Magnitude
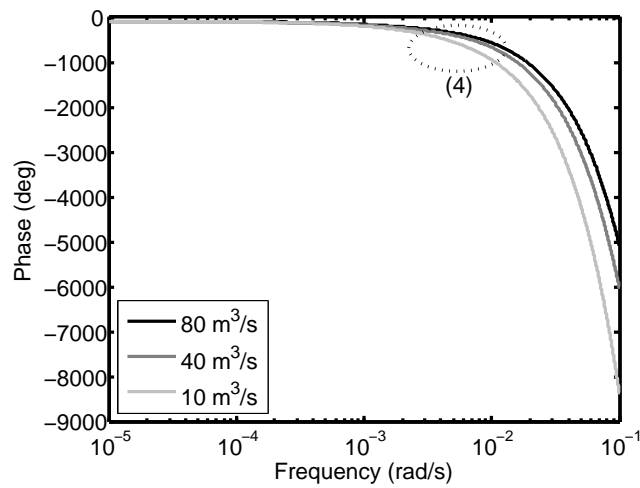
(b) Bode Phase

Figure 5.5: Bode diagram between q_i and $z_{s\,i}$ for long slopping pool

5.2.4.3 Discussion

It has been seen that the characteristics of a system like a pool depend on its particular design and on the water flow operational conditions.

All of them act as a simple integrator with delay in the long-term, but the integral gain and the amount of delay depend on the particular discharge that is passing through the pool.

Pools with small slopes have a natural tendency to oscillation, because of the continuous reflections of the shock waves that appear as consequence to discharge variations. This happens when the backwater covers the entire length of the pool. Consequently, pools with high slopes doesn't experience this type of phenomenon. The magnitude of this oscillations depend also on the discharge that is passing through the pool.

The length of the pool is also an important variable. Definitely, the delay augments with length, but more length also damps the oscillatory behavior of the pool.

In addition to the variables considered above, other like: friction, width, cross section, etc. also modify in less degree the hydraulic response of a pool.

5.2.5 About modifying the model to include gate equations or other structures

There are occasions when it is desired that a pool model includes the dynamical characteristics of hydraulic structures like undershot gates, overshoot gates, weirs or others. This task can be accomplished by taking (5.13) or (5.14) and replacing the respective discharge with the adequate structure equation. In order to preserve the linearity of the model, this equation should also be linear. When this is not the case, it is always possible to linearize the hydraulic structure equation around a working point. However, this approach changes the properties and dependencies of the original pool model. Next, some typical examples are presented.

Assuming that a general way to write (5.13) and (5.14) is:

$$z_{s\,i}(s) = \frac{1}{s}\left(F1(s)\,q_i(s) - F2(s)\,q_{i+1}(s) - F3(s)\,q_{L\,i}(s)\right) \tag{5.15}$$

the following models can be obtained:

- Overshoot gates (Z: water Level, O: gate Position) (see figure 5.6)

       Equation: $Q = C_d\,b\,\sqrt{2g}(Z - O)^{3/2}$

       Linearized equation: $q = c_1\,o + c_2\,z$

       Model structure: $z_{s\,i} = \dfrac{F1\,(c_1\,o_i + c_2\,z_{s\,i-1}) - F2\,c_3\,o_{i+1} - F3\,q_{L\,i}}{s + c_4\,F2}$
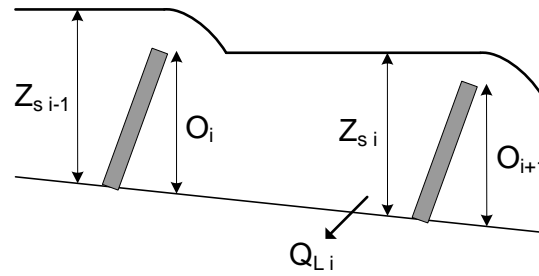
Figure 5.6: Pool with overshoot gates

- Undershoot gates (Ferro) (l: gate opening) (see figure 5.7)

(a) Free flow condition

(b) Submerged flow condition
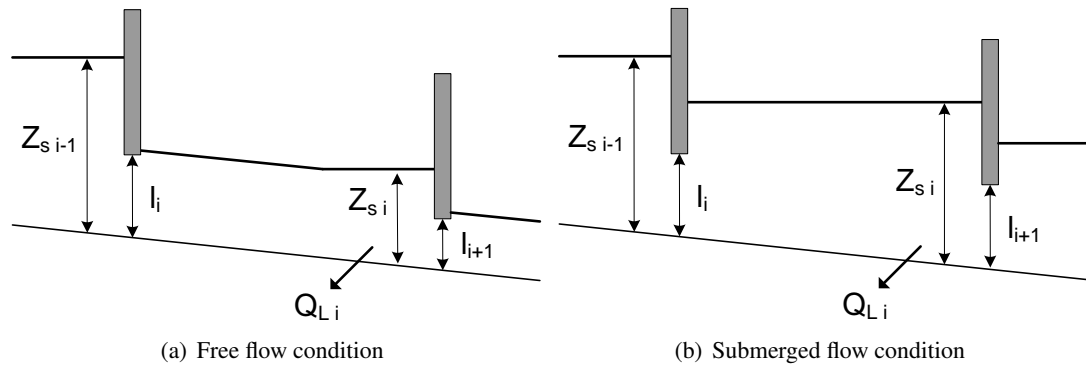
Figure 5.7: Pool with undershoot gates

Free Flow equation: $\qquad Q = b \sqrt{g \left(l\, k_0 \left(\dfrac{h_1}{l} \right)^{k_1} \right)^3}$

Submerged Flow equation: $\qquad Q = b \sqrt{g \left(l\, k_0' \left(\dfrac{h_1 - h_3}{l} \right)^{k_1'} \right)^3}$

FF Linearized equation: $\qquad q = c_1\, \delta l + c_2\, \delta h_1$

SF Linearized equation: $\qquad q = c_1\, \delta l + c_2\, \delta h_1 + c_3\, \delta h_3$

FF Model structure: $\qquad z_{s\,i} = \dfrac{F1 \left(c_1\, \delta l_i + c_2\, z_{s\,i-1} \right) - F2\, c_3\, \delta l_{i+1} - F3\, q_{L\,i}}{s + c_4\, F2}$

SF Model structure: $\qquad z_{s\,i} = f \left(z_{s\,k}, \delta l_k \right),\ k = 1, 2 \ldots, N$

- Rectangular weir offtake (Z: water level, O: weir height) (see figure 5.8)
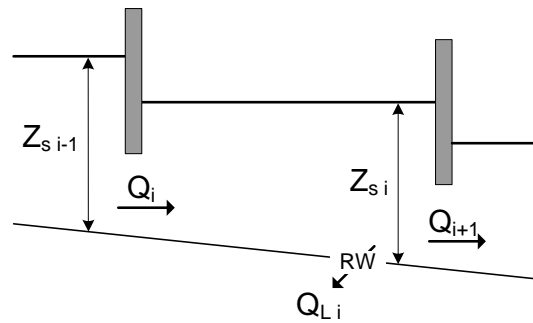
Figure 5.8: Pool with rectangular weir

Equation: $Q = C_d\, b\,(Z - O)^{3/2}$

Linearized equation: $q = c_1\, z$

Model structure: $z_{s\,i} = \dfrac{1}{s + c_1\, F3}\,(F1\, q_i - F2\, q_{i+1})$

In general and as the examples show, the inclusion of any hydraulic structure in the model cancels the integrator pole (these structures perform an output feedback in a natural manner). So, the model is no longer marginally stable: it is an absolutely stable model. However, this approach has two main drawbacks:

1. The number of variables and complexity of the pool model increases drastically.

2. The model inaccuracy increases because of the truncation error when linearizing the hydraulic equations of the structures.

To clarify the first point it is necessary to pay good attention to the input variables of the models. All the equations use water levels of other pools as inputs. These are output variables and should be replaced in order to obtain water levels as functions of gate openings or discharges only. Particularly, models with weirs, overshoot gates and undershoot gates working in free flow use recursively all downstream water levels $z_{s\,k}$. As a result, a particular pool model becomes a function of gate openings l_k, gate positions o_k or discharges of this and all the upstream pools ($k = 0, 1, \ldots, i$). Moreover, pool models with undershoot gates working in the submerged flow condition use variables of the whole canal for a single pool.

The second point needs less explanation. The original structure equations are highly non-linear and their linearization do not always give good results, specially when using equations of more accuracy than the ones used in this section (see Chapter 4).

These two points involve some other issues. For example, the linear system identification that is going to be performed in the next sections would be more complex and less accurate if the

discharges are not considered directly in the model. It is considered better, in the philosophy of this work, to identify each pool model using experimental data without considering the hydraulic structures. The structures can later be included if needed, using the original nonlinear equations or direct linearizations of them.

So, because of the reasons explained before, the next sections are going to focus only on the identification of discharge - water level pool models.

5.3   System identification of a pool

System Identification allows to build mathematical models of dynamic systems based on measured data, by adjusting parameters within a given model, until its output matches the measured output as good as possible.

Although system identification techniques apply to very general models, the most common models are difference equations descriptions.

In the next sections, the main aspects of the identification of a reach are treated, in order to obtain an appropriate discrete-time model.

5.3.1   Discrete-time modeling issues

Continuous-time models and controllers are not directly implementable on digital computers, which require signals changes only at discrete time instants. For this reason, in most situations, it is a general practice to use discrete-time models or difference equations. However, the choice of an adequate sampling time and a discrete system identification strategy is not trivial.

This section emphasizes some aspects that should be taken into account to obtain a good discrete-time model of a canal reach.

5.3.1.1   Sampling time

The sampling frequency or sampling rate defines the number of samples per second taken from a continuous signal to make a discrete signal. The inverse of the sampling frequency is the sampling period or sampling time, which is the time between samples. Once decided, the model will only work with data collected exactly at that particular rate. In order to identify a black-box model from a data set, the time between samples should also be the same as the one of the intended model. Generally, it is also recommended to sample faster than needed to filter the noisy components introduced by the measurement system and then create a filtered data set at the chosen sampling frequency.

To choose the length of the sampling time, it is very important to review some theoretical and practical recommended rules related to this subject:

- The Nyquist-Shannon sampling theorem states that the sampling frequency has to be, at least, twice the bandwidth of the signal being sampled. That means that the speed of sampling should be at least twice the speed of the fastest dynamic of the system to be sampled. The rule of thumb is to choose the sampling frequency between 6 and 25 times the bandwidth frequency.

- On the other hand, from the System Identification research area, it is known that a very fast sampling leads to numerical problems, model overfitting in high frequency bands

and poor returns for extra work (for example models with a huge amount of parameters) (Ljung, 1999). As the sampling interval increases over the natural time constants of the system, the variance of the estimated model parameters increases drastically. For system identification purposes, optimal choices of the sampling period for a fixed number of samples would lie in the range of the time constants of the system. These are, however, not exactly known and overestimating them may lead to very bad results. All these aspects recommend a sampling frequency that is about ten times the bandwidth of the system. In practice it is useful to first record a step response from a system, and then select the sampling interval so that it gives 4-6 samples during the "rise time" (time required to go from 10 to 90 percent of the final value).

- Additionally, if the model is going to be used for control purposes, several other aspects should be considered:

  - Generally, the sampling interval for which the model is build should be the same as the one in the control application (to avoid the recalculation from one sampling interval to another).

  - A too fast sampled model will often be non-minimum phase (there are unstable zeros in the transfer function).

  - A system with dead time may be modeled with delay of many sampling periods.

Such effects may cause problems for some control design techniques. On the other hand, depending on the particular process and the control strategy used, it is necessary to have more information on a certain band of frequencies than in others, having to choose the sampling frequency so as to maximize the accuracy in that region. For example, many frequency domain control techniques need an accurate representation of the frequency response at the gain crossover frequency, because of its relation with the maximum achievable "acceleration" of the closed loop system (plant+controller in feedback) before reaching instability. Another common design recommendation is to focus on the cutoff frequency ($-3\,\mathrm{dB}$ of input attenuation) of the desired frequency response for the closed loop system.

As it can be seen, in order to choose a correct sample time for a control model, it is necessary to know, a priori, the main dynamical characteristics of the system and then apply any appropriate rule with more or less care depending on each case.

To have a little insight of the difficulties that can arise when choosing the sampling time for a pool, an example is presented next.

Figures 5.9 and 5.10 show the step response and the Bode diagram of a pool with characteristics given by table 5.1.

Table 5.1: Reach's Characteristics

Characteristic	Value
Pool length	3000 m
Bottom slope	0.002 m/m
Bottom width	7 m
Pool shape	trapezoidal
Side slope	1.5 m/m
Manning's n	0.014
Operational flow	$10\,\mathrm{m}^3/\mathrm{s}$
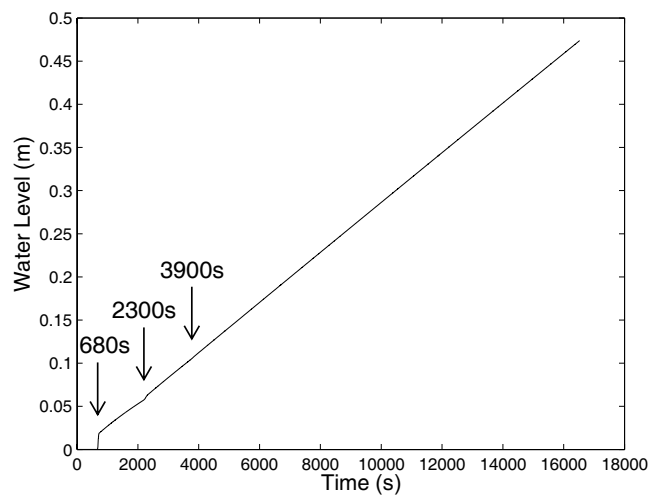
(a) Downstream water level response
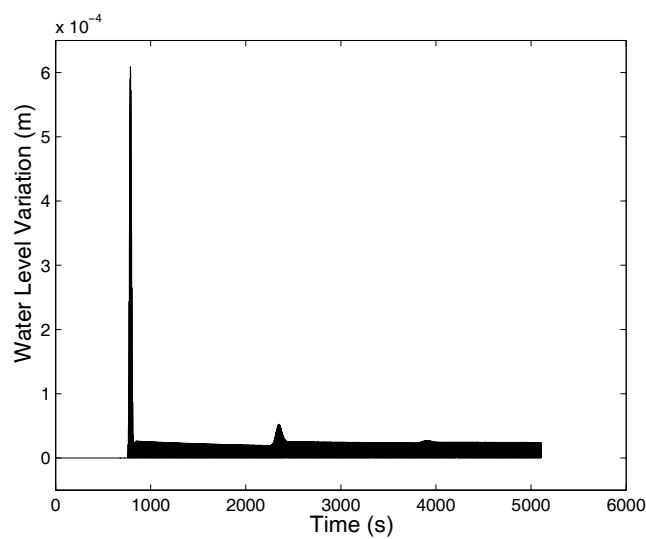
(b) Derivative of the water level response

Figure 5.9: Water level response for an inlet flow step change for the reach of table 5.1
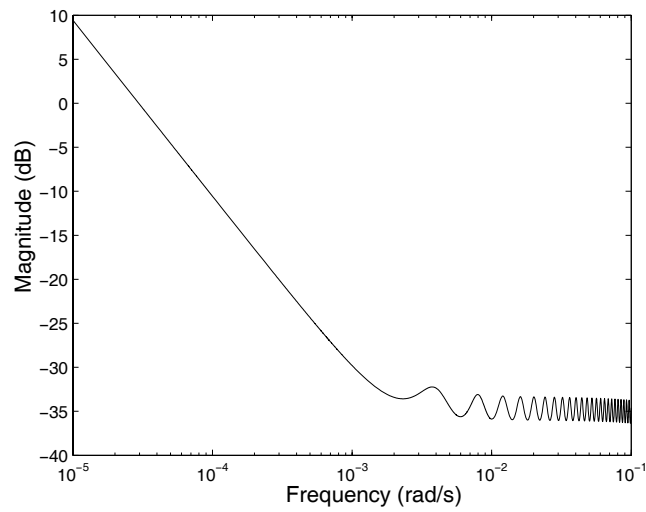
(a) Bode Magnitude
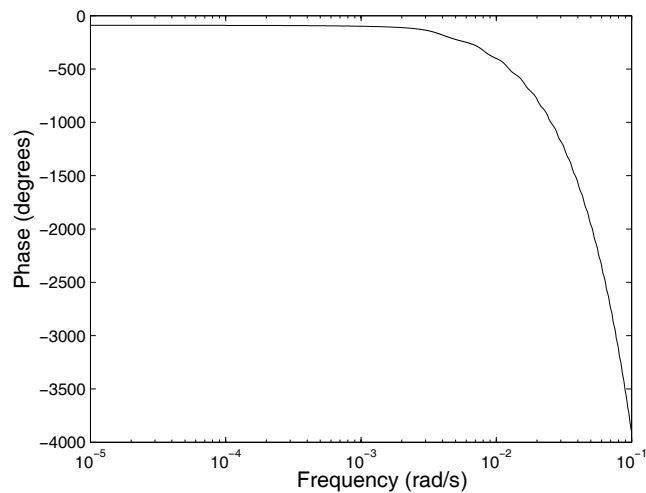
(b) Bode Phase

Figure 5.10: Bode diagram between q_i and $z_{s\,i}$ for the reach of table 5.1

The step response is obtained simulating, in a Saint-Venant based model, the downstream water level produced by a step increment in the inflow of this pool, maintaining the outflow constant.

The time history of the step response and the Bode diagram (obtained as in Section 5.2.4) for this particular configuration are presented next.

First of all, figure 5.9 shows that after the inflow change, there is a delay of approximately 680 seconds until noticing a change in the water level. At that time, a step increment occurs in the water level. Then, the level rises with a variable slope (including a big sudden slope change at time $2300\,s$) until time 4000 seconds. At that time the water level continue infinitely raising at a constant rate.

Looking in detail at the step response obtained, one can conclude that there are water level

variations (for example the first increment at 680 seconds) that, in order to be accurately reproduced, require the use of a very small sampling period. That would be the only way to sample the dynamical change with at least 4 points as recommended before. However, the variations do not have a clear and predictable tendency until time 4000 seconds. A linear discrete model that has to approximate this transient behavior with a so short sampling period, would have a great amount of parameters. So, a trade off should be made in the selection of the sampling period between accuracy and model complexity, having in mind all the possible control design and numerical problems discussed before.

The Bode diagram of figure 5.10 reveals that the linearized model has poles from very low to very high frequencies, standing out the dominance of the pole at the origin (integrator pole) as derived in Section 5.2.3. This is due to the resonant modes of the pool.

The existence of poles in an infinite range of frequencies shows that it is impossible to reproduce the exact dynamical behavior of the system by sampling it, because of the fact that the sampling frequency should lie 10 times away from the highest frequency present in the system. The only possibility is to approximate a smaller frequency band, i.e. to loose some fast changing dynamics. If this is the case, it is very important to remember that an approximation covering frequencies above the first resonant frequency, would need an exponentially increasing number of parameters.

After this analysis, a good choice for this particular case is a sampling time close to 221 seconds. It was selected having in mind the time needed by the water level to achieve a fixed course divided by 15:

$$\frac{4000\,\text{s} - 680\,\text{s}}{15} = 221\,\text{s}$$

With this sampling time, a correctly obtained linear model should be able to:

1. Reproduce the general tendency of the response properly.

2. Cover at least the first resonant modes.

3. Approximate the response at the gain crossover frequency.

4. Have a delay made up of few sampling times (in this case 3), to facilitate the control design and avoid possible performance problems.

Nevertheless, it is still probable that the model has unstable zeros making the model to have a non-minimum phase behavior. Unstable zeros can arise if the sampling time does not divide the delay period exactly.

In conclusion, the choice of the sampling period should always be taken thinking in the particular system dynamics and in the intended purpose, using all the design knowledge at hand.

This way of proceeding is indispensable to attain a linear model with the ability to adequately reproduce the hydraulic behavior of a pool.

5.3.1.2 Discrete transfer functions

It is important to remark that a discrete-time model will never be the same as a continuous one; it will only be an approximation to a model with similar characteristics, despite the technique used.

In general, a discrete-time representation can be viewed as the z-transform of the discrete-time impulse response of a system for a given sample time. In this case, transforming the continuous models (5.13) or (5.14) into a z-transform model would give:

$$z_{s\,i}(z) = F1(z)\,q_i(z) - F2(z)\,q_{i+1}(z) - F3(z)\,q_{L\,i}(z) \tag{5.16}$$

where z is the z-transform complex variable.[2]

The model given by (5.16) still maintains some characteristics of the continuous one. For example, it is also applicable to any type of reach. In addition, there are two aspects that have a direct correspondence in the discrete-time representation:

1. Any Laplace domain pole will have a direct counterpart in the z-transform domain with the relation given by $p_z = e^{p_s T}$, where p_s is the pole in the Laplace domain, T is the sampling period and p_z is the discrete-time pole. Because of this, the pole at $s = 0$ (integrator pole) of $\frac{1}{s}$ will produce always a discrete-time pole at $z = 1$ (discrete-time integrator pole); that means that a term $\frac{1}{z-1}$ will always appear in the z-transform of the model.

2. The time delays between the inputs (water discharges) and the output (water level) of the continuous time model will satisfy the following property:

$$\mathcal{Z}\left\{f(k-d)\right\} = z^{-d}F(z)$$

where $f(k-d)$ is the delayed discrete-time impulse response of the model, k is the discrete time instant variable, d is the delay expressed in amount of instants and z is the z-transform variable. This implies that the z-transform model (5.16) will always appear in the following manner:

$$z_{s\,i}(z) = z^{-d_1}F1'(z)\,q_i(z) - z^{-d_2}F2'(z)\,q_{i+1}(z) - z^{-d_3}F3'(z)\,q_{L\,i}(z) \tag{5.17}$$

---

[2]In the following any F(z) will correspond to $\mathcal{Z}\left\{f(kT)\right\}$, the Laplace transform of a sampled time function $f(kT)$ (called z-transform), with $k = 0, 1, 2, \ldots$ the sampling instant and T the sampling period. Besides for notation simplicity $f(kT)$ will normally be written as $f(k)$ only.

where d_1, d_2 and d_3 are the time periods, measured in discrete time instants, that takes each discharge to influence the downstream water level.

Point 1 presents a property that have to be taken with care in order to avoid possible modeling problems. Dynamically and numerically it is very difficult to identify a discrete-time model with a pole exactly located at $z = 1$. The problem is that a small variation in its position leads to a completely different dynamical behavior. For instance, a pole at $z = 1.01$ would produce an unstable model, i.e. the model output can go quickly to the infinite for finite input values. Conversely, a pole at $z = 0.99$ would produce a strictly stable model, whose response will always be bounded.

There are three approaches normally taken with respect to this problem when estimating a model by means of system identification:

1. To forget about the problem and obtain a model anyway.

2. To identify a model and afterwards correct the position of the pole in the estimated model.

3. To acknowledge the existence of the pole and apply its influence directly to the data in order to identify the other components of the model. This can be achieved in any of the two following ways:

$$
y(z) = F(z)u(z) = \left[\frac{1}{z-1} F'(z) \right] u(z)
$$
$$
\Rightarrow \begin{cases} y(z) &= F'(z) \left[\frac{1}{z-1} u(z) \right] &= F'(z)u'(z) \\ y'(z) &= y(z)(z-1) &= F'(z)u(z) \end{cases} \tag{5.18}
$$

The first way is generally more recommendable (especially in the presence of noise) and is equivalent to make a cumulative sum of the input data. The second way correspond to a differentiation of the output data. Unfortunately, both procedures modify the frequency characteristic of the original input signal. As a consequence, a maximally informative input signal specially designed to identify a model would lose it optimal properties.

From the three approaches presented above, 2 and 3 are the better ones. However, 3 has an additional drawback when modeling reaches; this procedure applied to large sample periods can induce long-term modeling bias errors. Therefore, the second option of identify and then correct would be the recommended one. This method is not always easy to apply to some discrete-time model structures. Moreover, there are some types of model structures that cannot deal with processes with integrators. For those cases the only choice is 3.

5.3.2 Discrete-time model structures

Generally, linear discrete-time models can be divided into three main classes:

Discrete transfer function models: Models based only on the input-output characteristics of a system by means of the z-transform.

Discrete state-space models: Time-domain models that incorporate all the information about the internal dynamics of a system.

Orthonormal basis models: Models that make use of the special approximation properties of some basis functions to mathematically represent systems.

Depending on the particular class and structure chosen, there are different types of parameter estimation methods. Examples of types of parameter estimation methods are Subspace methods for estimating state-space models, Prediction Error methods and Output Error methods for estimating transfer function models, etc.. These methods can estimate the parameter values of a model from only an enough informative data set collected from the true system.

In this section, only two model structures for modeling pools are going to be considered:

1. The Auto-Regressive with eXogenous Input (ARX) model, a transfer function based model.

2. The Laguerre model, an orthonormal basis based model.

The chosen models can only have a finite number of rational elements. This option has been taken despite the fact that the process is governed by irrational transfer functions. An approximation like this can be carried out because an irrational term can generally be approximated by a linear combination of rational ones, like in a Padè approximation of a function. However, depending on the particular irrational term, a good approximation can require a high number of rational terms to achieve good results.

In the following, all model parameters are going to be estimated using standard least-squares based algorithms.

The mathematical formulation of the ARX and Laguerre discrete-time pool models are explained in detail in the next sections.

5.3.2.1 ARX model

To derive the ARX model, it is first necessary to introduce the forward shift operator q and the backward shift operator q^{-1} respectively as:

$$qf(k) = f(k+1), \quad q^{-1}f(k) = f(k-1)$$

Then, assuming that $F1'(z)$, $F2'(z)$ and $F3'(z)$ of (5.17) can be approximated by quotients of polynomials in the following way:

$$F1'(z) = \frac{B1(z)}{A(z)}, \quad F2'(z) = \frac{B2(z)}{A(z)}, \quad F3'(z) = \frac{B3(z)}{A(z)}$$

with

$$A(z) = 1 + a_1 z^{-1} + \ldots + a_{na} z^{-na}$$
$$B1(z) = b1_1 + b1_2 z^{-1} + \ldots + b1_{nb1} z^{-nb1+1}$$
$$B2(z) = b2_1 + b2_2 z^{-1} + \ldots + b2_{nb2} z^{-nb2+1}$$
$$B3(z) = b3_1 + b3_2 z^{-1} + \ldots + b3_{nb3} z^{-nb3+1}$$

and replacing in (5.17), that yields after reordering:

$$A(z) z_{s\,i}(z) = z^{-d_1} B1(z) q_i(z) - z^{-d_2} B2(z) q_{i+1}(z) - z^{-d_3} B3(z) q_{L\,i}(z)$$

Finally, after applying the inverse z-transform to move the problem back in the time domain, the general model structure is:

$$A(q) z_{s\,i}(k) = B1(q) q_i(k - d_1) - B2(q) q_{i+1}(k - d_2) - B3(q) q_{L\,i}(k - d_3) \qquad (5.19)$$

with

$$A(q) = 1 + a_1 q^{-1} + \ldots + a_{na} q^{-na}$$
$$B1(q) = b1_1 + b1_2 q^{-1} + \ldots + b1_{nb1} q^{-nb1+1}$$
$$B2(q) = b2_1 + b2_2 q^{-1} + \ldots + b2_{nb2} q^{-nb2+1}$$
$$B3(q) = b3_1 + b3_2 q^{-1} + \ldots + b3_{nb3} q^{-nb3+1}$$

As can be seen, the parameters of the ARX model (5.19) are: the polynomial orders na, $nb1$, $nb2$ and $nb3$, the polynomial coefficients, and the a priori known time delays d_1, d_2 and d_3 expressed in sampling instants. Once the parameters are determined, this model can calculate the downstream water level $z_{s\,i}$ at instant k by a weighted sum of measurement data from past instants. Specifically, the historical data that is needed are the water levels $z_{s\,i}$ and the water discharges q_i, q_{i+1} $q_{L\,i}$, collected at a sampling interval T.

In some sense it is a little bit restrictive to force the three transfer functions, namely $\frac{B1(z)}{A(z)}$, $\frac{B2(z)}{A(z)}$, and $\frac{B3(z)}{A(z)}$ to have the same denominator polynomial $A(z)$. From (5.13) or (5.14) it is noticeable that they do not have really the same denominator. However, (5.13) or (5.14) show

in the same way that their transfer functions share some poles. Therefore, the assumption is not totally wrong. The reason for using the same denominator polynomial $A(q)$ have its roots in simplifying the parameter estimation process, because in that way it can be performed using a linear least squares approach.

This model can be applied to stable and unstable processes so, as mentioned before, there are two options in relation to the integrator parameter estimation problem. One is to estimate the model parameters and then fix the integrator pole location. This can be done following this procedure:

1. To perform the parameter estimation process obtaining $A(q)$, $B1(q)$, $B2(q)$ and $B3(q)$.

2. To calculate the roots of $A(q)$.

3. To replace the root of $A(q)$ that is close to 1 by exactly a 1.

4. To form a new $A(q)$ polynomial keeping the other roots locations.

The second option is:

1. To apply the cumulative sum on each input variable (discharges).

2. To estimate the model polynomials $A(q)$, $B1(q)$, $B2(q)$ and $B3(q)$.

3. To multiply the estimated $A(q)$ polynomial by $(1 - q^{-1})$.

5.3.2.2 Laguerre model

This model is based on the Laguerre functions, a complete orthonormal set of functions in $L_2(0, \infty)$, the space of square Lebesgue integrable functions in the $(0, \infty)$ interval (Zervos and Dumont, 1988). These functions are described in the time domain by:

$$l_i(t) = \sqrt{2p} \frac{e^{pt}}{(i-1)!} \frac{d^{i-1}}{dt^{i-1}} \left[t^{i-1} e^{-2pt} \right]$$

where i is the order of the function ($i \geq 1$) and p is a positive parameter. The laplace transform of the Laguerre functions produces rational functions in the s variable of the following form:

$$L_i(s) = \sqrt{2p} \frac{(s-p)^{i-1}}{(s+p)^i}$$

By using a linear combination of a truncated number of these functions, any impulse response (or its associated transfer function) that belongs to the intersection of $L_1(0, \infty) \cap L_2(0, \infty)$, can be approximated as follows:

$$f(t) = \sum_{i=1}^{N} c_i \, l_i(t) = \mathbf{c}^{\mathrm{T}} \mathbf{l} \qquad F(s) = \sum_{i=1}^{N} c_i \, L_i(s) = \mathbf{c}^{\mathrm{T}} \mathbf{L}$$

$$\mathbf{c}^{\mathrm{T}} = \begin{bmatrix} c_1 & c_2 & \cdots & c_N \end{bmatrix}$$

$$\mathbf{l}^{\mathrm{T}} = \begin{bmatrix} l_1(t) & l_2(t) & \cdots & l_N(t) \end{bmatrix}$$

$$\mathbf{L}^{\mathrm{T}} = \begin{bmatrix} L_1(s) & L_2(s) & \cdots & L_N(s) \end{bmatrix}$$

A discrete-time state-space version of this model can be obtained by applying a continuous network compensation method to each transfer function (Zervos and Dumont, 1988). The result of this operation yields:

$$\begin{aligned} \mathbf{l}(k+1) &= \mathbf{A}\,\mathbf{l}(k) + \mathbf{B}\,u(k) \\ y(k) &= \mathbf{c}^{\mathrm{T}}\,\mathbf{l}(k) \end{aligned} \tag{5.20}$$

where $\mathbf{l}(k)$ is the state vector of order N, $u(k)$ is the system input and $y(k)$ is the system output. In addition, if T is the discrete sampling time, $\mathbf{A}$ and $\mathbf{B}$ can be defined as:

$$\mathbf{A} = \begin{bmatrix} \tau_1 & 0 & \cdots & 0 \\ \dfrac{-\tau_1\tau_2 - \tau_3}{T} & \tau_1 & \ddots & \vdots \\ \vdots & \ddots & \ddots & 0 \\ \dfrac{(-1)^{N-1}\tau_2^{N-2}\left(\tau_1\tau_2 + \tau_3\right)}{T^{N-1}} & \cdots & \dfrac{-\tau_1\tau_2 - \tau_3}{T} & \tau_1 \end{bmatrix}$$

$$\mathbf{B}^{\mathrm{T}} = \begin{bmatrix} \tau_4 & \left(-\dfrac{\tau_2}{T}\right)\tau_4 & \cdots & \left(-\dfrac{\tau_2}{T}\right)^{N-1}\tau_4 \end{bmatrix}$$

with $\tau_1 = e^{-pT}$, $\tau_2 = T + \frac{2}{p}(\tau_1 - 1)$, $\tau_3 = -T\tau_1 - \frac{2}{p}(\tau_1 - 1)$ and $\tau_4 = \sqrt{2p}\frac{(1-\tau_1)}{p}$.

Making use of the Laguerre model structure for a pool, the particular model gives:

$$\begin{aligned} z_{s\,i}(k) &= \mathbf{c1}^{\mathrm{T}}\left[\mathbf{A1}\,\mathbf{l1}(k-1) + \mathbf{B1}\,q_i(k-1)\right] \\ &\quad - \mathbf{c2}^{\mathrm{T}}\left[\mathbf{A2}\,\mathbf{l2}(k-1) + \mathbf{B2}\,q_{i+1}(k-1)\right] \\ &\quad - \mathbf{c3}^{\mathrm{T}}\left[\mathbf{A3}\,\mathbf{l3}(k-1) + \mathbf{B3}\,q_{L\,i}(k-1)\right] \end{aligned} \tag{5.21}$$

In this type of model, the model output is obtained with just the inputs and the Laguerre functions values at time $k-1$ (always known for a particular p).

The parameters of the Laguerre-based model (5.21) are the vectors of coefficients $\mathbf{c1}$, $\mathbf{c2}$ and $\mathbf{c3}$; the designer-chosen number of Laguerre functions N and the Laguerre pole value (p) for each transfer function (to calculate $\mathbf{A1}$, $\mathbf{A2}$, $\mathbf{A3}$ and $\mathbf{B1}$, $\mathbf{B2}$, $\mathbf{B3}$). It is not necessary an a priori knowledge on the process orders or on any delay and the response produced by each input can be adjusted in a totally independent manner. On the other hand, for increasing complexity transfer functions, it is necessary a higher number of terms.

This model can not approximate systems that are not strictly stable. Hence, there is only one way to identify the model in this case:

1. To apply the cumulative sum (5.18) on each input variable (discharges).

2. To estimate the model parameters **c1**, **c2** and **c3**.

3. To augment the state-space representation in order to include the integrator.

5.3.3 Experiment design: Input signal

An input signal should excite a system with a rich frequency content, in order to successfully identify a model of a true real system. A rich frequency content means that the input signal can be decomposed into many frequencies of similar magnitude. In practice, it is appropriate to decide first upon which is the frequency band where it is important to have information about the system and then select a signal that has a more or less flat spectrum over it.

Such an input is provided by the Pseudo Random Binary Sequence (PRBS) signal (Biala-siewicz, 1995). The sequence is generated by a digital waveform generator, which produces a binary signal by switching randomly between two output levels (a, $-a$). It owes its name "pseudo-random" to the fact that it is characterized by a sequence length within which the pulse width varies randomly, while it is periodic over a large time period.

The PRBSs are generated by means of shift registers with feedback (implemented in hardware or software). The period is defined by the maximum sequence length:

$$L = 2^N - 1 \tag{5.22}$$

where N is the number of stages of the shift register. As an example, a fragment of a PRBS signal is presented in figure 5.11.

Assuming that $u(k)$ is a random binary process with a current value of a or $-a$ and that the value of $u(k)$ can change every T_{prbs} seconds, namely T_{prbs} is the switching period, the corresponding spectral density of the signal is:

$$S_{uu} = \frac{a^2}{\pi} \frac{T_{prbs}}{2} \left(\frac{\sin\left(\omega T_{prbs}/2\right)}{\omega T_{prbs}/2} \right)^2 \tag{5.23}$$

The spectral density function (5.23), can be assumed to be approximately flat up to a frequency about $0.3 f_{prbs} \, \mathrm{rad/s}$. If f_{prbs} is sufficiently high (as compared to the bandwidth of a plant to be identified), then the random binary process has a spectrum corresponding to a broad-band noise.

The spectrum of the pseudo-random binary signal is therefore an approximation of a broad band noise, provided that its clock frequency and its sequence length is large enough. However, there are two thinks to satisfy in order to enjoy the good properties of this signal:
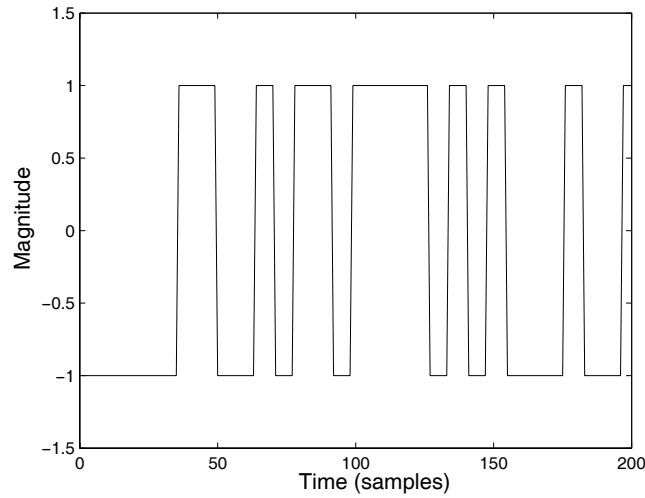
Figure 5.11: PRBS Test Signal

- One should work with an integer number of periods; that means: length$\{u(k)\} = nL$, with $n = \{1, 2, \ldots\}$. Usually one period of the signal meets the needs of the identification procedure.

- The amplitude of the signal a must ensure a good signal-to-noise ratio; normally ten times greater than the noise amplitude.

Additionally, in order to correctly identify the steady-state gain of the process, the duration of at least one of the pulses in the PRBS must be greater than stabilization time of the process. As the maximum duration of a pulse is NT_{prbs}, N and T_{prbs} have to be chosen to adequately cover that time period.

As can be seen, if the PRBS sampling period T_{prbs} is chosen equal to a well-chosen process sampling period T_s (see Section 5.3.1.1), the only way to augment the maximum duration of a pulse is increasing the number of registers N. However, higher values of N lead to very large signal sequences, increasing the experiment duration and the data length; e.g. $N = 10$ produces a sequence length of 1023 data points, when $N = 12$ produces a sequence length of 4095 data points. In that case it is useful to choose the PRBS sampling period T_{prbs} to be a multiple of the process sampling period T_s: $T_{prbs} = pT_s$. The problem of this approach is that reduces the frequency range corresponding to a constant spectral density, so usually p is chosen to be $p \leq 4$.

From a system identification point of view, the data length should range normally from 200 to 1000 data points, in order to have reliable values of the model parameters and less computational burden.

On the other hand, the proposed models are supposed to work only around an operational point of a pool. In order to have locally rich data, all movements induced to the system should be maintained sufficiently small. For normal systems this can be accomplished choosing a small

enough PRBS amplitude a. However, in this case where the system behaves like an integrator, it is additionally convenient to keep the experiment duration as short as possible to avoid letting the system to go to far away from the working point.

5.3.4 Parametric identification

System identification can be defined as the process of obtaining a model based on the plant input and output data. If a particular model structure is assumed, the identification problem is reduced to compute the parameters of the model. The usual way to calculate the parameters is finding the minimum of a function that measures how well the model, with a particular set of parameters, fits the existing input - output data. When process variables are perturbed by noise of a stochastic nature, the identification problem is usually interpreted as a parameter estimation problem. This problem has been extensively studied in the literature for the case of processes which are linear on the parameters and perturbed with white noise (Ljung, 1999; Camacho and Bordons, 2004). That is, processes that can be described by:

$$z_k = \boldsymbol{\Theta}\,\boldsymbol{\Phi}_k + e_k \tag{5.24}$$

where $\boldsymbol{\Theta}$ is the vector of parameters to be estimated, $\boldsymbol{\Phi}_k$ is the vector of past input and output measures, z_k is the latest output measure and e_k is a white noise.

Once a model is written in a form like in (5.24), the parameters can be identified by using a least-squares identification algorithm.

All the models proposed in this work can easily be expressed as in (5.24) as described in the subsequent subsections:

5.3.4.1 ARX model

Assuming that the residuals, the differences between the measured output and the output calculated by the model, can be described by $e_i(k)$ a white noise zero mean sequence, model equation (5.19) can be augmented as:

$$A(q)\,z_{s\,i}(k) = B1(q)\,q_i(k-d_1) - B2(q)q_{i+1}(k-d_2) - B3(q)q_{L\,i}(k-d_3) + e_i(k) \tag{5.25}$$

Then solving for $z_{s\,i}(k)$, (5.25) yields:

$$z_{s\,i}(k) = A'(q)\,z_{s\,i}(k-1) + B1(q)\,q_i(k-d_1) - B2(q)q_{i+1}(k-d_2) - B3(q)q_{L\,i}(k-d_3) + e_i(k) \tag{5.26}$$

with

$$A'(q) = (1 - A(q))\,q = -a_1 - a_2 q^{-1} + \ldots + a_{na}q^{-na-1}$$

This can be expressed as (5.24) by making

$$z_k = z_{s\,i}(k), \qquad \boldsymbol{\Theta}^{\mathrm{T}} = \begin{bmatrix} a_1 \\ a_2 \\ \vdots \\ a_{na} \\ b1_1 \\ b1_2 \\ \vdots \\ b1_{nb1} \\ b2_1 \\ b2_2 \\ \vdots \\ b2_{nb2} \\ b3_1 \\ b3_2 \\ \vdots \\ b3_{nb3} \end{bmatrix}, \qquad \boldsymbol{\Phi}_k = \begin{bmatrix} -z_{s\,i}(k-1) \\ -z_{s\,i}(k-2) \\ \vdots \\ -z_{s\,i}(k-na) \\ q_i(k-d_1) \\ q_i(k-d_1-1) \\ \vdots \\ q_i(k-d_1-nb1+1) \\ -q_{i+1}(k-d_2) \\ -q_{i+1}(k-d_2-1) \\ \vdots \\ -q_{i+1}(k-d_2-nb2+1) \\ -q_{L\,i}(k-d_3) \\ -q_{L\,i}(k-d_3-1) \\ \vdots \\ -q_{L\,i}(k-d_3-nb3+1) \end{bmatrix}$$

As a consequence, it is now possible to feed a least squares algorithm in a standard way and obtain a pool model. There are two ways to carry out this task:

Batch procedure: The parameter estimation is done in one step using the complete data set.

Recursive procedure: The parameter estimation is done in many steps. It is performed picking up one data point, calculating the best parameters for it and repeating using always the last values as initial guess for the next step.

5.3.4.2 Laguerre model

Assuming that the residuals of the model can be described in the same manner as before, that is by $e_i(k)$ a white noise zero mean sequence, model equation (5.21) can be rewritten as:

$$\begin{aligned} z_{s\,i}(k) = {} & \mathbf{c1}^{\mathrm{T}} \left[\mathbf{A1}\, \mathbf{l1}(k-1) + \mathbf{B1}\, q_i(k-1) \right] \\ & - \mathbf{c2}^{\mathrm{T}} \left[\mathbf{A2}\, \mathbf{l2}(k-1) + \mathbf{B2} q_{i+1}(k-1) \right] \\ & - \mathbf{c3}^{\mathrm{T}} \left[\mathbf{A3}\, \mathbf{l3}(k-1) + \mathbf{B3} q_{L\,i}(k-1) \right] \\ & + e_i(k) \end{aligned} \qquad (5.27)$$

Remembering that

$$\mathbf{l}(k) = \mathbf{A}\,\mathbf{l}(k-1) + \mathbf{B}\,u(k-1) \tag{5.28}$$

it is straightforward to show that (5.27) can be expressed as (5.24) in the following manner:

$$z_k = z_{s\,i}(k), \qquad \boldsymbol{\Theta}^{\mathrm{T}} = \begin{bmatrix} c1_1 \\ c1_2 \\ \vdots \\ c1_N \\ c2_1 \\ c2_2 \\ \vdots \\ c2_N \\ c3_1 \\ c3_2 \\ \vdots \\ c3_N \end{bmatrix}, \qquad \boldsymbol{\Phi}_k = \begin{bmatrix} l1_1(k) \\ l1_2(k) \\ \vdots \\ l1_N(k) \\ -l2_1(k) \\ -l2_2(k) \\ \vdots \\ -l2_N(k) \\ -l3_1(k) \\ -l3_2(k) \\ \vdots \\ -l3_N(k) \end{bmatrix}$$

As can be seen, in order to perform the parameter estimation procedure, first of all it is necessary to calculate the values of the N Laguerre functions responses at instant k for each model input, by means of the function (5.28). In that case the initial state vector should be $\mathbf{l}(0)^T = \begin{bmatrix} 0 & 0 & \cdots & 0 \end{bmatrix}$.

The parameter estimation procedure can also be done in this case in a batch or in a recursive way.

5.3.5 Simulation example

To check the degree of effectiveness that can be achieved when identifying a pool model from only data, an ARX model and a Laguerre model were identified for a pool with characteristics presented in table 5.1. This example will serve to put in practice all the knowledge developed in this chapter and particularly to study the performance that can be achieved using the proposed pool-model structures.

The initial water profile of the reach is presented in figure 5.12.

Following the recommendations made in Section 5.3.1.1, the sampling period was chosen to be $215\,\mathrm{s}$.

As commented before, an informative-rich input sequence is necessary in order to excite all the relevant dynamics of the system. Two maximum length PRBS signals were designed in a form that the maximum width of the PRBSs was greater than the tendency-stabilization time
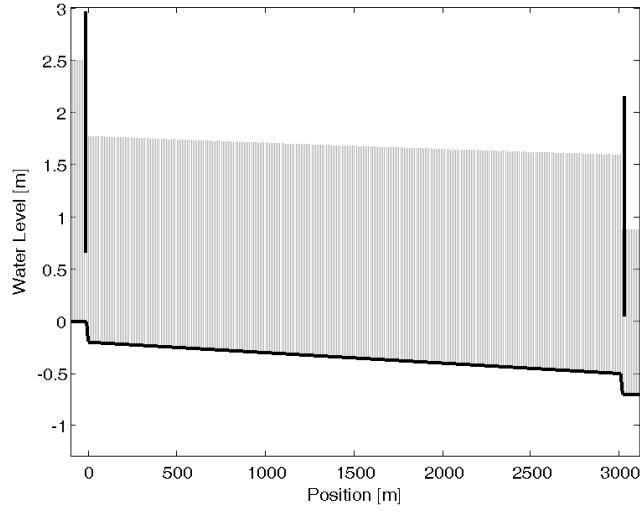
Figure 5.12: Initial water profile of the reach

of the step response of the pool: $4000\,\text{s} - 680\,\text{s} = 3320\,\text{s}$. In addition, having in mind "a not too large" sequence length, the following PRBS parameters were chosen: $p = 2$ and $N = 8$. Therefore, the total sequence length was:

$$p \times L = 2 \times \left(2^8 - 1\right) = 510\,\text{data points}$$

and the maximum pulse width was:

$$N \times T_s \times p = 8 \times 215\,\text{s} \times 2 = 3440\,\text{s} > 3320\,\text{s}$$

Using this information, two PRBS input sequences were generated by software; one for the inflow q_i and one for the outflow q_{i+1} (in this example $q_{L\,i}$ was not considered). Their amplitudes were chosen so as to obtain a variation of ± 0.4 around the working discharge, namely $10\,\text{m}^3/\text{s}$. The designed water discharges are depicted in figure 5.13 and figure 5.14.

The downstream water level ($z_{s\,i}$) response to the imposed water discharges can be viewed in figure 5.15.
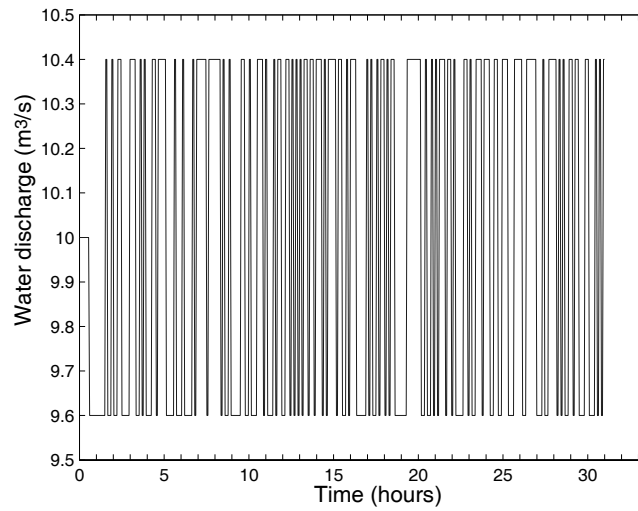
Figure 5.13: Imposed upstream water discharge
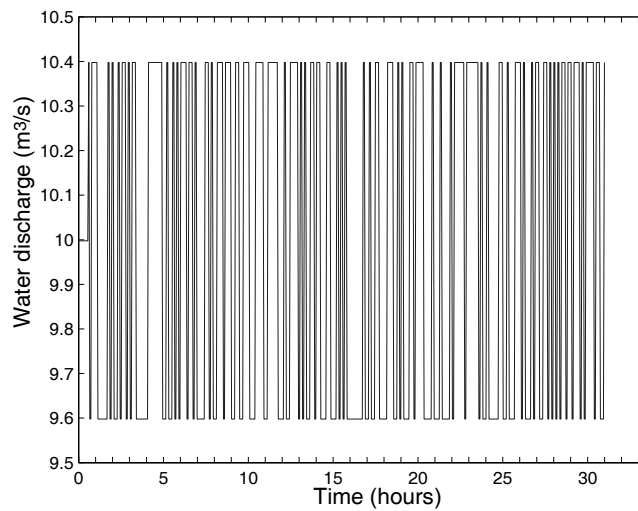
Figure 5.14: Imposed downstream water discharge
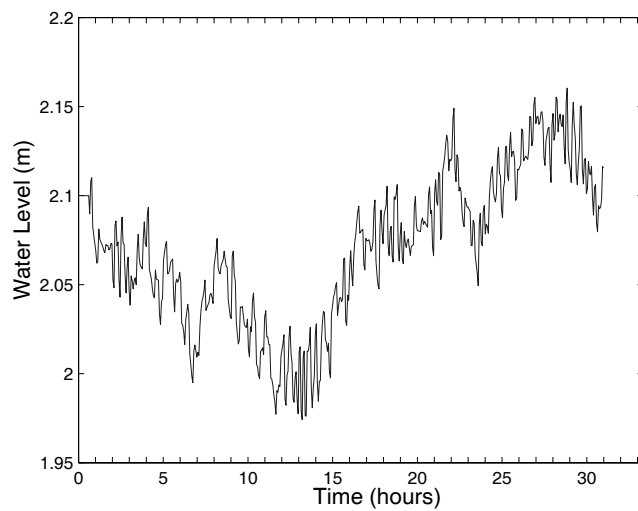
Figure 5.15: Reach's downstream water level

As can be observed in figure 5.15, the experiment was designed to achieve the following goals:

- To have the most information about the system dynamics.

- To have sufficient data points to feed the parameter estimation algorithms.

- To keep the water level around the operational point $(2.1\,\mathrm{m})$ in order to avoid the violation of the linearity assumption.

With the generated data set, the following models were obtained:

- ARX model with integrator position correction:

$$A(q) = 1 - 0.7791\,q^{-1} - 0.03589\,q^{-2} - 0.03576\,q^{-3} - 0.01423\,q^{-4}$$
$$- 0.01693\,q^{-5} - 0.01205\,q^{-6} - 0.2234\,q^{-7} + 0.1174\,q^{-8}$$
$$q^{-d_1}B1(q) = q^{-4}\left(0.0229 - 0.0113\,q^{-1}\right) \tag{5.29}$$
$$q^{-d_2}B2(q) = q^{-1}\left(-0.02598 + 0.01497\,q^{-1}\right)$$

- ARX model with a posteriori added integrator:

$$A(q) = 1 - 1.199\,q^{-1} + 0.1322\,q^{-2} + 0.01203\,q^{-3} + 0.03275\,q^{-4}$$
$$+ 0.005332\,q^{-5} + 0.009966\,q^{-6} - 0.2101\,q^{-7} + 0.2167\,q^{-8}$$
$$q^{-d_1}B1(q) = q^{-4}\left(0.02262 - 0.01995\,q^{-1}\right) \tag{5.30}$$
$$q^{-d_2}B2(q) = q^{-1}\left(-0.02617 + 0.02631\,q^{-1} - 0.002822\,q^{-2}\right)$$

- Laguerre model without integrator:

$$p1 = 0.0115$$
$$c1^{\mathrm{T}} = \begin{bmatrix} -0.0001 & -0.0017 & -0.0083 & -0.0168 & -0.0127 & -0.0032 \end{bmatrix}$$
$$p2 = 0.0053 \tag{5.31}$$
$$c2^{\mathrm{T}} = \begin{bmatrix} -0.0015 & -0.0022 & -0.0014 & -0.0008 & -0.0007 & -0.0003 \end{bmatrix}$$

In order to make an objective judgment, all model structures had been chosen so as to have to identify 12 unknown parameters.

The orders of the polynomials and the delays of models (5.29) and (5.30) were obtained comparing the results given by different combinations of them and then picking out the most appropriate ones.

In the case of model (5.31), the Laguerre pole p was determined by a Newton - Raphson iterative technique (Malti et al., 1998). This algorithm performed an optimal search in order to obtain the pole value with best fit.

All model parameters where obtained using least squares based parameter estimation algorithms (Ljung, 1999).

With respect to the integrator pole, model (5.29) includes the correction of the integrator pole position and model (5.30) was identified discarding the integrator in a first stage and then manually including it in $A(q)$. Model (5.31) is the Laguerre model obtained without integrator; the integrator had to be included augmenting the states of the identified model.

To compare the performances of the obtained models, they were tested in two different domains: the time domain and the frequency domain. A good performance in the time domain ensures that the model can accurately model a behavior for a given input, while a good fit in the frequency domain ensures that the identified model will approximate with good results, a response induced by a more general type of input.

In the time domain, the step response of a Saint-Venant modeled pool was compared against the step response of the identified linear models. This test was performed producing a step increase in the upstream water discharge, maintaining the downstream water discharge value constant. The results are given in figure 5.16.
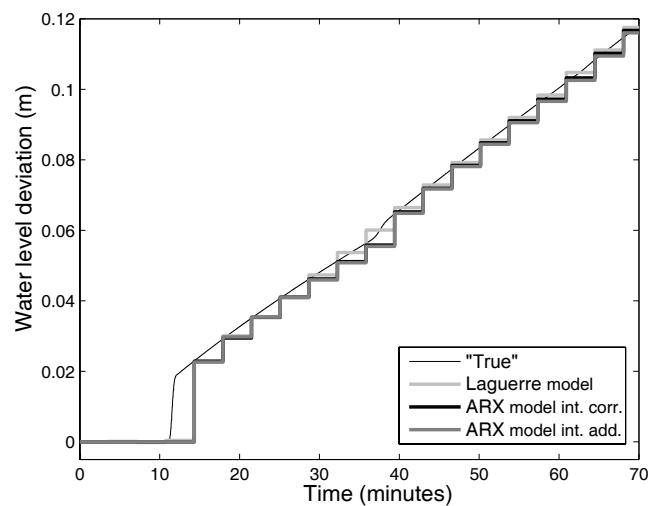
Figure 5.16: Step response of the reach v/s step response of the identified linear models

As can be observed in figure 5.16, all models performed relatively well in approximating the behavior of the Saint - Venant based simulation. However, looking in detail, there are two features that are worthy of note:

- The Laguerre model was less accurate in simulating the changes due to the water waves.

- After a large time period, all models tended slowly to deviate from the true response.

In order to study if the models can only perform well for a step-type input or if they are really representing the system in question, it was found useful to construct the frequency responses (or Bode diagrams) of the Saint - Venant modeled pool and of the identified linear models. In this case it is required the analysis of two relationships:

1. Upstream discharge (q_i) $\rightarrow$ Downstream water level ($z_{s\,i}$)

2. Downstream discharge (q_{i+1}) $\rightarrow$ Downstream water level ($z_{s\,i}$)

1 and 2 are presented in figure 5.17 and figure 5.18 respectively.
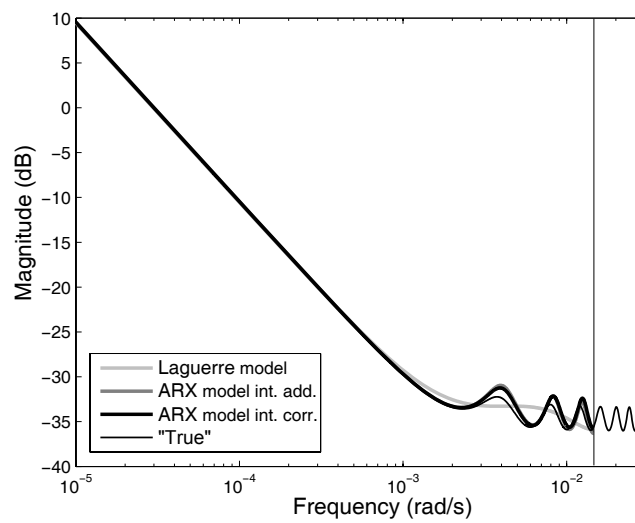
(a) Bode Magnitude
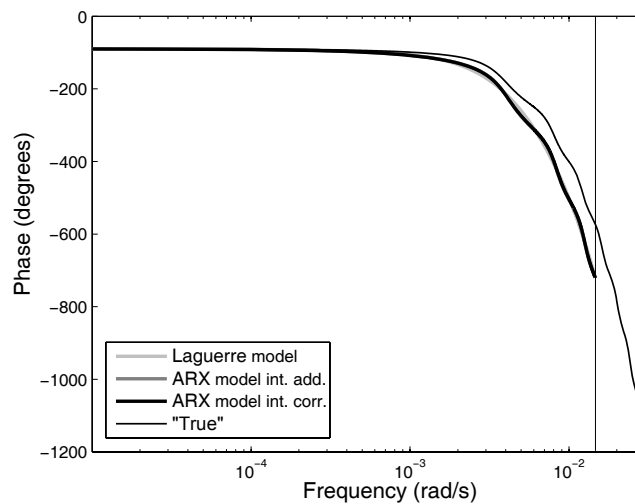
(b) Bode Phase

Figure 5.17: Bode diagram between q_i and $z_{s\,i}$ for pool of Table 5.1
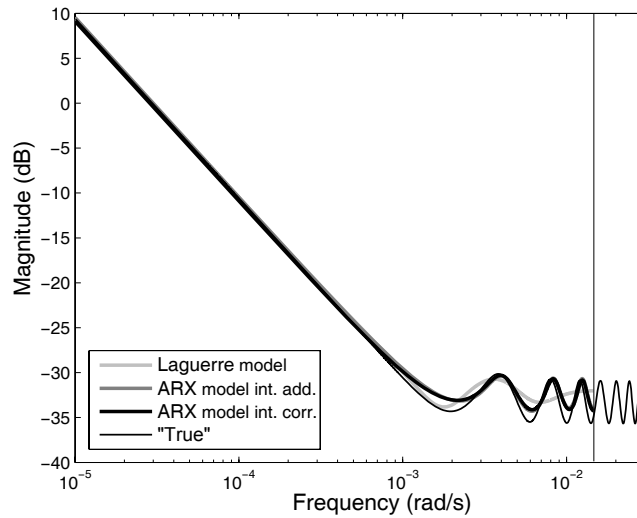
(a) Bode Magnitude
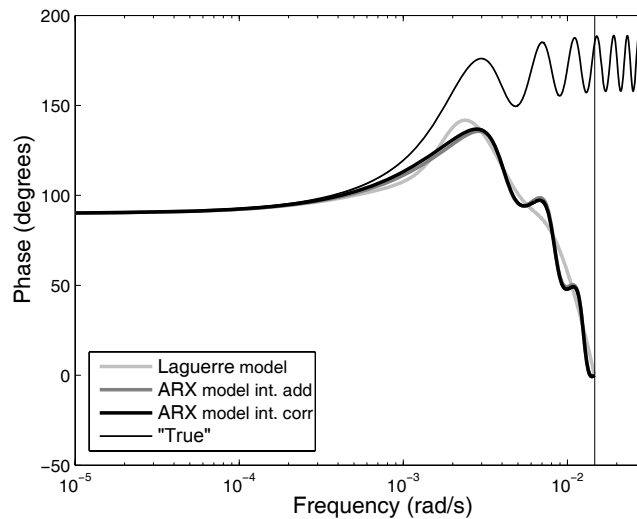
(b) Bode Phase

Figure 5.18: Bode diagram between q_{i+1} and $z_{s\,i}$ for pool of Table 5.1

Figures 5.17 and 5.18 show that there are no noticeable magnitude or phase errors for frequencies below $0.0005\,\mathrm{rad/s}$. Hence, all the identified models approximate the pool behavior with high accuracy in the low frequency region.

In the high frequency region, the magnitude plots show that the ARX models can approximate the location and magnitude of the resonant modes of the system with a medium-to-high accuracy until the Nyquist frequency (represented with a vertical line). In the same area, the Laguerre model tends to average the magnitudes of the frequencies, suggesting that the number of Laguerre functions is insufficient. In fact, doubling the number of terms improves the approximation of the resonant modes in a high degree (see figure 5.19).

On the other hand, a zoom on the high frequency region of the phase plots reveals the existence of notable phase errors. These errors appear at approximately 1/10 of the Nyquist fre-
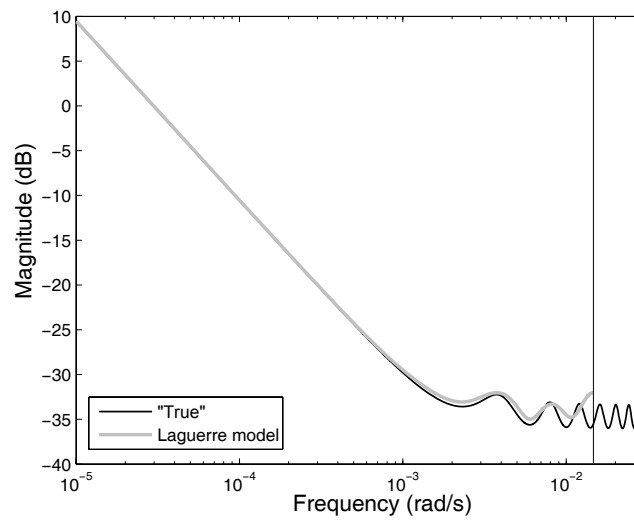
Figure 5.19: Bode diagram of Laguerre reach model with 24 parameters

quency and become more important when approaching to the Nyquist frequency. Nevertheless, this is a normal behavior of some discrete-time models working near the Nyquist frequency.

5.4 Canal model synthesis

In the previous sections, the issues concerning to pool models and their identification have been deeply studied. Now, it is the turn to explain how to construct a complete canal model.

For the purpose proposed, it is enough to describe a canal in a simplified way. A general scheme of a canal with N pools is presented in figure 5.20.
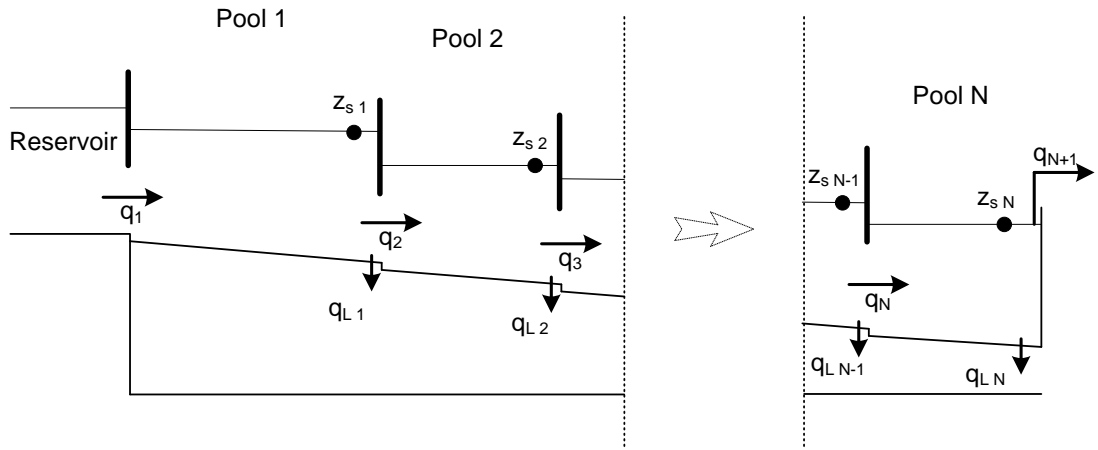
Figure 5.20: Canal scheme with N pools

The identification of each pool of the canal would produce several models with a structure like the one presented in (5.16). It is straightforward to show that the interconnection of all these discrete models would yield a discrete transfer function matrix of the form:

$$
\begin{bmatrix} z_{s\,1}(z) \\ z_{s\,2}(z) \\ \vdots \\ z_{s\,N}(z) \end{bmatrix} = \begin{bmatrix} F1_1(z) & F2_2(z) & 0 & \cdots & 0 \\ 0 & F1_2(z) & F2_3(z) & \ddots & \vdots \\ \vdots & \ddots & \ddots & \ddots & 0 \\ 0 & \cdots & 0 & F1_N(z) & F2_{N+1}(z) \end{bmatrix} \begin{bmatrix} q_1(z) \\ q_2(z) \\ \vdots \\ q_N(z) \\ q_{N+1}(z) \end{bmatrix}
$$
$$
+ \begin{bmatrix} F3_1(z) & 0 & \cdots & 0 \\ 0 & F3_2(z) & \ddots & \vdots \\ \vdots & \ddots & \ddots & 0 \\ 0 & \cdots & 0 & F3_N(z) \end{bmatrix} \begin{bmatrix} q_{L\,1}(z) \\ q_{L\,2}(z) \\ \vdots \\ q_{L\,N}(z) \end{bmatrix} \tag{5.32}
$$

The canal model structure presented in (5.32) is one way to express a Multiple-Input Multiple-Output (MIMO) process. Although its accurate analysis depends in a high degree on the particular canal characteristics, one can highlight the following points in general lines:

- Although it is possible that the interconnection can modify some individual pool dynamics, the pool properties and characteristics presented in other sections are still extrapolative to a complete irrigation canal. In other words, the system is likely to have delays, resonance, marginal stability, etc..

- There is an additional characteristic that appears from the union of pool models in (5.32): system coupling. That means that a single system input does not only influence a single output; it produces an action over other outputs too. In this case (5.32) shows that a particular gate discharge q_i acts over two water levels: the one immediately upstream ($z_{s\,i-1}$) and the one located in the downstream end of the pool ($z_{s\,i}$).

As explained in other sections, this canal model can be easily extended to include gate openings, weirs or other hydraulic structures by replacing discharges with appropriate hydraulic formulas. Those modifications would normally increase the coupling degree of the system (less zeros in (5.32)) and change some transient behaviors.

5.5   Experimental application

The general approach of this work has been to develop knowledge on a practical application basis. This section validates the use of system identification in canals by testing its application on the Canal PAC-UPC. This canal was already presented in Chapter 3 and is depicted in figure 5.21.
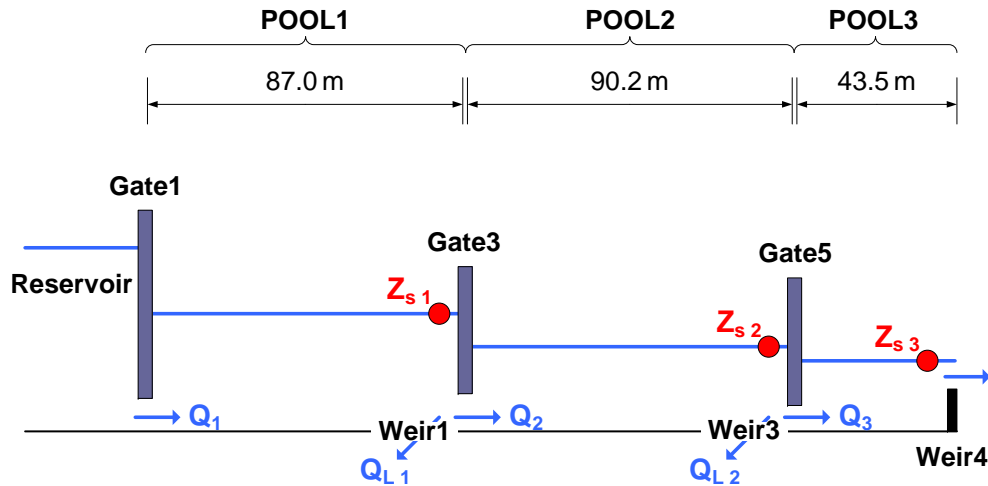
Figure 5.21: Scheme of the Canal PAC-UPC

Specifically, the recommendations and procedures developed in this chapter are applied in a modeling stage in order to produce an ARX MIMO model of this laboratory canal.

The necessary data comes from experiments performed on the real canal and the identification procedure is explained in the following subsections.

5.5.1   Sampling time

In order to determine an appropriate sampling time, it has been found helpful to obtain a step response of the system. For example, a true $20\,\mathrm{L/s}$ discharge increment at the upstream end of Pool 1 produced the downstream level variation plotted in figure 5.22.

Figure 5.22 marks two important time periods:

- Pool delay = $28\,\mathrm{s}$

- Tendency stabilization = $130\,\mathrm{s}$

The pool delay is time needed to see a downstream water level variation after an inflow change at the beginning of the pool. The tendency stabilization refers to the subsequent time period needed to observe a clear tendency in the downstream water level.

The pool sampling time selection procedure proposed in this thesis seeks a good trade off between accuracy, simplicity and control goals. One recommendation was to pick out a sam-
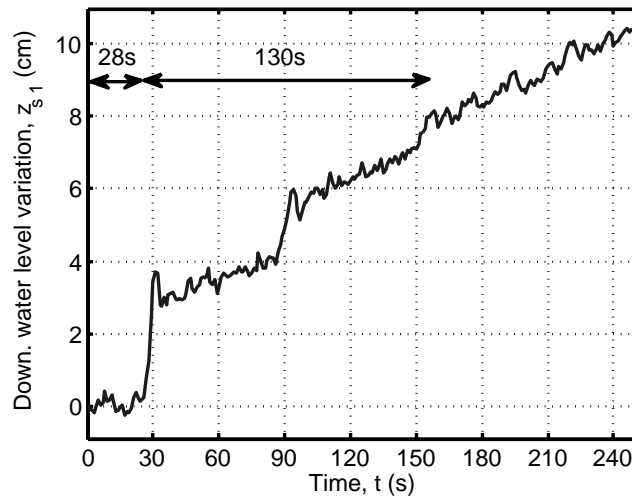
Figure 5.22: Inflow step response - Pool 1

pling time that divides the delay 2 or 3 times. Other suggestion was to divide the stabilization time by enough points. In this case it was found a good alternative to divide the stabilization time by 13:

- Sampling time = $130\,\text{s}$ / 13 = $10\,\text{s}$

This choice gives an acceptable discretization of the transient behavior and divides the delay by almost 3. Moreover, this choice gives a Nyquist frequency higher than the first resonant modes.

In a broader perspective, it is convenient to have only one sampling period for all pools in a canal. This permits the conception of a canal model with a unique sampling time. The decision should be made analyzing the step responses of all pools and picking out an average value. In this case it was not necessary; the step responses of the rest of the pools are rather similar. Furthermore, the shortest pool have a delay of approximately $20\,\text{s}$. The sampling time is contained twice in this period.

This decision is also adequate for control in this case. This value permits the use of a control time equal to the model sampling time. It was explained that this choice eliminates the need for control recalculation. This would not have been possible with a higher sampling frequency; it is not advisable to operate the servo-motorized gates of the canal at a higher rate.

5.5.2 PRBS design

The guidelines presented in this chapter suggest:

1. To remain around an operational point.

2. To maintain the experiment as short as possible.

3. A maximum pulse width bigger than the stabilization time.

4. Between 200 and 1000 data points to feed the parameter estimation algorithm.

In general, there are several PRBS signals that fulfill these requirements. Trial and error tests showed that a possible parameter set could be the one presented in table 5.2.

Table 5.2: PRBS parameters

Parameter	Value
PRBS time factor, p	4
Number of registers, N	6
PRBS amplitude, a (L/s)	10

These design parameters originate a PRBS signal with the following characteristics:

- Data points: 252 points

- Maximum pulse width: $240\,\text{s}$ ($>130\,\text{s}$)

- Minimum pulse width: $40\,\text{s}$

- Experiment duration: $2520\,\text{s}$

Two PRBS signals are required to perform the identification step because the pools of the canal have only two independent manipulable inputs: q_i and q_{i+1}. ($q_{L\,i}$ is not entirely manipulable in this canal) Generally, it is found better to excite both inputs at a time in order to capture the essential dynamics of the system and to reduce the length of the experiment. Hence, two maximally shifted PRBSs were constructed so as to have two different and statistically independent signals. These signals are shown in figure 5.23.
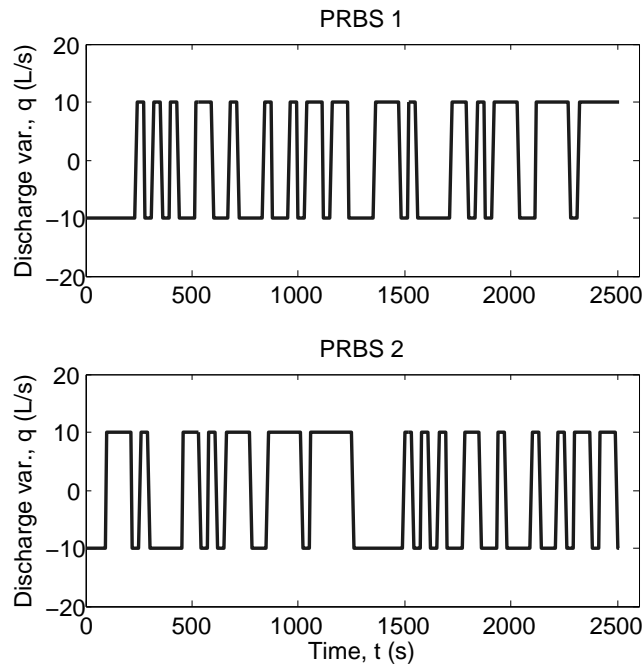
Figure 5.23: PRBSs designed for pool model identification

5.5.3 Identification experiment

The purpose of this step is to excite each pool so as to obtain the most information about their behavior. This procedure was applied pool by pool using the specifically designed PRBSs as discharge set points. These set points were transduced into real discharges by each gate discharge controller. Inevitably, real discharges were somewhat different from the designed ones. However, they were enough informative for identification.

In these experiments, all rectangular weirs were closed with the exception of the water way-out weir (Weir 4)(see figure 5.21). That is, all Q_{Li} were made zero in order to suppress their influence on the data. With weirs it is almost impossible to produce PRBS-like signals. However, the location of weirs is very close to the downstream ends of the pools in this canal. Hence, the process resembles model type (5.13) and this part of the model can be easily reconstructed once the rest of the model is known.

5.5.3.1 Pool 1

In this pool there are two manipulable variables: Q_1 and Q_2. Q_1 is the discharge that comes from the upstream reservoir through Gate 1. On the other hand, Q_2 is the discharge that leaves the pool through Gate 2. The PRBSs were applied around a stationary condition where the circulating discharge was $63 \, \text{L/s}$. The employed PRBS-like signals are presented in figure 5.24.

The controllable variable in this pool is the downstream water level Z_{s1}. At the time when
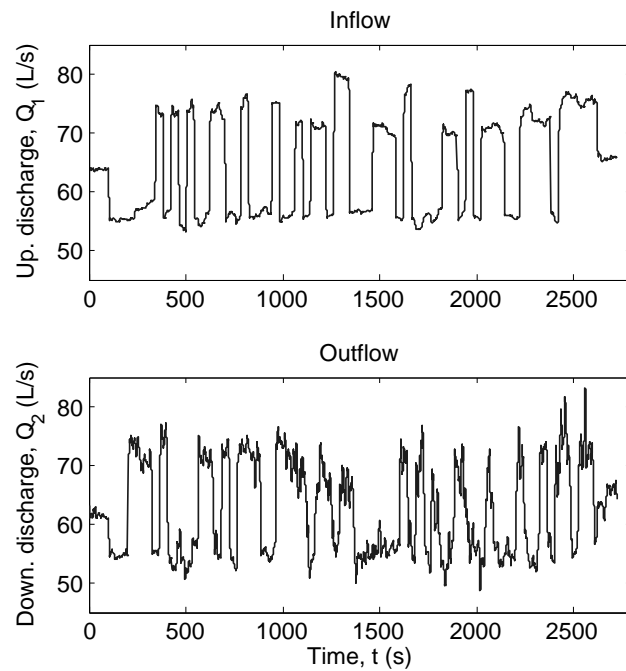
Figure 5.24: Excitation signals - Pool 1

the experiment began, the water level value was $86\,\mathrm{cm}$. The response produced by the discharge sequences is shown in figure 5.25.
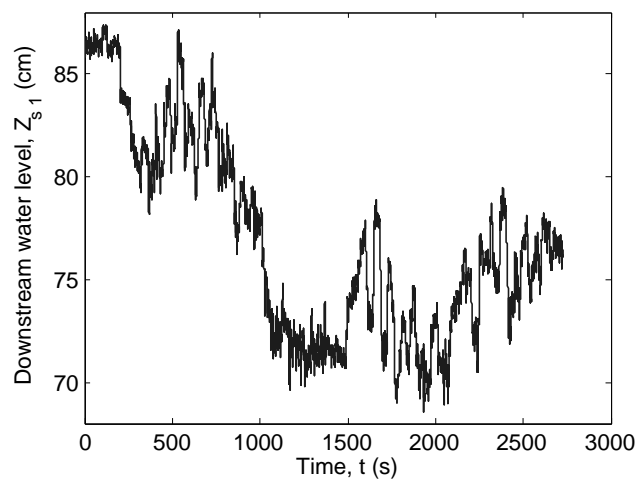
Figure 5.25: Level response- Pool 1

5.5.3.2 Pool 2

Just as Pool 1, this pool has two manipulated variables, Q_2 and Q_3. Q_2 is the discharge that enters the pool through Gate 2. Q_3 is the discharge that leaves the pool through Gate 3. The PRBS signals were applied around a stationary discharge value equal to $40\,\mathrm{L/s}$. These sequences are shown in figure 5.26.
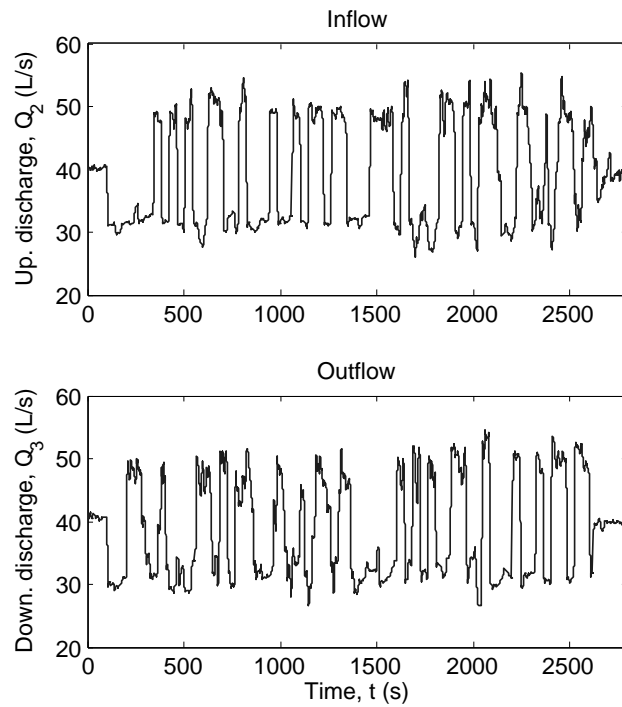
Figure 5.26: Excitation signals - Pool 2

In this case the dependent variable is the downstream water level $Z_{s\,2}$. It was perturbed from a stationary value of $60\,\mathrm{cm}$. The effect can be observed in figure 5.27.
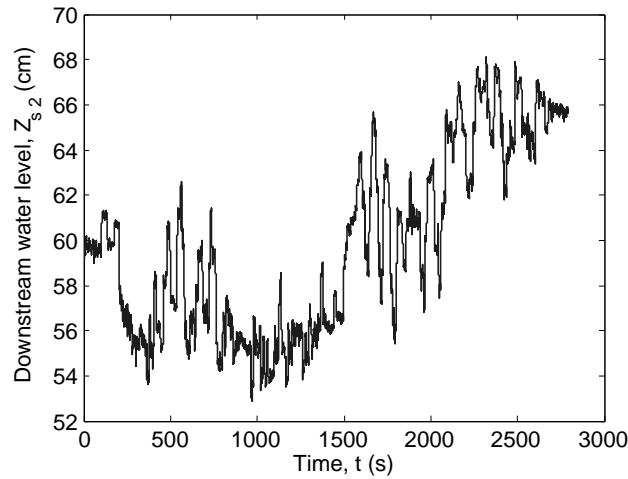
Figure 5.27: Level response- Pool 2

5.5.3.3   Pool 3

This pool is somewhat different because it is the last one. Here, the only independent manipulable variable is the inflow. It depends on the discharge Q_3 through Gate 3.

The outflow relies on the head-discharge weir relationship. Unfortunately, the head is equal

to the downstream water level $Z_{s\,3}$, the dependent variable. Thus, the outflow and the downstream water level are dependent on the inflow.

To sum up, in this case the excitation was applied only to the inflow. The discharge PRBS started from approximately $40\,\mathrm{L/s}$. The complete sequence is presented in figure 5.28.
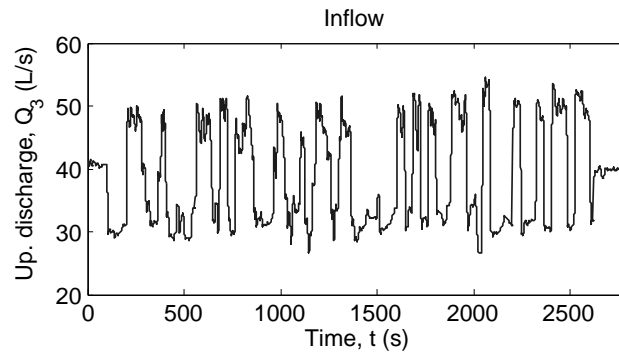
Figure 5.28: Excitation signal - Pool 3

The observed variable was the downstream water level $Z_{s\,3}$. It was perturbed from an original steady value of $49.5\,\mathrm{cm}$. The response is depicted in figure 5.29.
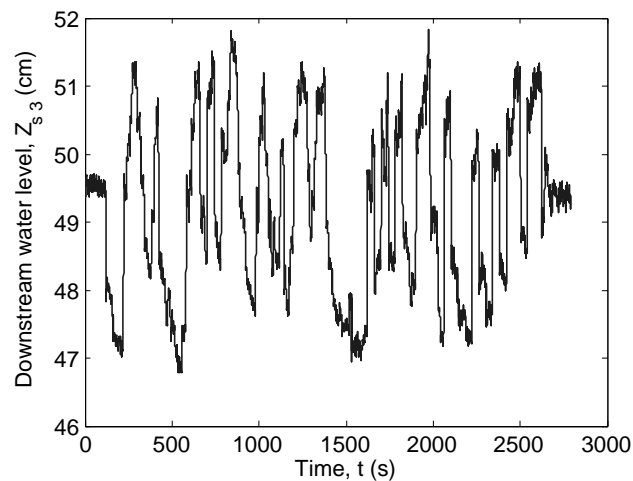
Figure 5.29: Level response- Pool 3

5.5.4   Data preprocessing

These data are not prepared for identification yet. Data has to be treated through two indispensable previous procedures:

1. To remove means or trends.

2. To apply antialias filtering and resample data.

The first step is usually performed in order to avoid biased model parameters. The second step is necessary when data is not sampled at the same frequency that is going to be used in the identification step. Sometimes, it is desirable to sample at a higher rate; measurement noise is reduced after the application of the antialias filter.

In this case the original sampling period was $0.1\,\text{s}$.

First, all initial stationary values were subtracted from the data so as to perform a kind of bias removal.

Then, an order 10 FIR antialias filter was applied to the data. This procedure ensures that after resampling, frequencies above the new Nyquist frequency will not corrupt the information of the rest of the bandwidth.

Finally, data was decimated (i.e. to pick up data samples at regular intervals greater than the data sampling) to achieve a new $10\,\text{s}$ sampling time.

The result of these operations is exemplified by the preprocessed Pool 1 signals that are shown in figures 5.30 and 5.31.
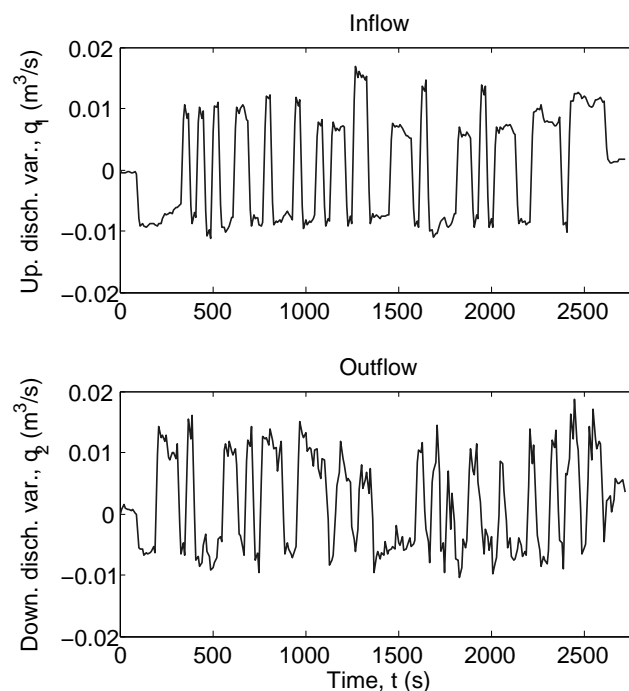
Figure 5.30: Preprocessed discharge signals - Pool 1
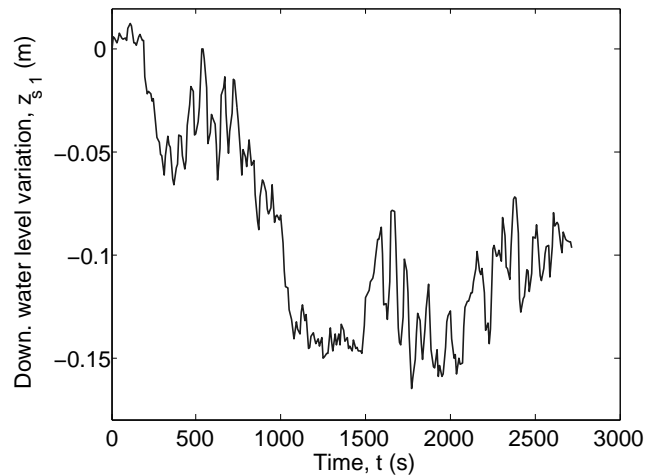
Figure 5.31: Preprocessed water level signal- Pool 1

5.5.5   Pool model identification

This step consists in using system identification tools to obtain a mathematical model that can fit the preprocessed data. Generally, some expertise and trial and error is required because it is not straightforward to find the correct model; there are many options to consider and the final model should balance model complexity, model accuracy and model generalization. Normally, it is a good practice to identify several models and analyze all these points before selecting the definitive model. In this case, this procedure was carried out in three consecutive stages using MATLAB$^{\circledR}$ and its System Identification Toolbox:

1. For each pool, a large set of ARX models was identified with the aid of the least squares parameter estimation algorithm provided by the software. This set was composed of models combining different values of polynomial orders by considering that na, $nb1$ and $nb2$ should take values between 1 and 10.

2. One model was selected from each set. This choice was performed seeking a final model with an acceptable performance and few parameters. The performance of each candidate model was evaluated in terms of:

   (a) *Simulation and prediction capability of the models* The former refers to the ability to reproduce process output data if the model is continuously fed with only input data; the latter denotes the model's ability to predict the system response up to a certain time instant in the future using current and past input and output data.

   (b) *Statistical residual analysis results* The residuals are the differences between the model output and the process output. This type of analysis calculates the cross-correlation function between the inputs and the residuals to verify if the output is

properly described by the model and computes the autocorrelation function of the residuals to determine if the model correctly describes the process disturbance or, what is the same thing, to check if the residuals are mutually independent.

3. The selected ARX models were corrected in the cases where a pure integrator should appear in the model according to Section 5.2. This was carried out pursuant to page 92 as follows:

   (a) The roots of the $A_i(q)$ polynomial were calculated.

   (b) The root q_x close to 1 was replaced with exactly an 1.

   (c) $A_i(q)$ was reconstructed using this new root value and the rest of the roots.

The result of the whole process gave the following ARX models:

- Pool 1 ARX model: $A_1(q) \, z_{s\,1}(k) = q^{-d1_1} B1_1(q) \, q_1(k) + q^{-d2_1} B2_1(q) \, q_2(k) + e_1(k)$

$$A_1(q) = 1 - 0.6918 \, q^{-1} + 0.09173 \, q^{-2} - 0.07062 \, q^{-3} + 0.1638 \, q^{-4}$$
$$- 0.2801 \, q^{-5} - 0.213 \, q^{-6}$$
$$q^{-d1_1} B1_1(q) = q^{-3} \left(1 - 0.2895 \, q^{-1}\right) \tag{5.33}$$
$$q^{-d2_1} B2_1(q) = q^{-1}(-1.154 + 0.4729 \, q^{-1} - 0.06765 \, q^{-2} + 0.4496 \, q^{-3}$$
$$- 0.4899 \, q^{-4})$$

- Pool 2 ARX model: $A_2(q) \, z_{s\,2}(k) = q^{-d1_2} B1_2(q) \, q_2(k) + q^{-d2_2} B2_2(q) \, q_3(k) + e_2(k)$

$$A_2(q) = 1 - 0.04315 \, q^{-1} - 0.1178 \, q^{-2} - 0.03932 \, q^{-3} + 0.03022 \, q^{-4}$$
$$- 0.1962 \, q^{-5} + 0.05333 \, q^{-6} - 0.3033 \, q^{-7} - 0.3838 \, q^{-8}$$
$$q^{-d1_2} B1_2(q) = q^{-4} \, (1.644) \tag{5.34}$$
$$q^{-d2_2} B2_2(q) = q^{-1}(-1.994 + 0.4728 \, q^{-1} - 0.1484 \, q^{-2} + 0.6077 \, q^{-3}$$
$$- 0.4835 \, q^{-4})$$

- Pool 3 ARX model: $A_3(q) \, z_{s\,3}(k) = q^{-d1_3} B1_3(q) \, q_3(k) + e_3(k)$

$$A_3(q) = 1 - 0.6495 \, q^{-1} - 0.2344 \, q^{-2} + 0.142 \, q^{-3} - 0.3175 \, q^{-4}$$
$$+ 0.2112 \, q^{-5}$$
$$q^{-d1_3} B1_3(q) = q^{-2} \left(1.422 - 0.9872 \, q^{-1}\right)$$

$$\tag{5.35}$$

5.5.6 Canal model

The union of pool models (5.33), (5.34) and (5.35) with the incorporation of two intermediate weir regulated offtakes produce the following discrete multivariable ARX model ($T = 10\,\mathrm{s}$):

$$
\begin{bmatrix} A_1(q) & 0 & 0 \\ 0 & A_2(q) & 0 \\ 0 & 0 & A_3(q) \end{bmatrix} \begin{bmatrix} z_{s\,1}(k) \\ z_{s\,2}(k) \\ z_{s\,3}(k) \end{bmatrix} = \begin{bmatrix} q^{-2}B1_1(q) & B2_1(q) & 0 \\ 0 & q^{-3}B1_2(q) & B2_2(q) \\ 0 & 0 & q^{-1}B1_3(q) \end{bmatrix} \begin{bmatrix} q_1(k-1) \\ q_2(k-1) \\ q_3(k-1) \end{bmatrix}
$$

$$
+ \begin{bmatrix} B2_1(q) & 0 \\ 0 & B2_2(q) \\ 0 & 0 \end{bmatrix} \begin{bmatrix} q_{L\,1}(k-1) \\ q_{L\,2}(k-1) \end{bmatrix} + \begin{bmatrix} e_1(k) \\ e_2(k) \\ e_3(k) \end{bmatrix}
$$

$$(5.36)$$

In some textbooks, it is also usual to rewrite a model like this in the following form:

$$
\begin{bmatrix} z_{s\,1}(k) \\ z_{s\,2}(k) \\ z_{s\,3}(k) \end{bmatrix} = \begin{bmatrix} 1 - A_1(q) & 0 & 0 \\ 0 & 1 - A_2(q) & 0 \\ 0 & 0 & 1 - A_3(q) \end{bmatrix} \begin{bmatrix} z_{s\,1}(k-1) \\ z_{s\,2}(k-1) \\ z_{s\,3}(k-1) \end{bmatrix}
$$

$$
+ \begin{bmatrix} q^{-2}B1_1(q) & B2_1(q) & 0 \\ 0 & q^{-3}B1_2(q) & B2_2(q) \\ 0 & 0 & q^{-1}B1_3(q) \end{bmatrix} \begin{bmatrix} q_1(k-1) \\ q_2(k-1) \\ q_3(k-1) \end{bmatrix} \qquad (5.37)
$$

$$
+ \begin{bmatrix} B2_1(q) & 0 \\ 0 & B2_2(q) \\ 0 & 0 \end{bmatrix} \begin{bmatrix} q_{L\,1}(k-1) \\ q_{L\,2}(k-1) \end{bmatrix} + \begin{bmatrix} e_1(k) \\ e_2(k) \\ e_3(k) \end{bmatrix}
$$

This canal model can be used for several purposes. For example, it can be used to simulate downstream water level responses to beforehand known discharge curves in a fast way. Another possibility is to use it to predict future water level variations from past discharge measurements and past water level readings. Nevertheless, its simpleness makes it specially attractive for control applications.

5.5.7 Model validation

A model validation stage determines the degree of validity of a model. It should be done by checking the model with data not used in its construction. In this case, the model was validated in the time domain and in the frequency domain.

5.5.7.1 Time domain

A totally new data set was taken from the Canal PAC-UPC in order to prove the effectiveness of the identified model.

This experiment consisted in following the evolution of the canal variables after closing $3\,\mathrm{cm}$ Gate 1 with Weir 1 completely closed. This test was somewhat severe because it produced a $33\,\%$ discharge reduction ($\Delta Q_1 \approx -20\,\mathrm{L/s}$). A variation like this, make the water levels go away from their initial conditions, occasionally violating the linearity assumption. However, the test was found appropriate in order to determine some model performance limits.

In order to study the efficiency of the model, two types of time-domain results were calculated: simulation results and prediction results.

Simulating a model means that the response of a model to a particular input is computed. On the other hand, predicting future outputs of a model from previous data over a time horizon of k samples or kT time units, requires both past inputs and past outputs. The main difference between simulation and prediction is whether it is used measured or computed previous outputs for calculating the next output.

A high simulation performance indicates that a model is a good representation of reality. However, the model purpose should also be considered when testing a model. Using a model for prediction is common in controls applications like predictive control, where it is wanted to predict output for a specific number of steps in advance. This type of control is going to be used later in this thesis, and therefore the relevance of these prediction results.

Both, simulation and prediction results using the identified ARX model were compared to measured output-data. Model inputs (measured discharges) are presented in figure 5.32 while the results are presented in figure 5.33 and 5.34 for simulation and prediction respectively.
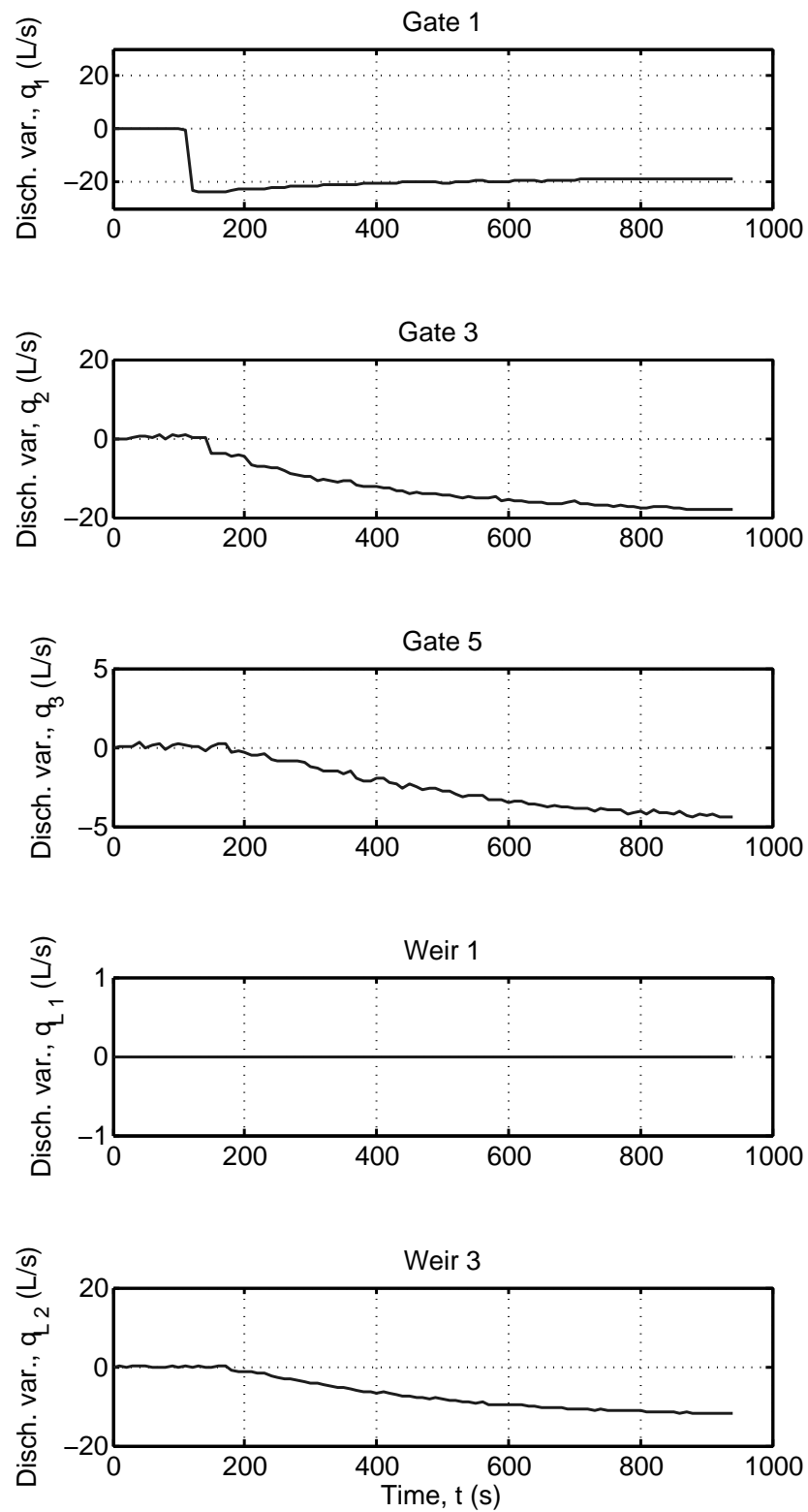
Figure 5.32: Discharge sequences used to feed the ARX model
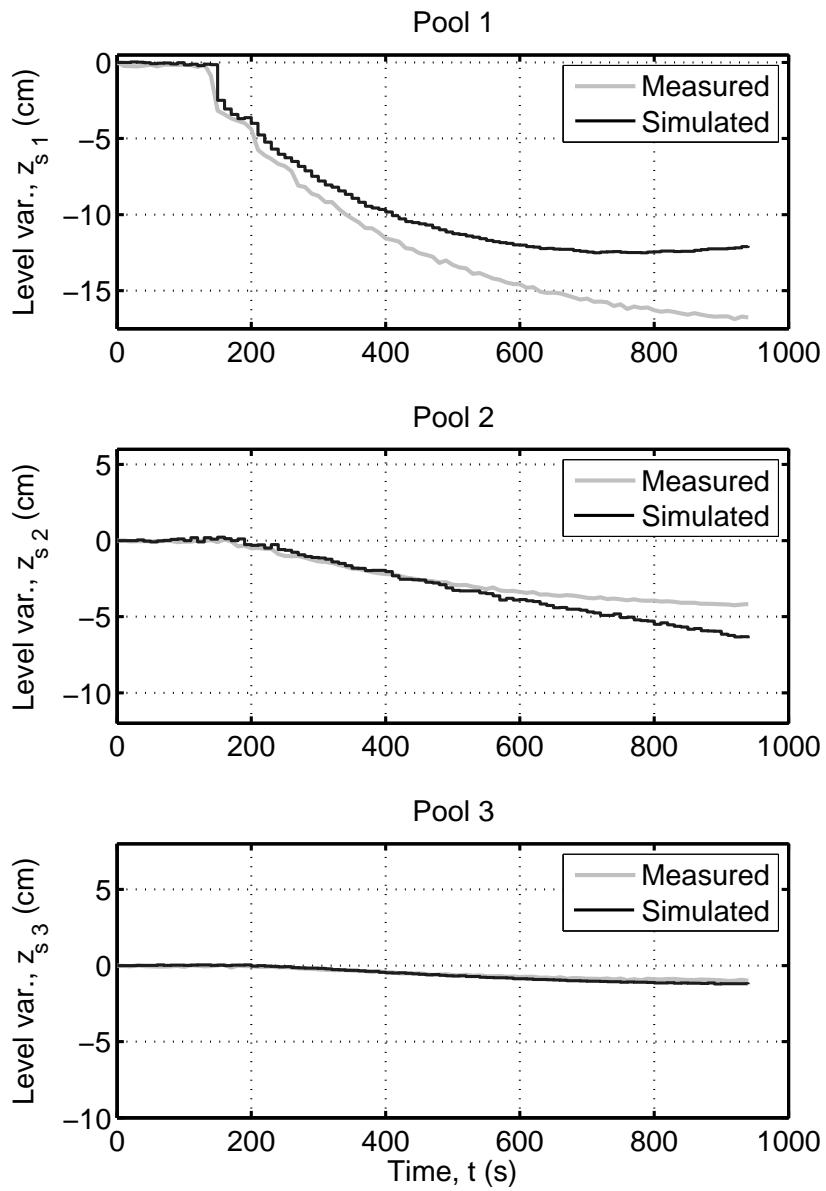
Figure 5.33: Comparison between measured water level deviations and model simulation
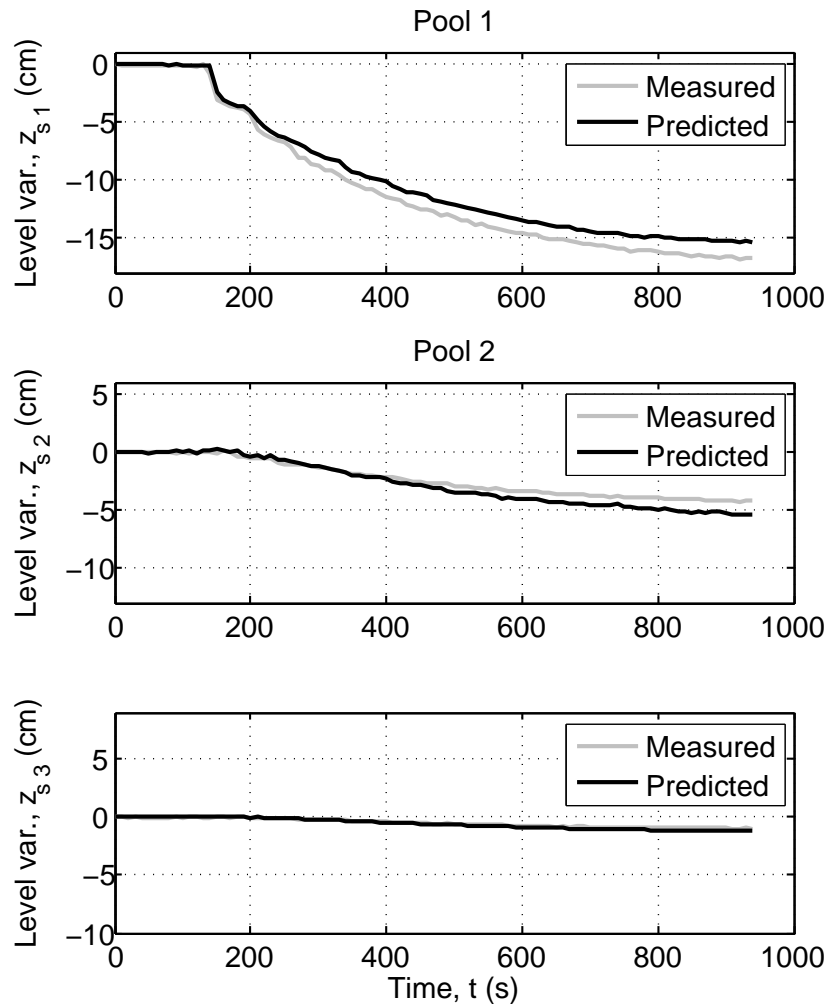
Figure 5.34: Comparison between measured water level deviations and a 20-step-ahead ($200\,\mathrm{s}$) model prediction

The simulation results of figure 5.33 show that the accuracy of the identified model deteriorates when the water level deviations exceed approximately the $5\,\mathrm{cm}$ value, a $10\,\%$ of the initial water level. Thus, the model gives good estimations within a $\pm 10\,\%$ operation area. This result is somewhat expected for a linearized model approximating a nonlinear process. Within this $\pm 10\,\%$ range, delays and transients are well approximated and there is a good agreement between measured and simulated water levels.

The prediction results of figure 5.34 look even better. The 20-step-ahead predictions (a $200\,\mathrm{s}$ forecast) are very accurate when compared to the measured water levels, inclusively beyond the $\pm 10\,\%$ operation range. The maximum residuals are only slightly higher than $1\,\mathrm{cm}$.

In summary, the model has successfully approximated the linearized behavior of the canal around an operation condition and is specially suitable for medium-term predictions. A model like this is accurate enough to be used in the design of any linear controller, but is particularly attractive for predictive controllers.

5.5.7.2   Frequency domain

In this case, the frequency response of the model was checked against the theoretical Bode diagram obtained from an unidimensional Saint-Venant canal model around an operation point. This model was configured using the geometrical dimensions of the real canal, but its roughness was not measured. Hence, the Manning number was arbitrarily taken as 0.02.

The comparison can be observed pool by pool in figures 5.35, 5.36 and 5.36 for Pool 1, Pool 2 and Pool 3 respectively.

(a) Bode Magnitude $q_1 \rightarrow z_{s\,1}$

(b) Bode Magnitude $q_2 \rightarrow z_{s\,1}$

(c) Bode Phase $q_1 \rightarrow z_{s\,1}$

(d) Bode Phase $q_2 \rightarrow z_{s\,1}$
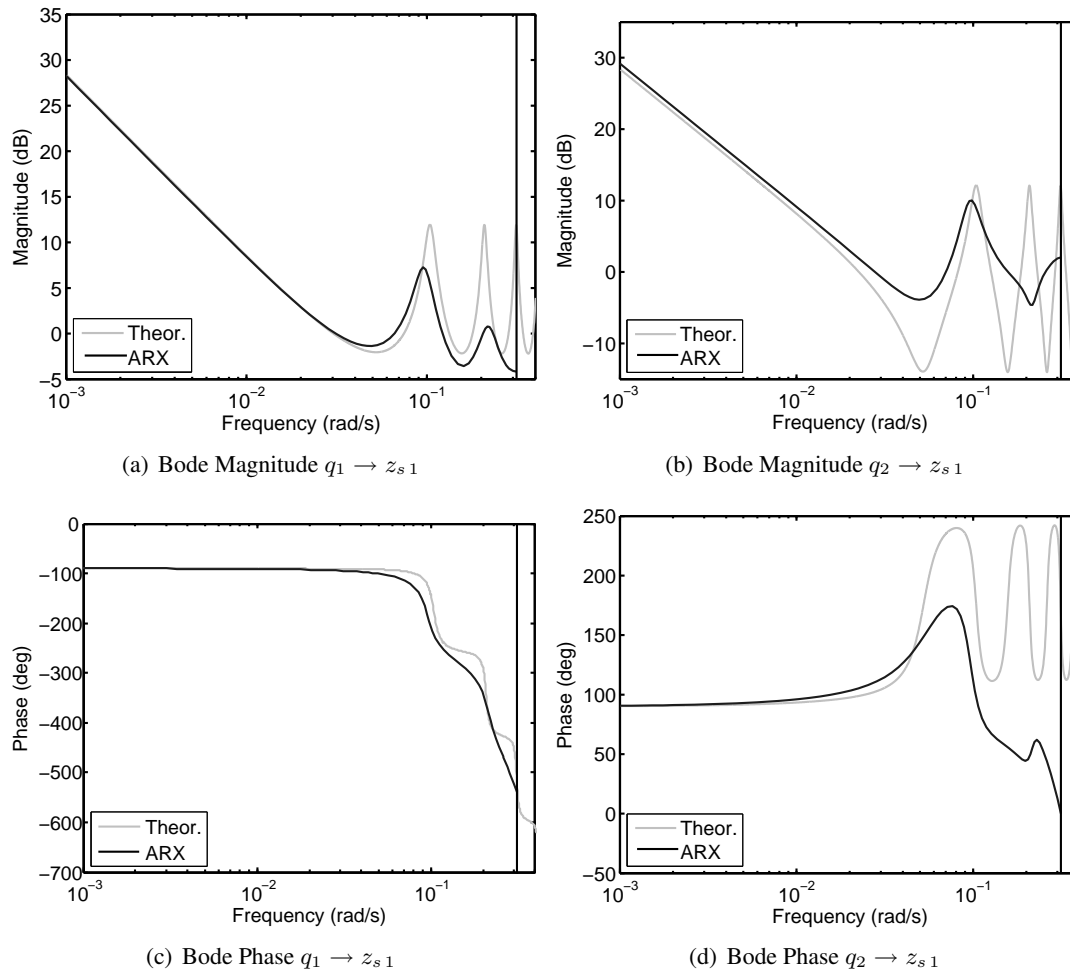
Figure 5.35: Theoretical Bode diagram v/s Bode diagram of identified ARX model - Pool 1

(a) Bode Magnitude $q_2 \rightarrow z_{s\,2}$

(b) Bode Magnitude $q_3 \rightarrow z_{s\,2}$

(c) Bode Phase $q_2 \rightarrow z_{s\,2}$

(d) Bode Phase $q_3 \rightarrow z_{s\,2}$
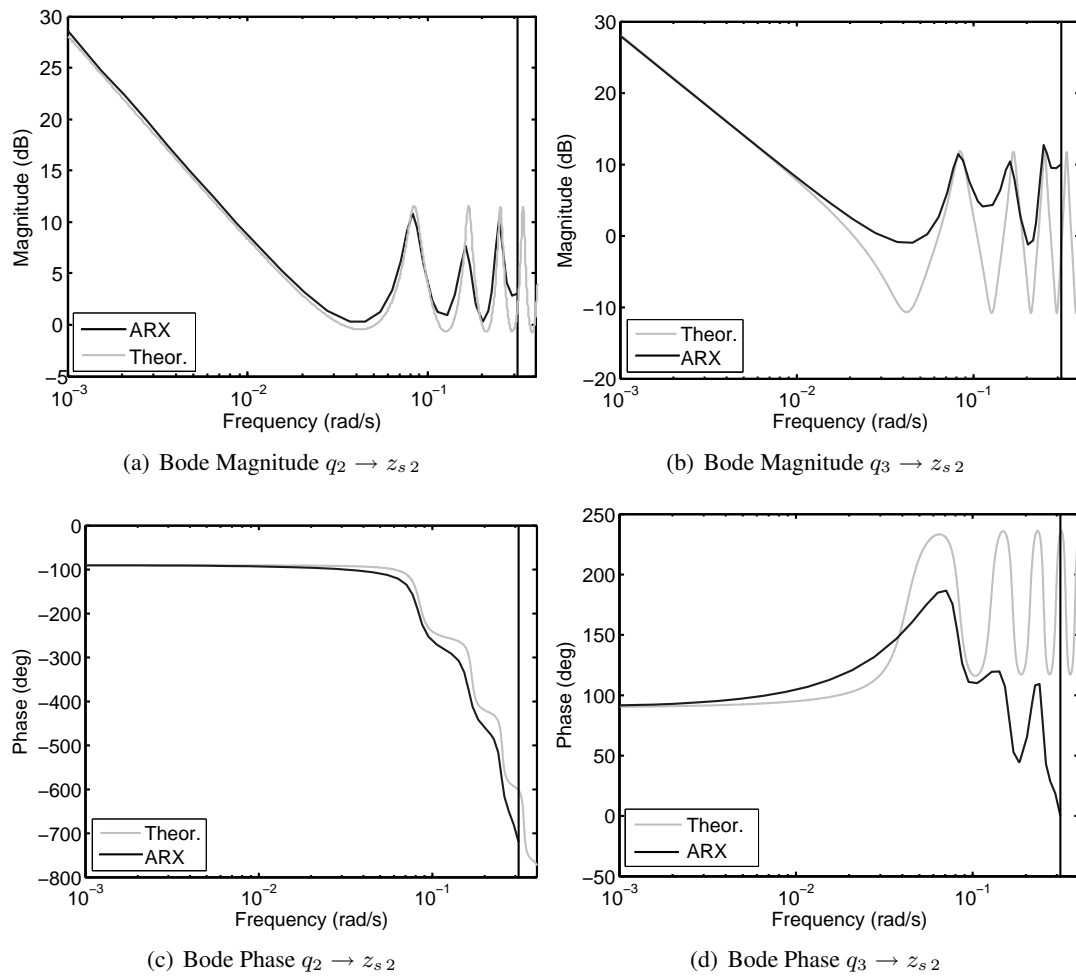
Figure 5.36: Theoretical Bode diagram v/s Bode diagram of identified ARX model - Pool 2
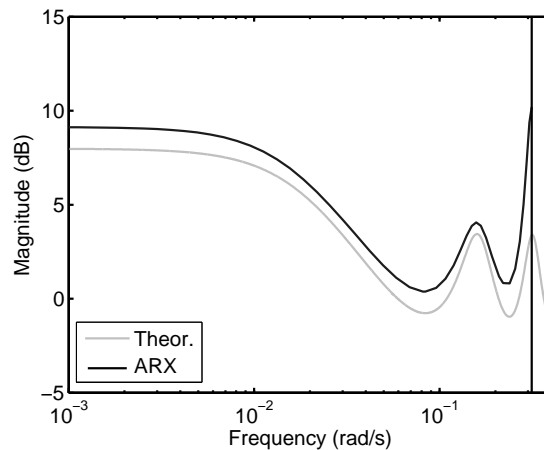
(a) Bode Magnitude $q_3 \rightarrow z_{s\,3}$
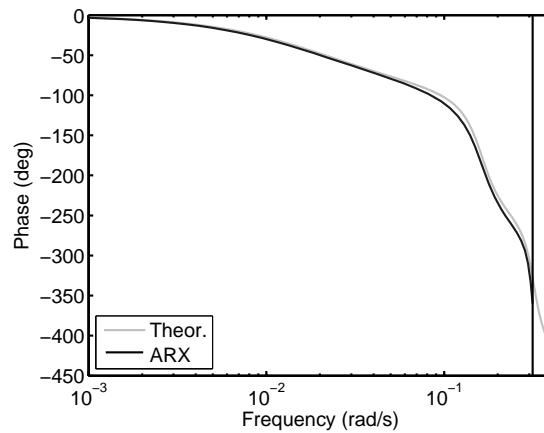
(b) Bode Magnitude $q_3 \rightarrow z_{s\,3}$

Figure 5.37: Theoretical Bode diagram v/s Bode diagram of identified ARX model - Pool 3

These figures show that the frequency responses of both models are in good agreement. The analysis is detailed in the following points:

- The magnitude plots display very small difference in the low frequency area.

- The first resonance peaks are located at identical frequencies in the magnitude plots, but their gains differ slightly, specially close to the Nyquist frequency.

- The concordance of the phase plots exhibits that the delays predicted by both models are almost identical.

The great similarity between the frequency responses of both models demonstrate that the ARX model does not only produce good results in the studied cases; it actually captured the behavior of the process around a working point. In fact, it is very likely that the magnitude differences correspond to the influence of dynamics that the unidimensional theoretical model has not considered and that the ARX model identified from the experimental data.

5.6 Conclusions

The main conclusion of this chapter is that an irrigation canal can be well modeled for control purposes by linear black-box models obtained by means of system identification techniques. Nevertheless, it is very important to take into account the "special characteristics" of the system (delays, resonant modes, integrator dynamics, etc.) when designing the identification procedure. If the process is performed in a blind manner, identified models are likely to be inaccurate and/or unappropriate and/or unstable.

Getting more in detail, the following concepts arose from this chapter:

- A detailed mathematical analysis has concluded that there is a general linear model structure that is applicable to any type of canal. One of the most relevant outcomes from this analysis, is that there are some new mathematical approximation results which reinforce and support the idea already suggested by some researchers, that there is always an integrator pole within this general structure.

- It is extremely important to take into account the structure, properties and characteristics of a pool before proceeding with system identification. This information is crucial to adequately select issues like: sampling time, model structure, experiment type, etc..

- A linearized pool model is only valid around a particular operation point. Among operation points, there are changes in the model gain, the time delay and in the amplitude and location of resonant modes.

- Long slopping pools are likely to have big transport delays. Short flat pools have also transport delays and in addition resonant modes. Both of them act as a swimming-pool or water tank in the long term behavior.

- It is recommendable to work with discharges and water levels in a pool identification procedure. Gate openings will always add additional nonlinearities and augment the identification complexity. In fact, the validity range of a pool linearization is generally shorter when using gate openings instead of gate discharges. Gates and other hydraulic structures can always be afterwards included in an already identified discharge-based model.

- There is not a unique solution in the sampling time selection. However, it was found useful to obtain the step response of a pool and divide approximately the time taken to reach a clear tendency by 15.

- PRBS type discharge signals are very appropriate to collect pool identification data.

- It is known that the identification of a system with integrators is very erratic about the exact location of these poles. The results indicated that it is helpful to rectify the location of the integrator pole after the model has been identified.

- The parameters of the models studied in this chapter can be easily obtained using linear least squares parameter estimation techniques. As a result, they can be also estimated during the normal operation of system. That opens the application of model adaptation.

- Simulation results have shown that ARX and Laguerre model structures can adequately approximate the pool behavior around an operation point. However, the ARX model performed better and with less parameters.

- Single identified pool models can be easily arranged to generate a complete irrigation canal model.

- A correctly identified MIMO ARX model can adequately model a real experimental canal around an operation point. Time domain and frequency domain results demonstrate that with a model order between 5 and 10, it is capable to approximate the principal dynamical characteristics of the system. Moreover, the results have shown that a linear model obtained in this way can perform very accurate predictions in the future. A model with this characteristics is very useful for control design applications and particularly for predictive control methods.

- The experimental validation of the specifically designed identification process demonstrate its ability to deal with real cases.

As an overall summary, two practical tools have been developed in this chapter:

1. A complete procedure to identify canal models from measured data.

2. A multivariable ARX model of the Canal PAC-UPC.

Both are mainly oriented for prediction and control purposes. These results will be recurrently used to design water level controllers for the Canal PAC-UPC in the next chapter of this thesis.

Chapter 6

Control of an Irrigation Canal

The automatic control of irrigation canals is the last issue that is treated in this thesis. As commented in other sections, the final goal of an irrigation canal control design is to deliver water to several farms with the highest achievable performance, flexibility and reliability.

The literature review chapter confirms that there are many control schemes and design strategies developed in the last decades. Thus, the focus of this chapter is to make a contribution in this area by pursuing the following objectives:

- To compare and study some control solutions developed by other researchers.

- To propose and present a new semi-decentralized control solution approach for irrigation canals.

- To show some advantages to be gained, if a predictive control strategy is used in the control of irrigation canals.

- To demonstrate the usefulness of well-designed data-based identified canal models, like the ones presented in the previous chapter, in control design problems.

- To remark the existence and influence of some practical implementation related problems.

- To automatize the operation of the Canal de Prueba de Algoritmos de Control - Universitat Politècnica de Catalunya (Canal PAC-UPC).

6.1   Control approach

In general, the overall control problem in irrigation canals can be viewed as the task of regulating either water levels, water volumes or water discharges in an open-channel. However, it is more common to use water levels as the controlled variables. The usual distribution of controlled water levels ($Z_{s\,i}$) in an irrigation canal is depicted with big dots in figure 6.1.
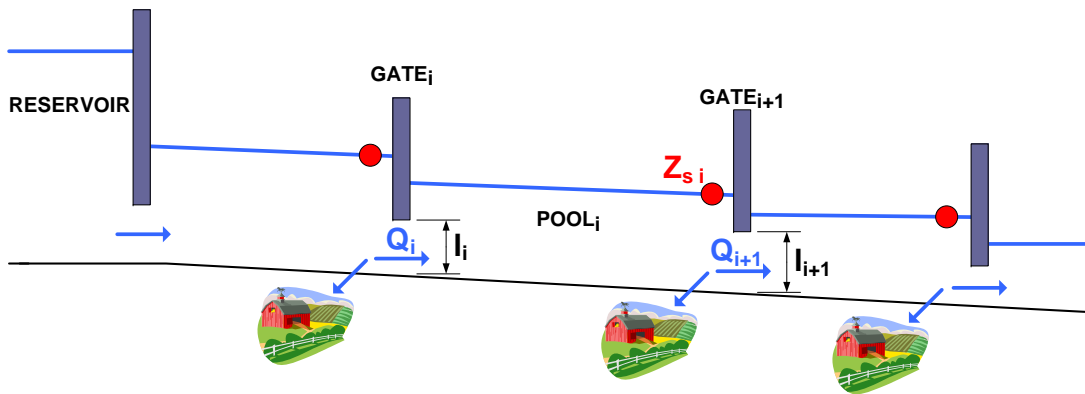
Figure 6.1: Sketch of an irrigation canal and its components

Regardless the approach used, the process is made up of several master-slave control loops shaping a control topology known as Cascade Control. This term is used when a set of control loops are placed one inside another. For irrigation canals, this is necessary because any of the aforementioned water variables can only be manipulated by controlling other variables like gate discharges (Q_i) and/or gate openings (l_i). In other words, to control the main canal variables, it is first necessary to control other set of secondary variables and so on. Hence, the control problem has to be tackled in different hierarchical layers. When controlling water levels, there are two global strategies that can be used to implement automatic control in irrigation canals:

1. (Figure 6.2) To consider a model where water levels depend directly on gate openings and:

    (a) to use a control algorithm to calculate required gate openings (SPl) so as to obtain desired water level values;

    (b) immediately afterwards, to act over each gate servomotor in order to move the gates to the requested positions (SPl).
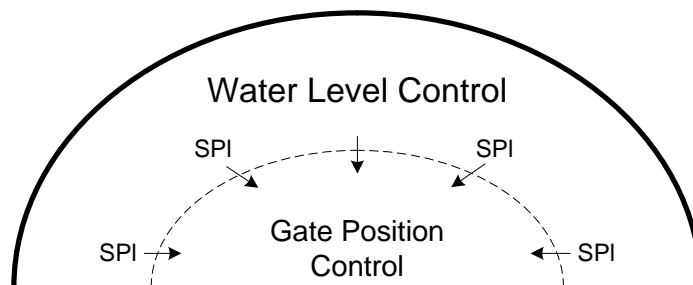
Figure 6.2: Possible irrigation canal control strategy

2. (Figure 6.3) To formulate a model where water levels depend explicitly on gate discharges and:

(a) to use a control algorithm to compute required gate discharges (SPq) in order to maintain water levels at desired values;

(b) to calculate required gate openings (SPl) so as to obtain the requested gate discharges (SPq) by using local controllers or by inverting the gate discharge equations;

(c) to operate the servos in order to move the gates to the demanded positions (SPl).
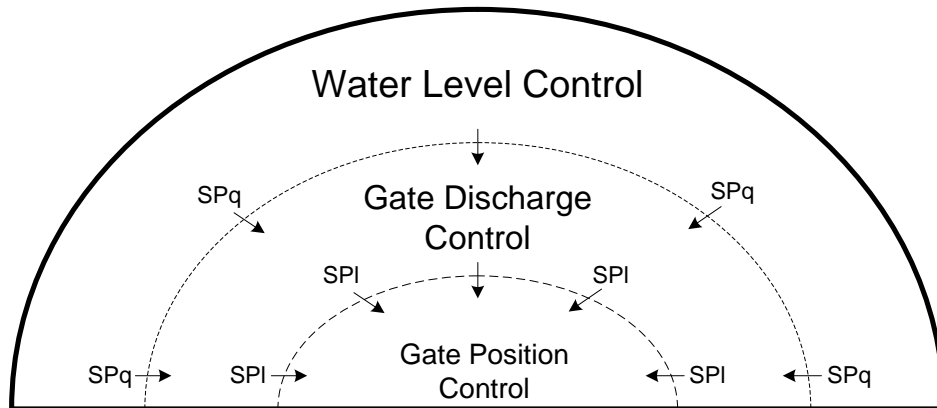
Figure 6.3: Canal control philosophy used in this research work

In this work, the preferred strategy is the second one (figure 6.3). The main reason is that the multivariable water level control problem is simplified by using this approach. As seen in the previous chapter, under this perspective it is possible to adequately approximate the canal behavior with pool models that depend only on the hydraulic variables between gates i and $i+1$ (Q_i, Q_{i+1}, Q_{Li} and Z_{si}). This type of modeling has some advantages for control. First of all, this abstraction of the multivariable water level control problem is weakly coupled as illustrated in (5.32) [page 109]. Furthermore, the actuator nonlinearities are not considered at this stage. Consequently, this control problem is easier to solve.

Inevitably, the problems related to unmodeled dynamics of gates (actuators) and other hydraulic structures are transferred to the gate discharge and to the gate position control layers. Therefore, the final success in regulating water levels in the canal depends in a high degree in the accuracy and performance of this two subordinate control layers.

6.2   Gate position control

This is the cornerstone of any irrigation canal control scheme. All other control layers depend, in a high degree, on the achieved gate opening accuracy after a control law computation. As a matter of fact, there are hydraulic conditions where the gate discharge is very sensitive to gate position errors. Additionally, there are researchers that have informed control performance degradation because of gate movement restrictions (Clemmens and Schuurmans, 2004b; Wahlin and Clemmens, 2002; Wahlin, 2004).

This section is focused on gates moved by servomotors, because it is the only type of motors in the Canal PAC-UPC. A typical gate position control scheme is sketched in figure 6.4.
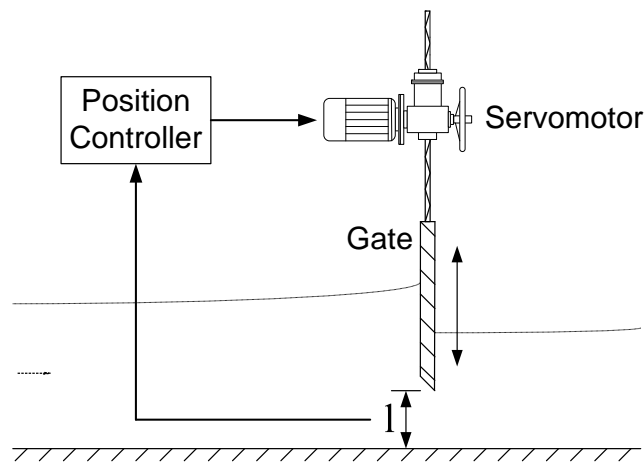
Figure 6.4: Gate position control

In general, the position control of servomotor-driven gates is performed by specialized electronic devices that already implement a built-in control. There are different alternatives depending on the electrical parameters of a particular servomotor. Their specific details are beyond the scope of this work.

In general, servomotors are configured to work either at a constant speed or at a variable speed. A servomotor operated at a constant speed have a longer lifetime than one controlled at a variable speed. Unfortunately, it is almost impossible to reach a highly precise position with a servomotor that works at a constant speed.

In the Canal PAC-UPC, there are only elementary constant speed motor drives. To improve the precision of the gate openings, the original position controllers were overridden by software. The main idea behind this decision was to tune the controllers as much as possible and to incorporate practical knowledge in the control law. The servos were operated at constant speeds and the controllers were forced to follow the following simple orders: open gate, off, close gate.

Using these orders, it was possible to implement the following simple position control algorithm:

Data: sp: desired position, pv: actual position, ξ: accepted error
Result: u: required action
begin
 $e \longleftarrow (sp - pv)$;
 if $e > \xi$ **then**
  $u \longleftarrow$ open;
 else if $e < -\xi$ **then**
  $u \longleftarrow$ close;
 else
  $u \longleftarrow$ off;
 end
end

Algorithm 1: Gate position control algorithm

This algorithm should be executed repeatedly at fast rate in order to obtain good results; in this case the repetitions were performed every $0.1\,\text{s}$.

The objective of the algorithm is to move a gate until reaching an acceptable positioning error ξ. Then, it switches the servomotor off. The reason to stop a gate before reaching a set point, is that the inertial forces make a gate to move farther than the switch off point. Thus, it is necessary to make ξ approximately equal to the inertial effect in order to get a gate position close to a set point.

A gate positioning error will always exists with a constant speed servomotor. It depends on the velocity of the servomotor, particular design of its gears, mechanical forces over the gate, etc.. This value should be determined for each gate. An overestimation of this parameter would lead to larger gate opening errors. In contrast, an underestimation of this value would unnecessarily force the servomotor by pursuing a positioning precision that is impossible to reach. Hence, an appropriate value will lead to accurate gate openings and will protect the lifetime of the servomotor.

The determination of the ξ parameter value was performed for every gate, measuring experimentally an average distance traveled by each gate after switching its servo off. The resulting values are presented in table 6.1.

Table 6.1: Determination of the ξ parameters

Gate name	ξ (mm)
Gate 1	8.0
Gate 3	9.5
Gate 5	10.1

With this simple control implementation, it was possible to obtain gate openings with a

precision of approximately $\pm 2\,\mathrm{mm}$. However, the control algorithm made evident a practical problem: the minimum gate movement restriction. In this case this restriction is equal to the ξ values. In other words, gates can not be moved less than their corresponding ξ values. This mechanical problem arises from the fact that it is impossible to try to move a gate a distance less than the inertial effect.

This is a known actuator nonlinearity in irrigation canals (but not always considered in some research papers) that produces an overall control performance deterioration. In general, it compels a water level control system to indefinitely oscillate around a working regime. Unfortunately, it is very difficult to implement a control scheme that deals with this actuator problem when it already exists.

This gate movement restriction can be considered as a dead zone on the slew rate of the actuators and for the superior control layers translates into a gate discharge supply restriction.

There is an alternative that could be useful in some cases. The position control loop acts generally at a faster frequency than the rest of the loops. Thus, a short additional transient in the position will not influence in a high degree the performance of the other master loops. It is possible to follow position set points that fall in the dead zone by forcing the gate to first move away from this area and then reverse to go after the desired position.

The proposed solution produces more gate movements and discharge transients, but offers a way to reach a higher positioning accuracy.

In general, this control will produce long trajectories for small positioning corrections. Hence, it is also necessary to limit the control sensitivity to avoid unnecessary gate movements owing to sensor noise.

An algorithm that fulfils the requirements could be the following:

Data: sp: desired position, pv: actual position, ξ: minimum movement, ν: noise level
Result: u: required action
begin
    $e \longleftarrow (sp - pv)$;
    if $e > \xi$ **then**
        $u \longleftarrow$ open;
    else if $\xi > e > \nu$ **then**   /* avoids dead zone */
        $u \longleftarrow$ close;
    else if $-\xi < e < -\nu$ **then**   /* avoids dead zone */
        $u \longleftarrow$ open;
    else if $e < -\xi$ **then**
        $u \longleftarrow$ close;
    else
        $u \longleftarrow$ off;
    end
end

Algorithm 2: Gate position control algorithm plus minimum gate movement restriction avoidance

---

6.3 Gate discharge control

The objective of this control layer is to transform desired gate discharges into required gate openings. Once the gate openings are known, they are passed to the gate position controllers as set points. There are to ways to perform this task according to Malaterre and Baume (1999):

1. To use a dynamic controller like a Proportional Integral Derivative (PID) controller.

2. To inverse the gate discharge equation so as to obtain an equation where, from a desired discharge value, it is possible to calculate the required gate opening.

The practical knowledge acquired during this research work, suggests that the second alternative would be better than the first one. The discharge measurement chapter has already stated the accuracy of gate discharge models. It has been seen that their precision is similar or better than some velocity measurement based discharge sensors. Thus, there is no reason to seek for the set point in a blind manner. Moreover, the minimum gate movement restriction is likely to easily destabilize any dynamic controller, especially when coming closer to the set point.

Going more into detail, the selection of the second alternative uses a gate discharge nonlinear relationship that is normally of the following form;

$$Q = f(h_1, h_3, l) \tag{6.1}$$

where h_1 and h_3 are the gate upstream and downstream water level respectively and l is the gate opening. These variables are illustrated in figure 6.5 for the submerged flow condition.
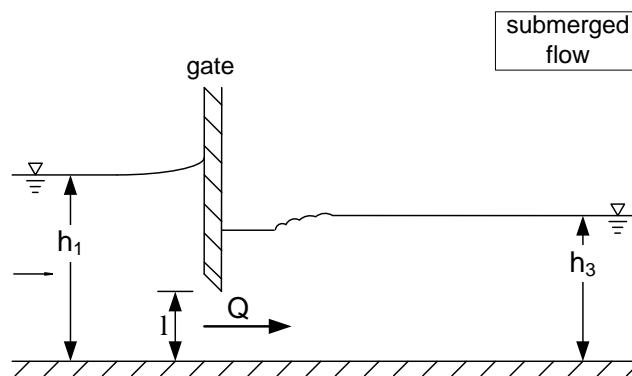
Figure 6.5: Sketch of the variables involved in gate discharge

Thus, assuming that a discrete-time discharge control algorithm is running at instant k, it is possible to calculate a gate opening that would make possible a given desired gate discharge (SPq) in a future time instant $k+1$ in the following way:

$$l(k+1) = f^{-1}(h_1(k+1), h_3(k+1), SP_Q(k+1)) \tag{6.2}$$

As can be observed, (6.2) needs at $k+1$ the upstream and downstream water levels (h_1 and h_3) and the discharge set point (SP_Q), in order to calculate the required gate opening. Unfortunately, $h_1(k+1)$ and $h_3(k+1)$ are not still known at instant k; their values have to be estimated in some way. There are two alternatives:

1. To consider that $h_1(k+1) \approx h_1(k)$ and $h_3(k+1) \approx h_3(k)$:

$$l(k+1) = f^{-1}\left(h_1(k), h_3(k), SP_Q(k+1)\right) \tag{6.3}$$

2. To estimate the water level variations (Δh_1 and Δh_3) due to the gate movement and calculate the future water levels as $h_1(k+1) = h_1(k) + \Delta h_1$ and $h_3(k+1) = h_3(k) + \Delta h_3$:

$$l(k+1) = f^{-1}\left(h_1(k) + \Delta h_1, h_3(k) + \Delta h_3, SP_Q(k+1)\right) \tag{6.4}$$

The second alternative is better than the first one, if the level variations are predicted with certain accuracy. In Malaterre and Baume (1999), the following formulas are proposed to calculate the water level variations:

$$\Delta h_1 = \frac{SP_Q(k+1) - Q(k)}{B(k)\,(V(k) - C(k))} \qquad \Delta h_3 = \frac{SP_Q(k+1) - Q(k)}{B(k)\,(V(k) + C(k))} \tag{6.5}$$

where B (surface width), V (flow velocity) and C (celerity) are calculated for present conditions. Both equations come from the Theory of Characteristics after some simplifications (no friction and uniform flow).

The experiments carried out in the Canal PAC-UPC suggested that the Ferro method equations are highly suitable for model inversion. This method performed the best among all the studied methods and has a very simple structure (see Chapter 4 conclusions [page 68]).

The derivation of a discharge control law for the submerged flow Ferro equation (4.19) [page 51] is going to be detailed next. The free flow case is not going to be developed but its derivation is almost identical.

In order to perform the model inversion it is first necessary to recall (4.19):

$$Q = b \sqrt{g\left(l\,k_0'\left(\frac{h_1 - h_3}{l}\right)^{k_1'}\right)^3}$$

where b is the gate width, g is the gravity acceleration and k_0', k_1' are numerical constants to be calibrated experimentally.

This equation can also be rewritten in the following form:

$$Q = b\,g^{0.5}\,l^{(1.5 - 1.5k_1')}\,k_0'^{1.5}\,(h_1 - h_3)^{1.5k_1'}$$

Now, the inversion of this equation leads to:

$$l = \left(\frac{Q}{b \, g^{0.5} \, k_0^{\prime 1.5} \, (h_1 - h_3)^{1.5 k_1^{\prime}}} \right)^{1/(1.5 - 1.5 k_1^{\prime})} \tag{6.6}$$

Therefore, employing (6.6) in (6.4) produces the following gate discharge control law:

$$l(k+1) = \left(\frac{SP_Q(k+1)}{b \, g^{0.5} \, k_0^{\prime 1.5} \, [(h_1(k) + \Delta h_1) - (h_3(k) + \Delta h_3)]^{1.5 k_1^{\prime}}} \right)^{1/(1.5 - 1.5 k_1^{\prime})} \tag{6.7}$$

where Δh_1 and Δh_3 should be formulated depending on their respective cross sections. For a rectangular cross section canal like the Canal PAC-UPC, equations yield the following expressions:

$$\Delta h_1 = \frac{SP_Q(k+1) - Q(k)}{Q(k)/h_1(k) - B\sqrt{g \, h_1(k)}} \qquad \Delta h_3 = \frac{SP_Q(k+1) - Q(k)}{Q(k)/h_3(k) + B\sqrt{g \, h_3(k)}} \tag{6.8}$$

In summary, using (6.7) with (6.8) in a real-time control algorithm enables the implementation of an efficient gate discharge control. However, there is still one practical problem: these equations assume a boundless availability of water to deliver. In general, this supposition is only valid for gates that receive water from big reservoirs; gates that take water from upstream pools can only deliver water until a certain limit. It is important to know this gate discharge deliverance limit for the following reasons:

1. In order to prevent gates to come out of water; gate discharge equations are only valid and can be used in this situation.

2. To feed this information back to a control algorithm and improve its performance.

3. To make this operational restriction known to the canal operators.

It has not been found in the literature a simple procedure that can estimate this maximum gate discharge value. However, an expression for calculating an approximation of the maximum discharge that would pass through a particular gate in the near future if it is completely opened, can be easily derived using (6.3).

It is known that the flow through a gate produces an appreciable upstream-downstream water level gradient ($h_3 - h_1 \gg 0$). On the other hand, when a gate is almost out of water it is clear that it is impossible to deliver more water. In that situation this gradient is almost zero. Consequently, it is possible to calculate an estimation of the maximum discharge that a gate can deliver in a particular instant, choosing a minimum water level gradient and calculating the

related discharge. In other words, the following relationship has to be verified:

$$(h_1(k) + \Delta h_1) - (h_3(k) + \Delta h_3) > \epsilon \tag{6.9}$$

where ϵ is a minimum admissible water level difference. Replacing (6.3) in (6.9) produces the following inequality after reordering:

$$SP_Q(k+1) < Q(k) + \frac{B(k)\,(V_1(k) - C_1(k))\,(V_3(k) + C_3(k))\,[-h_1(k) + h_3(k) + \epsilon]}{V_3(k) + C_3(k) - V_1(k) + C_1(k)} \tag{6.10}$$

where V_x and C_x ($x = 1, 3$) are velocities and celerities calculated at upstream and downstream positions.

Expression (6.10) gives an upper bound for the admissible discharge set point SP_Q so as to guarantee a minimum upstream-downstream water level difference ϵ.

The value of ϵ should be selected for each particular situation. For the gates of the Canal PAC-UPC, it was found appropriate to fix it to $7\,\mathrm{mm}$ in each case. Essentially, this choice is motivated by a discharge measuring concern: a smaller level difference ($h_1 - h_3$) leads to erratic discharge calculation results due to water level variations. This level variations can be more or less pronounced depending on the flow characteristics (Reynolds number). If in other cases the gate discharge measurement is carried out by other means, it is possible to select lower values that ensure that the gate is still under water ($\epsilon > 0$).

To sum up, a typical discharge control algorithm for the Canal PAC-UPC would be:

Data: sp: desired discharge, Q: current discharge value, h_1: current upstream water level
Data: h_3: current downstream water level, ϵ: minimum allowable water level gradient
Data: b: gate width, B: canal width, k'_0, k'_1: Ferro constants, g: acceleration of gravity
Result: l: required gate opening
begin

    $V_1 \longleftarrow \frac{Q}{B\,h_1}$;

    $C_1 \longleftarrow \sqrt{g\,h_1}$;

    $V_3 \longleftarrow \frac{Q}{B\,h_3}$;

    $C_3 \longleftarrow \sqrt{g\,h_3}$;

    $sp_{max} \longleftarrow (Q + \frac{B\,(V_1 - C_1)\,(V_3 + C_3)\,(-h_1 + h_3 + \epsilon)}{V_3 + C_3 - V_1 + C_1})$;   /* max.discharge */

    if $sp > sp_{max}$ **then**   /* limit the SP */

        $sp \longleftarrow sp_{max}$;

    end

    $\Delta h_1 \longleftarrow \frac{sp - Q}{B\,(V_1 - C_1)}$;

    $\Delta h_3 \longleftarrow \frac{sp - Q}{B\,(V_3 + C_3)}$;

    $l \longleftarrow \left(\frac{sp}{b\,g^{0.5}\,k'^{1.5}_0\,[(h_1 + \Delta h_1) - (h_3 + \Delta h_3)]^{1.5 k'_1}} \right)^{\frac{1}{1.5 - 1.5 k'_1}}$;   /* req.opening */

end

Algorithm 3: Gate discharge control algorithm plus discharge saturation constraint

Running this algorithm repeatedly at a given sampling time produces a recalculation of the required gate opening in order to maintain a gate discharge value at a desired set point. This gate opening is passed to the position controller as a position set point and it is this slave controller which finally moves the gate. Control design standards recommend that the slave loop should run at least 10 times faster than the master loop in order to insure the independence of the loops. In other words, the discharge control algorithm should be updated at a slower rate than the position control algorithm. When this is not possible, the control performance is likely to decrease. In this case the discharge control sampling time was chosen to be $10\,\mathrm{s}$.

6.4 Water level control

The water level control should be the final goal of an irrigation canal automation. Generally, the control objective is to maintain a constant level at the downstream end of each pool in a canal. This is the position where offtakes are normally located. As commented before, this regulation of water levels allows:

- a better management of an irrigation canal

- multiple offtakes at the same time

- more flexibility in the irrigation schedule

- improvements in the confidence level of the water delivery service

- the reduction of canal overflows

- the reduction of the wetting/drying cycles so as to protect the canal covering.

- etc.

The water level control problem in irrigation canals is exemplified in figure 6.6.
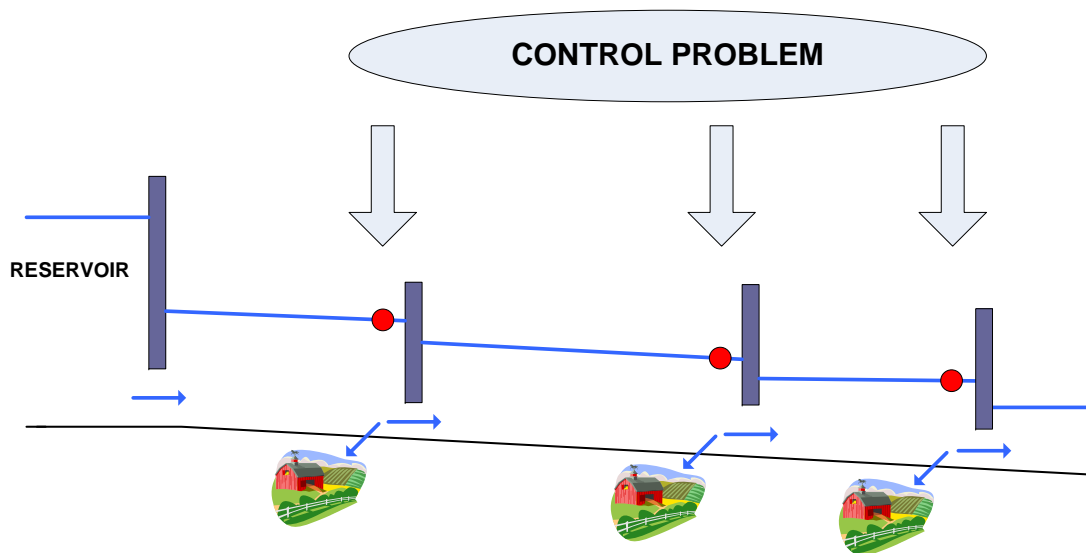
Figure 6.6: Usual location of controlled levels in irrigation canals

This control problem has been extensively studied in the last decades and there are many control algorithms and strategies that have been proposed by the canal automation research community.

An irrigation canal is a coupled Multiple-Input Multiple-Output (MIMO) system with many peculiar characteristics as was seen in the previous chapter. The automation of this type of

systems can be tackled by just one supervisory controller or by a number of less complex controllers. These two strategies are known respectively as

- Centralized Control

- Decentralized Control

A centralized control strategy takes into account all the objectives that should be fulfilled and finds the best solution for the whole system. A decentralized control strategy takes the system as a set of Single-Input Single-Output (SISO) processes and controls each one of them with a single controller. When the system is coupled, decoupling controllers are normally added in the control scheme in order to counteract the interactions among loops.

Both schemes have their own advantages and drawbacks. In general, the best control performance can be obtained with a centralized controller, but its design and implementation is complex. Conversely, a decentralized control scheme is normally based on simpler control methods but the overall performance is suboptimal. The decentralized approach has also some strategic benefits; a failure in the instrumentation is likely to affect only a part of the whole control system, the automation can be carried out in stages (to automate only some pools in the beginning), etc..

This work is intended to contribute in the development of an alternative irrigation canal control strategy that is going to be called

- Semi-decentralized Control

The reason behind the development of this new strategy is to gain some performance advantages of the centralized control while keeping the simplicity of the decentralized scheme. This scheme is formed by individual controllers that take over the regulation objectives of two water levels at the same time: one downstream water level and one upstream water level.

This scheme was not initially thought for a particular control method. However, its design needs a control method that can deal with multivariable systems. One control method that has proven its capability to handle both SISO and MIMO systems is Predictive Control. Predictive Control is more complex to design and implement than, for example, PID control, but offers some interesting control performance improvements. This research work has been based on the hypothesis that predictive control has nice properties to control irrigation canals.

In the following sections, irrigation canal centralized, decentralized and semi-decentralized control strategies are going to be designed for the Canal PAC-UPC. Two control methods are going to be used, namely Proportional Integral (PI) Control and Predictive Control. In the decentralized case, controllers from both methods are going to be designed, but only Predictive Control is going to be used for the other two schemes.

6.4.1 Decentralized control

In an irrigation canal automation, the decentralized management is carried out using one controller for each pool. This controller regulates the downstream water level by manipulating either the upstream gate discharge or the downstream gate discharge. When the upstream gate discharge is the manipulated variable the control strategy is called Downstream Control. On the opposite, when the manipulated variable is the downstream gate discharge it is called Upstream Control. In the following only Downstream Control schemes are going to be tested. A typical decentralized downstream control scheme is depicted in figure 6.7.
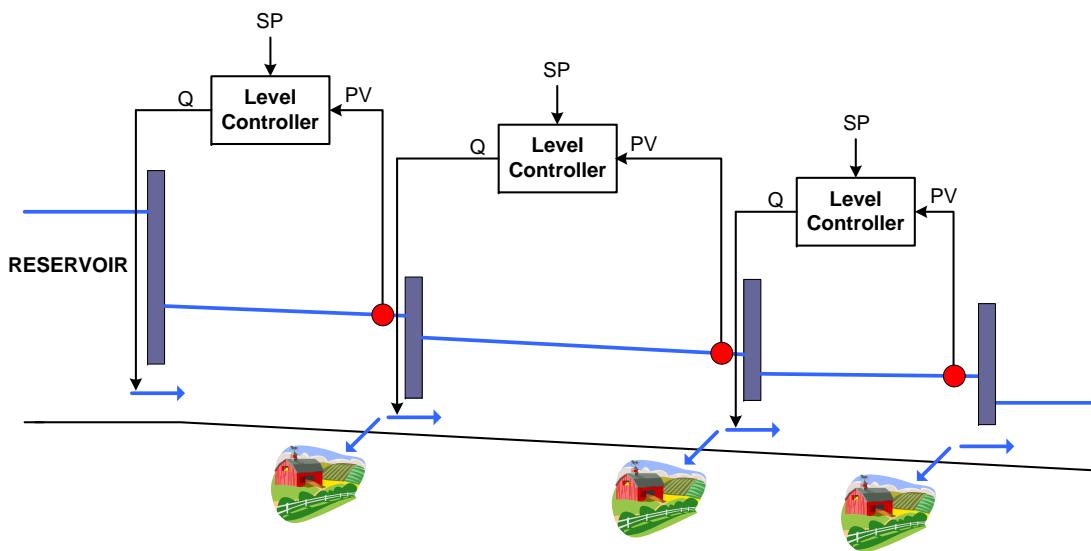
Figure 6.7: Typical downstream control example

In figure 6.7, Q is the gate discharge (control action), PV (Process Variable) is the controlled variable, which in this case corresponds to downstream water levels, and SP is the acronym for Set Point or, in other words, the value at which it is desired to maintain a water level.

This type of control can be implemented with any type of control method. In this case, it is going to be studied with PI controllers and with predictive controllers.

6.4.1.1 Level control with PI controllers

Controller derivation The control of irrigation canals using PI controllers has been studied by many researchers. This type of controllers are governed by the following control law:

$$u(t) = K_p\, e(t) + \frac{K_p}{T_i} \int\limits_0^t e(t)\, dt \tag{6.11}$$

where $e(t) = SP(t) - PV(t)$. K_p and T_i are control tuning constants and e is the difference between the desired value (or Set Point (SP)) and the measured value of the controllable variable

(or Process Variable (PV)): a downstream water level. u is called the control action which corresponds in this case to the required upstream gate discharge in order to maintain the water level at the desired value.

There are many ways to discretize (6.11). For instance, if the integration is approximated using the Forward Euler method, the discrete PI control law can be rewritten in the following form:

$$u(k) = K_p\, e(k) + \frac{K_p}{T_i} \left[T \sum_{i=0}^{k-1} e(i) \right] = K_p\, e(k) + \frac{K_p}{T_i} \left[I(k-1) + T\, e(k-1) \right] \qquad (6.12)$$

where T is the control recalculation period and $I(k-1)$ is the integration result obtained in the last control iteration.

A typical downstream water level PI control algorithm could be:

Data: sp_k: reference level value, pv_k: current water level
Data: K_p: proportional gain, T_i: integrative time, T: control period
Result: Q_k: required gate discharge
begin
    $e_k \longleftarrow (sp_k - pv_k)$;
    $I_k \longleftarrow (I_{k-1} + T\, e_{k-1})$;
    $Q_k \longleftarrow (K_p\, e_k + \frac{K_p}{T_i} I_k)$;   `/* req.discharge */`
    $e_{k-1} \longleftarrow e_k$;   `/* saves error for next iter */`
    $I_{k-1} \longleftarrow I_k$;   `/* saves integral for next iter */`
end

Algorithm 4: Example of a PI control algorithm

In theory, this simple algorithm should be able to control a process. However, some precautions have to be also taken in order to successfully implement this algorithm in practice. There are two problems that normally affect this type of implementation: Integrator Windup and Bump Transfer.

Integrator Windup and Bump Transfer   The first one is produced when the actuator is already saturated (e.g when gates are almost out of water) and the process is not at the set point value yet. In such a case, the integral part of the control law grows unbounded. This phenomenon is known as integrator windup.

The second one takes place when the controller is switched from manual mode to automatic mode. While the process is driven manually by the operators, the control calculations are still performed. As a result, the integral value becomes uncertain. When the system is switched back to the automatic mode, the incorrect integral value produces a bump in the control action value.

In controlled irrigation canals both situations are likely to occur. It is very normal to switch off the automatic mode and operate the gates "manually" under special circumstances. Like-

wise, and as already remarked in Section 6.3, gates convey a flow rate supplied from distant reservoirs. Thus, it is highly possible that a level controller, specially during operational transitions, computes a required gate discharge that is impossible to attain at that moment, but that the controller assumes accomplishable leading to the windup in the result of the integration.

Both problems have been studied by the control community and can be solved by modifying the original algorithm with suitable solutions. One solution that can solve both problems, consist in gradually modifying the integral value in order to equal the controller output with the saturated actuator value or the manually driven action. This operation can be accomplished adding a sort of feedback loop with an appropriately chosen gain T_t ($T_t = 0.5\,T_i$ gives usually good results). This solution is exemplified in the following control algorithm:

Data: sp_k: reference level value, pv_k: current water level, pvQ_k: current discharge
Data: K_p: proportional gain, T_i: integrative time, T: control period, T_t: anti-windup gain
Data: Q_{max}: maximum available discharge, Q_{min}: minimum permissible discharge
Result: Q_k: required gate discharge
begin
    $e_k \longleftarrow (sp_k - pv_k)$;
    $I_k \longleftarrow (I_{k-1} + \frac{K_p\,T}{T_i}\,e_{k-1})$;
    $Q_k \longleftarrow (K_p\,e_k + I_k)$;
    if *automatic mode* **then**
        if $Q_k > Q_{max}$ **then**   /* anti-windup protection */
            $I_{k-1} \longleftarrow (I_k + \frac{T}{T_t}\,(Q_{max} - Q_k))$;
            $Q_k \longleftarrow Q_{max}$;
        else if $Q_k < Q_{min}$ **then**
            $I_{k-1} \longleftarrow (I_k + \frac{T}{T_t}\,(Q_{min} - Q_k))$;
            $Q_k \longleftarrow Q_{min}$;
        else
            $I_{k-1} \longleftarrow I_k$;
        end
    else if *manual mode* **then**
        if $Q_k \neq pvQ_k$ **then**   /* bumpless transfer */
            $I_{k-1} \longleftarrow (I_k + \frac{T}{T_t}\,(pvQ_k - Q_k))$;
        else
            $I_{k-1} \longleftarrow I_k$;
        end
    end
    $e_{k-1} \longleftarrow e_k$;
end

Algorithm 5: Example of a PI control algorithm with anti-windup protection and bumpless transfer

---

PI control tuning   Focusing on the application of PI controllers to irrigation canals, there are a few researchers that have derived specific tuning rules for these systems. Particularly, these

tuning rules have been developed for pools represented by the Integrator Delay (ID) model:

$$A_i \frac{dz_{s\,i}}{dt} = q_i(t - T_d) - q_{i+1}(t) \tag{6.13}$$

It has been also stated that the resonant modes limit the achievable performance of PI controllers. As a consequence, the magnitude (R_p) and location (ω_r) of these modes are also needed to tune these controllers properly. There is also one alternative to overcome this restriction: to use a PI controller in series with a low pass filter (PIF controller) (Schuurmans et al., 1999b; Litrico et al., 2005; Litrico and Fromion, 2006). This type of scheme can diminish the controller sensibility to resonance, centering the controller attention on the long-term response. Any type of low pass filter can do the job. For instance, in Schuurmans et al. (1999b) it was proposed the use of the following first order discrete-time filter:

$$F(z^{-1}) = \frac{1 - e^{-T/T_f}}{1 - e^{-T/T_f}\,z^{-1}} = \frac{1 - a}{1 - a\,z^{-1}} \tag{6.14}$$

where T is the control period and T_f is the filter time constant.

Table 6.2 summarizes some PI tuning rules that are given in Schuurmans et al. (1999b) and in Litrico and Fromion (2006); Litrico et al. (2006). All these rules are can be applied to pools with a small slope.

Table 6.2: PI controller tuning rules

	Litrico PI		Schuurmans PI		Schuurmans PIF		
	K_p	T_i	K_p	T_i	T_f	K_p	T_i
Formula	$0.47\frac{A}{T_d}$	$6\,T_d$	$\frac{1}{2\,R_p}$	$\frac{1}{\sqrt{2}}\frac{A}{K_p}$	$\sqrt{\frac{A\,R_p}{\omega_r}}$	$\frac{A}{2\,T_f}$	$6\,T_f$

Decoupling and feedforward Decoupling and feedforward loops can also been added to any of the previously designed control schemes. In general, decoupling loops try to diminish the interrelationship among coupled variables in a MIMO system. Feedforward loops give an important feature to any control system: to take into account measurable disturbances in the control solution.

These issues have been already addressed in Schuurmans et al. (1999b) for this type of irrigation canal control solutions. A typical control scheme with decoupling and feedforward enhancements is depicted in figure 6.8.

The decoupling goal, in this case, is to reduce the effect that a gate discharge can produce over an upstream water level, i.e. to reduce the disturbing effects of control actions from "adja-
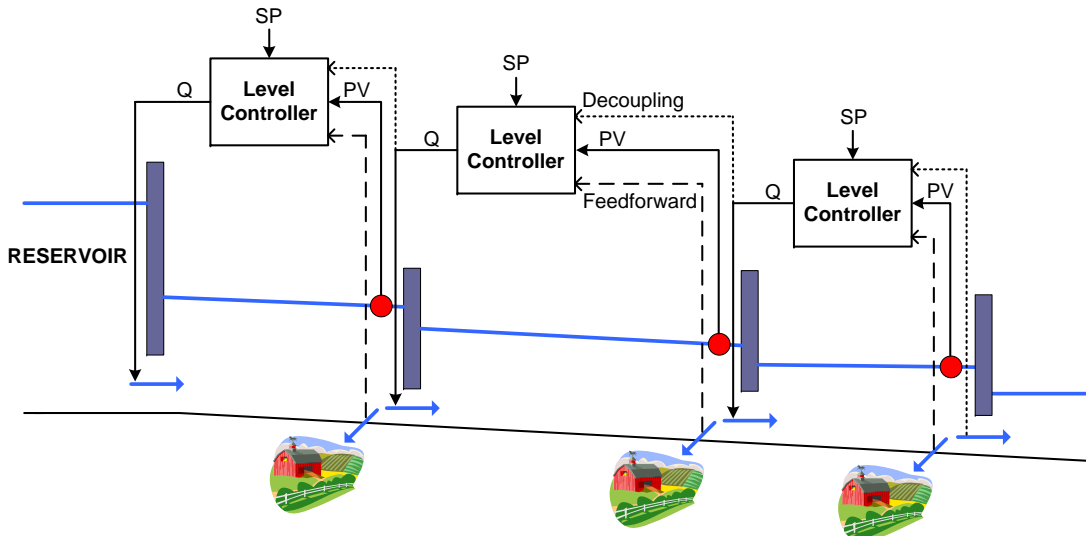
Figure 6.8: Downstream control with decoupling and feedforward capabilities

cent" controllers (Schuurmans et al., 1999b, page 191). The inclusion of a decoupling element
is very important in this type of PI control strategy; the use of the SISO design rules presented
before are strongly based on the loop independence assumption.

On the other hand, it is always helpful to feed a control scheme with the most available
information. If there are reliable measurements of the offtake discharges, the feedforward loops
can only benefit the control performance, specially when the results are not as good as required.

This type of strategies are implemented in a very simple way in Schuurmans et al. (1999b).
For a given pool i, it is only necessary to modify a recently calculated PI control action u_i
(upstream gate discharge) in the following form:

$$Q_i(k) = u_i(k) + Q_{i+1}(k) + Q_{Li}(k) \tag{6.15}$$

where Q_{i+1} is the discharge calculated by the controller of the next downstream pool (decou-
pling) and Q_{Li} is the offtake discharge measured value (feedforward).

6.4.1.2   PI control applied on the Canal PAC-UPC

With respect to the Canal PAC-UPC, the first two pools can be directly modeled using the ID
model (6.13). However, the last pool is somewhat different; the final weir eliminates the pure
integrator from the process as demonstrated in Section 5.2.5 (page 82). As a consequence, the
tuning rules presented in table 6.2 can not be applied to this particular pool. The PI controller of
this pool is alternatively tuned using a standard closed loop tuning rule such as the one proposed
in Åström and Hägglund (1995).

This tuning rule is based on the Ultimate Cycle Analysis, a procedure that determines the

stability limit of a controlled system by inducing a sustained output oscillation. Once this limit is known, the tuning is performed so as to ensure a stable response. The A-H tuning formulas are presented in table 6.3.

Table 6.3: Åström-Hägglund PI tuning rule

Parameter	Formula
K_p	$0.32\,k_u$
T_i	$0.94\,T_u$

In table 6.3, there are two parameters that have to be determined: the ultimate gain (k_u), which is the minimum controller gain that causes the system to continuously cycle and the ultimate period of oscillation (T_u).

In summary, it is necessary to estimate the ID model parameters of Pool 1 and Pool 2 and the ultimate cycle parameters of Pool 3 in order to calculate the parameters of the PI controllers. This information is given in table 6.4 and in table 6.5.

Table 6.4: ID model parameters for Pool 1 and Pool 2

	Backwater area, A (m^2)	Prop. delay, T_d (s)	Res. peak gain, R_p (s/m^2)	Lowest res. freq., ω_r (rad/s)
Pool 1	23.43	28.95	2.31	0.0955
Pool 2	24.30	34.45	3.47	0.0863

Table 6.5: Ultimate cycle parameters for Pool 3

	Ultimate gain, k_u (m^2/s)	Ultimate period, T_u (s)
Pool 3	0.6316	40

These parameters have been calculated from the Canal PAC-UPC identified ARX model (5.36) [page 121]. Hence, they are based on a system approximation around an operation point.

For Pool 3, the Ultimate Cycle Analysis was performed using a computer simulation of model (5.36) to avoid oscillations in the real canal.

These values were substituted in the PI tuning formulas and several sets of parameters were obtained. These formulas were developed in a continuous time framework so, in order to recover this performance using a sampled PI control, it is necessary to choose an appropriate control

time T. For systems with delays, this value should be around 0.5 or 0.33 times the delay. When the resulting operation rate is not tolerated by the actuator, it is better to consider this sampling constraint in the controller design (Litrico et al., 2006). The results are summarized in table 6.6.

Table 6.6: PI parameters tuned using different methods

	Litrico PI		Schuurmans PI		Schuurmans PIF			
	K_p (m²/s)	T_i (s)	K_p (m²/s)	T_i (s)	T_f (s)	K_p (m²/s)	T_i (s)	T (s)
Pool 1	0.381	173.7	0.216	76.5	23.8	0.492	142.8	10
Pool 2	0.332	206.7	0.144	119.2	31.2	0.389	187.5	10
	Åström and Hägglund PI							
Pool 3	0.202	37.6	0.202	37.6	—	0.202	37.6	10

MIMO based analysis It is worth to remark that the controller tunings were performed assuming simplified models in a SISO framework. At this stage, it is very useful to have a good multivariable linear model such as the one identified following the recommendations made in Chapter 5. A whole linear control scheme acting over an also linear MIMO process can be well analyzed inspecting the singular values of the system or using any Nyquist-like multivariable techniques (for details see Maciejowski (1989)). For instance, the characteristic locus of a MIMO process (plots of the eigenvalues of a system) gives the chance to apply the Generalized Nyquist theorem in order to test the stability of a final control design and to formulate some conclusions about the performance of a multivariable feedback system. This point can be exemplified by testing one of the suggested tunings. For example, the characteristic locus of the Canal PAC-UPC model controlled by the Litrico PI controller set is shown in figure 6.9.

The first aspect that should be noted is that this control scheme is absolutely unstable. Controlled irrigation canal systems are unstable when their characteristic locus encircles the point (-1,0), according to the Generalized Nyquist theorem. This behavior was somewhat expected. The authors themselves have remarked in Litrico and Fromion (2006) that, when there is a strong influence of resonant modes, they should be filtered in order to use their tuning recommendations. As a result, this tuning is going to be only implemented with appropriate filters from here on (Litrico PIF). For simplicity reasons, the same filters designed for Schuurmans PIF are going to be used.

Some performance conclusions can also be obtained from figure 6.9. This figure is plotted along with the so called "m-circles". If the characteristic locus penetrates the $3\,\mathrm{dB}$ m-circle, then at least one principal gain of the closed loop system will exhibit a resonance peak greater
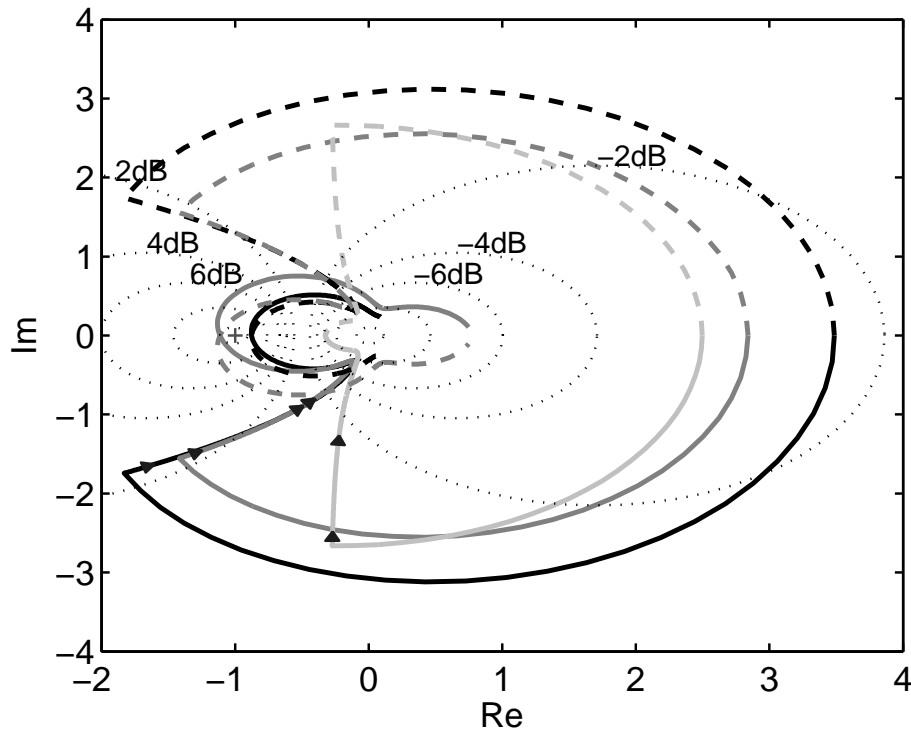
Figure 6.9: Characteristic locus of Canal PAC-UPC model controlled with Litrico PI tunings

than $\sqrt{2}$. This is usually not advisable because, in a system like this, measurement noise can easily destabilize the controlled system. In this case, each control scheme was analyzed and it was found that neither of them fulfil this requirement. Hence, the PI and PIF control schemes were retuned so as to remain outside the $3\,\mathrm{dB}$ m-circle. The resulting control parameter are shown in table 6.7.

Table 6.7: Retuned PI and PIF controller parameters in order to ensure stability against measurement noise

	MIMO Nyquist PI		MIMO Nyquist PIF			
	K_p ($\mathrm{m^2/s}$)	T_i (s)	T_f (s)	K_p ($\mathrm{m^2/s}$)	T_i (s)	T (s)
Pool 1	0.216	260.6	23.8	0.492	199.8	10
Pool 2	0.144	392.7	31.2	0.389	258.4	10
Pool 3	0.202	37.6	—	0.202	37.6	10

Later on in this chapter, all the set of PI tunings obtained in this section are going to be tested in identical situations in order to attain some performance results. In the next section, Predictive Control is briefly presented as a tool for designing decentralized controllers for canal pools.

6.4.1.3 Predictive control

Conceptual basis Predictive control methods (Martín Sánchez and Rodellar, 1996; Camacho and Bordons, 2004) aim to obtain a control action that can fulfil at best, certain time-performance criterions in the near future. In general lines, a process model is used to predict what is going to happen if a certain control action is taken and the result is evaluated in a near future time period called "prediction horizon". During the whole "prediction horizon", the control tries to keep the predicted process output close to a reference value or a reference trajectory. This goal and other minor objectives are usually collected in a single cost function, written as a function of possible control actions, to allow a mathematical treatment of the problem. A possible cost function given in Camacho and Bordons (2004) for the SISO case is:

$$J(N_1, N_2, N_u) = \sum_{j=N_1}^{N_2} \left[\hat{y}(k+j|k) - sp(k+j)\right]^2 + \sum_{j=1}^{N_u} \lambda \left[\Delta u(k+j-1)\right]^2 \qquad (6.16)$$

where $\hat{y}(k+j|k)$ is a j-step ahead prediction of the system output on data up to time instant k, N_1 and N_2 are the minimum and maximum costing horizons, N_u is the control horizon, λ is a control weighting factor and $sp(k+j)$ is a j-step ahead set point value, that can be also a part of a predefined reference trajectory. $\Delta u(k+j-1)$ with $j = 1 \ldots N_u$ is a sequence of control action increments which are left as the only independent variables in (6.16). The idea behind a predictive control is to calculate the optimum $\Delta u(k+j-1)$ values in order to minimize the cost function.

This cost function penalizes two things:

1. Deviations of the predicted outputs form a given reference trajectory.

2. An excessive control effort, i.e. large actuator movements.

In summary, a predictive controller calculates a sequence of moderate control actions in order to lead the system output to a given set point, as soon and as close as possible within a predefined time horizon according to some desired trajectory.

When the control problem is formulated without input or output constraints, it is possible to find the optimum solution of the minimization of (6.16) in an algebraic manner. The procedure is as follows.

Control law derivation First, it is necessary to write the j-step ahead optimal predictions in a convenient form by using an appropriate difference model.

Output predictions The Auto-Regressive Integrated with eXogenous input (ARIX) model is a type of difference model that uses a linear difference equation as model structure. It is well

suited for input-output modeling of linear processes. An ARIX model is normally expressed as follows:

$$A(z^{-1})\, y(k) = B(z^{-1})\, u(k-1) + \frac{e(k)}{\Delta} \qquad (6.17)$$

where $\Delta = 1 - z^{-1}$ is the backward difference operator written in the complex variable z, y is the process output, u is the process input and e is a white noise sequence that by itself does not represent any physical variable, but that is used to represent the differences between the measured output and the output calculated by the model (i.e. the model residuals). $A(z^{-1})$, $B(z^{-1})$ are polynomials in the backward shift operator given by:

$$A(z^{-1}) = 1 + a_1 z^{-1} + a_2 z^{-2} + \cdots + a_{n_a} z^{-n_a}$$
$$B(z^{-1}) = b_0 + b_1 z^{-1} + b_2 z^{-2} + \cdots + b_{n_b} z^{-n_b}$$

Following the same approach used in Camacho and Bordons (2004), and taking the control actions $u(k+j)$ constant and equal to $u(k+N_u-1)$ when $N_u \leq j < N_2$, the predictions using this type of model can be expressed in a matricial form as:

$$\mathbf{y} = \mathbf{Gu} + \mathbf{f} \qquad (6.18)$$

with

$$\mathbf{y} = \begin{bmatrix} \hat{y}(k+N_1|k) \\ \hat{y}(k+N_1+1|k) \\ \vdots \\ \hat{y}(k+N_2|k) \end{bmatrix} \qquad \mathbf{u} = \begin{bmatrix} \Delta u(k) \\ \Delta u(k+1) \\ \vdots \\ \Delta u(k+N_u-1) \end{bmatrix}$$

$$\mathbf{f} = \begin{bmatrix} f_{N_1} \\ f_{N_1+1} \\ \vdots \\ f_{N_2} \end{bmatrix} \qquad \mathbf{G} = \begin{bmatrix} g_{N_1-1} & g_{N_1-2} & \cdots & g_{N_1-N_u} \\ g_{N_1} & g_{N_1-1} & \cdots & g_{N_1+1-N_u} \\ \vdots & \ddots & \ddots & \vdots \\ g_{N_2-1} & g_{N_2-2} & \cdots & g_{N_2-N_u} \end{bmatrix}$$

In this form, the output predictions contained in $\mathbf{y}$ are explicitly written as a linear function of the control action increments contained in $\mathbf{u}$. On the other hand, $\mathbf{G}$ is a matrix of constants and $\mathbf{f}$ is a vector of constants that complete this representation. There are different ways to compute $\mathbf{G}$ and $\mathbf{f}$. One way is the following.

It is known that the elements of $\mathbf{G}$ can be computed by calculating the step response of the

model. Particularly, each g_i correspond to the value of the step response at instant $k = i+1$, i.e.

$$g_i = \begin{cases} 0, & \text{if } i < 0 \\ y(i+1) \,|\, u\text{=step}(k), & \text{if } i \geq 0 \end{cases}$$

where step(k) is the discrete unit step function starting at instant $k = 0$.

On the other hand, vector $\mathbf{f}$, called free response in some textbooks, can be calculated recursively using the following formula:

$$f_{j+1} = z(1 - \Delta A(z^{-1})) f_j + B(z^{-1})\Delta u(k+j)$$

with $f_0 = y(k)$, $f_{-1} = y(k-1), \ldots, f_{-n_a} = y(k-n_a)$ and $\Delta u(k+j) = 0$ for $j \geq 0$.

This prediction equation collects the expected values of the process output in between a time window $[k + N_1, k + N_2]$, in which it is desired to make the system follow a reference value. In SISO processes with dead time (d), there is no reason to make N_1 less than d because the output will not begin to evolve until instant $k + d$.

Output predictions with disturbances When the process is affected by disturbances that can be measured or whose evolution is beforehand surely known, it is also possible to include them in the prediction. For example, a process described by the following ARIX model:

$$A(z^{-1})y(k) = B(z^{-1})u(k-1) + D(z^{-1})v(k-1) + \frac{e(k)}{\Delta} \tag{6.19}$$

where $v(k-1)$ is the measured disturbance at time instant $k-1$ and $D(z^{-1})$ is a polynomial defined as:

$$D(z^{-1}) = d_0 + d_1 z^{-1} + d_2 z^{-2} + \cdots + d_{n_d} z^{-n_d}$$

have the following prediction equation:

$$\mathbf{y} = \mathbf{Gu} + \mathbf{Hv} + \mathbf{f} \tag{6.20}$$

In this case, the elements of the matrix $\mathbf{H}$ correspond to the coefficients of the system step response to the disturbance and the shape of the matrix is similar to the configuration of $\mathbf{G}$, i.e.

$$\mathbf{v} = \begin{bmatrix} \Delta v(k) \\ \Delta v(k+1) \\ \vdots \\ \Delta v(k + N_2 - 1) \end{bmatrix} \quad \mathbf{H} = \begin{bmatrix} h_{N_1-1} & h_{N_1-2} & \cdots & h_{N_1-N_2} \\ h_{N_1} & h_{N_1-1} & \cdots & h_{N_1+1-N_2} \\ \vdots & \ddots & \ddots & \vdots \\ h_{N_2-1} & h_{N_2-2} & \cdots & h_0 \end{bmatrix} \tag{6.21}$$

In this formulation, the free response $\mathbf{f}$ does not entirely coincide with the one of the disturbance-free case; all past disturbances should be considered in the free response vector when performing the recursive calculation.

By making $\mathbf{f'} = \mathbf{Hv} + \mathbf{f}$, the prediction equation is now:

$$\mathbf{y} = \mathbf{Gu} + \mathbf{f'} \tag{6.22}$$

which has the same shape as the general prediction equation used in the case of zero measured disturbances. Conclusively, the prediction can be written in the same way, simply using as free response the process response due to initial conditions (including external disturbances) and future "known" disturbances. Particularly, if these future disturbances are supposed to be constant and equal to the last measured value, then $\Delta v(k + j) = 0$ for $j \geq 0$.

Control problem solution Focusing on the predictive control problem, the minimization of (6.16) can be written as a Quadratic Programming (QP) problem in the following way:

$$\min_{\mathbf{u}} J = \min_{\mathbf{u}} (\mathbf{Gu} + \mathbf{f} - \mathbf{sp})^{\mathrm{T}} (\mathbf{Gu} + \mathbf{f} - \mathbf{sp}) + \lambda \mathbf{u}^{\mathrm{T}} \mathbf{u} \tag{6.23}$$

with $\mathbf{sp} = \begin{bmatrix} sp(k + N_1) & sp(k + N_1 + 1) & \cdots & sp(k + N_2) \end{bmatrix}^{\mathrm{T}}$.

The minimum of J can be found by making the gradient equal to zero. That leads to the following expression for the optimum solution:

$$\mathbf{u}^* = (\mathbf{G}^{\mathrm{T}}\mathbf{G} + \lambda \mathbf{I})^{-1} \mathbf{G}^{\mathrm{T}} (\mathbf{sp} - \mathbf{f}) \tag{6.24}$$

Vector $\mathbf{u}^*$ contains a sequence of control action increments that should be applied to the process in order to lead the output to the set point. However, it is common to apply only the first element of vector $\mathbf{u}^*$, i.e. $\Delta u(k)$. Thus, the control signal that is actually sent to the process is given by:

$$\Delta u(k) = \mathbf{K}(\mathbf{sp} - \mathbf{f}) \qquad \text{or} \qquad u(k) = u(k - 1) + \mathbf{K}(\mathbf{sp} - \mathbf{f}) \tag{6.25}$$

where $\mathbf{K}$ is the first row of matrix $(\mathbf{G}^{\mathrm{T}}\mathbf{G} + \lambda \mathbf{I})^{-1} \mathbf{G}^{\mathrm{T}}$.

This calculation should be repeated the next control time and so forth. This type of implementation is known as Receding strategy.

When the model parameters and the controller tuning values are chosen fixed, it is only necessary to calculate $\mathbf{K}$ once and it is possible to formulate f as an unchangeable function of past inputs and outputs. Thus, an explicit control law expression can be found. This expression allows a simple and fast implementation of the controller as a product of process data and constant coefficients.

Control tuning recommendations In addition to the usual controller sampling time T, there are four parameters in this predictive controller that can modify the controller response: the minimum prediction horizon N_1, the maximum prediction horizon N_2, the control horizon N_u and the control weighting factor λ. A control technique having so many tuning parameters would induce to think that the tuning procedure is complicated and troublesome. However, this is not the case; the tuning parameters can be easily selected from the process model response.

Minimum prediction horizon, N_1 In general, it is recommended to select its value depending on the dead time of the process. If the dead time consist of d sampling periods, N_1 should be equal to $d + 1$. There is no sense in making N_1 less than this value because the process would depend only on past values. On the other hand, a higher N_1 would make the controller loose the most certain predictions.

Maximum prediction horizon, N_2 The value of this parameter should be selected high enough so as to have a prediction horizon $N = N_2 - N_1 + 1$ where the evolution of the system can reach a stable condition. In general, an increment in this parameter leads to a softer and less oscillating output response.

Control horizon, N_u The higher this parameter is chosen, more complex is the control sequence that can be computed. If the process has a simple response, a low value should be enough. However, if the process present nonminimum phase behaviors, unstable modes, etc. it is recommended to choose a value close to the prediction horizon, i.e. $N_u = N_2 - N_1 + 1$.

Control weighting factor, λ This parameter attaches more or less importance to the strength of the control actions that are going to be applied to the process. A too low value would focus the controller in reaching the set point forgetting about the magnitude of the control actions, whereas a too high value would limit the actions in such a way, that the controller would no longer control the system. In addition, it can play an important role in the type of response that can be obtained (overdamped or underdamped) and in the controller sensibility to measurement noise. It is very difficult to select a value beforehand. It is better to test different values starting with a value near to one and raise it or lower it depending on the desired response.

Controller sampling time T The same recommendations given for other types of controllers can be applied here. The simplest choice is to select its value equal to the sampling time of the controller model in order to avoid unnecessary recalculations. When the control time is different from the model sampling time, a predictive controller can also be obtained but the control law should be modified in an adequate way.

6.4.1.4 Predictive control applied on the Canal PAC-UPC

Three predictive controllers were designed for the Canal PAC-UPC; one for each pool. Their respective Auto-Regressive with eXogenous Input (ARX) models are given in page 120 by equations (5.33), (5.34) and (5.35). Taking into account the delays and dynamics of each pool, several sets of tuning values were chosen and tested in simulation. The finally selected tuning values are presented in table 6.8.

Table 6.8: Tuning values for each predictive controller

Pool	N_1	N_2	N_u	λ	T
Pool 1	3	62	60	50	10 s
Pool 2	4	63	60	50	10 s
Pool 3	2	61	60	50	10 s

The search for adequate tuning values was not a difficult task. The minimum horizons were chosen to be greater than the delays, the maximum horizons were selected big enough in order to ensure a smooth response and the controller rates were chosen to be equal to the sampling times of the prediction models. The selection of a value for the control weighting factor λ was more delicate. In real applications, the noise sensitivity of the controllers can be dependent on the value of this factor. In this case, this parameter was tuned in the real laboratory canal by supervising the control responses. The value of λ was successively increased until achieving a not too noisy control signal.

To test different tuning values, the implementation of the decentralized predictive controllers was performed in the easiest possible way. In this case, it was found appropriate to choose a particular set of tuning values and then calculate directly the corresponding control law. As a result, the predictive control law is just a product of data and constants, that can be computed very fast and efficiently in a real-time computer program.

The procedure to obtain the explicit control law is very simple; it is only necessary to multiply the product in (6.25) keeping any reference to past or present data as variables. Then, after collecting and reordering terms, it is possible to obtain an explicit equation to implement a predictive controller with fixed tuning values.

It was decided to make the following assumptions to develop the controllers:

- A constant reference signal for the whole prediction horizon, i.e. $sp(k + N_1) = sp(k + N_1 + 1) = \cdots = sp(k + N_2)$

- Control actions $u(k + j)$ constant and equal to $u(k + N_u - 1)$ for $N_u \leq j < N_2$

- Future disturbances ($v(k + j)$ for $j > 0$) are considered constant and equal to the last measured disturbance value $v(k)$.

The first assumption is due to the fact that water level control in irrigation canals is more a regulation problem than a set point change problem or a trajectory tracking task. Consequently, to consider that the reference will not vary during the prediction horizon is usually true.

The second assumption is usual in many predictive control formulations and gives usually good performance results.

The third assumption is only a simplification of the problem. However, it is not ruled out that more accurate predictions of disturbances in the future (see for example Gómez et al. (2002)) can improve the control performance.

Taking into account all the aforementioned control assumptions, and using the tuning values of table 6.8, the following control law expressions were computed for each pool:
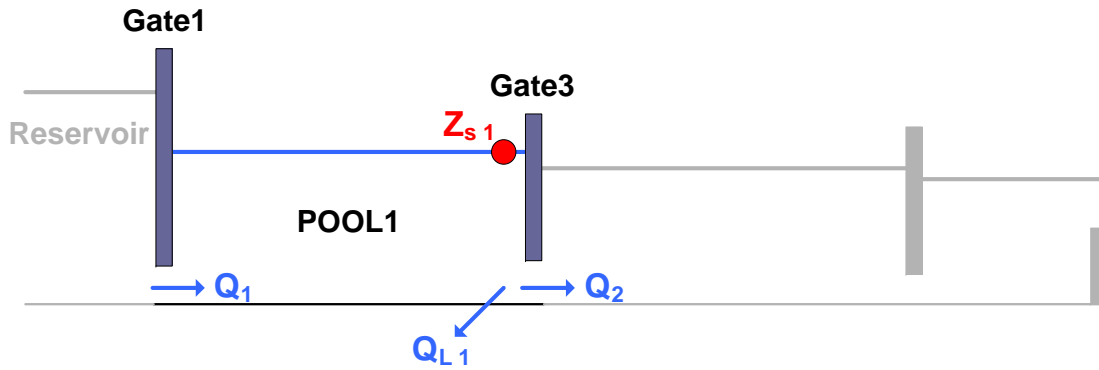
Figure 6.10: Variables involved in the control of Pool 1

Pool1 predictive controller:

$$Q_1(k) = 0.1221\, sp_{Z_{s1}} + \mathbf{K_y}\, \mathbf{Z}_{s1} + \mathbf{K_u}\, \mathbf{Q}_1 + \mathbf{K_v}\, \mathbf{Q}_v \tag{6.26}$$

with

$$\mathbf{K_y}^T = \begin{bmatrix} -0.4543 \\ 0.2744 \\ -0.0617 \\ 0.0102 \\ -0.0888 \\ 0.1091 \\ 0.0890 \end{bmatrix} \quad \mathbf{Z}_{s1} = \begin{bmatrix} Z_{s1}(k) \\ Z_{s1}(k-1) \\ Z_{s1}(k-2) \\ Z_{s1}(k-3) \\ Z_{s1}(k-4) \\ Z_{s1}(k-5) \\ Z_{s1}(k-6) \end{bmatrix} \quad \mathbf{K_u}^T = \begin{bmatrix} 0.7164 \\ -0.0244 \\ 0.4289 \\ -0.1210 \end{bmatrix}$$

$$\mathbf{Q}_1 = \begin{bmatrix} Q_1(k-1) \\ Q_1(k-2) \\ Q_1(k-3) \\ Q_1(k-4) \end{bmatrix} \quad \mathbf{K_v}^T = \begin{bmatrix} 0.3097 \\ -0.4971 \\ 0.2086 \\ -0.0227 \\ 0.2063 \\ -0.2047 \end{bmatrix} \quad \mathbf{Q}_v = \begin{bmatrix} Q_2(k) + Q_{L1}(k) \\ Q_2(k-1) + Q_{L1}(k-1) \\ Q_2(k-2) + Q_{L1}(k-2) \\ Q_2(k-3) + Q_{L1}(k-3) \\ Q_2(k-4) + Q_{L1}(k-4) \\ Q_2(k-5) + Q_{L1}(k-5) \end{bmatrix}$$

Figure 6.11: Variables involved in the control of Pool 2

Pool2 predictive controller:

$$Q_2(k) = 0.1202\, sp_{Z_{s\,2}} + \mathbf{K_y}\, \mathbf{Z_{s\,2}} + \mathbf{K_u}\, \mathbf{Q_2} + \mathbf{K_v}\, \mathbf{Q_v} \tag{6.27}$$

with

$$\mathbf{K_y}^{\mathrm{T}} = \begin{bmatrix} -0.2206 \\ -0.0126 \\ 0.0061 \\ -0.0164 \\ -0.0263 \\ 0.0328 \\ -0.0199 \\ 0.0576 \\ 0.0791 \end{bmatrix} \quad \mathbf{Z_{s\,2}} = \begin{bmatrix} Z_{s\,2}(k) \\ Z_{s\,2}(k-1) \\ Z_{s\,2}(k-2) \\ Z_{s\,2}(k-3) \\ Z_{s\,2}(k-4) \\ Z_{s\,2}(k-5) \\ Z_{s\,2}(k-6) \\ Z_{s\,2}(k-7) \\ Z_{s\,2}(k-8) \end{bmatrix} \quad \mathbf{K_u}^{\mathrm{T}} = \begin{bmatrix} 0.7037 \\ -0.0215 \\ -0.0211 \\ 0.3389 \end{bmatrix}$$

$$\mathbf{Q_2} = \begin{bmatrix} Q_2(k-1) \\ Q_2(k-2) \\ Q_2(k-3) \\ Q_2(k-4) \end{bmatrix} \quad \mathbf{K_v}^{\mathrm{T}} = \begin{bmatrix} 0.3067 \\ -0.4034 \\ 0.0970 \\ -0.0321 \\ 0.1315 \\ -0.0997 \end{bmatrix} \quad \mathbf{Q_v} = \begin{bmatrix} Q_3(k) + Q_{L\,2}(k) \\ Q_3(k-1) + Q_{L\,2}(k-1) \\ Q_3(k-2) + Q_{L\,2}(k-2) \\ Q_3(k-3) + Q_{L\,2}(k-3) \\ Q_3(k-4) + Q_{L\,2}(k-4) \\ Q_3(k-5) + Q_{L\,2}(k-5) \end{bmatrix}$$
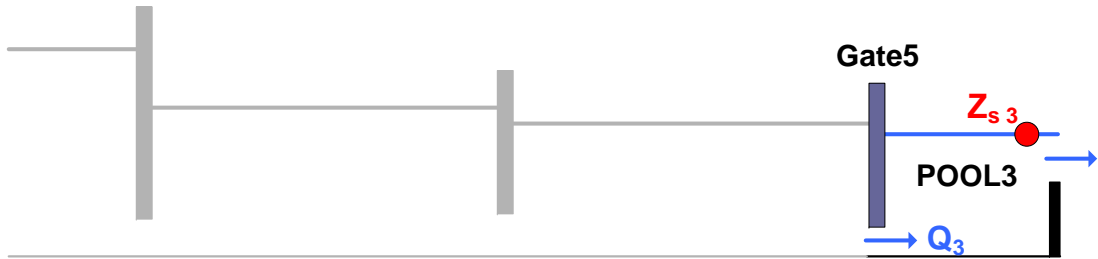
Figure 6.12: Variables involved in the control of Pool 3

Pool3 predictive controller:

$$Q_3(k) = 0.1238 \, sp_{Z_{s\,3}} + \mathbf{K_y} \, \mathbf{Z}_{s\,3} + \mathbf{K_u} \, \mathbf{Q}_3 \qquad (6.28)$$

with

$$\mathbf{K_y}^T = \begin{bmatrix} -0.4845 \\ 0.2685 \\ 0.0984 \\ -0.0643 \\ 0.1489 \\ -0.0908 \end{bmatrix} \qquad \mathbf{Z}_{s\,3} = \begin{bmatrix} Z_{s\,3}(k) \\ Z_{s\,3}(k-1) \\ Z_{s\,3}(k-2) \\ Z_{s\,3}(k-3) \\ Z_{s\,3}(k-4) \\ Z_{s\,3}(k-5) \end{bmatrix}$$

$$\mathbf{K_u}^T = \begin{bmatrix} 0.7554 \\ 0.6691 \\ -0.4245 \end{bmatrix} \qquad \mathbf{Q}_3 = \begin{bmatrix} Q_3(k-1) \\ Q_3(k-2) \\ Q_3(k-3) \end{bmatrix}$$

It should be noted that in the first two predictive controllers, i.e. (6.26) and (6.27), the control law expressions include the gate discharge calculated by a downstream controller (Q_{i+1}) and the offtake discharge ($Q_{L\,i}$). These variables appear in the control laws because the original ARX models include their influence on the downstream water level ($Z_{s\,i}$).

Taken into account explicitly these variables in predictive control of irrigation canal pools, produce an effect similar to what was presented as "decoupling" and "feedforward" in Section 6.4.1.1. The difference lies in the way these elements are incorporated in the controllers; PI controllers should add additional control loops while predictive controllers incorporate these capabilities intrinsically from the process model.

It is not compulsory to incorporate these external disturbances in the controller. However, they generally improve the control performance in a high degree, specially when used in decoupling loops. If Q_{i+1} or $Q_{L\,i}$ are not available, it is only necessary to feed the controller with zero values instead; the predictive controllers will consider these unmodeled dynamics as an effect of unmeasured disturbances and will still manage to maintain the water levels.

Later on in this chapter, it is going to be studied the real benefits that the use of available disturbance information produce in the framework of a whole irrigation canal control scheme. To highlight when predictive controllers use the measurement of a particular disturbance and to denote the capability that can be acquired when using this information, it is going to be added the term "feedforward" when a predictive controller is fed with offtake discharges $Q_{L\,i}$ and the term "decoupling" when it is fed with gate discharges Q_{i+1} computed by other controllers. However, the use of these terms do not mean that an additional controller or filter is going to be used working in combination with these predictive controllers.

One final remark on the use of offtake discharges: the predictive controllers have been designed in a way where only current and past measurements are used. It would has been also possible to incorporate future offtake discharges, especially if they are known beforehand or can be estimated in a more or less accurate manner. Some research works use this additional information to improve the control performance (e.g Gómez et al. (2002)) whereas others like Schuurmans et al. (1999b) do not consider recommendable to include this information in advance in order to increase the flexibility of water deliveries.

6.4.2 Centralized control

As mentioned before, this type of control concentrates the operation burden of the entire system in a single multivariable controller. The performance that can be achieved with a centralized strategy is usually very high, because it takes into account all the interactions that occur among the inputs and outputs of the system. However, the design and implementation of this type of controllers are considerably more complex and laborious than any SISO based strategy. A conceptual scheme of an irrigation canal controlled by a centralized controller is illustrated in figure 6.13.
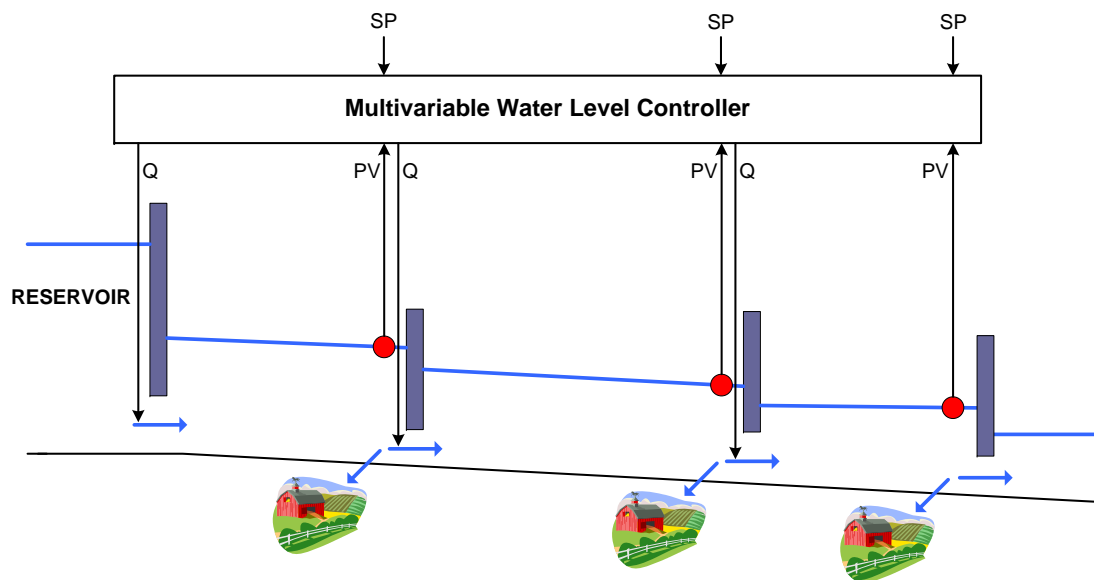
Figure 6.13: Example of an irrigation canal controlled by a centralized controller

There are several control techniques that can deal with multivariable systems. In this case, it is considered suitable to test the centralized control strategy using multivariable predictive controllers, because of their performance and design strengths. In this case, it was chosen the multivariable formulation of the predictive controller of Section 6.4.1.3 in order to facilitate the comparison between centralized and decentralized designs.

6.4.2.1 Multivariable Predictive Control

Controller derivation The derivation of the MIMO predictive controller is very similar to the SISO case.

Cost function This controller aims to minimize the following finite horizon quadratic criterion:

$$J(N_1, N_2, N_u) = \sum_{j=N_1}^{N_2} \|\hat{\mathbf{y}}(k+j|k) - \mathbf{sp}(k+j)\|_{\mathbf{Q}}^2 + \sum_{j=1}^{N_u} \|\Delta\mathbf{u}(k+j-1)\|_{\mathbf{R}}^2 \qquad (6.29)$$

where $\hat{\mathbf{y}}(k+j|k)$ is an optimum j-step ahead prediction of the system output on data up to instant k, i.e. the expected value of the output vector at k if the past input and output vectors and the future control sequence are known. N_1 and N_2 are the minimum and maximum prediction horizon and $\mathbf{sp}(k+j)$ is a future setpoint or reference sequence for the output vector. $\mathbf{Q}$ and $\mathbf{R}$ are positive definite weighting matrices.

This cost function pursues the same goal than (6.16), i.e. to drive the system output to a reference sequence during a particular future time period with a moderate control effort. The only difference is that in this case the system output is a vector of controllable variables and the system input is a vector of manipulable variables.

In order to reach an expression for optimum solution like in the SISO case, it is first necessary to obtain a formula for the output predictions $\hat{\mathbf{y}}(k+j|k)$ in the time horizon $[N_1, N_2]$.

Output predictions A multivariable ARIX model of an n-output, m-input MIMO process can be expressed as:

$$\mathbf{A}(z^{-1})\mathbf{y}(k) = \mathbf{B}(z^{-1})\mathbf{u}(k-1) + \frac{1}{\Delta}\mathbf{e}(k) \qquad (6.30)$$

In (6.30), $\mathbf{A}(z^{-1})$ is a $n \times n$ monic polynomial matrix and $\mathbf{B}(z^{-1})$ is a $n \times m$ polynomial matrix, which are defined by:

$$\mathbf{A}(z^{-1}) = \mathbf{I}_{n \times n} + \mathbf{A}_1 z^{-1} + \mathbf{A}_2 z^{-2} + \cdots + \mathbf{A}_{n_a} z^{-n_a} \qquad (6.31)$$

$$\mathbf{B}(z^{-1}) = \mathbf{B}_0 + \mathbf{B}_1 z^{-1} + \mathbf{B}_2 z^{-2} + \cdots + \mathbf{B}_{n_b} z^{-n_b} \qquad (6.32)$$

The operator Δ is defined as $\Delta = 1 - z^{-1}$. The variables $\mathbf{y}(k)$, $\mathbf{u}(k)$ and $\mathbf{e}(k)$ are the $n \times 1$ output vector, the $m \times 1$ input vector and the $n \times 1$ noise vector at instant k. The noise vector is supposed to be a white noise with zero mean.

Following the same approach used in Camacho and Bordons (2004), the predictions using this MIMO model can be expressed in a condensed form as:

$$\mathbf{y} = \mathbf{Gu} + \mathbf{f} \qquad (6.33)$$

with

$$
\mathbf{y} = \begin{bmatrix} \hat{\mathbf{y}}(k + N_1|k) \\ \hat{\mathbf{y}}(k + N_1 + 1|k) \\ \vdots \\ \hat{\mathbf{y}}(k + N_2|k) \end{bmatrix} \qquad \mathbf{u} = \begin{bmatrix} \Delta\mathbf{u}(k) \\ \Delta\mathbf{u}(k + 1) \\ \vdots \\ \Delta\mathbf{u}(k + N_u - 1) \end{bmatrix}
$$

$$
\mathbf{f} = \begin{bmatrix} \mathbf{f}_{N_1} \\ \mathbf{f}_{N_1+1} \\ \vdots \\ \mathbf{f}_{N_2} \end{bmatrix} \qquad \mathbf{G} = \begin{bmatrix} \mathbf{G}_{N_1-1} & \mathbf{G}_{N_1-2} & \cdots & \mathbf{G}_{N_1-N_u} \\ \mathbf{G}_{N_1} & \mathbf{G}_{N_1-1} & \cdots & \mathbf{G}_{N_1+1-N_u} \\ \vdots & \ddots & \ddots & \vdots \\ \mathbf{G}_{N_2-1} & \mathbf{G}_{N_2-2} & \cdots & \mathbf{G}_{N_2-N_u} \end{bmatrix}
$$

The first column of matrix $\mathbf{G}$ correspond to the step response of the MIMO process when a unit step is applied to the first control signal. Column j can be obtained in a similar way by applying a unit step to the j-input. In general, each matrix $\mathbf{G}_e$ can be obtained as follows:

$$
(\mathbf{G}_e)_{i,j} = \begin{cases} 0, & \text{if } e < 0 \\ y_i(k + e + 1) \,|\, u_j\text{=step}(k), & \text{if } e \geq 0 \end{cases}
$$

where $(\mathbf{G}_e)_{i,j}$ is the (i, j) element of matrix $\mathbf{G}_e$ and $y_i(k + e + 1) \,|\, u_j$=step(k) is the i-output of the system when a unit step has been applied to control input j at time instant k.

The free response terms can be calculated recursively using the following formula:

$$
\mathbf{f}_{j+1} = z(\mathbf{I}_{n\times n} - \Delta\mathbf{A}(z^{-1}))\,\mathbf{f}_j + \mathbf{B}(z^{-1})\Delta\mathbf{u}(k + j)
$$

with $\mathbf{f}_0 = \mathbf{y}(k), \mathbf{f}_{-1} = \mathbf{y}(k - 1), \ldots, \mathbf{f}_{-n_a} = \mathbf{y}(k - n_a)$ and $\Delta\mathbf{u}^{\mathrm{T}}(k + j) = \begin{bmatrix} 0 & \cdots & 0 \end{bmatrix}_{1\times m}$ for $j \geq 0$.

Control problem solution　Formulating the predictions in a matricial way makes possible to rewrite (6.29) as

$$
J = (\mathbf{G}\mathbf{u} + \mathbf{f} - \mathbf{sp})^{\mathrm{T}}\,\overline{\mathbf{Q}}\,(\mathbf{G}\mathbf{u} + \mathbf{f} - \mathbf{sp}) + \mathbf{u}^{\mathrm{T}}\,\overline{\mathbf{R}}\,\mathbf{u} \tag{6.34}
$$

where $\overline{\mathbf{Q}} = \begin{bmatrix} \mathbf{Q} & & 0 \\ & \ddots & \\ 0 & & \mathbf{Q} \end{bmatrix}$ and $\overline{\mathbf{R}} = \begin{bmatrix} \mathbf{R} & & 0 \\ & \ddots & \\ 0 & & \mathbf{R} \end{bmatrix}$.

If there are no constrains, the optimum solution of the minimization of (6.34) can be expressed as:

$$
\mathbf{u}^* = (\mathbf{G}^{\mathrm{T}}\,\overline{\mathbf{Q}}\,\mathbf{G} + \overline{\mathbf{R}})^{-1}\mathbf{G}^{\mathrm{T}}\,\overline{\mathbf{Q}}(\mathbf{sp} - \mathbf{f}) = \mathbf{K}(\mathbf{sp} - \mathbf{f}) \tag{6.35}
$$

Because of the receding control strategy, only $\Delta\mathbf{u}(k)$ is needed at instant k. Thus, only the

first m rows of $\mathbf{K}$ have to be computed. Hence, the control signal that is actually sent to the process is given by the following control law:

$$\Delta\mathbf{u}(k) = \mathbf{K}(\mathbf{sp} - \mathbf{f}) \qquad \text{or} \qquad \mathbf{u}(k) = \mathbf{u}(k-1) + \mathbf{K}(\mathbf{sp} - \mathbf{f}) \qquad (6.36)$$

In summary, the MIMO control law is very similar to the SISO case; it consists of a linear gain matrix K multiplying the predicted differences between the references and the "free response" of the system.

As in the SISO case, it is also possible to reach an explicit control law, if the controller model has fixed parameters and the controller tuning values are chosen beforehand.

Multivariable Predictive Control with measurable disturbances   A centralized control scheme does not need decoupling elements; coupling effects are inherently lessened in the control problem. Nevertheless, other measurable disturbance variables can also been added to the controller so as to feed a feedforward path. An irrigation canal centralized controller including feedforward capabilities is illustrated in figure 6.14.
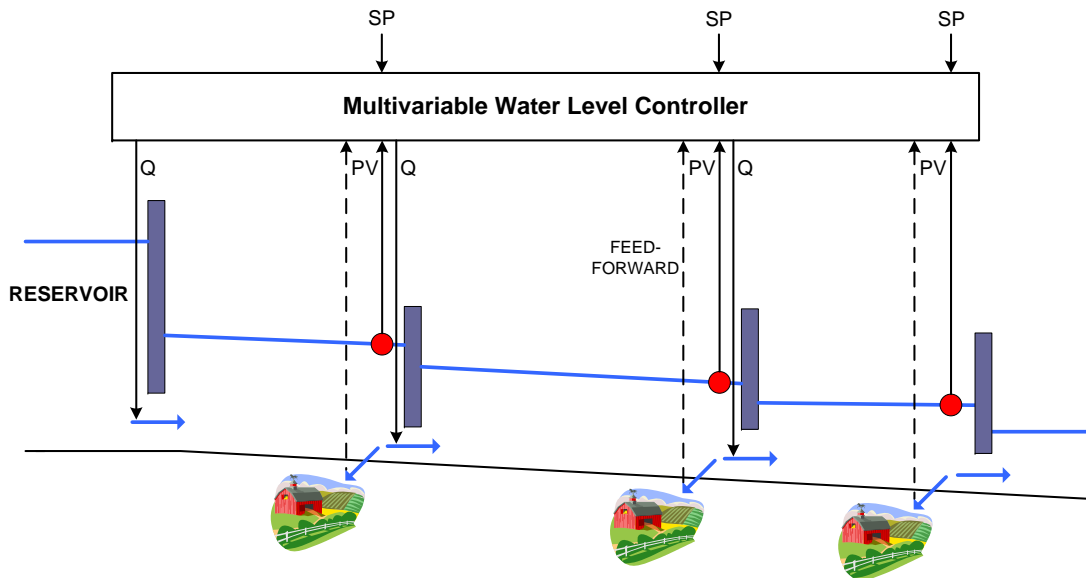
Figure 6.14: Scheme of an irrigation canal controlled by a centralized controller with feedforward capabilities

In the multivariable Predictive control as in the SISO case, it is only necessary to incorporate the influence of measurable disturbances in the free response term $\mathbf{f}$ of the prediction equation in order to include them in the control problem.

A multivariable ARIX model including measurable disturbances can be expressed as:

$$\mathbf{A}(z^{-1})\mathbf{y}(k) = \mathbf{B}(z^{-1})\mathbf{u}(k-1) + \mathbf{D}(z^{-1})\mathbf{v}(k-1) + \frac{1}{\Delta}\mathbf{e}(k) \qquad (6.37)$$

where $\mathbf{v}(k-1)$ is a $n \times 1$ vector of measured disturbances at instant $k-1$ and $\mathbf{D}(z^{-1})$ is a $n \times n$ polynomial matrix defined as:

$$\mathbf{D}(z^{-1}) = \mathbf{D}_0 + \mathbf{D}_1 z^{-1} + \mathbf{D}_2 z^{-2} + \cdots + \mathbf{D}_{n_d} z^{-n_d} \qquad (6.38)$$

It is demonstrated in Camacho and Bordons (2004) that the predictions given by this model can be expressed in a condensed form as:

$$\mathbf{y} = \mathbf{G}\mathbf{u} + \mathbf{H}\mathbf{v} + \mathbf{f} \qquad (6.39)$$

where $\mathbf{v}$ is a vector with present and future disturbances and $\mathbf{f}$ should contain the influence of past disturbances. $\mathbf{H}$ is a matrix similar to matrix $\mathbf{G}$ in structure. With a minimum prediction horizon N_1 and a maximum prediction horizon N_2, $\mathbf{v}$ and $\mathbf{H}$ are given by:

$$\mathbf{v} = \begin{bmatrix} \Delta\mathbf{v}(k) \\ \Delta\mathbf{v}(k+1) \\ \vdots \\ \Delta\mathbf{v}(k+N_2-1) \end{bmatrix} \quad \mathbf{H} = \begin{bmatrix} \mathbf{H}_{N_1-1} & \mathbf{H}_{N_1-2} & \cdots & \mathbf{H}_{N_1-N_2} \\ \mathbf{H}_{N_1} & \mathbf{H}_{N_1-1} & \cdots & \mathbf{H}_{N_1+1-N_2} \\ \vdots & \ddots & \ddots & \vdots \\ \mathbf{H}_{N_2-1} & \mathbf{H}_{N_2-2} & \cdots & \mathbf{H}_0 \end{bmatrix} \qquad (6.40)$$

where each $\mathbf{H}_e$ is a $n \times m$ matrix. $\mathbf{H}$ can be obtained applying unit steps to the disturbance signals. Specifically, each matrix $\mathbf{H}_e$ can be computed in the following way:

$$(\mathbf{H}_e)_{i,j} = \begin{cases} 0, & \text{if } e < 0 \\ y_i(k+e+1) \,|\, v_j{=}\text{step}(k), & \text{if } e \geq 0 \end{cases}$$

where $(\mathbf{H}_e)_{i,j}$ is the (i,j) element of matrix $\mathbf{H}_e$ and $y_i(k+e+1)_{v_j:\text{step}(k)}$ is the i-output of the system when a unit step has been applied to disturbance j at time instant k.

By making $\mathbf{f}' = \mathbf{H}\mathbf{v} + \mathbf{f}$, the prediction equation can be rewritten as

$$\mathbf{y} = \mathbf{G}\mathbf{u} + \mathbf{f}' \qquad (6.41)$$

This formula has the same shape as the as the prediction equation used for the case of zero external measured disturbances. As a result, the attainment of the final control law follows the same steps presented in the last section.

Tuning recommendations The tuning procedure of a multivariable predictive controller is very similar to the one of the SISO case. Hence, the same recommendations can be applied in this case (details in page 156). There are only three parameters that deserve special attention in the multivariable case:

Minimum prediction horizon, N_1 The recommendation made for the predictive SISO controller was to select this value as $N_1 = d + 1$, where d is the delay expressed in sampling instants. A multivariable process is likely to present different delay magnitudes depending on which input-output pair is taken. Thus, there are many choices for d. The simplest option is to use the delay of less value, i.e. $N_1 = d_{min} + 1$.

Error weighting matrix, $\mathbf{Q}$ This matrix is normally taken equal to the identity matrix ($\mathbf{Q} = \mathbf{I}$). A modification of the diagonal values is only justified when it is necessary to equalize outputs with different units or when it is required to prioritize the control of some outputs over others.

Control weighting matrix, $\mathbf{R}$ This matrix plays the same role that plays the control weighting factor in the SISO predictive controller, i.e. to give more or less importance to the resulting control effort. The recommendations presented in the SISO case (page 156) are still valid if this matrix is taken as $\mathbf{R} = \lambda\mathbf{I}$. There are also few research papers (Wahlin, 2004; Clemmens and Schuurmans, 2004a,b) that have proposed to reflect the relative capacity of the pools in the diagonal elements of the matrix, in order to equalize the effect that each control action can cause over the entire system.

6.4.2.2   Canal PAC-UPC multivariable 3×3 predictive controller

Taking the system as a whole, the Canal PAC-UPC can be considered as a three input - three output system with two measurable disturbance variables. The inputs correspond to the manipulable gate discharges, the outputs to the three water levels that should be controlled and the measurable disturbances to the offtake discharges.

The goal of this section is to obtain an explicit control law in order to easily implement a multivariable predictive controller for this laboratory canal. The design procedure followed the guidelines detailed in the previous section using as controller model the multivariable ARX model given by (5.36) [page 121].

No special tuning is carried out in this particular case; the controller parameters were selected as close as possible to the ones chosen for the SISO predictive controllers from section 6.4.1.4. The weighting matrices $\mathbf{Q}$ and $\mathbf{R}$ where chosen equal to $\mathbf{I}$ and $\lambda\mathbf{I}$ respectively, where $\mathbf{I}$ is the identity matrix and λ was the control weighting factor used in the SISO case. The minimum prediction horizon N_1 was selected equal to one ($N_1 = 1$), because the minimum delay in the discrete ARX model is $d = 0$. On the other hand, the maximum prediction horizon N_2 was chosen equal to the highest value in the Predictive Control SISO tuning ($N_2 = 63$) and the control horizon was calculated using $N_u = N_2 - N_1 + 1$. All this tuning information is summarized in table 6.9.

Table 6.9: Tuning values for 3×3 predictive controller

Min. pred. horiz., N_1 (samp. time units)	Max. pred. horiz., N_2 (samp. time units)	Control horiz., N_u (samp. time units)	Control time, T (s)
1	63	63	10

Error weighting matrix, $\mathbf{Q}$	Control weighting matrix, $\mathbf{R}$
$\begin{bmatrix} 1 & 0 & 0 \\ 0 & 1 & 0 \\ 0 & 0 & 1 \end{bmatrix}$	$\begin{bmatrix} 50 & 0 & 0 \\ 0 & 50 & 0 \\ 0 & 0 & 50 \end{bmatrix}$

By fixing the tuning values in the multivariable predictive controller formulation, it was possible to derive an explicit control law expression for the multivariable predictive controller.

The assumptions made to develop the controllers where the same than in the SISO case, namely:

- A constant reference signal for the whole prediction horizon, i.e. $\mathbf{sp}(k + N_1) = \mathbf{sp}(k + N_1 + 1) = \cdots = \mathbf{sp}(k + N_2)$

- Control actions $\mathbf{u}(k + j)$ constant and equal to $\mathbf{u}(k + N_u - 1)$ for $N_u \leq j < N_2$

- Future disturbances ($\mathbf{v}(k + j)$ for $j > 0$) are considered constant and equal to the last measured disturbance value $\mathbf{v}(k)$.

The procedure was very similar as the one used in Section (6.4.1.4), that is to multiply the product in (6.29) keeping any reference to past or present data as variables and to conveniently collect and reorder terms. It enabled the attainment of a controller equation which, given some measurement data and reference values for the three controlled water levels, can calculate the necessary gate discharges in order to lead the water levels to the desired values. As is in the SISO case, the resulting controller can also compute the control action very fast and efficiently in a real-time computer program.

The final controller equation is presented next.
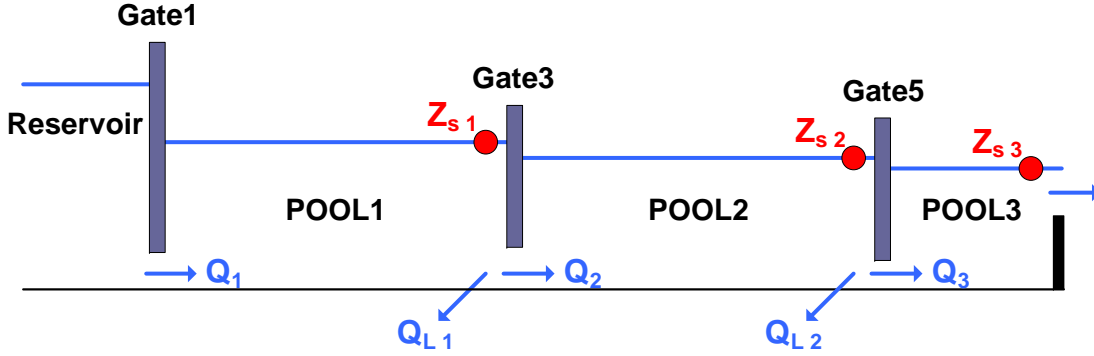
Figure 6.15: Variables involved in the control of the Canal PAC-UPC

MIMO predictive controller equation:

$$\mathbf{Q}(k) = \mathbf{K_{sp}}\mathbf{sp}_{Z_s} + \overbrace{\mathbf{K_{y_1}}\mathbf{Z}_{s\,1} + \mathbf{K_{y_2}}\mathbf{Z}_{s\,2} + \mathbf{K_{y_3}}\mathbf{Z}_{s\,3}}^{\mathbf{K_y}\times\text{level data}}$$
$$+ \underbrace{\mathbf{K_{u_1}}\mathbf{Q}_1 + \mathbf{K_{u_2}}\mathbf{Q}_2 + \mathbf{K_{u_3}}\mathbf{Q}_3}_{\mathbf{K_u}\times\text{gate discharge data}} + \underbrace{\mathbf{K_{v_1}}\mathbf{Q}_{L\,1} + \mathbf{K_{v_2}}\mathbf{Q}_{L\,2}}_{\mathbf{K_v}\times\text{offtake discharge data}}$$

(6.42)

where $\mathbf{Q}$ is a vector which contains the required gate discharges calculated by the controller, i.e. $\mathbf{Q}^{\mathrm{T}}(k) = \begin{bmatrix} Q_1(k) & Q_2(k) & Q_3(k) \end{bmatrix}$, and the rest of the matrices and vectors in the equation are given by:

$$\mathbf{K_{sp}} = \begin{bmatrix} 0.0901 & 0.0460 & 0.0746 \\ -0.0748 & 0.0662 & 0.0636 \\ -0.0156 & -0.0852 & 0.0777 \end{bmatrix} \qquad \mathbf{sp}_{Z_s} = \begin{bmatrix} sp_{Z_{s\,1}} \\ sp_{Z_{s\,2}} \\ sp_{Z_{s\,3}} \end{bmatrix}$$

$$\mathbf{K_{y_1}}^{\mathrm{T}} = \begin{bmatrix} -0.3599 & 0.1795 & 0.0495 \\ 0.2193 & -0.1018 & -0.0289 \\ -0.0492 & 0.0185 & 0.0062 \\ 0.0089 & -0.0033 & -0.0011 \\ -0.0686 & 0.0442 & 0.0103 \\ 0.0883 & -0.0313 & -0.0110 \\ 0.0712 & -0.0311 & -0.0094 \end{bmatrix} \qquad \mathbf{Z}_{s\,1} = \begin{bmatrix} Z_{s\,1}(k) \\ Z_{s\,1}(k-1) \\ Z_{s\,1}(k-2) \\ Z_{s\,1}(k-3) \\ Z_{s\,1}(k-4) \\ Z_{s\,1}(k-5) \\ Z_{s\,1}(k-6) \end{bmatrix}$$

$$\mathbf{K_{y_3}}^{\mathrm{T}} = \begin{bmatrix} -0.4214 & -0.3344 & -0.2712 \\ 0.2629 & 0.2042 & 0.1435 \\ 0.0965 & 0.0757 & 0.0517 \\ -0.0591 & -0.0467 & -0.0350 \\ 0.1329 & 0.1051 & 0.0824 \\ -0.0864 & -0.0675 & -0.0491 \end{bmatrix} \qquad \mathbf{Z}_{s\,3} = \begin{bmatrix} Z_{s\,3}(k) \\ Z_{s\,3}(k-1) \\ Z_{s\,3}(k-2) \\ Z_{s\,3}(k-3) \\ Z_{s\,3}(k-4) \\ Z_{s\,3}(k-5) \end{bmatrix}$$

$$
\mathbf{K_{y_2}}^{\mathrm{T}} =
\begin{bmatrix}
-0.1457 & -0.1271 & 0.1185 \\
-0.0025 & -0.0082 & 0.0022 \\
0.0094 & 0.0041 & -0.0045 \\
-0.0005 & -0.0112 & -0.0003 \\
-0.0094 & -0.0155 & 0.0164 \\
0.0233 & 0.0214 & -0.0108 \\
-0.0119 & -0.0099 & 0.0248 \\
0.0388 & 0.0343 & -0.0188 \\
0.0526 & 0.0459 & -0.0423
\end{bmatrix}
\qquad
\mathbf{Z}_{s2} =
\begin{bmatrix}
Z_{s2}(k) \\
Z_{s2}(k-1) \\
Z_{s2}(k-2) \\
Z_{s2}(k-3) \\
Z_{s2}(k-4) \\
Z_{s2}(k-5) \\
Z_{s2}(k-6) \\
Z_{s2}(k-7) \\
Z_{s2}(k-8)
\end{bmatrix}
$$

$$
\mathbf{K_{u_1}}^{\mathrm{T}} =
\begin{bmatrix}
0.7710 & 0.0819 & 0.0287 \\
-0.0158 & 0.0350 & 0.0043 \\
0.3415 & -0.1592 & -0.0457 \\
-0.0967 & 0.0423 & 0.0127
\end{bmatrix}
\qquad
\mathbf{Q}_1 =
\begin{bmatrix}
Q_1(k-1) \\
Q_1(k-2) \\
Q_1(k-3) \\
Q_1(k-4)
\end{bmatrix}
$$

$$
\mathbf{K_{u_2}}^{\mathrm{T}} =
\begin{bmatrix}
-0.3514 & 0.8900 & 0.1071 \\
0.1575 & -0.0745 & 0.0101 \\
-0.0301 & 0.0041 & 0.0653 \\
0.3877 & 0.1089 & -0.2040 \\
-0.1637 & 0.0715 & 0.0215
\end{bmatrix}
\qquad
\mathbf{Q}_2 =
\begin{bmatrix}
Q_2(k-1) \\
Q_2(k-2) \\
Q_2(k-3) \\
Q_2(k-4) \\
Q_2(k-5)
\end{bmatrix}
$$

$$
\mathbf{K_{u_3}}^{\mathrm{T}} =
\begin{bmatrix}
-0.2554 & -0.2103 & 0.9154 \\
0.6602 & 0.5267 & 0.3157 \\
-0.4253 & -0.3339 & -0.1990 \\
0.0868 & 0.0753 & -0.0854 \\
-0.0662 & -0.0579 & 0.0533
\end{bmatrix}
\qquad
\mathbf{Q}_3 =
\begin{bmatrix}
Q_3(k-1) \\
Q_3(k-2) \\
Q_3(k-3) \\
Q_3(k-4) \\
Q_3(k-5)
\end{bmatrix}
$$

$$
\mathbf{K_{v_1}}^{\mathrm{T}} =
\begin{bmatrix}
0.2466 & -0.1229 & -0.0334 \\
-0.3951 & 0.1928 & 0.0532 \\
0.1678 & -0.0665 & -0.0212 \\
-0.0182 & 0.0128 & 0.0026 \\
0.1625 & -0.0878 & -0.0227 \\
-0.1637 & 0.0715 & 0.0215
\end{bmatrix}
\qquad
\mathbf{Q}_{L1} =
\begin{bmatrix}
Q_{L1}(k) \\
Q_{L1}(k-1) \\
Q_{L1}(k-2) \\
Q_{L1}(k-3) \\
Q_{L1}(k-4) \\
Q_{L1}(k-5)
\end{bmatrix}
$$

$$
\mathbf{K_{v_2}}^{\mathrm{T}} =
\begin{bmatrix}
0.2121 & 0.1743 & -0.1880 \\
-0.2755 & -0.2287 & 0.2450 \\
0.0646 & 0.0555 & -0.0551 \\
-0.0217 & -0.0186 & 0.0303 \\
0.0868 & 0.0753 & -0.0854 \\
-0.0662 & -0.0579 & 0.0533
\end{bmatrix}
\qquad
\mathbf{Q}_{L2} =
\begin{bmatrix}
Q_{L2}(k) \\
Q_{L2}(k-1) \\
Q_{L2}(k-2) \\
Q_{L2}(k-3) \\
Q_{L2}(k-4) \\
Q_{L2}(k-5)
\end{bmatrix}
$$

6.4.3   Semi-decentralized control

As mentioned previously in this chapter, this type of control strategy tries to acquire the most of the performance benefits that a centralized scheme can offer, while keeping the implementation simplicity of a decentralized scheme.

To describe how this type of strategy was conceived, it is useful to recall once again an irrigation canal scheme like the one sketched in figure 6.16.
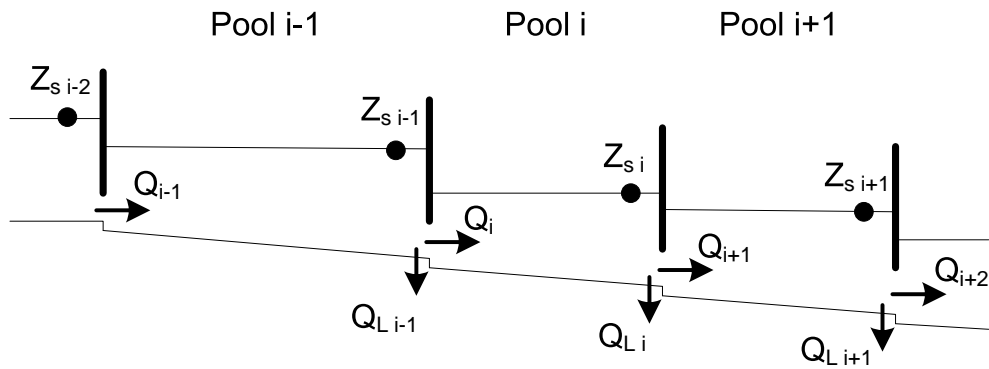
Figure 6.16: Conceptual scheme of an irrigation canal

Focusing on the conception of the idea, it arose from two main concepts:

- In a decentralized irrigation canal control scheme, each controller tries to regulate its downstream end water level $Z_{s\,i}$, forgetting completely about the effect that the controller action can produce over all the upstream pools. In a scheme like this, the responsibility for counteracting this effect fall on the upstream controllers. This type of disturbance affects mainly the upstream pool close to it (i.e. Pool i-1). A particular gate movement to regulate a downstream water level $Z_{s\,i}$ disturbs the immediately adjacent upstream water level $Z_{s\,i-1}$ with the highest intensity in the shortest time. So, why not perform this downstream water level regulation considering also that it is going to disturb the adjacent upstream water level? A controller like this would reduce in a high degree the sooner and most important part of the coupling effect.

- It sometimes happens that it is not the best option to regulate a circumstantial water level deviation with an upstream gate discharge adjustment (downstream control), but with a downstream gate discharge change (upstream control). As a matter of fact, there are cases where a particular gate discharge adjustment could be beneficial to both, an upstream and a downstream water level regulation task. These capabilities can only be provided by a multivariable controller that supervises, at least, two contiguous pools.

As a result, it was thought that solving the irrigation canal control problem taking pairs of pools, would be a much better option to approximate the centralized control performance than

a totally decentralized strategy.

The attainment of such a control scheme is visualized as follows. The irrigation canal semi-decentralized control strategy can be implemented using a series of multivariable Two-Input Two-Output (TITO) controllers (controller sketch in figure 6.17).
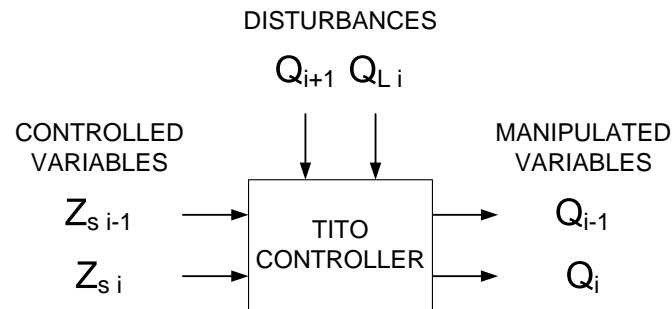
Figure 6.17: General scheme of a TITO controller

If each TITO controller takes into account an additional upstream water level, it is necessary to overlap the fields of action of the controllers as illustrated in figure 6.18.
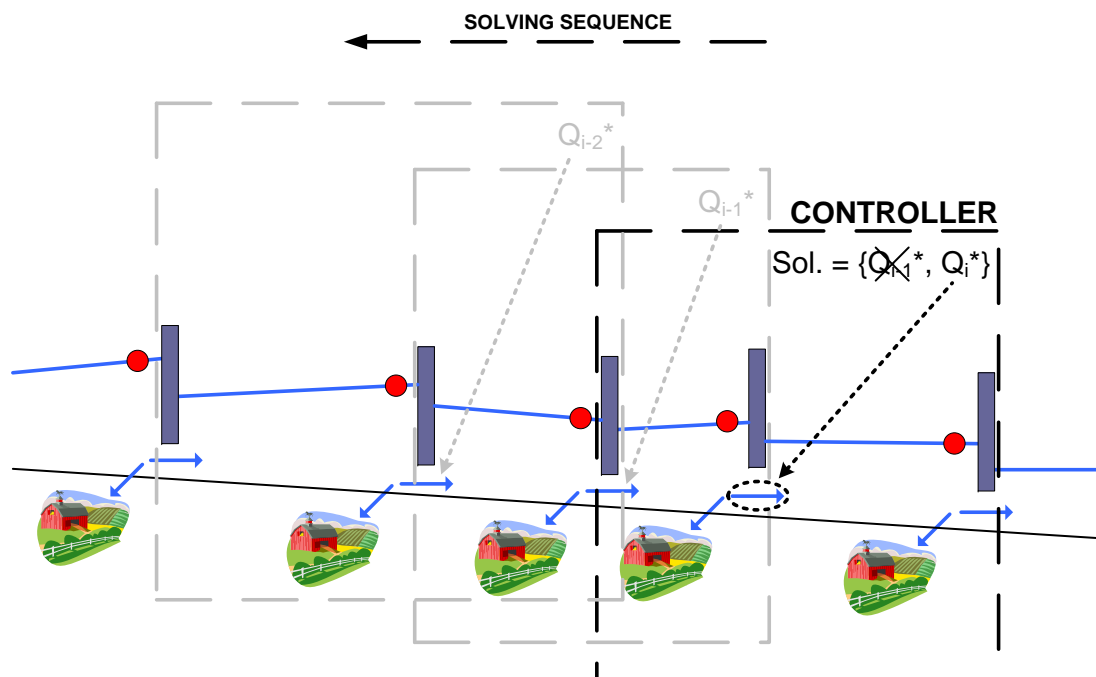
Figure 6.18: Irrigation canal semi-decentralized control philosophy

To grant the possibility of using gate discharges calculated by other controllers in the same control instant, the operation sequence should start with the controller located at the downstream end of the canal, then continue with the closest upstream controller and so on. Specifically, each "Pool i"-controller should regulate two downstream water levels, e.g. $Z_{s\,i}$ and $Z_{s\,i-1}$, with two gate discharges: Q_i and Q_{i-1}. However, only one gate discharge is actually applied, namely

Q_i. The Q_{i-1} value calculated by this controller is discarded. This control problem formulation ensures that the calculation of Q_i is performed in order to regulate $Z_{s\,i}$, but having also in mind the contiguous upstream pool objectives.

Continuing, the upstream "Pool i-1"-controller calculates the best Q_{i-1} and Q_{i-2} values to regulate $Z_{s\,i-1}$ and $Z_{s\,i-2}$. It applies only the calculated Q_{i-1} value and so on. The procedure is repeated until reaching the most upstream located controller.

This strategy allows to use the gate discharge calculated by a downstream controller and the offtake discharge as known measurable disturbances. Their incorporation depend only on the particular control technique used to implement the required two-input two-output controllers.

6.4.3.1 Semi-decentralized strategy applied on the Canal PAC-UPC
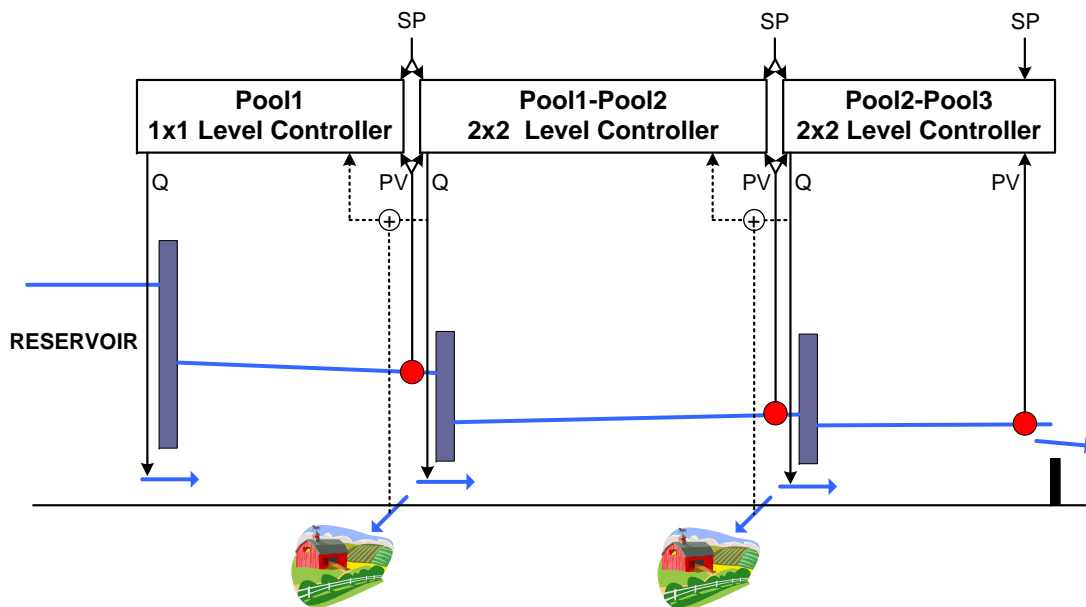
Figure 6.19: Simplified scheme of the Canal PAC-UPC with semi-decentralized control

The Canal PAC-UPC has three pools. A semi-decentralized implementation would require only two TITO controllers to tackle this particular control problem. However, in order to show that the strategy works fine for larger sequences of controllers, it has been arbitrarily decided to incorporate an additional SISO controller at the head of the canal. A simplification of the scheme that is going to be implemented in the Canal PAC-UPC is shown in figure 6.19.

It has been decided to design the required TITO controllers using the multivariable Predictive Control technique. This method is able to develop controllers for TITO systems and can also include measurable disturbances in the control law. The controller synthesis and some tuning recommendation were already explained in section 6.4.2.1 and were successfully used to obtain an explicit control law expression for a centralized controller. The same type of control

law expressions is pursued in this case.

The tuning parameters of the TITO controllers were selected so as to coincide with the previously designed controllers. The minimum prediction horizon (N_1), the maximum prediction horizon (N_2) and the control horizon (N_u) were chosen equal to the ones used to design the centralized controller. The weighting matrices Q and R were selected in similar way; it was only necessary to readjust the dimensions of the matrices maintaining the weights. The tuning of both TITO controllers is shown in table 6.10

Table 6.10: Tuning values for each 2×2 predictive controller

Min. pred. horiz., N_1 (samp. time units)	Max. pred. horiz., N_2 (samp. time units)	Control horiz., N_u (samp. time units)	Control time, T (s)
1	63	63	10
Error weighting matrix, $\mathbf{Q}$		Control weighting matrix, $\mathbf{R}$	
$\begin{bmatrix} 1 & 0 \\ 0 & 1 \end{bmatrix}$		$\begin{bmatrix} 50 & 0 \\ 0 & 50 \end{bmatrix}$	

With respect to the SISO controller that should control Pool1, the same controller designed for the decentralized Predictive Control scheme can be used. Their tuning values can be reviewed in table 6.8 from section 6.4.1.4.

To summarize, three controllers were designed to implement the semi-decentralized control strategy on the three-pool Canal PAC-UPC, one predictive SISO controller and two TITO predictive controllers. In addition to their regulation capabilities, this controllers were formulated in a way that enables the controllers to take advantage of additional information, like offtake discharges or a downstream controller action. The resulting controller formulas are presented next.
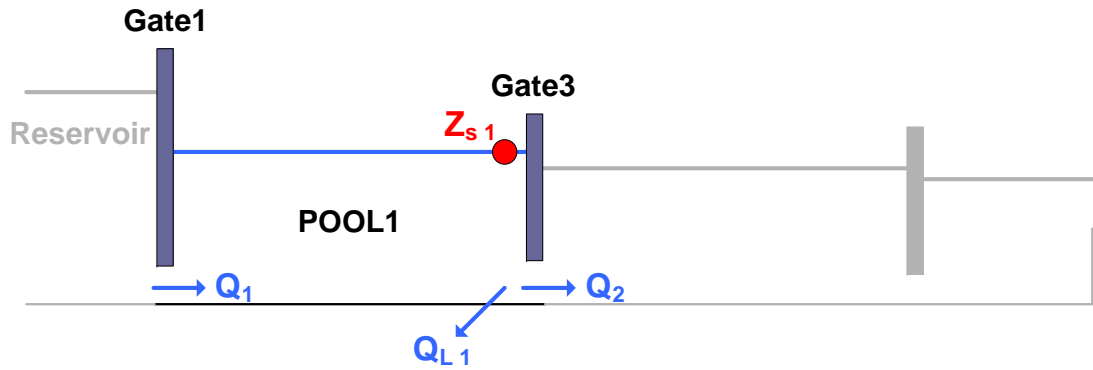
Figure 6.20: Variables involved in the control of Pool 1

Pool1 predictive controller:

$$Q_1(k) = 0.1221 \, sp_{Z_{s\,1}} + \mathbf{K_y} \, \mathbf{Z}_{s\,1} + \mathbf{K_u} \, \mathbf{Q}_1 + \mathbf{K_v} \, \mathbf{Q}_v \qquad (6.43)$$

with

$$\mathbf{K_y}^\mathbf{T} = \begin{bmatrix} -0.4543 \\ 0.2744 \\ -0.0617 \\ 0.0102 \\ -0.0888 \\ 0.1091 \\ 0.0890 \end{bmatrix} \quad \mathbf{Z}_{s\,1} = \begin{bmatrix} Z_{s\,1}(k) \\ Z_{s\,1}(k-1) \\ Z_{s\,1}(k-2) \\ Z_{s\,1}(k-3) \\ Z_{s\,1}(k-4) \\ Z_{s\,1}(k-5) \\ Z_{s\,1}(k-6) \end{bmatrix} \quad \mathbf{K_u}^\mathbf{T} = \begin{bmatrix} 0.7164 \\ -0.0244 \\ 0.4289 \\ -0.1210 \end{bmatrix}$$

$$\mathbf{Q}_1 = \begin{bmatrix} Q_1(k-1) \\ Q_1(k-2) \\ Q_1(k-3) \\ Q_1(k-4) \end{bmatrix} \quad \mathbf{K_v}^\mathbf{T} = \begin{bmatrix} 0.3097 \\ -0.4971 \\ 0.2086 \\ -0.0227 \\ 0.2063 \\ -0.2047 \end{bmatrix} \quad \mathbf{Q}_v = \begin{bmatrix} Q_2(k) + Q_{L\,1}(k) \\ Q_2(k-1) + Q_{L\,1}(k-1) \\ Q_2(k-2) + Q_{L\,1}(k-2) \\ Q_2(k-3) + Q_{L\,1}(k-3) \\ Q_2(k-4) + Q_{L\,1}(k-4) \\ Q_2(k-5) + Q_{L\,1}(k-5) \end{bmatrix}$$

Figure 6.21: Variables involved in the control of Pools 1 and 2

Pool1-Pool2 MIMO predictive controller

$$
\begin{bmatrix} Q_1(k) \\ Q_2(k) \end{bmatrix} = \mathbf{K_{sp}sp}_{Z_s} + \overbrace{\mathbf{K_{y_1}Z}_{s\,1} + \mathbf{K_{y_2}Z}_{s\,2}}^{\mathbf{K_y}\times\text{level data}} + \overbrace{\mathbf{K_{u_1}Q}_1 + \mathbf{K_{u_2}Q}_2}^{\mathbf{K_u}\times\text{gate discharge data}} + \overbrace{\mathbf{K_{v_1}Q}_{L\,1} + \mathbf{K_{v_2}Q}_v}^{\mathbf{K_v}\times\text{outflow data}}
$$

$$(6.44)$$

with

$$
\mathbf{K_{sp}} = \begin{bmatrix} 0.1016 & 0.0712 \\ -0.0623 & 0.0981 \end{bmatrix} \qquad \mathbf{sp}_{Z_s} = \begin{bmatrix} sp_{Z_{s\,1}} \\ sp_{Z_{s\,2}} \end{bmatrix}
$$

$$
\mathbf{K_{y_1}}^{\mathrm{T}} = \begin{bmatrix} -0.3998 & 0.1388 \\ 0.2432 & -0.0776 \\ -0.0541 & 0.0135 \\ 0.0099 & -0.0025 \\ -0.0769 & 0.0356 \\ 0.0973 & -0.0222 \\ 0.0788 & -0.0234 \end{bmatrix} \qquad \mathbf{Z}_{s\,1} = \begin{bmatrix} Z_{s\,1}(k) \\ Z_{s\,1}(k-1) \\ Z_{s\,1}(k-2) \\ Z_{s\,1}(k-3) \\ Z_{s\,1}(k-4) \\ Z_{s\,1}(k-5) \\ Z_{s\,1}(k-6) \end{bmatrix}
$$

$$
\mathbf{K_{y_2}}^{\mathrm{T}} = \begin{bmatrix} -0.1917 & -0.1793 \\ -0.0041 & -0.0106 \\ 0.0111 & 0.0051 \\ -0.0021 & -0.0144 \\ -0.0145 & -0.0222 \\ 0.0286 & 0.0272 \\ -0.0173 & -0.0158 \\ 0.0500 & 0.0473 \\ 0.0689 & 0.0645 \end{bmatrix} \qquad \mathbf{Z}_{s\,2} = \begin{bmatrix} Z_{s\,2}(k) \\ Z_{s\,2}(k-1) \\ Z_{s\,2}(k-2) \\ Z_{s\,2}(k-3) \\ Z_{s\,2}(k-4) \\ Z_{s\,2}(k-5) \\ Z_{s\,2}(k-6) \\ Z_{s\,2}(k-7) \\ Z_{s\,2}(k-8) \end{bmatrix}
$$

$$\mathbf{K_{u_1}}^T = \begin{bmatrix} 0.7475 & 0.0582 \\ -0.0191 & 0.0314 \\ 0.3787 & -0.1214 \\ -0.1071 & 0.0318 \end{bmatrix} \qquad \mathbf{Q}_1 = \begin{bmatrix} Q_1(k-1) \\ Q_1(k-2) \\ Q_1(k-3) \\ Q_1(k-4) \end{bmatrix}$$

$$\mathbf{K_{u_2}}^T = \begin{bmatrix} -0.4225 & 0.8097 \\ 0.1671 & -0.0656 \\ -0.0394 & -0.0053 \\ 0.4760 & 0.2074 \\ -0.1813 & 0.0538 \end{bmatrix} \qquad \mathbf{Q}_2 = \begin{bmatrix} Q_2(k-1) \\ Q_2(k-2) \\ Q_2(k-3) \\ Q_2(k-4) \\ Q_2(k-5) \end{bmatrix}$$

$$\mathbf{K_{v_1}}^T = \begin{bmatrix} 0.2740 & -0.0950 \\ -0.4385 & 0.1486 \\ 0.1851 & -0.0490 \\ -0.0203 & 0.0107 \\ 0.1809 & -0.0690 \\ -0.1813 & 0.0538 \end{bmatrix} \qquad \mathbf{Q}_{L1} = \begin{bmatrix} Q_{L1}(k) \\ Q_{L1}(k-1) \\ Q_{L1}(k-2) \\ Q_{L1}(k-3) \\ Q_{L1}(k-4) \\ Q_{L1}(k-5) \end{bmatrix}$$

$$\mathbf{K_{v_2}}^T = \begin{bmatrix} 0.2782 & 0.2484 \\ -0.3627 & -0.3270 \\ 0.0849 & 0.0790 \\ -0.0284 & -0.0260 \\ 0.1147 & 0.1069 \\ -0.0868 & -0.0813 \end{bmatrix} \qquad \mathbf{Q}_v = \begin{bmatrix} Q_3(k) + Q_{L2}(k) \\ Q_3(k-1) + Q_{L2}(k-1) \\ Q_3(k-2) + Q_{L2}(k-2) \\ Q_3(k-3) + Q_{L2}(k-3) \\ Q_3(k-4) + Q_{L2}(k-4) \\ Q_3(k-5) + Q_{L2}(k-5) \end{bmatrix}$$

To be coherent with the procedure explained in Section 6.4.3, from (6.44) only $Q_2(k)$ should be applied to the process to implement the Semi-decentralized strategy.
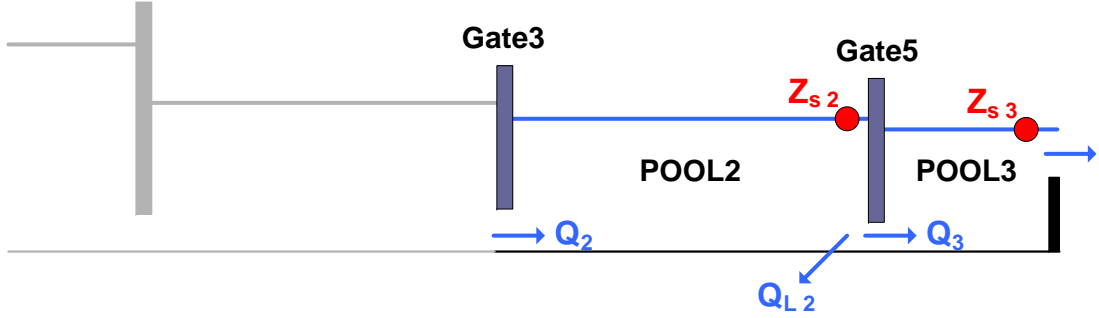
Figure 6.22: Variables involved in the control of Pools 2 and 3

Pool2-Pool3 MIMO predictive controller

$$\begin{bmatrix} Q_2(k) \\ Q_3(k) \end{bmatrix} = \mathbf{K_{sp}sp}_{Z_s} + \overbrace{\mathbf{K_{y_1}Z}_{s\,2} + \mathbf{K_{y_2}Z}_{s\,3}}^{\mathbf{K_y}\times\text{level data}} + \overbrace{\mathbf{K_{u_1}Q}_2 + \mathbf{K_{u_2}Q}_3}^{\mathbf{K_u}\times\text{gate discharge data}} + \overbrace{\mathbf{K_v Q}_{L\,2}}^{\mathbf{K_v}\times\text{offtake discharge data}}$$

(6.45)

with

$$\mathbf{K_{sp}} = \begin{bmatrix} 0.0879 & 0.0870 \\ -0.0781 & 0.0868 \end{bmatrix} \qquad \mathbf{sp}_{Z_s} = \begin{bmatrix} sp_{Z_s\,2} \\ sp_{Z_s\,3} \end{bmatrix}$$

$$\mathbf{K_{y_1}}^{\mathrm{T}} = \begin{bmatrix} -0.1741 & 0.1006 \\ -0.0103 & 0.0017 \\ 0.0057 & -0.0036 \\ -0.0129 & -0.0006 \\ -0.0195 & 0.0150 \\ 0.0284 & -0.0081 \\ -0.0141 & 0.0232 \\ 0.0463 & -0.0142 \\ 0.0626 & -0.0360 \end{bmatrix} \qquad \mathbf{Z}_{s\,2} = \begin{bmatrix} Z_{s\,2}(k) \\ Z_{s\,2}(k-1) \\ Z_{s\,2}(k-2) \\ Z_{s\,2}(k-3) \\ Z_{s\,2}(k-4) \\ Z_{s\,2}(k-5) \\ Z_{s\,2}(k-6) \\ Z_{s\,2}(k-7) \\ Z_{s\,2}(k-8) \end{bmatrix}$$

$$\mathbf{K_{y_2}}^{\mathrm{T}} = \begin{bmatrix} -0.4574 & -0.3199 \\ 0.2793 & 0.1734 \\ 0.1035 & 0.0627 \\ -0.0638 & -0.0418 \\ 0.1437 & 0.0977 \\ -0.0923 & -0.0589 \end{bmatrix} \qquad \mathbf{Z}_{s\,3} = \begin{bmatrix} Z_{s\,3}(k) \\ Z_{s\,3}(k-1) \\ Z_{s\,3}(k-2) \\ Z_{s\,3}(k-3) \\ Z_{s\,3}(k-4) \\ Z_{s\,3}(k-5) \end{bmatrix}$$

$$\mathbf{K_{u_1}}^{\mathrm{T}} = \begin{bmatrix} 0.7579 & 0.0634 \\ -0.0123 & 0.0298 \\ -0.0135 & 0.0609 \\ 0.2680 & -0.1540 \end{bmatrix} \qquad \mathbf{Q}_2 = \begin{bmatrix} Q_2(k-1) \\ Q_2(k-2) \\ Q_2(k-3) \\ Q_2(k-4) \end{bmatrix}$$

$$\mathbf{K_{u_2}}^{\mathrm{T}} = \begin{bmatrix} -0.2879 & 0.8851 \\ 0.7204 & 0.3922 \\ -0.4567 & -0.2477 \\ 0.1031 & -0.0748 \\ -0.0788 & 0.0453 \end{bmatrix} \qquad \mathbf{Q_3} = \begin{bmatrix} Q_3(k-1) \\ Q_3(k-2) \\ Q_3(k-3) \\ Q_3(k-4) \\ Q_3(k-5) \end{bmatrix}$$

$$\mathbf{K_v}^{\mathrm{T}} = \begin{bmatrix} 0.2408 & -0.1624 \\ -0.3154 & 0.2116 \\ 0.0759 & -0.0473 \\ -0.0256 & 0.0276 \\ 0.1031 & -0.0748 \\ -0.0788 & 0.0453 \end{bmatrix} \qquad \mathbf{Q}_{L2} = \begin{bmatrix} Q_{L2}(k) \\ Q_{L2}(k-1) \\ Q_{L2}(k-2) \\ Q_{L2}(k-3) \\ Q_{L2}(k-4) \\ Q_{L2}(k-5) \end{bmatrix}$$

To be coherent with the procedure explained in Section 6.4.3, from (6.45) only $Q_3(k)$ should be applied to the process to implement the Semi-decentralized strategy.

6.4.4   Simulation results

The aim of this section is to test each one of the water level control schemes designed for the Canal PAC-UPC, without the interference of the other slave control layers. In particular, it is desired to observe their control performances in terms of disturbance rejection capabilities (unscheduled offtake discharge changes) and compare the results. It is expected that these tests will be revealing in order to expose the main advantages and drawbacks of each scheme.

In order to carry out the tests, the previously identified multivariable ARX model (5.36) (page 121) was used as the "true" plant. Each control solution was implemented, linked to the ARX model and simulated in Simulink®, a toolbox of the software package MATLAB®.

The experiment is based on a situation were the following events take place:

- Time = 1000 s: A +20 L/s offtake discharge increment in Pool1.

- Time = 3000 s: A +20 L/s offtake discharge increment in Pool2.

- Time = 5000 s: A +2 cm downstream water level set point increment in Pool3.

These events are shown graphically in figure 6.23.

(a) Unscheduled offtake discharge signals   (b) Water level reference signals
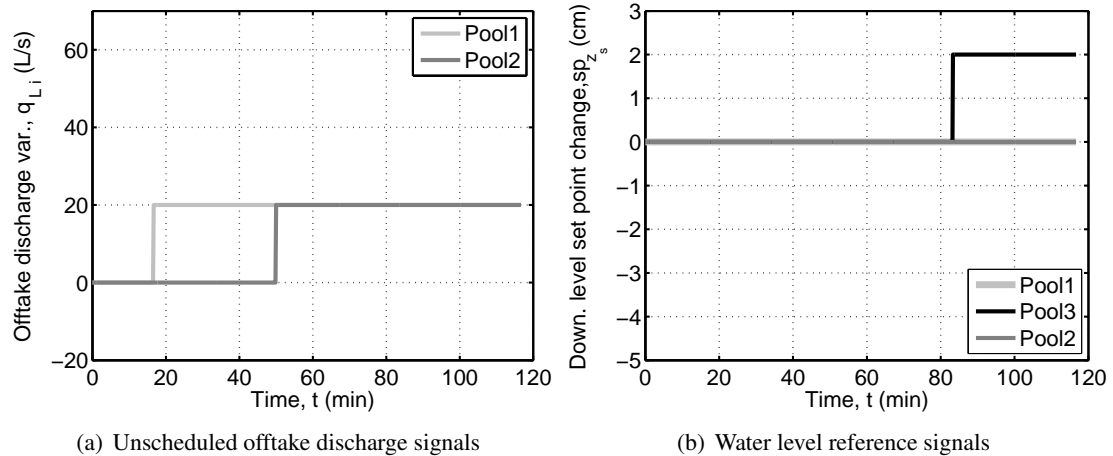
Figure 6.23: Experimental conditions

The simulation results are divided into two groups that are going to be detailed in the following pages.

The first group collects results of PI-based strategies tuned with different methods. Among these strategies, it is also possible to find different types of PI-based implementations such as PIF controllers and PIF controllers with decoupling. This first group of results are presented in two figures; figure 6.24 presents the water level variations that take place when the PI based control solutions try to counteract the aforementioned operation events and figure 6.25 presents the control actions applied in each case. Both figures are presented next.

(a) Schuurmans PI

(b) MIMO Nyquist PI

(c) Schuurmans PIF

(d) Litrico PIF

(e) MIMO Nyquist PIF

(f) MIMO Nyquist PIF + decoupling
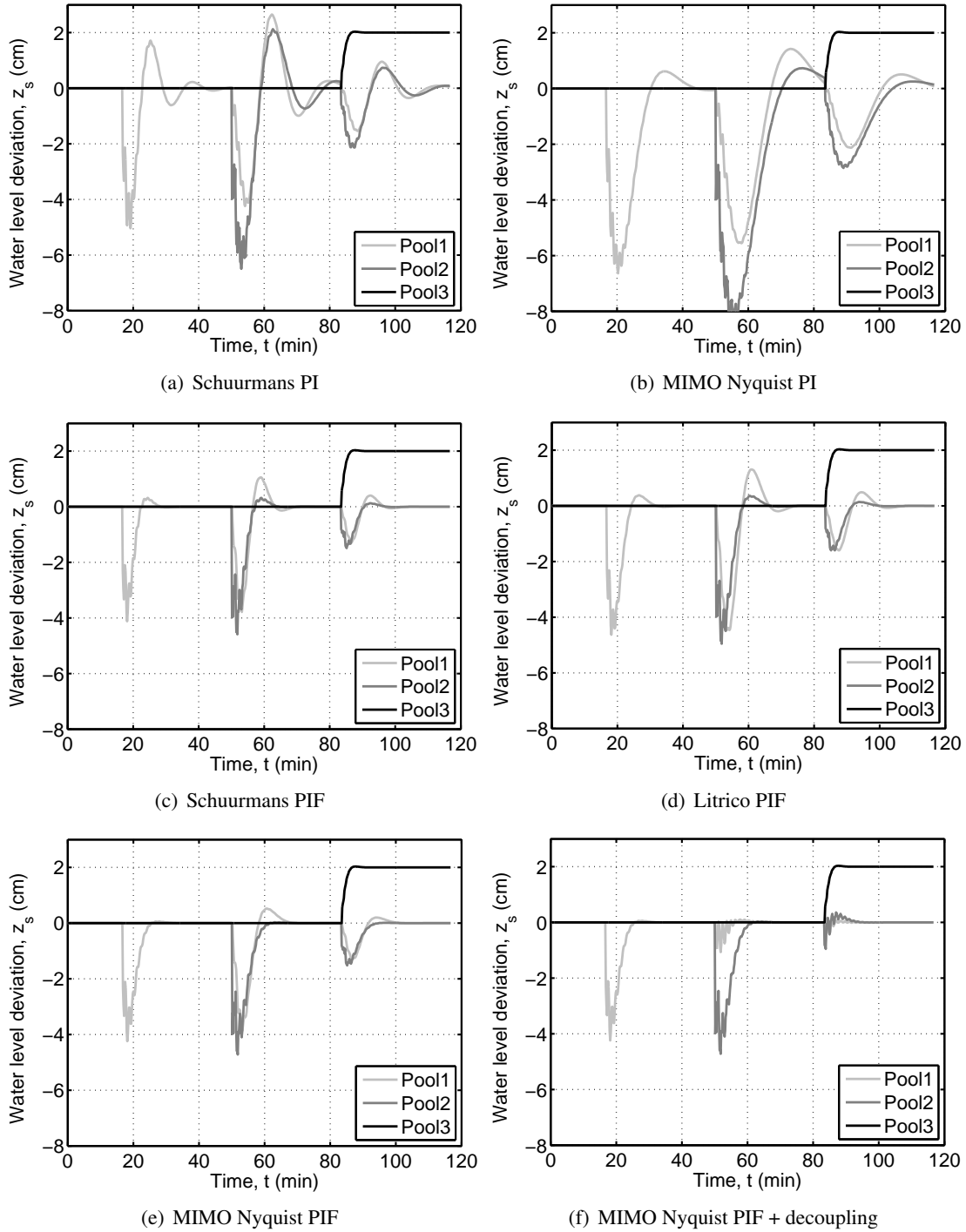
Figure 6.24: Regulation of water levels using different PI based solutions

(a) Schuurmans PI

(b) MIMO Nyquist PI

(c) Schuurmans PIF

(d) Litrico PIF

(e) MIMO Nyquist PIF

(f) MIMO Nyquist PIF + decoupling
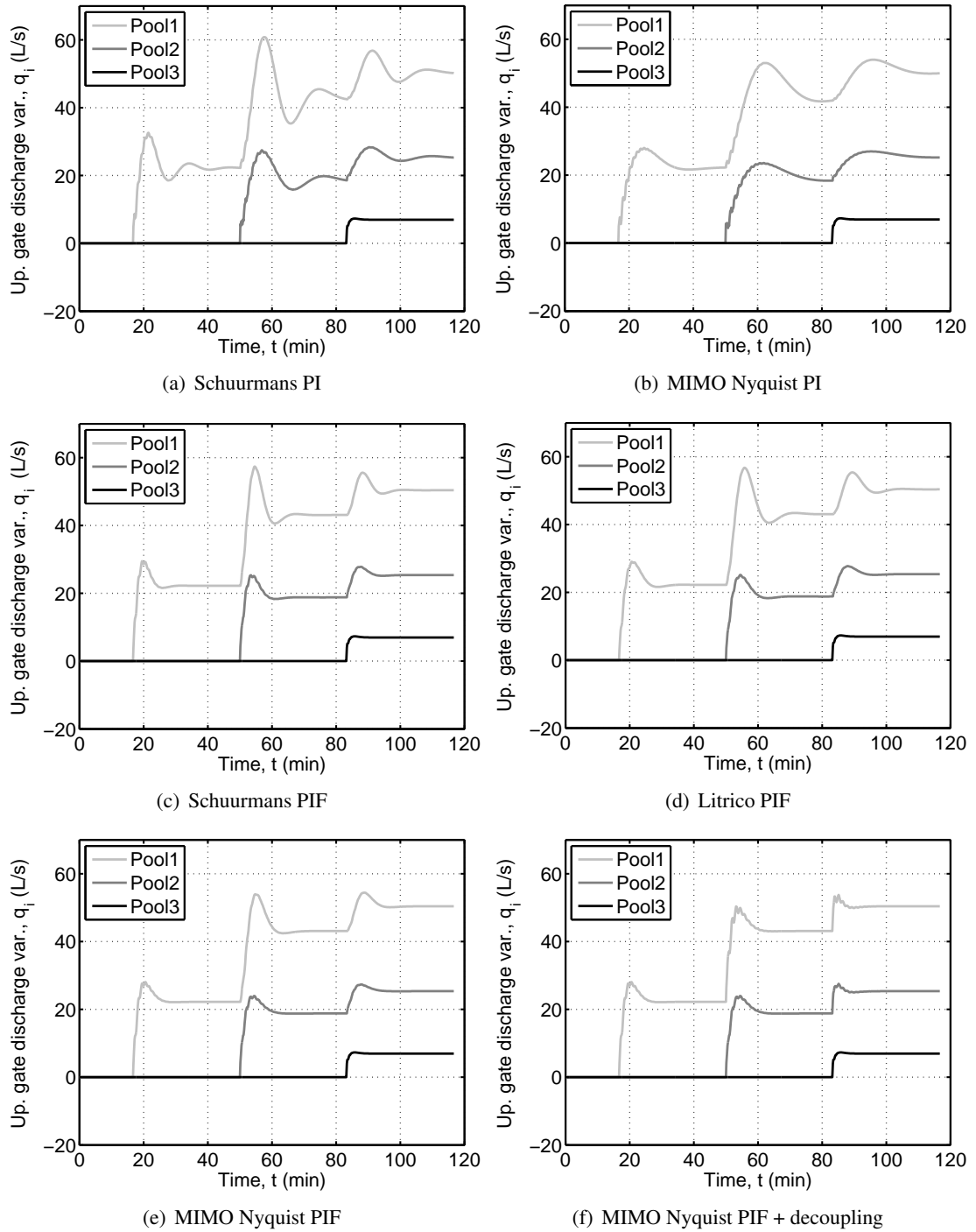
Figure 6.25: Gate discharges required by the PI based solutions

Generally speaking, the inspection of both figures reveals that all the tested schemes were able to control this particular situation. At first glance, this fact suggests that all of them are perfectly capable of managing this laboratory canal, but with different performance degrees.

There are interesting performance peculiarities. For instance, the control schemes based on standard PI controllers ("Schuurmans PI" and "MIMO Nyquist PI") exhibit the worst performances. The magnitude of the water level deviations using this type of schemes were the group highest. Additionally, they took a lot of time in order to return the system to a stationary condition.

The schemes using PIF controllers without decouplers ("Schuurmans PIF", "Litrico PIF" and "MIMO Nyquist PIF") behave all in a similar manner. Water level deviations were lessened in less time than the aforementioned schemes and the peak values were sensible smaller. As expected, the "MIMO Nyquist PIF" required the shorter times to stabilize the system and exhibited the less oscillating behavior. Because of this, this control scheme was selected to be implemented with decouplers. The so called "MIMO Nyquist PIF + decoupling" scheme presented the best performance results of the whole group, achieving the smallest level deviations during the shortest time periods.

Focusing on the control efforts required by each method, the inspection of figure 6.25 revealed that the best level regulation performances were normally in accordance with the lowest control efforts.

The best PI-based results, namely the ones of the "MIMO Nyquist PIF + decoupling" scheme, were also included in the second group of simulation results for comparison purposes. This second group contains the results obtained by controlling the Canal PAC-UPC with decentralized, semi-decentralized and centralized predictive control strategies. The decentralized and the semi decentralized control strategies were implemented so that each controller knows the control action (gate discharge) that a downstream controller is going to execute. This information is fed into each controller as a measurable disturbance and provide the schemes with decoupling capabilities.

As before, these results are presented in two figures; figure 6.26 presents the water level variations results and figure 6.27 show the gate discharges calculated in each case. Both figures are presented in the next pages.[1]

---

[1]Notice the change in the y-axis scale factor of figure 6.26 with respect to figure 6.24

(a) MIMO Nyquist PIF + decoupling

(b) Decentralized PC + decoupling

(c) Semi-decentralized PC + decoupling

(d) Centralized PC
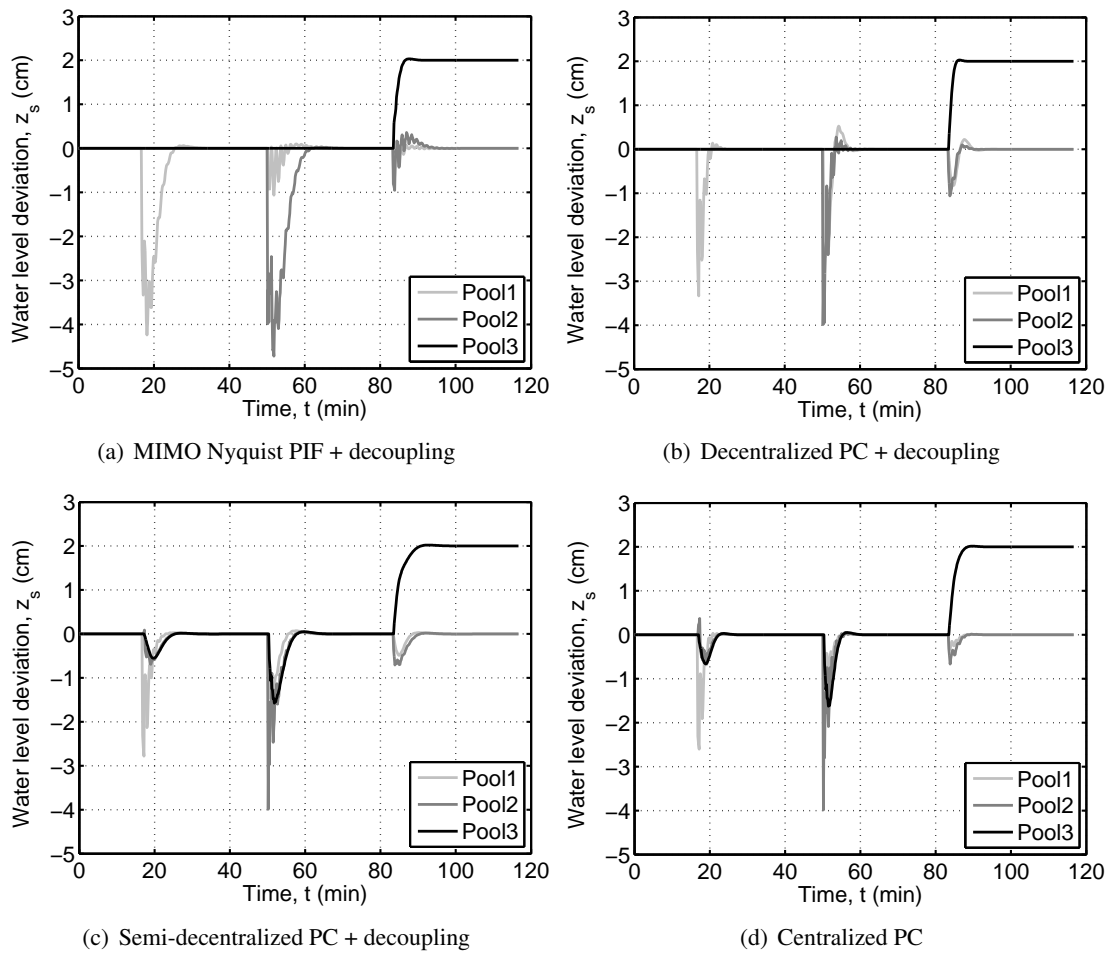
Figure 6.26: Regulation of water levels using different control strategies

(a) MIMO Nyquist PIF + decoupling

(b) Decentralized PC + decoupling

(c) Semi-decentralized PC + decoupling

(d) Centralized PC
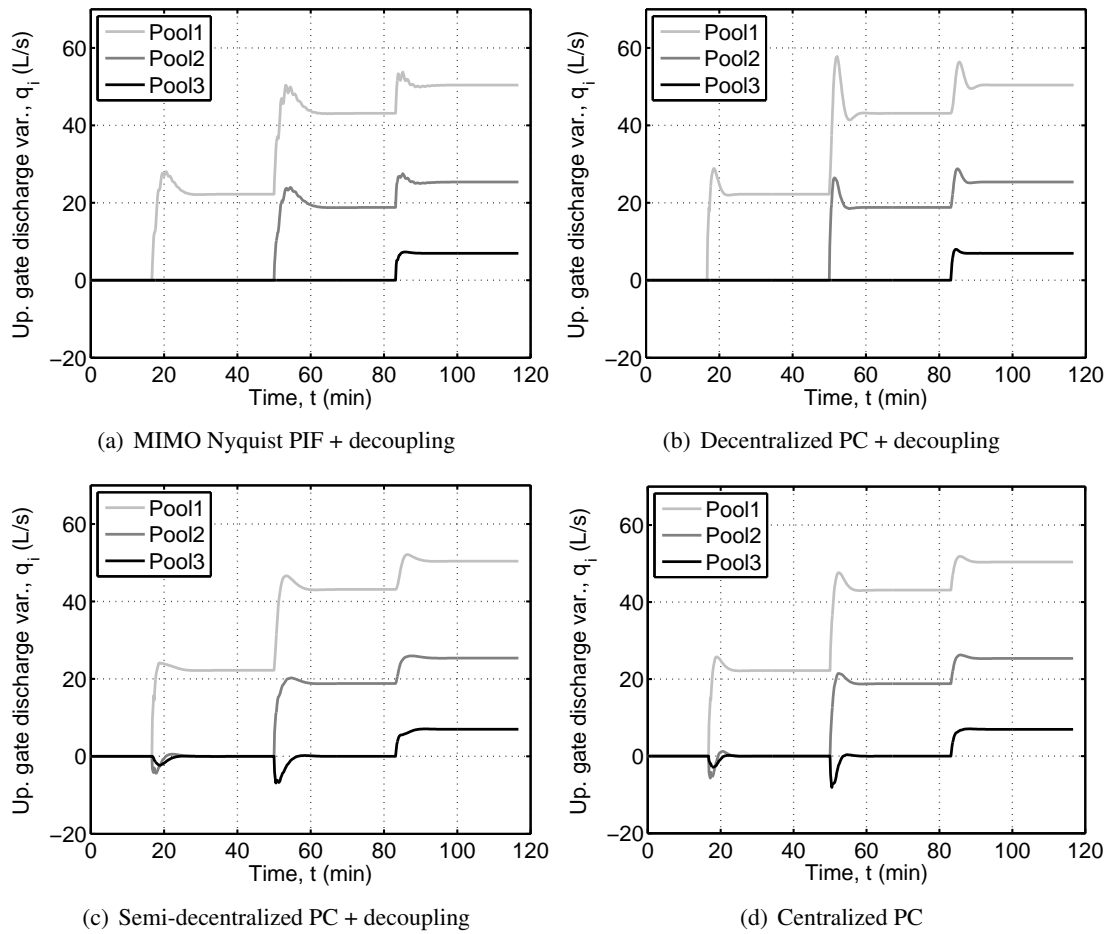
Figure 6.27: Gate discharges calculated by each control method

An overall inspection of both figures reveals that the Predictive Control (PC)-based control schemes did better than the best PI-based control scheme; their water level deviations were always smaller with shorter recovery times. There is also one additional peculiarity in the "MIMO Nyquist PIF + decoupling" results; the controller response and particularly the water levels, seem to be slightly oscillating in the transitions in comparison to the other schemes. This behavior is attributable to the way decoupling is implemented in this case; the control action calculated by a downstream controller is directly added to the output of an upstream controller. Thus, the controller is working under a condition that is slightly different from the designed one.

Among the PC-based strategies, the performance differences were small. As expected, the centralized strategy ("Centralized PC") achieved the best results: the smallest level deviations during the shorter time periods (see figure 6.26). The control actions and the results obtained using the semi-decentralized control scheme ("Semi-decentralized PC + decoupling") were very similar to the ones exhibited by the centralized controller. The only difference between their responses was that the semi-decentralized scheme responded in a slightly slower manner than the centralized scheme. Finally, the decentralized and decoupled predictive control scheme

("Decentralized PC + decoupling") obtained similar performance results, but with much more aggressive control actions; figure 6.27 show that the gate discharges calculated by this control solution achieved noticeable transient peaks compared to the other schemes.

It should be noticed that these results were obtained from simulating linear model (5.36) (page 121) with the different control schemes. That means that these results correspond to the nominal performance of the level controllers. In other words, the ideal and most favorable case. However, these performance results may vary if these control schemes are tested in a Saint-Venant model or in a real canal.

6.4.4.1 Special test: minimum gate movement restriction

A few research works (Bautista and Clemmens, 1999; Wahlin and Clemmens, 2002; Wahlin, 2004; Clemmens and Schuurmans, 2004b) have remarked the existence of a water level control performance deterioration because of this real actuator nonlinearity. All motorized gates are affected by this physical constraint; it is impossible to move a gate less than a certain minimum distance. This minimum distance varies depending on each gate's particular design. For the Canal PAC-UPC gates, these minimum values were already given in page 135. This information is recalled in table 6.11

Table 6.11: Determination of the ξ parameters

Gate name	ξ (mm)
Gate 1	8.0
Gate 3	9.5
Gate 5	10.1

For the water level control layer, this gate movement restriction converts into a gate discharge constraint. Required gate discharge increments or decrements can only be accomplished if their absolute values are greater than a certain limit ($|\Delta Q_i|$>limit). However, this limit value is not fixed; it depends on the particular water level and gate opening conditions. Nevertheless, this value do not change considerably around a particular operation condition.

A simple implementation of this constraint can be attained by using a fixed constraint value. All tested controllers, without exception, had problems when this constraint was included in the simulations. For example, the simulation test results of the "Centralized PC" and of the "MIMO Nyquist PIF + decoupling" schemes are presented in figure 6.28 when it is not possible to realize gate discharge changes less than $\pm 2\,\mathrm{L/s}$.

It is easily noticeable in figure 6.28 that neither of these control solutions is able to lead the

(a) MIMO Nyq. PIF + dec. – Levels

(b) Centralized PC – Levels

(c) MIMO Nyq. PIF + dec. – Gate discharges

(d) Centralized PC – Gate discharges
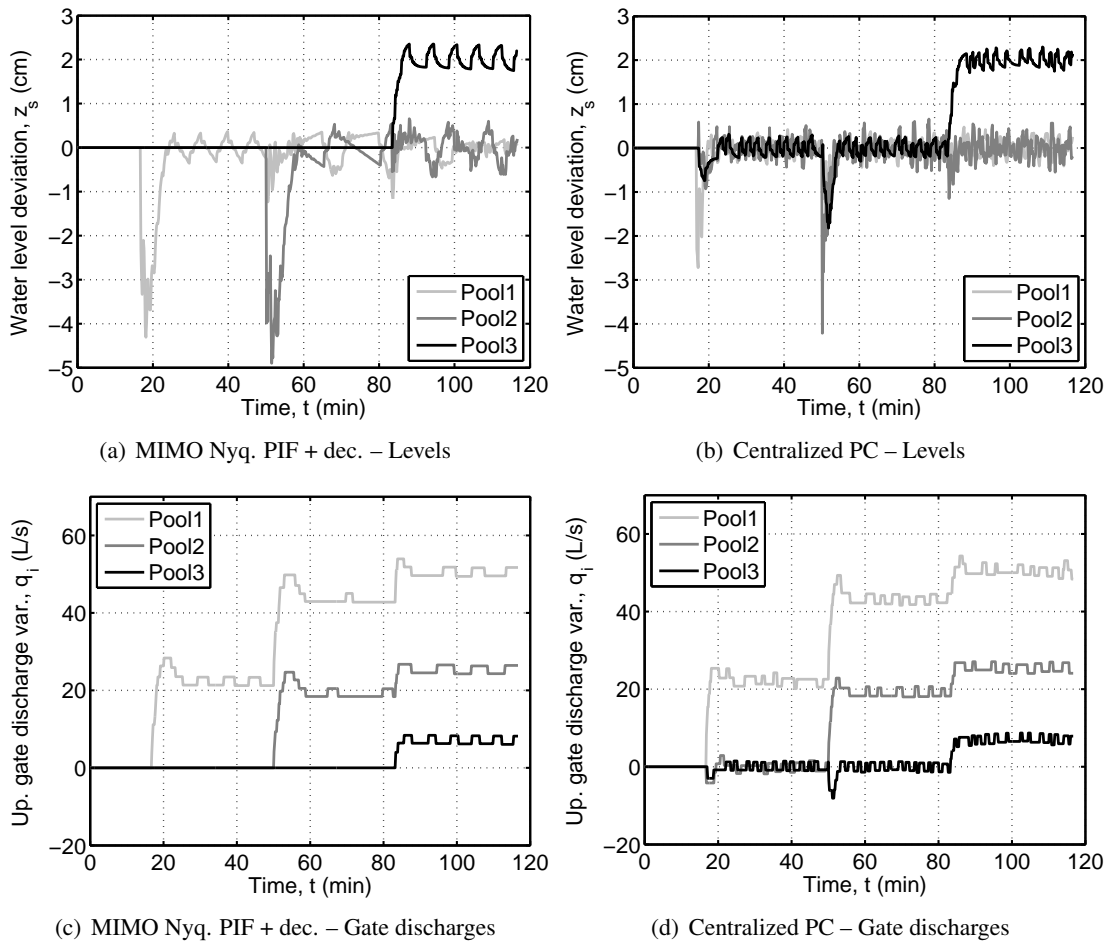
Figure 6.28: Influence of the minimum gate movement constraint on control performance

system to a steady state value, when dealing with this particular gate discharge constraint. In general, the oscillations increase when this constraint value is higher, whereas they decrease in the opposite case. If this value is very small, this effect is hardly noticed.

A real solution to the complete control problem is very difficult to implement in practice. For instance, a predictive controller with the capability to incorporate this type of constraint would require a very complex and time-consuming type of optimization problem solver. Hence, it is advisable to try to reduce the minimum movement constraint of control gates to the greatest possible extent.

When the position control runs at a much faster rate than the rest of the control layers, it is also possible to achieve smaller gate movements by repositioning the gate with longer trajectories that should avoid this minimum movement. In that case, this would produce greater transient peaks that should not disturb the water level control performance. However this gate repositioning should also be limited to a certain value in order to prevent the gate to move due to noisy or unnecessary accurate orders.

In summary, it is better to reduce this problem from the source when possible. However, most of the cases, this is not possible, and actuator and level oscillations around stationary values are likely to appear.

6.5 Experimental results

6.5.1 Experiment description

In order to reveal the real strengths and weaknesses of each control scheme, an appropriate performance test situation was designed. This test is based on the most common control task that a real automated irrigation canal has to face: regulation of water levels to counteract changes in offtake discharges. The details are given next.

The performance test starts from the initial condition that is illustrated in figure 6.29.
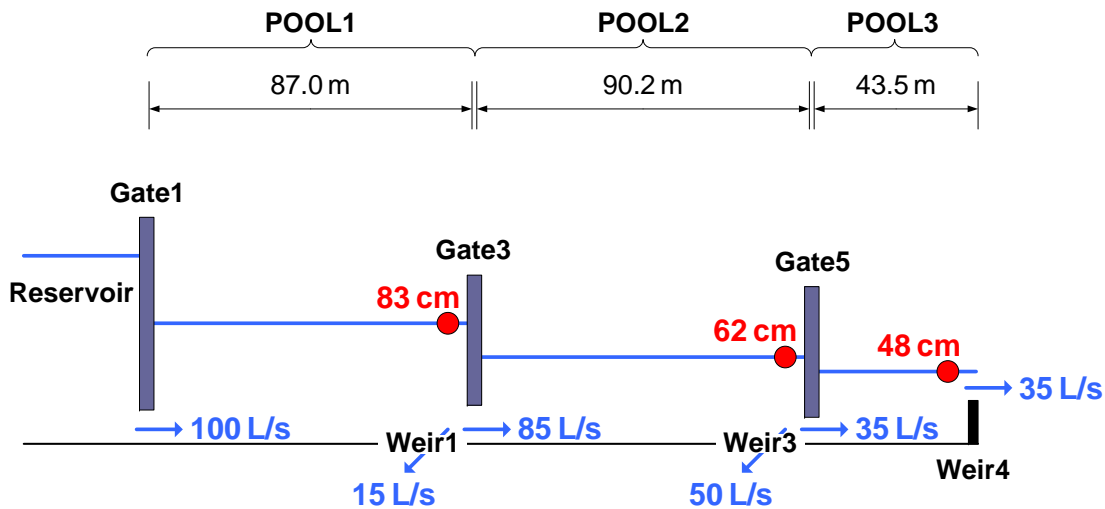
Figure 6.29: Initial condition for the performance test

From this stationary state, the following events are executed:

1. Weir3 is **closed** at time $t = 20\,\text{min}$.

2. Weir3 is **opened** at time $t = 55\,\text{min}$.

These simple actions involve two different types of disturbances. When Weir3 is suddenly closed, the offtake discharge is varied from $50\,\text{L/s}$ to $0\,\text{L/s}$. Thus, the controlled system is affected by a step disturbance. On the other hand, when Weir3 is opened the offtake discharge is time-varying until the level is returned to the reference value, because of the dependence of the weir discharge on the head.

These disturbances produce an important variation in the downstream water level of each pool. Consequently, the task of each control scheme is to bring these levels back to their reference values as soon as possible and minimize the eventual deviations. As explained in the previous section, it is almost impossible to avoid the small steady state oscillations that occur due to the minimum gate movement restrictions, but it is also important that the control schemes do not amplify these oscillations. Hence, it is also desirable to obtain the smaller water level oscillation amplitudes in the long term response.

This test is also appropriate to test the noise sensitivity of the different control schemes. In general, discharges bigger than $70\,\mathrm{L/s}$ agitate the downstream water levels a few centimeters around the references. This situation occurs before Weir3 is closed and after Weir3 is re-opened. Thus, the control schemes has to deal with these noisy signals during these time periods. In contrast, when Weir3 is closed the required head discharge should be $50\,\mathrm{L/s}$. Under this situation, the water is more calm. If there is a remarkable difference in the response of a particular control scheme when facing the closing and the opening of Weir3, it is an evidence that noise affects the control performance.

It is worth to remark that the first offtake discharge variation (at $t = 20\,\mathrm{min}$) represent the $50\,\%$ of the discharge entering the canal and that the second event (at $t = 55\,\mathrm{min}$) force the control to double the canal inflow. Hence, this performance test is really demanding in terms of relative units although a maximum offtake discharge change of $\pm 50\,\mathrm{L/s}$ could be relatively small for a big irrigation canal.

6.5.2 Tested schemes

The majority of the control solutions designed in previous sections were implemented and tested in the true Canal PAC-UPC. In particular the following control schemes were tested:

- Decentralized PIF control (tuned with MIMO Nyquist-like techniques)

- Decentralized PIF control with decoupling

- Decentralized PIF control with decoupling and feedforward capabilities

- Decentralized PC control

- Decentralized PC control with decoupling

- Decentralized PC control with decoupling and feedforward capabilities

- Semi-decentralized PC control

- Semi-decentralized PC control with decoupling

- Semi-decentralized PC control with decoupling and feedforward capabilities

- Centralized PC control

- Centralized PC control with feedforward capabilities

The term "decoupling" means that each level controller calculates an upstream gate discharge to fulfil its own water level regulation objectives and then gives this information to the controller of the upstream pool. In this way, the upstream controller can know the flow rate

change that is going to be performed in the downstream gate of its pool and counteract its effect. This is why the term "decoupling" is used; it refers to the scheme capability to reduce the interference among control actions taken by different controllers.

The controllers without feedforward capabilities can not make use of offtake discharge information. Hence, they are submitted to unexpected or unknown disturbances when the test is performed. Conversely, the controllers with feedforward capabilities are fed with actual offtake discharge weir measurements (known disturbances). However, no future information or scheduled changes in flow are given to the controllers.

6.5.3 Results

The response of the canal controlled with the aforementioned schemes was recorded during a $90\,\mathrm{min}$ time period at a $0.1\,\mathrm{s}$ sampling rate. The dynamics occurring at periods smaller than $5\,\mathrm{s}$ were later on filtered in order to center the attention on the response trends.

Three physical variables were followed: downstream water levels, gate discharges and gate openings. This data was represented in different graphs following the same order cited before. There are eleven tested control schemes, so the total amount of graphs is 33. In order to facilitate the comparisons, the graphs of the resulting pool water levels were grouped into three categories:

1. Control schemes where controllers do not share information

2. Control schemes where controllers share information

3. Control schemes where controllers share information and the disturbances are measured

The graphs and a detailed analysis of the results are presented in the following pages.

6.5.3.1 Pool water levels

These results are presented in figures 6.30, 6.31 and 6.32.

Control schemes where controllers do not share information (figure 6.30) The disturbance effect is more notorious in the decentralized PIF scheme. There are large water level deviations in Pool1 and in Pool2. This control scheme takes approximately $10\,\mathrm{min}$ and $15\,\mathrm{min}$ to bring the levels back to the references when facing disturbance 1 and 2 respectively. However the response seems to be very stable.

The decentralized PC exhibit smaller transient deviations, but a clear oscillatory behavior. The oscillations have a magnitude that is higher for Pool1 when water levels are more noisy. The oscillation amplitude is close to $5\,\mathrm{cm}$ in that case. However, the time to bring the system back to the reference values is the shortest among these schemes: less than $5\,\mathrm{min}$.

(a) Decentralized PIF

(b) Decentralized PC

(c) Semi-decentralized PC
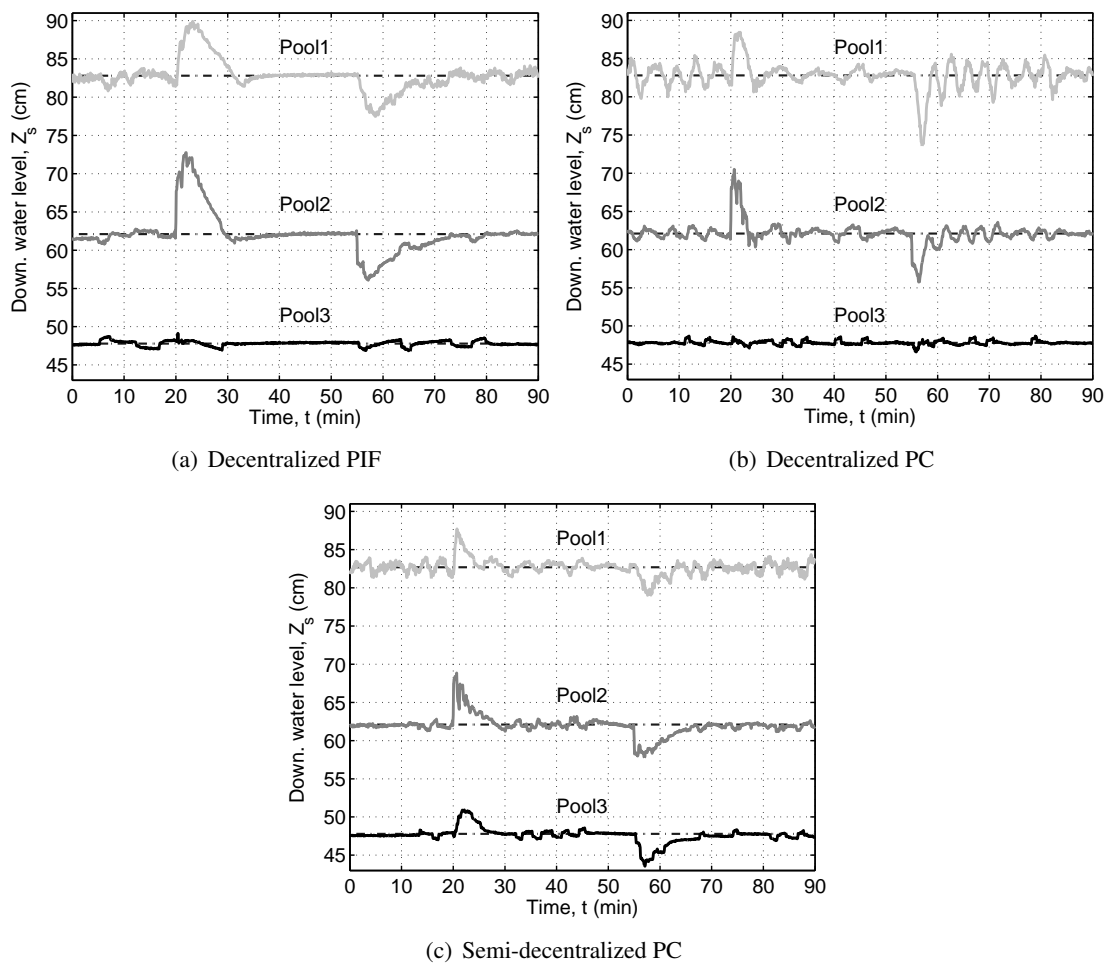
Figure 6.30: Control schemes where controllers do not share information: Regulation of water levels

The smallest deviations are obtained by the semi-decentralized PC scheme. This scheme sacrifice a little the Pool3 level regulation to avoid larger deviations in the other pools. Levels are returned in less than $10\,\mathrm{min}$ and in a very stable manner. Moreover, the influence of the Pool2 events on Pool1 are highly dampened using this scheme. However, this issue was somehow expected. Indeed, the semi-decentralized concept considers some type of decoupling since each controller uses information from two adjacent pools. In cases (a) and (b) each individual controller uses only local information of its pool.

(a) Decentralized PIF + decoupling

(b) Decentralized PC + decoupling

(c) Semi-decentralized PC + decoupling
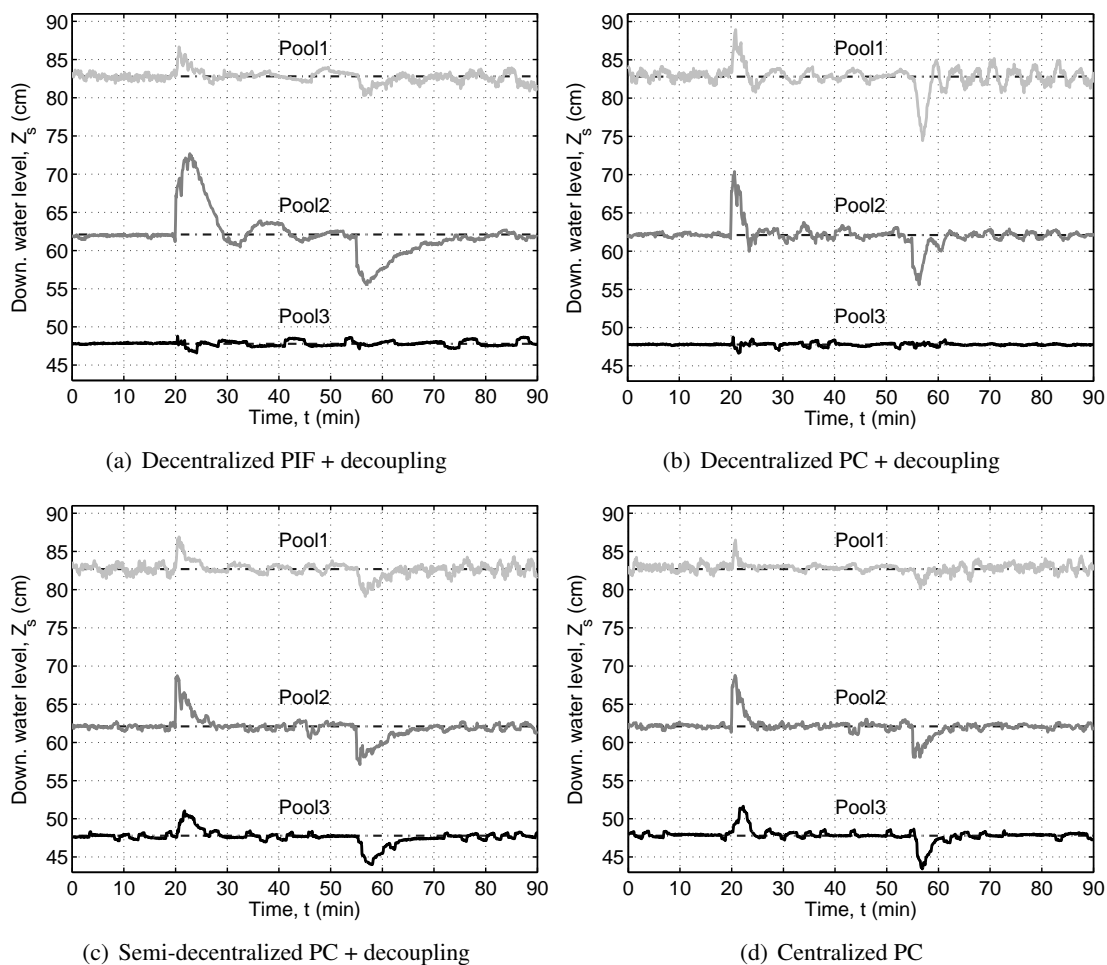
(d) Centralized PC

Figure 6.31: Control schemes where controllers share information: Regulation of water levels

Control schemes where controllers share information (figure 6.31) The inclusion of decoupling strategies has more impact on the decentralized PIF scheme. The time needed to return the canal to its original state and the level deviations in Pool2 are exactly the same, but the effect on Pool1 has been greatly reduced (approx. $50\,\%$).

The decoupling effect is less noticeable in the decentralized and in the semi-decentralized PC schemes. However, a closer inspection reveals that the maximum level deviations in Pool1

are a couple of centimeter smaller than before. The other differences among these three schemes remain. The predictive control schemes return the levels in half the time than the PIF scheme and the smaller deviations are still obtained by the semi-decentralized strategy. Level oscillations are still noticeable in the decentralized PC scheme.

The results obtained with the centralized PC controller are also given. It achieved the best results, i.e. the smaller deviations and the shorter recovery times. Its results are very similar to the semi-decentralized ones; level deviations are almost the same and recovery times are slightly shorter.

(a) Decentralized PIF + dec. + feedforward

(b) Decentralized PC + dec. + feedforward

(c) Semi-decentralized PC + dec. + feedforward

(d) Centralized PC + feedforward
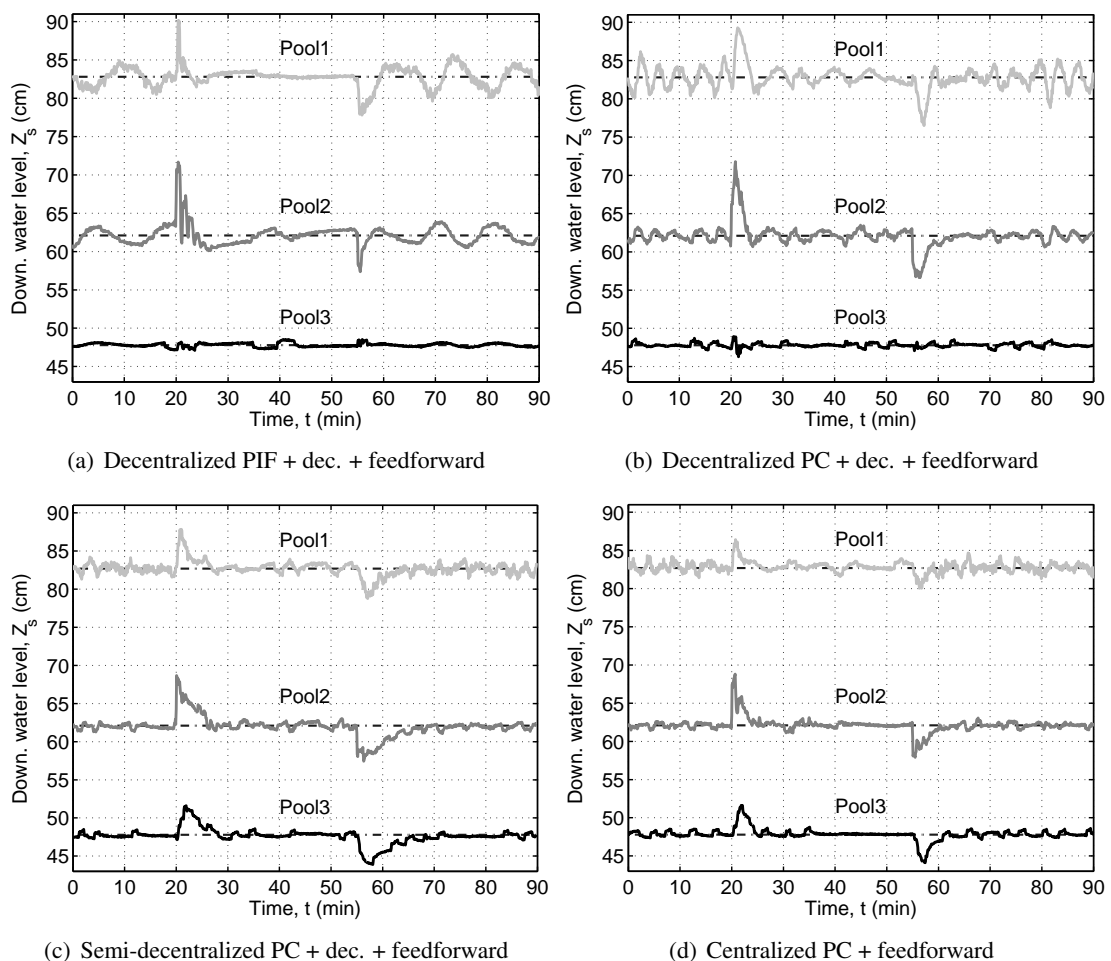
Figure 6.32: Control schemes where controllers share information and the disturbances are measured: Regulation of water levels

Control schemes where controllers share information and the disturbances are measured (figure 6.32) To feed the control schemes with offtake discharge information does not seem to improve the control performance any further.

It is true that larger deviation are controlled more quickly using feedforward in the decen-

tralized PIF control. However, the PIF control scheme is now clearly oscillating, inclusively before starting the performance test. It seems that the direct inclusion of the offtake discharge measurements induced high oscillations in the controlled system. There is also a more plausible explanation for this. The detailed inspection of case (a) reveals that oscillations only occur when the flow rate is high. Consequently, it is a controller response to slightly turbulent water levels. This is an evidence that the stability margins of the controlled system are no longer the ones originally designed. Thus, the direct inclusion of offtake discharge measurements in the control has modified the original control design so much that now it is no longer valid.

The predictive control schemes exhibit no noticeable changes in general. Only the decentralized PC response seems to be a little more oscillating than without feedforward.

6.5.3.2   Gate discharges and gate openings

These results are shown graphically in figures 6.33 and 6.34 respectively.

These figures confirm the existence of sustained system oscillations in all the decentralized PC schemes and in the decentralized PIF scheme with decoupling and feedforward capabilities. This type of response appeared when the canal was operating with higher discharges and the water levels were more fluctuating. Thus, it is supposed that these schemes are likely to be affected by fluctuating level measurements under the current particular controller tunings.

It can be also appreciated that all the predictive control schemes demand gate movements at a more frequent rate than the PIF schemes to maintain the levels close to their reference values. In this respect, it is also noticeable that the semi-decentralized and the centralized predictive control solutions are the only ones that produce gate discharge transitions without overshoot.

(a) Decentralized PIF

(b) Decentralized PIF + dec.

(c) Decentralized PIF + dec. + ff

(d) Decentralized PC

(e) Decentralized PC + dec.

(f) Decentralized PC + dec. + ff

(g) Semi-decentr. PC

(h) Semi-decentr. PC + dec.

(i) Semi-decentr. PC + dec. + ff

(j) Centralized PC

(k) Centralized PC + ff
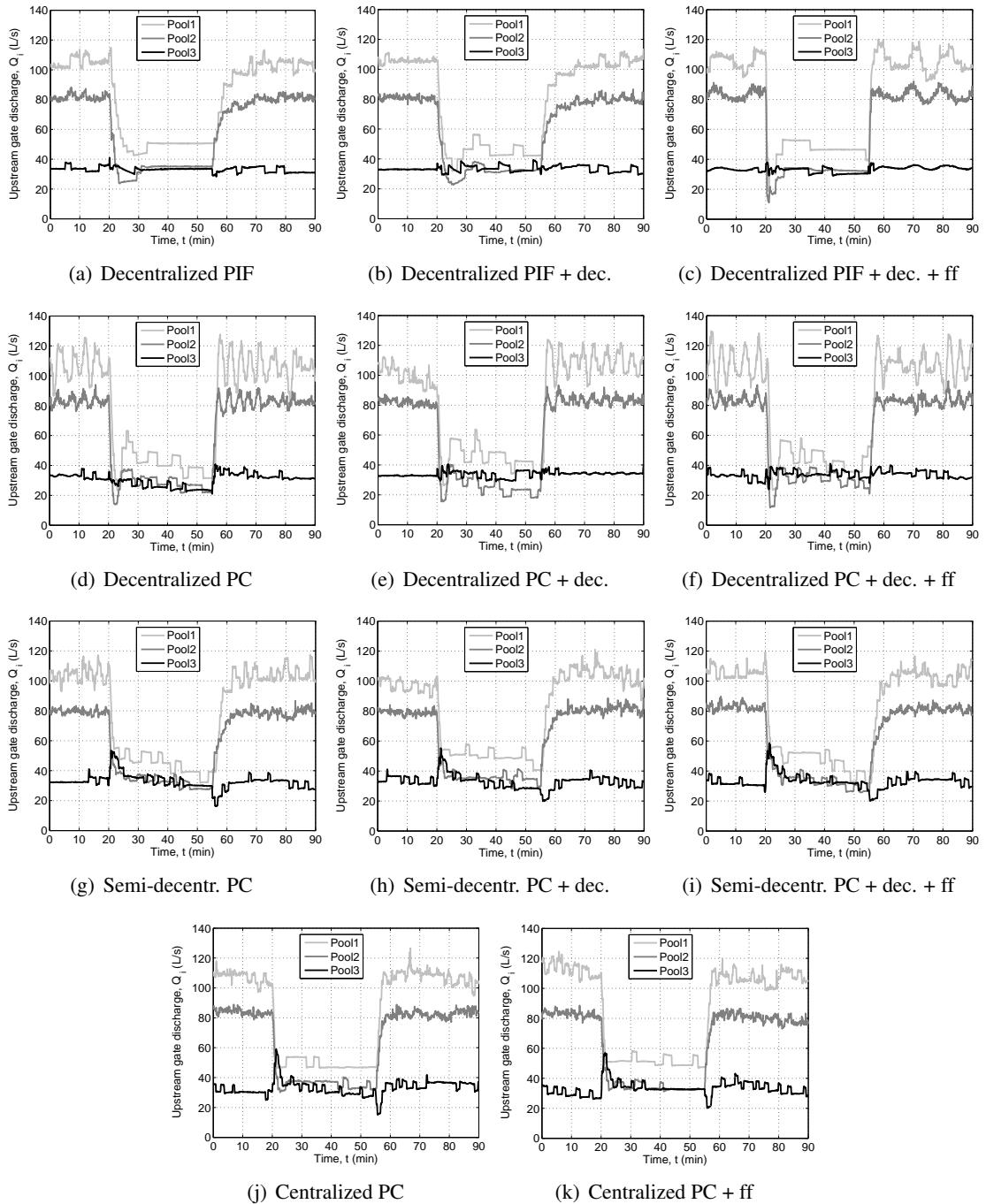
Figure 6.33: Calculated gate discharges

(a) Decentralized PIF   (b) Decentralized PIF + dec.   (c) Decentralized PIF + dec. + ff

(d) Decentralized PC   (e) Decentralized PC + dec.   (f) Decentralized PC + dec. + ff

(g) Semi-decentr. PC   (h) Semi-decentr. PC + dec.   (i) Semi-decentr. PC + dec. + ff

(j) Centralized PC   (k) Centralized PC + ff
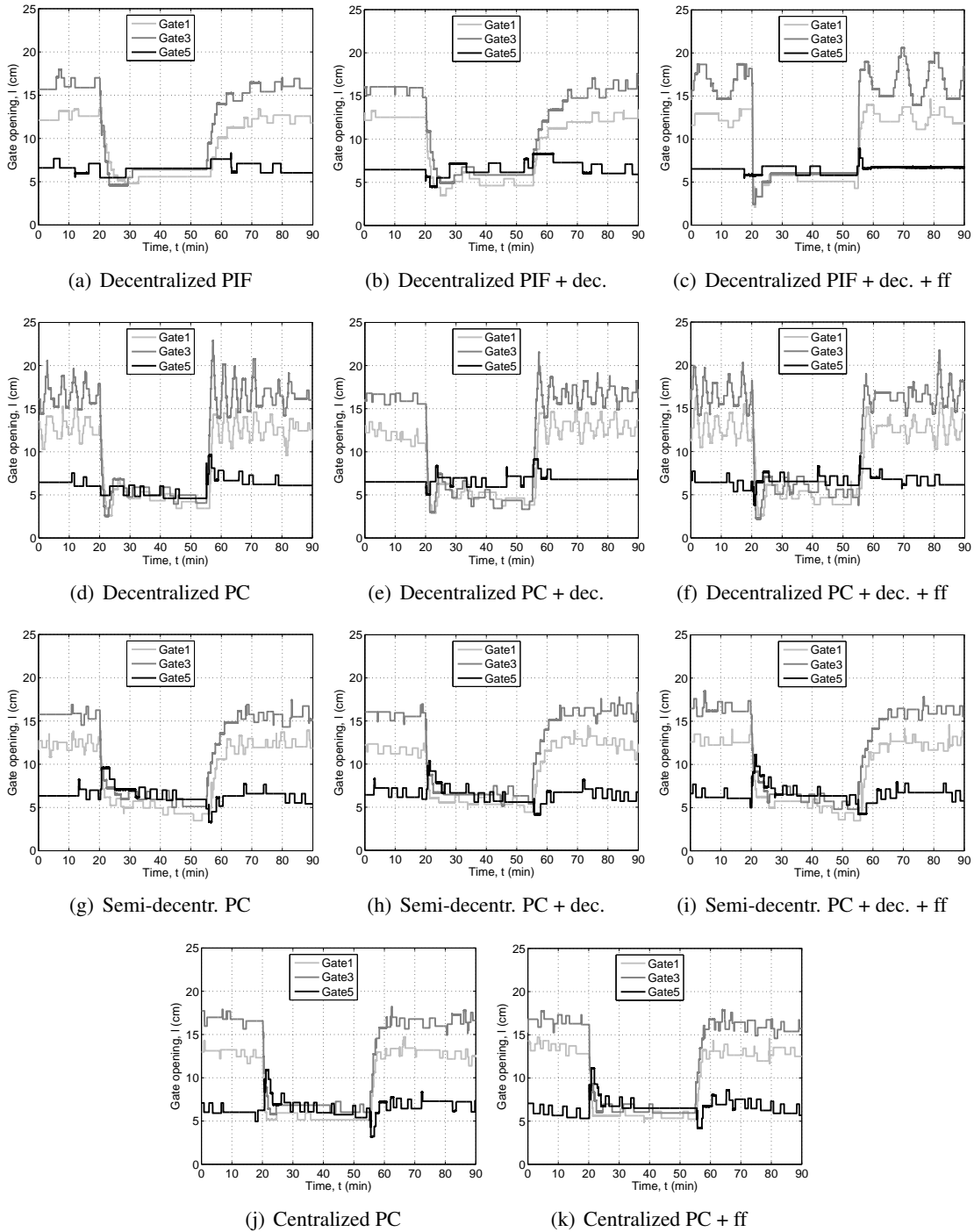
Figure 6.34: Applied gate openings

6.6   Discussion

The simulation results have shown that the use of a low pass filter can improve to a great extent the control performance of PI-based control strategies when dealing with canals with a marked resonant behavior, a characteristic that is typical of canals with subcritical flow. This filter is necessary because PI controllers can not deal directly with these transient oscillations. In that way, controllers focus mainly on the long-term response. Predictive Control has no structural restriction to deal with a system with resonance problems, unless this phenomena is not modeled by the controller model. In that case it is possible that the controller will not perform better than other simpler controls because the controller does not foresees this particular response peculiarity. This concept is also applicable to other types of irrigation canals where shock waves do not travel in the upstream direction (supercritical flow). If the predictive controller model does not consider this traveling effect, Predictive control will not exhibit a better performance than PI control as shown in Wahlin (2004). However, if the predictive controller model include these peculiar dynamics, these complex transients are likely to be well controlled without the need of any type of filtering action.

In general, the PI control tuning recommendations given in Schuurmans et al. (1999b) and in Litrico et al. (2006) gave good and similar performance results. However, it was found that the control performance could be slightly improved by using multivariable Nyquist-like analysis tools and a good linear MIMO canal model.

The simulation results predicted that a decentralized PIF scheme using a simple decoupling strategy could obtain very good results, but that a predictive control strategy would be capable to achieve a much better performance. For instance, simulations of the Canal PAC-UPC using predictive control schemes showed smaller level deviations and approximately a $50\,\%$ reduction of the time needed to recover the system from an offtake discharge change. These results also emphasized that all methods produce small steady state oscillations because of the minimum movement restriction of typical gates. All these results were confirmed by the experimental data.

The use of these control schemes in the real canal proved that all of them are capable to manage irrigation canal systems and counteract offtake discharge change effects. However, there were appreciable differences in their resulting performances. The gate and the discharge control layers were the same for all. Hence, differences are due to more appropriate or less appropriate water level control schemes.

The PIF control achieved an acceptable performance, specially when used with the decoupling scheme proposed by Schuurmans et al. (1999b). The incorporation of this type of strategies do not seem to affect the stability margins of well tuned decentralized controllers. In contrast, the direct incorporation of the offtake discharge measurements in the way proposed in the

same paper, end up producing high oscillations of the controlled system. Large and continuous oscillations were observed with higher velocities when the water levels were more fluctuating due to the discharge conditions and the canal geometry.

The same thing happened with all the decentralized predictive control schemes. It seems that this group of designed schemes turned out to be more sensitive to this type of noisy signal.

In both cases it is not ruled out that a fine controller re-tuning might reduce the noise sensitive and eliminate the oscillations.

What is clear from the experimental results is that the semi-decentralized and the centralized predictive control schemes do not present this performance degradations either including offtake discharge measurements or facing noisy level signals.

Furthermore, these two schemes exhibited always the best level regulation results. They outperformed all PIF based schemes with smaller level deviations during shorter time periods. In this respect, the absolute sum of all pool level deviations in figure 6.31 and the sum of the respective gate openings in figure 6.34 during the period after closing and before reopening Weir3 are plotted in figure 6.35.
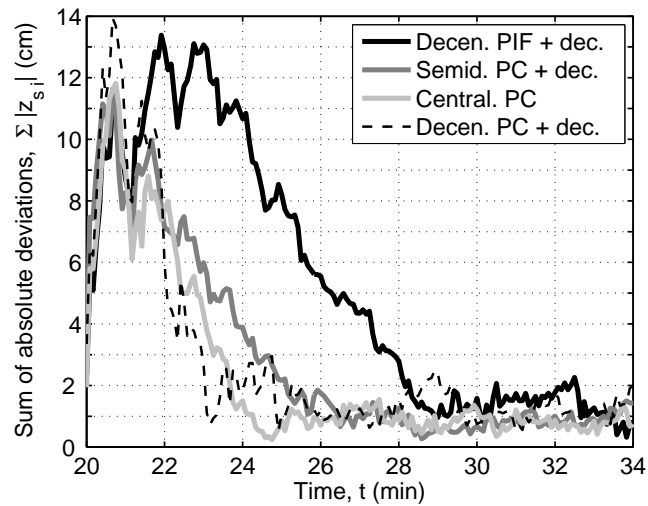
(a) Sum of level deviations
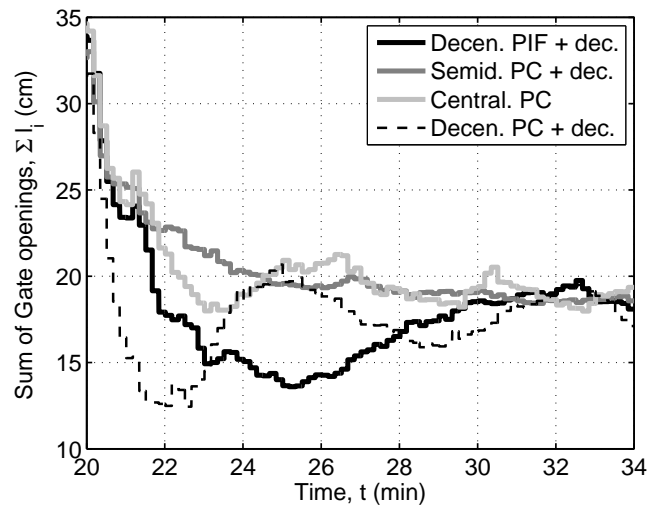
(b) Sum of gate openings

Figure 6.35: Comparison of the overall regulation performance when using different controls

This figure shows that the centralized and the semi-decentralized predictive control schemes controlled the unknown offtake discharge change situation in approximately $50\,\%$ and $66\,\%$ of the time required by the PIF scheme respectively. In addition, they attain a maximum sum of deviations that was $10\,\%$ less than the one of the PIF response. Furthermore, these control schemes attained these performance improvements using appreciable shorter gate trajectories than the other two schemes (see figure 6.35b). In other words, better level regulation results were achieved with less control effort.

In figure 6.35 and in all the rest, it is remarkable how similar the responses of the semi-decentralized and the centralized predictive control schemes are. The only appreciable difference is the longer period that takes the former to return the levels to their references. These results are manifesting that the semi-decentralized strategy is a very good approximation of the centralized control approach. The outcome of this analysis is that bigger irrigation canals with many pools can resemble a centralized control behavior with a series of less complex Two-Input Two-Output (TITO) controllers, maintaining the strategic benefits of a decentralized scheme. In fact, the only signalling difference between a decentralized controller and a basic semi-decentralized controller is that the latter needs additionally the upstream-pool downstream water level measurement. No gate discharge measurements are used by this water level controller, this data is fed back from the calculated controller output.

The implementation of these type of controllers is not necessarily more complex than a normal PI controller. As a matter of fact, all the predictive controllers developed in this chapter were implemented as a sum of weighted data. The additional complexity locates in the design stage. However, the design of TITO controllers is completely accessible and several regulation control performance benefits can be gained.

Regarding to the use of offtake discharge measurements in the control, neither of the tested schemes showed any appreciable performance improvement. However, it is not ruled out that this type of strategy could be helpful in the control of other canals or with other control algorithms. The use of the offtake discharge predictions have not been tested in this work.

6.7 Conclusions

This chapter has treated the overall control process of a real canal, particularly the Canal PAC-UPC. The main conclusion of the chapter is that a well designed control solution is completely capable to handle the multiple water level regulation problem that is produced by offtake discharge changes in real irrigation canals. However, the attainable regulation performance may vary depending on the selected method.

Getting into details, the following conclusions were obtained:

- It is possible to deduce a simple gate discharge saturation formula, i.e. a formula that calculates bounds on the attainable gate discharge value at a given time instant, useful to prevent gates come out of water and to feed anti-windup control schemes.

- A gate discharge controller based on the Ferro equation is enough accurate and simple to achieve the discharge set points calculated by a water level control layer.

- The minimum gate movement restriction deteriorates the performance of any feedback control scheme that does not take that problem explicitly into account. The effect of this actuator nonlinearity consists in producing steady state oscillations around the operating points.

- The use of a low pass filter in series with PI controllers can improve to a great extent the attainable performance in pools with backwater effects.

- The tuning recommendations given in Schuurmans et al. (1999b) and in Litrico et al. (2006) for PI level controllers give acceptable results in practice. However the control performance can be further improved using multivariable Nyquist-like tuning techniques with a good multivariable model.

- A predictive controller is capable of rejecting a change in the offtake discharge in almost half the time and with less level deviations than a PI-based controller.

- Well tuned not centralized control schemes can achieve higher performance results by introducing simple decoupling strategies.

- Irrigation control schemes based on predictive controllers tuned with the same prediction horizons and control weights, can exhibit different regulation performances. For instance, the decentralized predictive control scheme presented large oscillations around the operating points when level conditions were more fluctuating (higher flow velocities) in the laboratory tests, unlike the centralized and semi-decentralized predictive control schemes

that exhibited very stable and soft responses. It is possible that these last two configurations have intrinsic robust characteristics, especially against noisy signals and unmodeled dynamics.

- The centralized predictive control scheme offers the best results when rejecting offtake discharge changes in practice with more stable, smaller and shorter level deviations. However, the semi-decentralized scheme proposed in this thesis achieve almost identical performance results and can be implemented in a virtually decentralized way, thus being more robust against instrumentation failures, making possible the gradual automation of irrigation canals, etc..

- The analysis of the results suggests that the semi-decentralized scheme approximates very closely the centralized control behavior. In front of same offtake discharge changes, both of them react in a very similar form. The only really distinguishable difference is the response speed of both control strategies; the semi-decentralized scheme is slightly slower and conservative in the actions.

- It is not clear that the inclusion of offtake discharge measurements in the control schemes would always improve the control performance. In this case, this feedforward control element destabilized a well tuned decoupled PIF scheme and added no noticeable benefits in the level regulations results of the predictive control schemes.

- The success of these control schemes in managing this laboratory canal qualifies the application of these strategies on real irrigation canals. Although the size of the canal is smaller than real irrigation canals, real water transport problems, instrumentation inaccuracies and actuator constraints were confronted. Furthermore, level sensors, motor drives and other elements were acquired from irrigation-related suppliers.

In a broader context, two major contributions have been made through this chapter:

1. A new irrigation canal control strategy, called semi-decentralized control, was proposed, developed and tested with very good results. This control strategy has the performance advantages of a centralized controller and the implementation benefits of a decentralized control strategy.

2. The Canal PAC-UPC was totally automatized, leaving a consistent and already tested platform that can be used by other researchers to deploy and prove other irrigation canal control algorithms.

Chapter 7

Conclusions and Future Work

7.1 Summary of Conclusions

The objectives of this thesis have required to cover knowledge of two very wide and different engineering areas, namely hydraulic engineering and control engineering. The mix of this theoretical requirement with the responsibility to design and implement the instrumentation and gate motorization in a laboratory canal to fulfil the experimentation necessities of this thesis work, has lead to a meticulous investigation exploiting several research lines in parallel. Each one of these research lines were developed in different chapters that, in conjunction, lead to one important and general conclusion: the automation of irrigation canals is entirely feasible and can produce very good performance results, if the peculiar characteristics of this type of systems are taken into account and ad-hoc control solutions are carefully chosen and designed.

Going more in detail, each one of the different working lines has provided important conclusions that are worth to mention. These conclusions are divided by chapters in the following paragraphs.

Chapter 3: "The Canal PAC-UPC"

- A laboratory canal has been completely instrumented and the gates motorized to test control algorithms for irrigation canals. This canal was described in detail in this chapter, from which it was possible to acquire a practical knowledge related to the instrumentation of canals, touching on topics like treatment of measurement errors, signal processing techniques, calibration of sensors, etc.. All this know-how is indispensable when working with real canals.

- This chapter has also presented one of the products of this thesis: an own, non-commercial, Supervisory Control And Data Acquisition (SCADA) software for the Canal PAC-UPC.

Many of the elements, solutions and procedures used in its development are applicable to similar systems in real canals.

- Based on the overall chapter content, it is possible to confirm that this laboratory canal provides a good platform where to test irrigation canal automation issues for future research.

Chapter 4: "Calibration of Weirs and Sluice Gates"

- Hydraulic structures, like weirs and gates, have demonstrated a great skill in measuring water flow rates. In particular, it was observed that appropriate hydraulic relationships, carefully calibrated with field measurement data, can provide higher measurement accuracies than typical flow gages at very reduced costs.

- It is known that accurate gate discharges measurements are very important in the management and control of irrigation canals. However, the determination of gate discharge values with hydraulic relationships is sometimes very inaccurate, specially when working under the submerged flow condition. A study which evaluated many methods to compute gate discharges in this condition, has found that with very accurate level measurements (the best situation), the majority of the methods produce mean errors around 10% or more. However, there are highly remarkable exceptions. When calibration data were available, a very simple method recently proposed in Ferro (2001) achieved mean errors smaller than 3%. When no a priori data was available, it was found that using a fixed contraction value of 0.611 in classical theoretical equations was a very good option because the mean errors were always smaller than 6%.

- Due to the very good results produced by the method proposed in Ferro (2001), it is found to be one of the best candidates to implement a gate discharge controller by inverting the hydraulic equation.

- The good success in calibrating the hydraulic structures of the laboratory canal using methods from other researchers, validate their design to use them as commonly encountered irrigation canal devices.

Chapter 5: "Canal Identification for Control Purposes"

- The main conclusion of this chapter is that an irrigation canal can be well modeled for control purposes by linear black-box models obtained by means of system identification techniques. Nevertheless, it is very important to take into account the special characteristics of the system (delays, resonant modes, integrator dynamics, etc.) when designing

the identification procedure. If the process is performed in a blind manner, identified models are likely to be inaccurate and/or unappropriate and/or unstable. Thus, it is necessary to inspect the structure, properties and characteristics of each pool before proceeding because this information is crucial when selecting issues like: sampling time, model structure, experiment type, etc..

- A detailed mathematical analysis has concluded that there is a general linear model structure that is applicable to any type of canal. One of the most relevant outcomes from this analysis, is the derivation of new mathematical approximation results which reinforce and support the idea already suggested by some researchers, that there is always an integrator pole within this general structure. This result is very important because it is known that the identification of a system with integrators is very erratic about the exact location of these poles. To circumvent this problem, it was found recommendable to rectify the location of the integrator pole after the model has been identified.

- It is recommendable to work with discharges and water levels in a pool identification procedure. Gate openings will always add additional nonlinearities and augment the identification complexity. In fact, the validity range of a pool linearization is generally shorter when using gate openings instead of gate discharges. Gates and other hydraulic structures can always be afterwards included in an already identified discharge-based model.

- When designing the identification experiment, there is not a unique solution in the data sampling time selection. Nevertheless, it was found useful to obtain the step response of a pool and divide approximately the time taken to reach a clear tendency by a value around 15 to adequately characterize the most important elements in the pool behavior.

- Simulation results have shown that Auto-Regressive with eXogenous Input (ARX) and Laguerre model structures can adequately approximate the pool behavior around an operation point. However, the ARX model performed better and with less parameters.

- A correctly identified Multiple-Input Multiple-Output (MIMO) ARX model can adequately model a real canal around an operation point. Time domain and frequency domain results demonstrate that with a model order between 5 and 10, it is capable to approximate the principal dynamical characteristics of the system. Moreover, the results have shown that a linear model obtained in this way can perform very accurate predictions in the future. A model with this characteristics is very useful for control design applications and particularly for predictive control methods.

- The experimental validation of the specifically designed identification process demonstrates its ability to deal with real cases.

Chapter 6: "Control of an Irrigation Canal"

- The main conclusion of the chapter is that any well designed control solution is completely capable to handle the multiple water level regulation problem that is produced by offtake discharge changes in real irrigation canals. However, the attainable regulation performance may considerably vary depending on the selected control strategy. For instance, irrigation canal control schemes focusing the managing problem more centrally offer the best results when rejecting offtake discharge changes in practice with more stable, smaller and shorter level deviations. Nevertheless, it is not necessary to totally centralize the control problem; a semi-decentralized control scheme proposed in this thesis achieve much better performance results than decentralized control schemes and an almost identical efficiency than a centralized controller. This control scheme is slightly slower and more conservative than a centralized controller, but its design and implementation is far more simple; instead of controlling only one water level, controllers in this scheme should control two water levels. Consequently, its implementation is almost decentralized and offers benefits like: to be more robust against instrumentation failures, to make possible the gradual automation of irrigation canals, etc..

- The type of control method used to implement the controllers for these irrigation canal control schemes, plays also an important role in the resulting control performance. It has been observed that schemes based on predictive controllers are capable of rejecting a change in the offtake discharge in almost half the time and with less level deviations than a scheme with PI controllers. In this respect, it has been seen that the use of a low pass filter in series with PI controllers can improve to a great extent the attainable performance in pools with backwater effects, and even better results can be obtained by introducing simple decoupling strategies like the one presented in Schuurmans et al. (1999b), but never superior than when using predictive controllers.

- Regarding to PI controllers in irrigation canals, it has been proven that the tuning recommendations given in Schuurmans et al. (1999b) and in Litrico et al. (2006) for PI level controllers give acceptable results in practice. However the control performance can be further improved using multivariable Nyquist-like tuning techniques with a good multivariable model.

- Focusing on less centralized or more centralized predictive control schemes, it has been observed that different schemes tuned with the same prediction horizons and control weights can exhibit different regulation performances. For instance, while for a particular set of tuning values, decentralized predictive control schemes presented large oscillations around the operating points when level conditions were more fluctuating (higher flow

velocities) in the laboratory tests, centralized and semi-decentralized predictive control schemes exhibited always very stable and soft responses. It is possible that these last two configurations have intrinsic robust characteristics, especially against noisy signals and unmodeled dynamics.

- It is not clear that the inclusion of offtake discharge measurements in the control schemes would always improve the control performance. In this case, this feedforward control element destabilized a well tuned and decoupled scheme based on PI controllers with low pass filters and added no noticeable benefits in the level regulations results of the predictive control schemes.

- It is very useful to view the irrigation canal control problem in a simplified way when designing a global control strategy, but the influence of gates, the real actuators in irrigation canals, should not be forgotten. Their operational constraints or the way they accomplish the orders given by supervisory controllers, can reduce the control performance drastically. As a matter of fact, the minimum gate movement restriction deteriorates the performance of any feedback irrigation canal control scheme that does not take that limitation explicitly into account. The effect of this actuator nonlinearity consists in producing steady state oscillations around the operating points. This type of response is almost unavoidable for the majority of the really implementable control methods to date. However, there are other actuator constraints that are not too difficult to handle. This is the case of gate discharge saturation limits. In this thesis, it was deduced a simple gate discharge saturation formula, i.e. a formula that calculates bounds on the attainable gate discharge value at a given time instant, useful to prevent gates come out of water and to feed anti-windup control schemes. The existence of such constraints (actuator nonlinearities) makes almost inadvisable the use of integral control to attain specific gate discharge values or gate openings because oscillations are likely to occur. In this perspective, it was found in this thesis that a gate discharge controller based on the inversion of the static discharge equation presented in Ferro (2001) is enough accurate and simple, to achieve the discharge set points calculated by a water level control layer.

- The success in the automation of this laboratory canal qualifies the application of these techniques on real irrigation canals. Although the size of the canal is smaller than real irrigation canals, real water transport problems, instrumentation inaccuracies and actuator constraints were confronted. Furthermore, level sensors, motor drives and other elements were acquired from irrigation-related suppliers.

7.2   Future work

Following the investigations described in this thesis, a number of projects could be taken up:

- To further study the relationships among the gate discharges methods for the submerged flow condition and for the free flow condition, in order to find a more accurate description of this hydraulic phenomena. In particular, some preliminary analysis carried out during this thesis, have shown that gate discharge equations calibrated using Ferro (2001) fit almost perfectly distinct zones of the empirical curve developed for gate discharge coefficients in Henry (1950), but neither of them the entire graph. Thus, it is necessary to perform more experiments to discover the true link between these two approaches and, moreover, if these relationships can be unified with the other methods proposed in the research literature.

- To compare the performance of models computed using the proposed system identification guidelines for irrigation canals with other identification approaches used in other research works (e.g. the ones in Weyer (2001), in Ooi et al. (2005), in Eurén and Weyer (2007) and in Rivas Pérez et al. (2007)).

- To test the performance of adaptive system identification algorithms in approximating the true nonlinear behavior of the system.

- To test the performance of other types of control algorithms in the Canal PAC-UPC, using other pool configurations and other flow conditions. With this canal, it is possible to change the working conditions with small effort, providing an excellent opportunity to extend the results obtained in this thesis.

- To study the real benefits that a predictive control algorithm can exhibit, if the minimum gate movement restriction is considered explicitly in the control problem. The implementation of such an actuator constraint is complex and requires much computation effort. However, if there is a clear improvement in the management of irrigation canals, it should be considered as a promising alternative.

- To extend the results of the semi-decentralized control strategy by testing its implementation in large canals and by simulating its response in the ASCE test cases (Clemmens et al., 1998).

References

K. Akouz, A. Benhammou, P.-O. Malaterre, B. Dahhou, and G. Roux. Predictive control applied to ASCE Canal 2. In *IEEE International Conference on Systems, Man, and Cybernetics*, volume 4, pages 3920–3924, San Diego, USA, Oct. 1998.

M. Ansar. Discussion of 'Simultaneous flow over and under a gate' by V. Ferro. *Journal of Irrigation and Drainage Engineering*, 127(5):325–326, 2001.

E. Bautista and A. J. Clemmens. Response of ASCE Task Committee Test Cases to open-loop control measures. *Journal of Irrigation and Drainage Engineering*, 125(4):179–188, 1999.

O. Begovich, C. Aldana, V. Ruiz, D. Georges, and G. Besançon. Real-time predictive control with constraints of a multi-pool open irrigation canal. In *XI Congreso Latinoamericano de Control Automatico, CLCA2004*, La Habana, Cuba, May 2004.

J. T. Bialasiewicz. Advanced system identification techniques for wind turbine structures with special emphasis on modal parameters. *NASA STI/Recon Technical Report N*, 96:11276–+, 1995.

C. M. Burt and X. Piao. Advances in PLC-based irrigation canal automation. *Irrigation and Drainage*, 53(1):29–37, 2004.

E. F. Camacho and C. Bordons. *Model Predictive Control*. Springer-Verlag, London, second edition, 2004.

CEMAGREF. *Simulation of Irrigation Canals (SIC) version 4.08: user's guide & theoretical concepts*, Feb. 2004.

A. J. Clemmens and J. Schuurmans. Simple optimal downstream feedback canal controllers: theory. *Journal of Irrigation and Drainage Engineering*, 130(1):26–34, 2004a.

A. J. Clemmens and J. Schuurmans. Simple optimal downstream feedback canal controllers: ASCE test case results. *Journal of Irrigation and Drainage Engineering*, 130(1):35–46, 2004b.

A. J. Clemmens, T. F. Kacerek, B. Grawitz, and W. Schuurmans. Test cases for canal control algorithms. *Journal of Irrigation and Drainage Engineering*, 124(1):23–30, 1998.

A. J. Clemmens, T. S. Strelkoff, and J. A. Replogle. Calibration of submerged radial gates. *Journal of Hydraulic Engineering*, 129(9):680–687, 2003.

J. de Halleux, C. Prieur, J.-M. Coron, B. d'Andréa Novel, and G. Bastin. Boundary feedback control in networks of open channels. *Automatica*, 39(8):1365–1376, 2003.

J.-F. Dulhoste, D. Georges, and G. Besançon. Nonlinear control of open-channel water flow based on collocation control model. *Journal of Hydraulic Engineering*, 130(3):254–266, 2004.

Ö. F. Durdu. Control of transient flow in irrigation canals using Lyapunov fuzzy filter-based gaussian regulator. *International Journal for Numerical Methods in Fluids*, 50(4):491–509, 2005.

K. Eurén and E. Weyer. System identification of open water channels with undershot and overshot gates. *Control Engineering Practice*, 15(7):813–824, 2007.

V. Ferro. Simultaneous flow over and under a gate. *Journal of Irrigation and Drainage Engineering*, 126(3):190–193, 2000.

V. Ferro. Closure to 'Simultaneous flow over and under a gate' by V. Ferro. *Journal of Irrigation and Drainage Engineering*, 127(5):326–328, 2001.

M. Ghodsian. Flow through side sluice gate. *Journal of Irrigation and Drainage Engineering*, 129(6):458–4636, 2003.

M. Gómez, J. Rodellar, and J. A. Mantecón. Predictive control method for decentralized operation of irrigaton canals. *Applied Mathematical Modelling*, 26(11):1039–1056, 2002.

HEC. *Hydrologic Engineering Center - River Analysis System (HEC-RAS) version 3.1: hydraulic reference manual*, Nov. 2002.

F. M. Henderson. *Open channel flow*. MacMillan Publishing Co., Inc., New York, 1966.

H. R. Henry. Discussion of 'Diffusion of submerged jets' by M. L. Albertson, Y. B. Dai, R. A. Jensen and H. Rouse. *Trans. ASCE*, 115:687–694, 1950.

C. H. Lin, J. F. Yen, and C. T. Tsai. Influence of sluice gate contraction coefficient on distinguishing condition. *Journal of Irrigation and Drainage Engineering*, 128(4):249–252, 2002.

X. Litrico. Nonlinear diffusive wave modeling and identification of open channels. *Journal of Hydraulic Engineering*, 127(4):313–320, 2001a.

X. Litrico. Robust flow control of single input multiple outputs regulated rivers. *Journal of Irrigation and Drainage Engineering*, 127(5):281–286, 2001b.

X. Litrico and V. Fromion. Simplified modeling of irrigation canals for controller design. *Journal of Irrigation and Drainage Engineering*, 130(5):373–383, 2004a.

X. Litrico and V. Fromion. Analytical approximation of open-channnel flow for controller design. *Applied Mathematical Modelling*, 28(7):677–695, 2004b.

X. Litrico and V. Fromion. Frequency modeling of open-channel flow. *Journal of Hydraulic Engineering*, 130(8):806–815, 2004c.

X. Litrico and V. Fromion. Tuning of robust distant downstream PI controllers for an irrigation canal pool. I: Theory. *Journal of Irrigation and Drainage Engineering*, 132(4):359–368, 2006.

X. Litrico and D. Georges. Robust continuous-time and discrete-time flow control of a dam-river system. (I) Modelling. *Applied Mathematical Modelling*, 23(11):809–827, 1999a.

X. Litrico and D. Georges. Robust continuous-time and discrete-time flow control of a dam-river system. (II) Controller design. *Applied Mathematical Modelling*, 23(11):829–846, 1999b.

X. Litrico, V. Fromion, J.-P. Baume, C. Arranja, and M. Rijo. Experimental validation of a methodology to control irrigation canals based on Saint-Venant equations. *Control Engineering Practice*, 13(11):1425–1437, 2005.

X. Litrico, V. Fromion, and J.-P. Baume. Tuning of robust distant downstream PI controllers for an irrigation canal pool. II: Implementation issues. *Journal of Irrigation and Drainage Engineering*, 132(4):369–379, 2006.

X. Litrico, P.-O. Malaterre, J.-P. Baume, P.-Y. Vion, and J. Ribot-Bruno. Automatic tuning of PI controllers for an irrigation canal pool. *Journal of Irrigation and Drainage Engineering*, 133(1):27–37, 2007.

L. Ljung. *System identification. Theory for the user.* Prentice-Hall, Inc., Upper Saddle River, New Jersey, second edition, 1999.

J. M. Maciejowski. *Multivariable Feedback Design*. Addison-Wesley, Wokingham, UK, first edition, 1989.

P.-O. Malaterre. Pilote: Linear quadratic optimal controller for irrigation canals. *Journal of Irrigation and Drainage Engineering*, 124(4):187–194, 1998.

P.-O. Malaterre and J.-P. Baume. Modeling and regulation of irrigation canals: existing applications and ongoing researches. In *IEEE International Conference on Systems, Man, and Cybernetics*, volume 4, pages 3850–3855, San Diego, USA, Oct. 1998.

P.-O. Malaterre and J.-P. Baume. Optimum choice of control action variables and linked algorithms: comparison of different alternatives. In *ASCE-ICID Workshop on Modernization of Irrigation Water Delivery Systems*, Phoenix, USA, Oct. 1999.

P.-O. Malaterre and J. Rodellar. Multivariable predictive control of irrigation canals. Design and evaluation on a 2-pool model. In *International Workshop on the Regulation of Irrigation Canals: State of the Art of Research and Applications*, pages 230–238, Marakech, Morocco, Apr. 1997.

P.-O. Malaterre, D. C. Rogers, and J. Schuurmans. Classification of canal control algorithms. *Journal of Irrigation and Drainage Engineering*, 124(1):3–10, 1998.

R. Malti, S. B. Ekongolo, and J. Ragot. Dynamic SISO and MIMO system approximations based on optimal Laguerre models. *IEEE transactions on Automatic Control*, 43(9):1318–1323, 1998.

I. Mareels, E. Weyer, S. K. Ooi, M. Cantoni, Y. Li, and G. Nair. Systems engineering for irrigation systems: Successes and challenges. In *Annual Reviews in Control (IFAC)*, volume 29, pages 191–204, 2005.

J. M. Martín Sánchez and J. Rodellar. *Adaptive Predictive Control. From the Concepts to Plant Optimization.* Prentice Hall International, Hemel Hempstead, first edition, 1996.

A. Montazar, P. J. van Overloop, and R. Brouwer. Centralized controller for the Narmada Main Canal. *Irrigation and Drainage*, 54(1):79–89, 2005.

J. S. Montes. Irrotational flow and real fluid effects under planar sluice gates. *Journal of Hydraulic Engineering*, 123(3):219–232, 1997.

J. S. Montes. Closure to 'Irrotational flow and real fluid effects under planar sluice gates' by J. S. Montes. *Journal of Hydraulic Engineering*, 125(2):212–213, 1999.

S. K. Ooi, M. Krutzen, and E. Weyer. On physical and data driven modelling of irrigation channels. *Control Engineering Practice*, 13(4):461–471, 2005.

N. Rajaratnam and K. Subramanya. Flow equation for the sluice gate. *Journal of Irrigation and Drainage Engineering*, 93(3):167–186, 1967.

J. M. Reddy and R. G. Jacquot. Stochastic optimal and suboptimal control of irrigation canals. *Journal of Water Resources Planning and Management*, 125(6):369–378, 1999.

R. Rivas, C. Prada, J. R. Perán, and P. I. Kovalenko. Robust adaptive predictive control of water distribution in irrigation canals. In *15th IFAC World Congress*, Barcelona, Spain, July 2002.

R. Rivas Pérez, V. Feliu Batlle, and L. Sánchez Rodríguez. Robust system identification of an irrigation main canal. *Advances in Water Resources*, 30(8):1785–1796, 2007.

J. Rodellar, M. Gómez, and J. P. Martín Vide. Stable predictive control of open-channel flow. *Journal of Irrigation and Drainage Engineering*, 115(4):701–713, 1989.

J. Rodellar, M. Gómez, and L. Bonet. Control method for on-demand operation of open-channel flow. *Journal of Irrigation and Drainage Engineering*, 119(2):225–241, 1993.

J. Rodellar, C. Sepúlveda, D. Sbarbaro, and M. Gómez. Constrained predictive control of irrigation canals. In *Proceedings of the 2nd International Conference on Irrigation and Drainage*, pages 477–486, Phoenix, Arizona, May 2003. USCID.

D. C. Rogers and J. Goussard. Canal control algorithms currently in use. *Journal of Irrigation and Drainage Engineering*, 124(1):11–15, 1998.

V. M. Ruiz and J. Ramírez. Predictive control in irrigation canal operation. In *IEEE International Conference on Systems, Man, and Cybernetics*, volume 4, pages 3897–3901, San Diego, USA, Oct. 1998.

V. M. Ruiz, A. J. Clemmens, and J. Schuurmans. Canal control algorithms formulations. *Journal of Irrigation and Drainage Engineering*, 124(1):31–39, 1998.

B. F. Sanders and N. D. Katopodes. Control of canal flow by adjoint sensitivity method. *Journal of Irrigation and Drainage Engineering*, 125(5):287–297, 1999.

S. Sawadogo, R. M. Faye, P.-O. Malaterre, and F. Mora-Camino. Decentralized predictive controller for delivery canals. In *IEEE International Conference on Systems, Man, and Cybernetics*, volume 4, pages 3880–3884, San Diego, USA, Oct. 1998.

S. Sawadogo, R. M. Faye, A. Benhammou, and K. Akouz. Decentralized adaptive predictive control of multi-reach irrigation canal. In *IEEE International Conference on Systems, Man, and Cybernetics*, pages 3437–3442, Nashville, USA, Oct. 2000.

J. Schuurmans, O. H. Bosgra, and R. Brouwer. Open-channel flow model approximation for controller design. *Applied Mathematical Modelling*, 19(9):525–530, 1995.

J. Schuurmans, A. J. Clemmens, S. Dijkstra, A. Hof, and R. Brouwer. Modeling of irrigation and drainage canals for controller design. *Journal of Irrigation and Drainage Engineering*, 125(6):338–344, 1999a.

J. Schuurmans, A. Hof, S. Dijkstra, O. H. Bosgra, and R. Brouwer. Simple water level controller for irrigation and drainage canals. *Journal of Irrigation and Drainage Engineering*, 125(4): 189–195, 1999b.

C. Seatzu. Design and robustness analysis of decentralized constant volume-control for open-channels. *Applied Mathematical Modelling*, 23(6):479–500, 1999.

C. Seatzu. Decentralized controllers design for open-channel hydraulic systems via eigenstructure assignment. *Applied Mathematical Modelling*, 24(12):915–930, 2000.

C. Seatzu and G. Usai. A decentralized volume variations observer for open channels. *Applied Mathematical Modelling*, 26(10):975–1001, 2002.

M. A. Shahrokhnia and M. Javan. Dimensionless stage–discharge relationship in radial gates. *Journal of Irrigation and Drainage Engineering*, 132(2):180–184, 2006.

D. S. Shook, C. Mohtadi, and S. L. Shah;. A control-relevant identification strategy for GPC. *IEEE Transactions on Automatic Control*, 37(7):975–980, 1992.

P. Silva, M. Ayala Boto, J. Figueiredo, and M. Rijo. Model predictive control of an experimental water canal. In *Proceedings of the European Control Conference 2007*, pages 2977–2984, Kos, Greece, July 2007.

J. Soler, M. Gómez, and J. Rodellar. Una herramienta de control de transitorios en canales de regadío. *Ingeniería del Agua*, 11(3):297–313, 2004.

J. Speerli and W. H. Hager. Discussion of 'irrotational flow and real fluid effects under planar sluice gates' by J. S. Montes. *Journal of Hydraulic Engineering*, 125(2):208–210, 1999.

K. J. Åström and T. Hägglund. *PID controllers: Theory, design, and tuning.* Instrument Society of America, Research Triangle Park, North Carolina, second edition, 1995.

P. K. Swamee. Sluice-gate discharge equations. *Journal of Irrigation and Drainage Engineering*, 118(1):56–60, 1992.

P. K. Swamee, S. K. Pathak, and M. S. Ali. Analysis of rectangular side sluice gate. *Journal of Irrigation and Drainage Engineering*, 119(6):1026–1035, 1993.

P. K. Swamee, S. K. Pathak, T. Mansoor, and C. S. P. Ojha. Discharge characteristics of skew sluice gates. *Journal of Irrigation and Drainage Engineering*, 126(5):328–334, 2000.

P. J. van Overloop, J. Schuurmans, R. Brouwer, and C. M. Burt. Multiple-model optimization of proportional integral controllers on canals. *Journal of Irrigation and Drainage Engineering*, 131(2):190–196, 2005.

B. T. Wahlin. Performance of model predictive control on ASCE Test Canal 1. *Journal of Irrigation and Drainage Engineering*, 130(3):227–238, 2004.

B. T. Wahlin and A. J. Clemmens. Performance of historic downstream canal control algorithms on ASCE Test Canal 1. *Journal of Irrigation and Drainage Engineering*, 128(6):365–375, 2002.

B. T. Wahlin and A. J. Clemmens. Automatic downstream water-level feedback control of branching canal networks; theory. *Irrigation and Drainage Engineering*, 132(3):198–207, 2006.

M. G. Webby. Discussion of 'Irrotational flow and real fluid effects under planar sluice gates' by J. S. Montes. *Journal of Hydraulic Engineering*, 125(2):210–212, 1999.

E. Weyer. System identification of an open water channel. *Control Engineering Practice*, 9(12): 1289–1299, 2001.

J.-F. Yen, C.-H. Lin, and C.-T. Tsai. Hydraulic characteristics and discharge control of sluice gates. *Journal of the Chinese Institute of Engineers*, 24(3):301–310, 2001.

C. C. Zervos and G. A. Dumont. Deterministic adaptive control based on Laguerre series representation. *International Journal of Control*, 48(1):2333–2359, 1988.

Appendix A

Procedure to obtain the structure of the linearized model

Replacing with letters the most common expressions in (5.9), (5.12) can be calculated for any reach using a finite number of uniform areas, in a manner that the equation structure can be easily identified.

So, approximating a reach with an increasing numbers of areas yields:

One uniform area:

$$
e^{A(x_0, s) h_0} =
\begin{bmatrix}
\dfrac{\lambda_2\, e^{\lambda_1 h_0} - \lambda_1\, e^{\lambda_2 h_0}}{\lambda_2 - \lambda_1} & \dfrac{c\, s\left(e^{\lambda_1 h_0} - e^{\lambda_2 h_0}\right)}{\lambda_2 - \lambda_1} \\[3mm]
\dfrac{\lambda_1\, \lambda_2\left(e^{\lambda_2 h_0} - e^{\lambda_1 h_0}\right)}{c\, s\left(\lambda_2 - \lambda_1\right)} & \dfrac{\lambda_2\, e^{\lambda_2 h_0} - \lambda_1\, e^{\lambda_1 h_0}}{\lambda_2 - \lambda_1}
\end{bmatrix}
$$

$$
=
\begin{bmatrix}
\dfrac{a_{11}}{a} & \dfrac{c_a\, s\, a_{12}}{a} \\[3mm]
-\dfrac{\lambda_a\, a_{12}}{c_a\, s\, a} & \dfrac{a_{22}}{a}
\end{bmatrix}
$$

$$
z_{s\,i}(s) = \frac{\lambda_a\, a_{12}{}^2 + a_{22}\, a_{11}}{s\, a\left(a_{22}\, A_{s\,i} - c_a\, a_{12}\right)}\, q_i(s) - \frac{a_{22}}{s\left(a_{22}\, A_{s\,i} - c_a\, a_{12}\right)}\left(q_{i+1}(s) + q_{L\,i}(s)\right)
$$

Two uniform areas:

$$
e^{A(x_1, s) h_1} \times e^{A(x_0, s) h_0} =
\begin{bmatrix}
\dfrac{b_{11}}{b} & \dfrac{c_b\, s\, b_{12}}{b} \\[3mm]
-\dfrac{\lambda_b\, b_{12}}{c_b\, s\, b} & \dfrac{b_{22}}{b}
\end{bmatrix}
\times
\begin{bmatrix}
\dfrac{a_{11}}{a} & \dfrac{c_a\, s\, a_{12}}{a} \\[3mm]
-\dfrac{\lambda_a\, a_{12}}{c_a\, s\, a} & \dfrac{a_{22}}{a}
\end{bmatrix}
$$

$$z_{s\,i}(s) =$$

$$-\frac{c_b\left(\lambda_b\, b_{12}{}^2\, a_{11}\, a_{22} + b_{22}\, \lambda_a\, a_{12}{}^2\, b_{11} + \lambda_b\, b_{12}{}^2\, a_{12}{}^2\, \lambda_a + b_{22}\, a_{22}\, b_{11}\, a_{11}\right)}{s\, b\, a\left((\lambda_b\, b_{12}\, c_a\, a_{12} - b_{22}\, a_{22}\, c_b)\, A_{s\,i} + b_{11}\, c_a\, a_{12}\, c_b + c_b{}^2\, b_{12}\, a_{22}\right)}\, q_i(s)$$

$$-\frac{\lambda_b\, b_{12}\, c_a\, a_{12} - b_{22}\, a_{22}\, c_b}{s\left((\lambda_b\, b_{12}\, c_a\, a_{12} - b_{22}\, a_{22}\, c_b)\, A_{s\,i} + b_{11}\, c_a\, a_{12}\, c_b + c_b{}^2\, b_{12}\, a_{22}\right)}\, (q_{i+1}(s) + q_{L\,i}(s))$$

Three uniform areas:

$$e^{A(x_2,\,s)\, h_2} \times e^{A(x_1,\,s)\, h_1} \times e^{A(x_0,\,s)\, h_0} =$$

$$\begin{bmatrix} \dfrac{c_{11}}{c} & \dfrac{c_c\, s\, c_{12}}{c} \\[2mm] -\dfrac{\lambda_c\, c_{12}}{c_c\, s\, c} & \dfrac{c_{22}}{c} \end{bmatrix} \times \begin{bmatrix} \dfrac{b_{11}}{b} & \dfrac{c_b\, s\, b_{12}}{b} \\[2mm] -\dfrac{\lambda_b\, b_{12}}{c_b\, s\, b} & \dfrac{b_{22}}{b} \end{bmatrix} \times \begin{bmatrix} \dfrac{a_{11}}{a} & \dfrac{c_a\, s\, a_{12}}{a} \\[2mm] -\dfrac{\lambda_a\, a_{12}}{c_a\, s\, a} & \dfrac{a_{22}}{a} \end{bmatrix}$$

$$z_{s\,i}(s) =$$

$$-\frac{c_b\, c_c\left(a_{11}c_{22}\lambda_b b_{12}{}^2 a_{22}c_{11} + \lambda_a a_{12}{}^2 \lambda_c c_{12}{}^2 b_{12}{}^2 \lambda_b + \lambda_a a_{12}{}^2 c_{22}b_{22}c_{11}b_{11}\right)\, q_i(s)}{s\, c\, b\, a\left(\star A_{s\,i} + c_a a_{12}c_c c_{11}b_{11}c_b - c_a a_{12}c_c{}^2 c_{12}\lambda_b b_{12} + a_{22}c_c c_b{}^2 c_{11}b_{12} + a_{22}c_c{}^2 c_b c_{12}b_{22}\right)}$$

$$-\frac{c_b\, c_c\left(a_{12}{}^2 \lambda_c c_{12}{}^2 b_{11}\lambda_a b_{22} + a_{11}\lambda_c c_{12}{}^2 b_{11}a_{22}b_{22} + a_{12}{}^2 c_{22}\lambda_b b_{12}{}^2 \lambda_a c_{11}\right)\, q_i(s)}{s\, c\, b\, a\left(\star A_{s\,i} + c_a a_{12}c_c c_{11}b_{11}c_b - c_a a_{12}c_c{}^2 c_{12}\lambda_b b_{12} + a_{22}c_c c_b{}^2 c_{11}b_{12} + a_{22}c_c{}^2 c_b c_{12}b_{22}\right)}$$

$$-\frac{c_b\, c_c\left(a_{22}\lambda_c c_{12}{}^2 b_{12}{}^2 a_{11}\lambda_b + a_{22}c_{22}b_{22}a_{11}c_{11}b_{11}\right)\, q_i(s)}{s\, c\, b\, a\left(\star A_{s\,i} + c_a a_{12}c_c c_{11}b_{11}c_b - c_a a_{12}c_c{}^2 c_{12}\lambda_b b_{12} + a_{22}c_c c_b{}^2 c_{11}b_{12} + a_{22}c_c{}^2 c_b c_{12}b_{22}\right)}$$

$$-\frac{\star\, (q_{i+1}(s) + q_{L\,i}(s))}{s\left(\star A_{s\,i} + c_a a_{12}c_c c_{11}b_{11}c_b - c_a a_{12}c_c{}^2 c_{12}\lambda_b b_{12} + a_{22}c_c c_b{}^2 c_{11}b_{12} + a_{22}c_c{}^2 c_b c_{12}b_{22}\right)}$$

$$\star = \left(c_a a_{12}\lambda_c c_{12}b_{11}c_b + c_a a_{12}c_{22}\lambda_b b_{12}c_c + c_b{}^2 a_{22}\lambda_c c_{12}b_{12} - c_b a_{22}c_{22}b_{22}c_c\right)$$

A detailed observation of all the above cases, reveals that all of them can be rewritten in the following form:

$$z_{s\,i}(s) = \frac{1}{s}\left(\frac{n_1(s)}{d_1(s)\, d_2(s)}\, q_i(s) - \frac{n_2(s)}{d_2(s)}\, q_{i+1}(s) - \frac{n_2(s)}{d_2(s)}\, q_{L\,i}(s)\right) \tag{A.1}$$

The succession has been followed until 6 areas (for lack of space they haven't been included), obtaining always the same result. The strength of the evidence suggests that this structure is always valid independently on the number of areas, therefore generalizing the equation structure for any type of reach under any operational condition.

If the offtake is located in a middle section of the pool, a similar equation structure can be obtained. For example, approximating the backwater curve with two uniform zones and

performing a discharge withdrawal in between both zones yields:

$$
\begin{bmatrix} q(X,s) \\ z(X,s) \end{bmatrix} = \begin{bmatrix} \dfrac{b_{11}}{b} & \dfrac{c_b\,s\,b_{12}}{b} \\[2ex] -\dfrac{\lambda_b\,b_{12}}{c_b\,s\,b} & \dfrac{b_{22}}{b} \end{bmatrix} \times \left[\begin{bmatrix} q_{L\,i}(s) \\ 0 \end{bmatrix} + \begin{bmatrix} \dfrac{a_{11}}{a} & \dfrac{c_a\,s\,a_{12}}{a} \\[2ex] -\dfrac{\lambda_a\,a_{12}}{c_a\,s\,a} & \dfrac{a_{22}}{a} \end{bmatrix} \begin{bmatrix} q(0,s) \\ z(0,s) \end{bmatrix} \right]
$$

$$
z_{s\,i}(s) =
$$

$$
-\frac{c_b\left(\lambda_b b_{12}^2 a_{11} a_{22} + \lambda_b b_{12}^2 a_{12}^2 \lambda_a + b_{22}\lambda_a a_{12}^2 b_{11} + b_{22} a_{22} b_{11} a_{11}\right)}{s\,b\,a\left((\lambda_b b_{12} c_a a_{12} - b_{22} a_{22} c_b) A_{s\,i} + b_{11} c_a a_{12} c_b + c_b^2 b_{12} a_{22}\right)}\, q_i(s)
$$

$$
-\frac{\lambda_b b_{12} c_a a_{12} - b_{22} a_{22} c_b}{s\left((\lambda_b b_{12} c_a a_{12} - b_{22} a_{22} c_b) A_{s\,i} + b_{11} c_a a_{12} c_b + c_b^2 b_{12} a_{22}\right)}\, q_{i+1}(s)
$$

$$
+\frac{c_b a_{22}\left(\lambda_b b_{12}^2 + b_{22} b_{11}\right)}{s\,b\left((\lambda_b b_{12} c_a a_{12} - b_{22} a_{22} c_b) A_{s\,i} + b_{11} c_a a_{12} c_b + c_b^2 b_{12} a_{22}\right)}\, q_{L\,i}(s)
$$

In this case the equation can be rewritten in the following form:

$$
z_{s\,i}(s) = \frac{1}{s}\left(\frac{n_1(s)}{d_1(s)\,d_2(s)\,d_3(s)}\, q_i(s) - \frac{n_3(s)}{d_3(s)}\, q_{i+1}(s) - \frac{n_2(s)}{d_2(s)\,d_3(s)}\, q_{L\,i}(s)\right) \tag{A.2}
$$

Appendix B

Weir discharge calibration data

Table B.1: Weir 1 calibration data

Discharge, Q (m^3/s)	Head, h (m)	Weir height, O (m)	General coefficient, C_{gen} (m$^{3/2}$/s)	h/O (m/m)
0.02768	0.1231	0.393	0.6332	0.3132
0.03448	0.1416	0.393	0.6403	0.3603
0.02775	0.1245	0.493	0.6242	0.2525
0.03916	0.1558	0.493	0.6307	0.3160
0.02963	0.1292	0.443	0.6307	0.2916
0.04916	0.1770	0.443	0.6546	0.3995
0.06166	0.2049	0.443	0.6599	0.4625

Table B.2: Weir 3 calibration data

Discharge, Q (m^3/s)	Head, h (m)	Weir height, O (m)	General coefficient, C_{gen} (m$^{3/2}$/s)	h/O (m/m)
0.03370	0.1389	0.493	0.6439	0.2817
0.04588	0.1699	0.493	0.6494	0.3446
0.06343	0.2080	0.493	0.6638	0.4219
0.02932	0.1265	0.393	0.6441	0.3219
0.04953	0.1756	0.393	0.6674	0.4468
0.06203	0.2012	0.393	0.6822	0.5120

Table B.3: Weir 4 calibration data

Discharge, Q (m^3/s)	Head, h (m)	Weir height, O (m)	General coefficient, C_{gen} $(\text{m}^{3/2}/\text{s})$	h/O (m/m)
0.03314	0.1324	0.543	0.6802	0.2438
0.05657	0.1851	0.393	0.7047	0.4710
0.05156	0.1755	0.443	0.6953	0.3962
0.02732	0.1154	0.343	0.6880	0.3364
0.05238	0.1765	0.393	0.7004	0.4491

Appendix C

Gate discharge calibration data

Table C.1: Gate 1 calibration data

Discharge, Q ($\mathrm{m^3/s}$)	Gate opening, l (m)	Upstream level, h_1 (m)	Downstream level, h_3 (m)
0.01729	0.0300	0.8480	0.6318
0.02056	0.0240	1.1210	0.6647
0.02064	0.0300	1.0320	0.7311
0.02260	0.0440	0.8180	0.6387
0.02269	0.0930	0.6026	0.5487
0.02375	0.0310	1.0443	0.6694
0.02381	0.0240	1.2615	0.6564
0.02838	0.0300	0.7979	0.2667
0.02838	0.0418	0.5379	0.2637
0.02858	0.0485	0.4746	0.2667
0.02899	0.0328	1.1149	0.6159
0.02909	0.0443	1.0380	0.7532
0.03792	0.0800	0.9335	0.7762
0.03800	0.0930	0.9155	0.7997
0.03827	0.0710	0.9008	0.7063
0.05228	0.0525	1.1820	0.5647
0.05242	0.0485	1.2877	0.5652
0.05247	0.0590	1.0545	0.5662
0.05252	0.0568	1.2438	0.6970
0.05252	0.0490	1.2685	0.5637

Table C.1: Continued on next page...

Table C.1: (continued)

Discharge, Q	Gate opening, l	Upstream level, h_1	Downstream level, h_3
(m^3/s)	(m)	(m)	(m)
0.05262	0.0585	1.1850	0.6749
0.05267	0.0765	0.9938	0.6896
0.05512	0.0500	1.1395	0.4072
0.05512	0.0675	0.8030	0.4062
0.05940	0.0600	1.2910	0.6752
0.05981	0.0710	1.1435	0.6981
0.05981	0.0660	1.2120	0.6895

Table C.2: Gate 3 calibration data

Discharge, Q	Gate opening, l	Upstream level, h_1	Downstream level, h_3
(m^3/s)	(m)	(m)	(m)
0.01729	0.0418	0.6433	0.5330
0.02056	0.0458	0.6768	0.5467
0.02064	0.0415	0.7431	0.5891
0.02260	0.0613	0.6496	0.5624
0.02269	0.0765	0.5589	0.5029
0.02375	0.0588	0.6798	0.5754
0.02381	0.0543	0.6665	0.5451
0.02899	0.0788	0.6224	0.5385
0.02909	0.0738	0.7618	0.6641
0.03792	0.0998	0.7836	0.6938
0.03800	0.0765	0.8053	0.6553
0.03827	0.1268	0.7120	0.6569
0.05252	0.0830	0.6926	0.4618
0.05262	0.1498	0.6688	0.6020
0.05267	0.1623	0.6850	0.6269
0.05981	0.1695	0.6860	0.6204
0.05981	0.1643	0.6810	0.6098

Table C.3: Gate 5 calibration data

Discharge, Q (m^3/s)	Gate opening, l (m)	Upstream level, h_1 (m)	Downstream level, h_3 (m)
0.01729	0.0388	0.5316	0.4273
0.02056	0.0465	0.5444	0.4387
0.02064	0.0388	0.5865	0.4377
0.02260	0.0485	0.5605	0.4441
0.02269	0.0700	0.4987	0.4455
0.02375	0.0495	0.5731	0.4483
0.02381	0.0568	0.5417	0.4483
0.02899	0.0802	0.5307	0.4645
0.02909	0.0488	0.6603	0.4639
0.03792	0.0890	0.6869	0.5882
0.03800	0.0700	0.6443	0.4885
0.03827	0.1115	0.6486	0.5893
0.05262	0.1540	0.5756	0.5263
0.05267	0.1295	0.6047	0.5254
0.05981	0.1758	0.5887	0.5427
0.05981	0.1930	0.5767	0.5422